

MOMENT CONNECTIONS BETWEEN STEEL BEAMS AND
CONCRETE COLUMNS

by

Tauqir Muhammad Sheikh, B.Sc., M.S.

DISSERTATION

Presented to the Faculty of the Graduate School of

The University of Texas at Austin

in Partial Fulfillment

of the Requirements

for the Degree of

DOCTOR OF PHILOSOPHY

THE UNIVERSITY OF TEXAS AT AUSTIN

December 1987

MOMENT CONNECTIONS BETWEEN STEEL BEAMS AND
CONCRETE COLUMNS

APPROVED:

Joseph A. Gern
James Gern
Richard W. Furberg
Joe W. Roessel
Edward H. ...

ACKNOWLEDGEMENTS

The experimental work reported herein was carried out at the Phil M. Ferguson Structural Engineering Laboratory, Balcones Research Center, The University of Texas at Austin. The research was sponsored by (i) National Science Foundation, grant number MSM-8412111, (ii) American Institute of Steel Construction, and (iii) CBM Engineers, Inc., Houston, TX. The author is grateful to each sponsor, especially Dr. P.V. Banavalkar of CBM Engineers who provided necessary support and funds to initiate the project.

The research was carried out under the direction of Dr. Joseph A. Yura and Dr. James O. Jirsa, author's dissertation supervisors. The author is deeply indebted to them for the continuous support and valuable advice that made this work possible. The encouragement of Dr. Yura and his generously devoted time is greatly appreciated. The author also acknowledges other members of the dissertation committee for their helpful suggestions.

The author is greatly obliged to his fellow graduate student Gregory Deierlein without whose suggestions, ideas and help, this research program would not have run smoothly. The assistance of other graduate students, Leo Linbeck, III, David Hartmann, David Yates, Paul Tikalsky and Robert Treece is also acknowledged. The help of undergraduates Leo Sanchez and David Inlow is greatly appreciated.

The technical assistance of Blake Stasney, Patrick Ball, Alex Tahmassebi, Richard Marshall, Jean Gehrke and G. Hinckley is gratefully acknowledged. The contributions of other staff including Laura Golding and Sharon Cunningham are appreciated.

Tauqir M. Sheikh

The University of Texas at Austin
December, 1987

MOMENT CONNECTIONS BETWEEN STEEL BEAMS AND
CONCRETE COLUMNS

Publication No. _____

Tauqir Muhammad Sheikh, Ph.D.
The University of Texas at Austin, 1987

Supervising Professors: Dr. Joseph A. Yura
Dr. James O. Jirsa

In recent years mixed steel-concrete structural systems have gained popularity for the construction of buildings, especially those over 30 stories high. Although these systems are termed "mixed", the structural members within a subsystem are made of a single material, steel or concrete. These systems traditionally make use of only simple shear connections between steel beams and concrete columns. As a result, there is a minimum interaction between the two materials. The efficiency of mixed systems can be substantially enhanced by combining members of structural steel and reinforced concrete by developing moment connections between steel beams and concrete columns.

Several methods are available for the transfer of steel beam flange forces to the connection panel. Lever Mechanisms and face bearing plates (FBP) were experimentally investigated. FBPs are steel plates welded to the beam at column faces. Steel panel thickness, and thickness, width and configuration of FBP were chosen as variables. Nine, 1/2 to 2/3 scale steel beam-concrete column subassemblages, representing interior connections, were tested under simulated monotonic lateral loads to examine strength and stiffness of the connections.

The test results show that face bearing plates substantially enhanced joint strength. Variations in the thickness of these plates did not affect the joint capacity. The joint capacity, however, was increased by increasing the width of the FBP. Extending the FBPs above and below the beam was most effective and increased both the joint strength and stiffness.

Based on the test data, a design model which identifies principal forces on the connection panel was developed. The resistance to joint shear is furnished by a) steel panel in pure shear and b) concrete panel through diagonal compression strut. A design approach is proposed which can be used to detail the connections.

TABLE OF CONTENTS

Chapter		Page
1	MIXED STEEL CONCRETE STRUCTURAL SYSTEMS	1
	1.1 Introduction.....	1
	1.2 Mixed Steel-Concrete Systems	3
	1.3 The Connection Problem	7
	1.4 Possible Connection Details	12
	1.5 Scope and Objectives	16
2	REVIEW OF PAST RESEARCH AND PRACTICES	19
	2.1 Developments in the United States	19
	2.2 Research in Japan	24
	2.3 Research in Australia	33
3	EXPERIMENTAL PROGRAM.....	35
	3.1 Test Series Description	35
	3.2 Specimen design and details	39
	3.2.1 Beam details	43
	3.2.2 Column details	49
	3.2.3 Specimen fabrication	51
	3.3 Material Properties	57
	3.4 Test Set-Up	59
	3.5 Load System	63
	3.6 Instrumentation and Data Acquisition	66
	3.6.1 Joint distortion, drift and load measurements	66
	3.6.2 Strain measurements	69
	3.6.3 Data acquisition.....	74
	3.7 General Test Procedure.....	74
4	EXPERIMENTAL RESULTS	78
	4.1 General Specimen Behavior	78
	4.2 Stiffness Characteristics	106
	4.2.1 Components of Joint Distortion	106
	4.2.2 Member Contribution	110
	4.2.3 Load vs. Joint Distortion Relationship	114
	4.3 Flange and Face Bearing Plate Stresses	121
	4.3.1 Transverse and Longitudinal Flange Stresses	123

TABLE OF CONTENTS

Chapter		Page
	4.3.2 Transverse and Vertical Stresses in Face Bearing Plates	127
4.4	Reinforcing Bar Behavior	129
	4.4.1 Column Vertical Bars	131
	4.4.2 Joint Ties	137
4.5	Connection Panel Behavior	139
	4.5.1 Steel Panel Behavior	139
	4.5.2 Concrete Panel Behavior	141
5	EVALUATION OF JOINT STRENGTH	147
	5.1 Failure Criteria	147
	5.2 Summary of Test Results	148
	5.3 Mechanisms for Resisting Joint Forces	151
	5.4 Joint Shear	158
	5.5 Modes of Failure	163
	5.6 Thickness of Face Bearing Plates	167
	5.7 Width of Face Bearing Plate	168
	5.8 Configuration of Face Bearing Plate	169
	5.9 Thickness of Steel Panel	171
6	DESIGN RECOMMENDATIONS	172
	6.1 Parameters Governing Design	173
	6.2 Proposed Model for Joint Forces	174
	6.3 Explicit Considerations	178
	6.3.1 Bearing Block Size and Intensity ...	178
	6.3.2 Face Bearing Plate Size and Configuration	180
	6.3.3 Steel Panel Capacity	185
	6.3.4 Concrete Panel Size and Capacity ...	185
	6.4 Other Considerations	190
	6.4.1 Flange Size	190
	6.4.2 Beam Embedment and Aspect Ratio	192
	6.4.3 Joint Reinforcement	193
	6.4.4 Bond Conditions	194
	6.4.5 Joint Stiffness	194
	6.5 Design Approach	195
	6.6 Limitations of Design Approach	199
	6.7 Comparison with Test Results	202
7	CONCLUSIONS AND RECOMMENDATIONS	205
	7.1 Summary	205
	7.2 Conclusions	205
	7.3 Future Research Needs	206

TABLE OF CONTENTS

Chapter	Page
APPENDIX A: REVIEW OF JOINT DESIGN	208
APPENDIX B: DESIGN EXAMPLE	231
LIST OF SELECTED NOTATIONS	238
REFERENCES	244
VITA	

LIST OF TABLES

Table		Page
3.1	Summary of Test Series	36
3.2	Material Properties	60
3.3	Concrete Cylinder Strength	60
4.1	Significant Load Points	81
4.2	Summary of Joint Distortion	115
5.1	Summary of Test Results	149
5.2	Estimated Joint Shear	160
6.1	Revised Analysis of Test Results	187
6.2	Comparison of Design Approach with Test Results ...	202
6.3	Salient Features of Japanese Tests	204

LIST OF FIGURES

Figure		Page
1.1	Typical floor plan - composite framed tube system .	5
1.2	Conventional composite framed tube system details .	5
1.3	Composite framed tube system details with steel spandrel beam	8
1.4	Typical steel beam simple connections	8
1.5	Typical connection details used by O'Leary and Undrill	10
1.6(a)	Behavior of framed tube under lateral loads	11
1.6(b)	Forces on the joint	11
1.7	Forces on the connection panel	13
1.8	Lever arm mechanism	13
1.9	Means of stress transfer from steel beam to concrete column	15
2.1	Resistance of embedded bracket at ultimate	20
2.2	Typical test specimen used by Mattock and Gaafar ..	22
2.3	Actual and assumed stresses and strains in concrete adjacent to embedded steel section	22
2.4	Typical specimen used by Hawkins and Roeder	25
2.5	Typical SRC assemblage	25
2.6	SRC beam-to-column connection	27
2.7	Stress transferring mechanism in exterior joint ...	31
3.1	Modelling of beam-column subassemblage	40

LIST OF FIGURES

Figure		Page
3.2	Test specimens 1 and 2	41
3.3	Test specimens 3 thru 9	42
3.4	Beam details in the joint area for specimens 1 and 2	44
3.5	Beam details in the joint area for specimens 3, 4 and 5	45
3.6	Beam details in the joint area for specimens 6 and 7	46
3.7	Beam details in the joint area for specimens 8 and 9	47
3.8(a)	Joint reinforcement for specimens 1 and 2	50
3.8(b)	Joint reinforcement for specimens 3 thru 7 and 9 ..	52
3.9	Joint reinforcement for specimen 8	53
3.10	A view of joint area of specimen 1	54
3.11	Joint area of specimen 5	54
3.12	Joint area of specimen 8	55
3.13	A typical reinforcement cage	55
3.14	A view of formwork	56
3.15	Concreting operation	56
3.16	Typical load vs strain plot for tension coupons ...	58
3.17	Test set-up for specimens 3 thru 9	61
3.18	A view of test set-up	62

LIST OF FIGURES

Figure		Page
3.19	Detail at the column base	62
3.20	Detail at the column top	64
3.21	Detail at the beam end	64
3.22	Schematic of load system	65
3.23	Components of beam deflection	67
3.24	Location of LVDTs - looking north	68
3.25	LVDTs for joint distortion	70
3.26	Steel frame to measure joint distortion	70
3.27	Electronic digital inclinometer to measure the column face rotation	71
3.28	Location for rotation measurements with electronic inclinometer	71
3.29	Instrumentation on reinforcing bars for specimens 1 and 2	72
3.30	Instrumentation on reinforcing bars and concrete -- specimens 3 thru 9	73
3.31	Instrumentation on beam for specimens 1 and 2	75
3.32	Instrumentation on beam for specimens 3 thru 9	76
4.1	Member stress zones under loading in the primary direction	79
4.2	Typical loading curve	79
4.3	Critical cracks in concrete column	82

LIST OF FIGURES

Figure		Page
4.4	Load-drift plot of specimen 1	82
4.5	A view of joint 1 after failure	83
4.6	Load-drift plot of specimen 2	85
4.7	A view of joint 2 after cycle U1	85
4.8	A view of Joint 2 after failure	86
4.9	Load-drift plot of specimen 3	87
4.10	A view of Joint 3 after failure	87
4.11	Joint 3 after failure	89
4.12	Load-drift plot of specimen 4	89
4.13	Joint 4 after cycle U1	90
4.14	Joint 4 after failure	90
4.15	Joint 4 after failure	91
4.16	Load-drift plot of specimen 5	91
4.17	Joint 5 after cycle U1	93
4.18	Joint 5 after failure	93
4.19	Load-drift plot of specimen 6	95
4.20	Joint 6 after cycle U1	95
4.21	Joint 6 after failure	96
4.22	Joint 6 after failure	96
4.23	Load-drift plot of specimen 7	98

LIST OF FIGURES

Figure		Page
4.24	Joint 7 after cycle U1	98
4.25	Joint 7 after failure	99
4.26	Joint 7 after failure	99
4.27	Load-drift plot of specimen 8	100
4.28	Joint 8 after cycle U1	100
4.29	Joint 8 after failure	102
4.30	Joint 8 after failure	102
4.31	Joint 8 after failure	103
4.32	Joint 8 after failure	103
4.33	Load-drift plot of specimen 9	104
4.34	Joint 9 after cycle U1	104
4.35	Joint 9 after failure	105
4.36	Joint 9 after failure	105
4.37	Joint size correction for shear distortion	108
4.38	Schematic diagram of the test specimen	111
4.39	Sources of error in panel separation and steel panel distortion	111
4.40	Composition of joint distortion in specimen 5	115
4.41	Comparison of distortion in steel and concrete panels of specimen 5	116
4.42	Load vs TJD plot for specimens 3, 4, 5 and 7	116

LIST OF FIGURES

Figure		Page
4.43	Load vs TJD plot for specimens 3, 6, 8 and 9	118
4.44	Load vs TJD plot for specimens 1 and 2	121
4.45	Forces on a typical joint	122
4.46	Transfer of column flexural compression to the connection panel	122
4.47	Longitudinal stress in flanges of specimen 5	124
4.48	Transverse stress in flanges of specimen 5	124
4.49	Diagrammatic representation of concrete settlement under flanges	126
4.50	Transverse stress in flanges of specimen 6	126
4.51	Transverse stress in face bearing plates of specimen 6	128
4.52	Vertical stress in face bearing plates of specimen 5	128
4.53	Transfer of vertical bar tension to the concrete strut through friction	130
4.54	Vertical stress in face bearing plate of specimen 6	130
4.55	Stress in vertical bars of specimen 5 near bottom flange	132
4.56	Stress in vertical bars of specimen 5 near top flange	132
4.57	Flexural forces on a typical joint	134
4.58	Stress in vertical bars of specimen 8 near bottom flange	135

LIST OF FIGURES

Figure		Page
4.59	Mechanism of transfer of partial flange forces to the diagonal compression strut	136
4.60	Stress in vertical bars of specimen 8 near top flange	138
4.61	Stress in ties located within beam depth of specimen 5	138
4.62	Stress in ties located above beam of specimen 5 ...	140
4.63	Maximum shear stress in the steel panel of specimen 5	140
4.64	Concrete stress-strain curve in uniaxial compression	143
4.65	Strain in the concrete panel of specimen 5	143
4.66	Strain in the concrete panel of specimen 7	145
4.67	Strain in the concrete panel of specimen 9	145
5.1	Forces on a connection	152
5.2	Stress in column vertical bars	152
5.3	Vertical bar forces inside the joint	154
5.4	Assignment of force C'_c to steel and concrete panels	154
5.5	Assignment of external forces to steel and concrete panels	155
5.6	Forces at the panel boundaries	155
5.7	Forces on the connection panel at failure load	159

LIST OF FIGURES

Figure		Page
5.8	Simplified analysis of joint	159
5.9	Forces on face bearing plates	165
5.10	Load vs TJD plot for specimens 5 and 8	170
5.11	Load vs TJD plot for specimens 5 and 9	170
6.1	Forces on a steel beam-to-concrete column connection due to lateral loads	175
6.2	Modelling of external forces on the joint	175
6.3	Modelling of forces on the connection panel	177
6.4	Forces on steel beam	177
6.5	Forces on extended face bearing plate	182
6.6	Transfer of forces on the flanges to the steel panel	191
A.1	Forces on a beam-column joint	209
A.2	Mechanism for joint core shear resistance	209
A.3	Forces on a joint after bond slip	217
A.4	Continuous beam-to-column connections	219
A.5	Strength of column web	220
A.6	Strength of column flange in tension region of connection	222
A.7	Forces on a typical rigid connection	226
A.8	Connection panel at ultimate shear capacity	228

CHAPTER ONE

MIXED STEEL-CONCRETE STRUCTURAL SYSTEMS

1.1 Introduction

In the last twenty years or so, several structural systems for the construction of buildings have evolved to exploit the best characteristics of both reinforced concrete and structural steel. These structural systems are termed mixed steel-concrete systems, composite systems or hybrid systems, and are especially popular for the construction of tall buildings.

A structural system for buildings is composed of two primary subsystems; lateral load resisting subsystem and gravity load subsystem. Mixed structural systems invariably use structural steel for the gravity load subsystem. For the lateral load subsystem, reinforced concrete or composite members in various forms are used. The lateral load subsystem is designed to carry its share of gravity forces and resist all the lateral loads. This subsystem is also required to provide the stiffness required for:

- a) limiting lateral sway (drift) to prevent cladding and partition distress;
- b) limiting acceleration to prevent disturbing perception to lateral motion; and
- c) providing overall system stability under the entire gravity loads and lateral loads.

The overall effectiveness of a given combination of steel and concrete components is controlled not only by structural efficiency, but is controlled significantly by other factors like

material availability and cost, construction technology and labor, and constraints from architectural and mechanical disciplines. A structural system most efficient under one set of constraints may not be applicable in other situations. Mixed systems, in general, utilize the most desirable characteristics and assets of each material so that the combination may result in a higher order of overall efficiency.

Mixed systems use structural steel for light and simple floor framing, smaller size steel columns, and flexibility for space planning, especially in the core. A typical steel beam and composite metal deck floor system weighs approximately 60% of a typical reinforced concrete floor system. Although the costs of the two are comparable, reduced weight from steel framing can still result in large savings in columns and foundation costs. Another particular asset of steel construction is that elements are prefabricated in plants under mechanized and controlled conditions resulting in higher speed of construction which is a major factor in determining the cost of most tall buildings.

Mixed systems use concrete for its moldability to any shape, durability in different weather conditions, fire resistance, insulating qualities, easy availability in any strength at relatively low cost, better damping characteristics, and above all, its inherent stiffness characteristics. Motion perception and lateral stiffness are the most important structural considerations, especially for tall buildings. Reinforced concrete lateral load resisting subsystems, because of their larger mass and better mechanical damping properties, reduce the problem of perception to motion. The development of readily available high strength concrete in the range of 7000 to 14000 psi has resulted in much improved rigidity since the concrete elastic modulus increases with the strength. High strength concrete has also

made it possible to keep the columns reasonable in size. Cost analyses indicate [18] reinforced concrete columns are almost 11 times more cost effective in strength and about eight times more cost effective in terms of the axial stiffness as compared to steel columns. However, the concrete columns weigh about 25% more and are almost three to four times the size of steel columns. Also concrete is at a distinct disadvantage when it comes to beams and floor framing because of higher labor costs for formwork and shoring, and slower speed of construction.

In the current practice of mixed structural system design, individual components within each of the primary subsystems are still made of a single structural material, i.e. reinforced concrete or structural steel. The connections between the steel floor beams and lateral load resisting concrete members are designed as simple shear connections. Hence, there is minimum interaction between the two materials.

The economy of mixed systems can be substantially enhanced by using members of two different materials within a subsystem, e.g. steel beams with concrete columns/walls for lateral load resistance. However, in this case a moment connection between steel beams and concrete columns or walls is required.

Currently there is no data available for the design of such connections and they are not covered in any design specifications. Various authors (Iyengar, 24; Griffis, 18) have emphasized that research is critically needed for design methods and standardization of connections between steel beams and reinforced concrete and composite columns.

1.2 Mixed Steel-Concrete Systems

Most mixed structural systems have been developed for construction of tall buildings. Therefore, lateral load resis-

tance has perhaps been the most controlling subsystem into and around which are fitted other subsystems required for gravity loads. To date, most tall buildings of mixed construction are in regions where wind resistance is of prime concern, but there is growing interest in their use as economical structures in earthquake regions. Most of the mixed systems, with some adjustments, can be adapted readily to seismic design and construction.

Some of the common mixed structural systems are: composite framed tube system, concrete core braced system, multiple concrete core support system, panel braced frame system, and encased steel frame system. These systems are described in detail in Refs. 22, 23 and 46. Only one of these structural systems, composite framed tube system, is discussed in the following to illustrate the possible use of steel beams with concrete columns using moment connections.

The composite frame tube system is perhaps the most popular mixed structural system. Like other mixed systems, the gravity load subsystem consists of steel beams composite with composite metal deck. The concept is shown in schematic form in Figs. 1.1 and 1.2. The floor beams are connected to the steel columns at the interior using simple shear connections. At the exterior these beams are connected to small steel erection columns which are later embedded in the concrete columns. Small steel beams are required at the exterior to brace the floor framing during construction. These beams are also embedded in the concrete spandrel beams as shown in Fig. 1.2. The floor framing and the interior steel columns are designed to carry the gravity loads only. A reinforced concrete exterior framed tube is used as the lateral load-resisting subsystem. It consists of closely spaced concrete columns at the perimeter of the building with deep concrete spandrel beams. A typical section of the spandrel beam

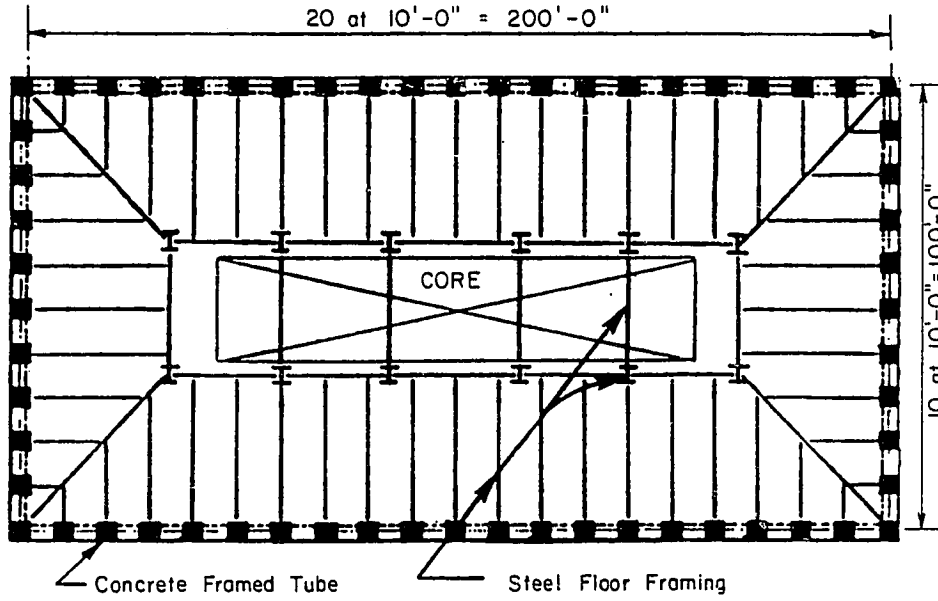


Fig. 1.1 Typical floor plan - composite framed tube system.

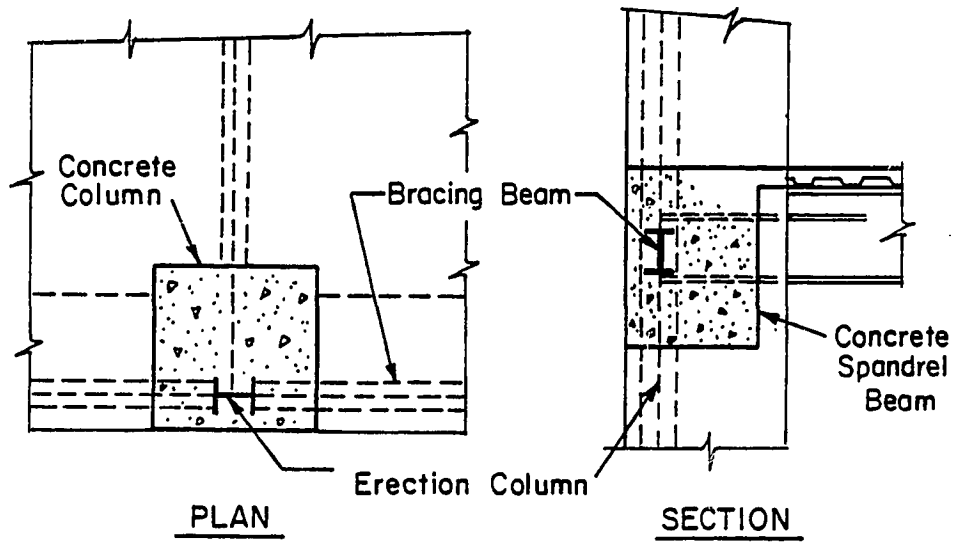


Fig. 1.2 Conventional composite framed tube system details.

and exterior columns is shown in Fig. 1.2. The exterior framed tube is designed to resist all the lateral loads.

Concrete placement for the exterior columns and spandrel beams typically lags about 10-12 floors behind the steel erection. Metal deck installation quickly follows erection of the steel framing after which concrete on the deck is placed. The completed slab is also used as a construction platform for lifting prefabricated reinforcement cages and gang forms for the construction of the framed tube. The small exterior steel erection columns are designed to carry a maximum of 5-6 concreted floors and 5-6 floors with metal deck only plus any construction load. The contribution of the embedded steel column to the concrete column's strength and stiffness is generally neglected.

The exterior framed tube form offers considerable flexibility for variations in shape without significant loss of structural efficiency of lateral load resistance. Partial or incomplete framed tubes, cluster of tubes, and bundled tubes have been used.

The total stiffness of the framed tube is controlled by the axial deformation of the columns, the flexural deformation of the beams and columns, and the shear distortion of the beam-column joints. As the height-to-width ratio of a building increases from two-to-five or more, the contribution of axial stiffness of the columns to the overall stiffness increases from 10-20% to well over 50%. The reinforced concrete columns are found to be cost effective in providing strength, as well as axial stiffness, when compared to steel columns. The size of the concrete columns would not be unreasonably large, especially when readily available high strength concrete is used. The weight would be slightly more than that of steel columns.

The economy of the composite framed tube system could be further enhanced if steel spandrel beams are used with reinforced concrete columns, as shown in Fig. 1.3. This combination would eliminate the formwork cost of spandrels. Steel spandrels would simply replace the bracing beams and fuse with the remaining steel floor framing. Similarly, steel beams could be used as link beams with reinforced concrete walls in other mixed structural systems. As mentioned earlier, this combination of steel beams and concrete columns/walls requires information regarding the moment connections between them.

1.3 The Connection Problem

In the current practice of mixed systems there is limited interaction between the members of two different materials i.e. steel and concrete. The connections between steel floor beams and concrete columns or walls are generally made using simple shear connections. A few commonly used simple connection details are shown in Fig. 1.4. These connections can be designed using the recommendations of the Prestressed Concrete Institute (PCI) committee on connection details [40, 41] and the American Concrete Institute (ACI) building code [4].

In order to use steel and concrete together in the lateral load resisting subsystem, a moment connection between steel beams and concrete columns or walls would be required. Currently, there is no information available for the design of such moment connections. There is an urgent need for data to establish the design guidelines for such moment connections so more economical mixed systems can be developed.

In recent years there has been a growing interest among design engineers to combine structural steel beams with reinforced concrete or composite columns/walls. Despite the lack

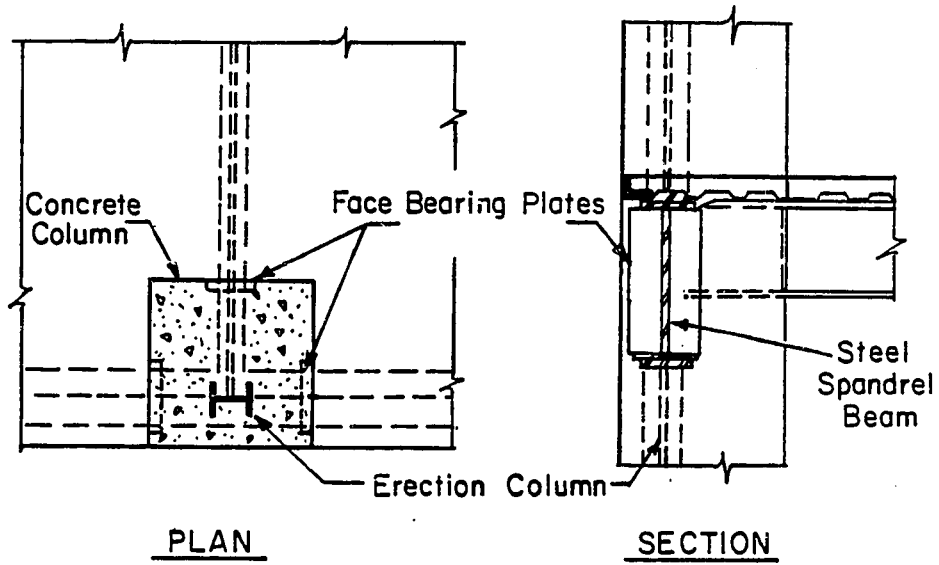


Fig. 1.3 Composite framed tube system details with steel spandrel beam.

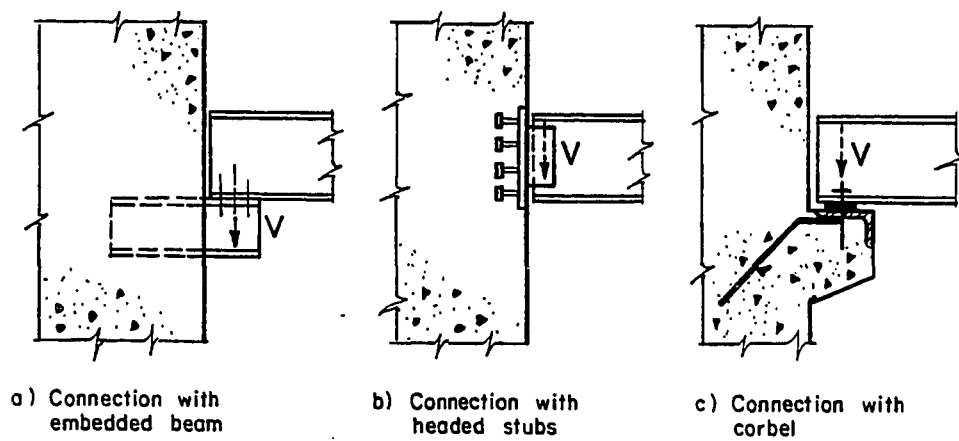


Fig. 1.4 Typical steel beam simple connections.

of design information, a few examples of their use have been reported. Griffis [18], and Moore and Gosain [35] have described their use in the structural system of two buildings; the 52-story Three Houston Center Gulf Tower, Houston, Texas, and the 49-story First City Tower, Houston, Texas. The perimeter composite framed tube or frame, consisting of steel spandrel beams and composite columns, were designed to provide resistance to lateral loads. Concrete shear walls linked with steel beams were used for additional lateral resistance in the First City Tower. Unfortunately, the details of the connections between these steel beams and composite columns or concrete walls, employed in these two buildings, are not published.

O'Leary and Undrill [37] have described a structural system using steel beams and concrete columns. In this system plane frames were used at the perimeter of the building to resist the entire seismic forces of the building. These frames consisted of rectangular structural steel beams and closely spaced reinforced concrete columns. O'Leary and Undrill used the system in four completed multi-story buildings ranging from 14 to 17 stories. Typically, the columns were 3'-4" to 3'-9" deep with about 3'-4" clear spacing between columns. Beams were solid rectangular sections, ranging from 2 in. wide X 12 in. deep to 1-1/2 in. wide X 6 in. deep in cross section. The moment connections between the steel beams and the concrete columns were made using bearing plates, as shown in the Fig. 1.5., which were clamped to the beam with one long bolt at each side of the rectangular beams. The concrete bearing stresses were limited to those allowed in ACI 318 Code [4]. However, special supplementary hoops were used adjacent to the plates. O'Leary and Undrill claim the system achieved the ductility of structural steel beams without utilizing field bolted or welded connections

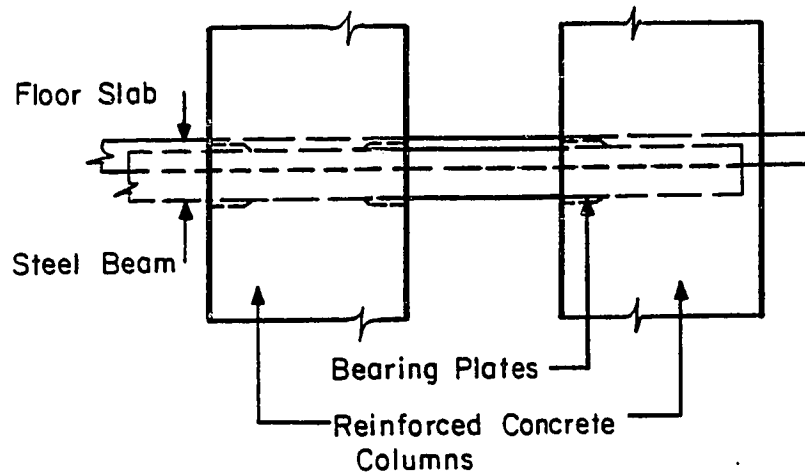


Fig. 1.5 Typical connection details used by O'Leary and Undrill (Ref. 37).

with steel columns. Several construction problems were noted including congested reinforcing in relatively narrow columns, beam placement, etc.

The behavior of a framed tube or a rigid frame, when subjected to lateral loads, is shown in a partial view in Fig. 1.6a drawn at exaggerated scale. Overturning moments cause axial forces in columns. These forces, coupled with lateral shear and relative axial movement of columns, cause reversed curvature moments in beams and columns. In addition to resisting these forces, the framed tube or rigid frame is required to furnish adequate stiffness to limit the lateral drift, perception to lateral motion, and $P-\Delta$ effects due to gravity loads. Lateral stiffness is comprised of axial stiffness of columns, flexural stiffness of beams and columns, and joint rigidity.

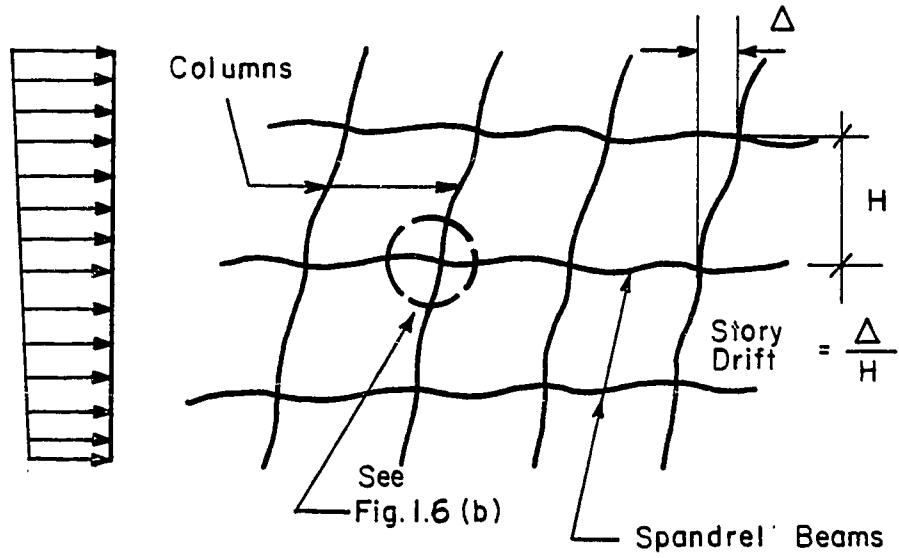


Fig. 1.6(a) Behavior of framed tube under lateral loads.

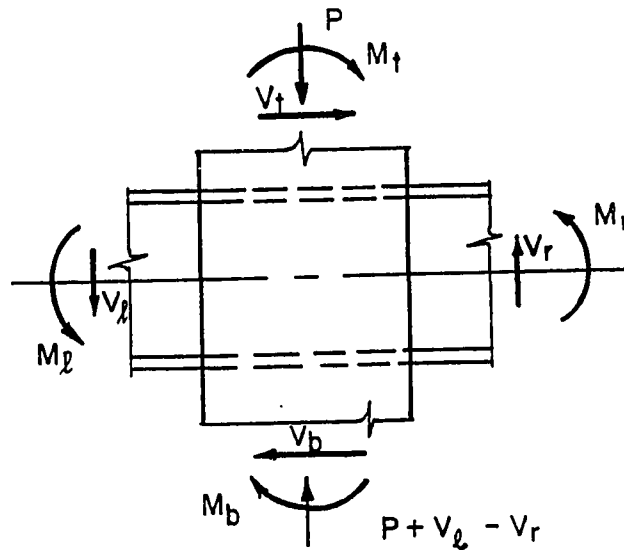


Fig. 1.6(b) Forces on the joint.

Under lateral loads, a typical joint is subjected to the forces from the adjoining members as shown in Fig. 1.6b. A moment connection between steel beam and concrete column should be designed to resist these forces and provide adequate rigidity.

1.4 Possible Connection Details

As described in the last section, moment connection between a steel beam and concrete column must provide enough strength to resist the forces from the adjoining members and ensure adequate stiffness to limit total joint distortion. Designing for strength involves, a) the transfer of steel beam flange forces (shown as T_1 , C_1 , T_r and C_r in Fig. 1.7) to the joint or connection panel; b) the resistance of high shear forces generated in the connection panel (shown as V_h in Fig. 1.7); and c) the transfer of the column axial load through the joint. The term "joint" or "connection panel" refers to the concrete and structural steel within the depth of the beam bounded by the column faces, as indicated in Fig. 1.7. The structural steel and concrete are called "steel panel" and "concrete panel", respectively. It is clear that most attention should be directed to transferring flange forces to the connection panel, since the joint should have substantial strength to resist shear as well as axial load, if mobilized. If needed, the steel panel can be strengthened with doubler plates. A review of concrete joints and steel joints is given in Appendix A.

Several means of transferring stress from the steel flanges to the connection panel are possible. However, bond forces may not be relied upon as they are small in magnitude and vary substantially under different steel surface conditions. Also, as the load is increased, the bond is likely to break and it is not

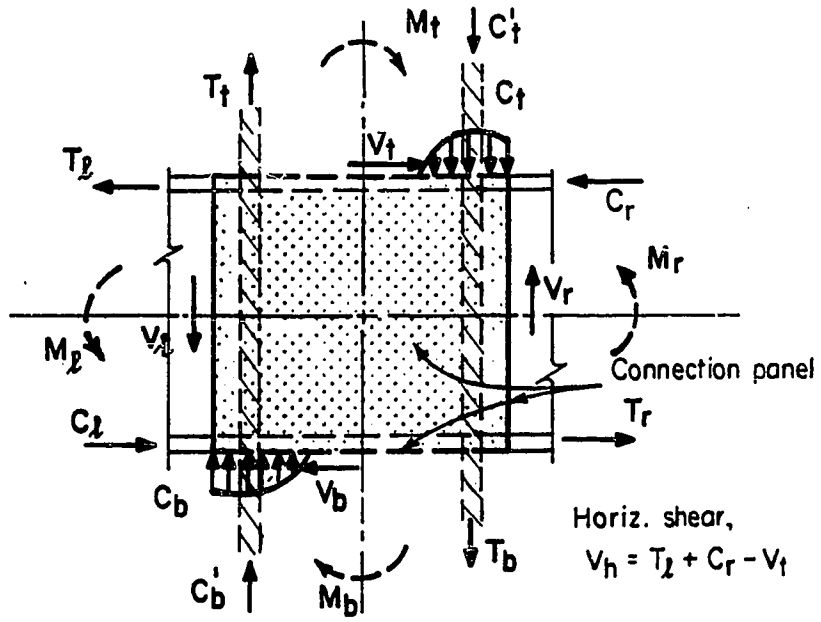


Fig. 1.7 Forces on the connection panel.

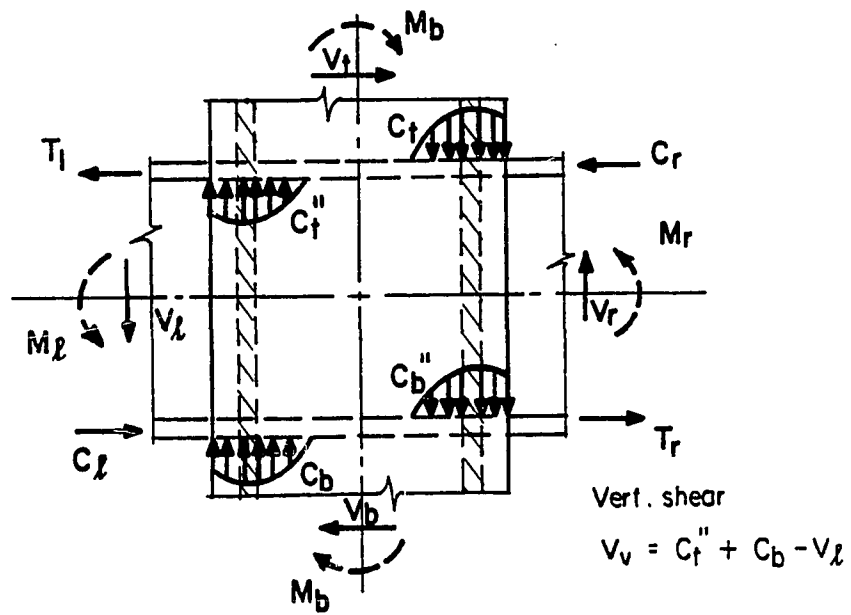


Fig. 1.8 Lever arm mechanism.

recoverable. Therefore, the bond forces are ignored. Five methods of flange stress transfer are shown in Fig. 1.9 and are described below.

Beam Embedment. If a steel beam is embedded in the concrete column without any attachments, the flange forces would be transferred to the steel panel by forming four reaction or compression blocks, C_t , C_t'' , C_b , and C_b'' as shown in Fig 1.8. This mechanism of stress transfer is called a "Lever Arm Mechanism." It should be noted that in this mechanism only the steel panel is mobilized and no flange force is transferred to the concrete panel. The vertical shear force in the steel panel at the column centerline, as shown in Fig. 1.8, is

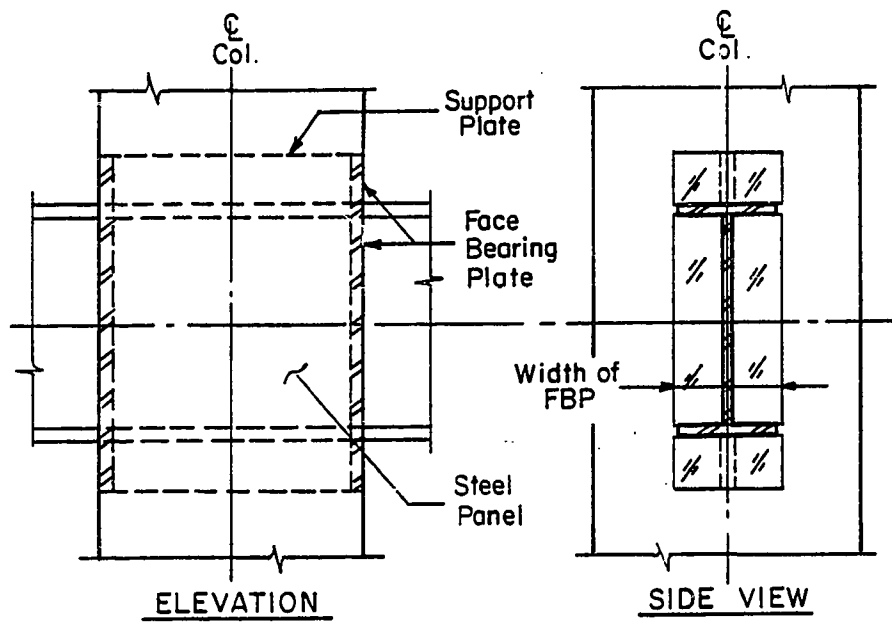
$$V_v = C_t'' + C_b - V_\ell \quad (1.1)$$

Complementary horizontal shear is equal to,

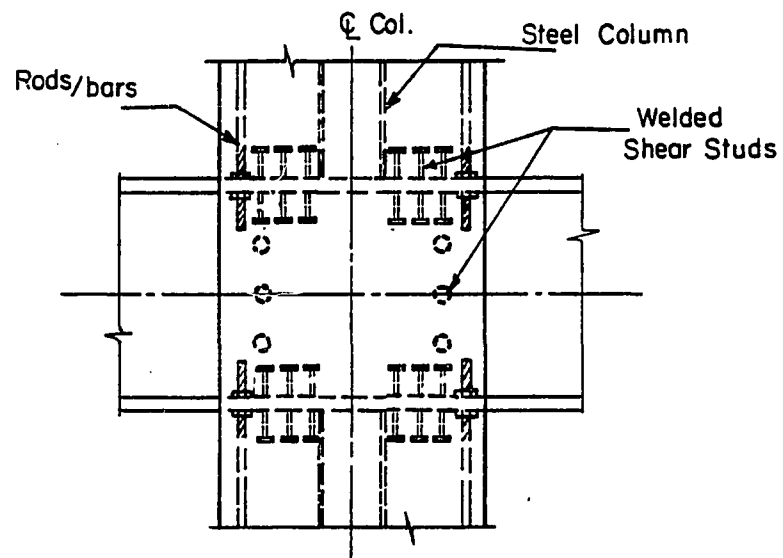
$$V_h = T_\ell + C_r - V_t \quad (1.2)$$

The maximum shear force is limited by the steel panel strength.

Face Bearing Plates. Flange forces may be transferred to the concrete panel through the use of face bearing plates (FBP), shown in Fig. 1.9a. These plates may be placed between the flanges only at each side of the web and welded all around in which case they will look like ordinary web stiffeners. Bearing plates may also be extended above and below the beam in which case they may require support plates as shown in Fig. 1.9a. The face bearing plates would be welded to the beam before the column is cast. As such, these plates would eliminate the need for formwork between flanges. The face bearing plates could be equal in width or wider than the beam flange.



a) Face bearing plates and steel panel.



b) Other methods.

Fig. 1.9 Means of stress transfer from steel beam to concrete column.

Steel Column. A small steel column (Fig. 1.9b) required for the erection of steel framing, may improve the transfer of flange forces to the concrete panel or may reduce the joint distortion. The erection column may be welded directly to the beam flanges or it may be field-bolted if a column base plate is used. If, for ease of steel erection, the column must be continuous, it can be offset from the beam centerline.

Shear Studs. Headed shear studs could be welded on the outside and/or inside faces of the flanges to transfer the flange forces to the concrete panel. Shear studs may also be welded on each side of the web panel as shown in Fig. 1.9b to hold the steel and concrete panels together. Shear studs might reduce the joint distortion and in addition might increase the strength of the connection.

Rods or Bars. As shown in Fig. 1.9b, threaded rods or reinforcing bars may be fastened to the beam flanges near the column faces. Alternatively reinforcing bars could be welded directly to the flanges or through pieces of steel angles pre-welded to the flanges. These rods/bars might improve the efficiency of the "lever arm mechanism" or enhance the rigidity of the connection.

1.5 Scope and Objectives

After identifying various connection details it is clear that in order to understand and evaluate fully the moment connection between steel beams and concrete columns, a large number of parameters need to be investigated for their influence, both qualitatively and quantitatively. The parameters include: thickness and width of the flanges of the steel beam; thickness of steel panel and its aspect ratio, i.e. ratio of column depth, D_c , to beam depth, D_b ; thickness, width, and configuration of

face bearing plates; size and orientation of steel erection column; size, spacing and location of shear studs; size and quantity of rods/bars; etc. In addition, the influence of column axial load, concrete strength, reinforcement details inside and adjacent to the joint, and type of loading need to be investigated.

The effect of steel beam web thickness; and thickness, width, and configuration of face bearing plates on the performance of steel beam-to-concrete column moment connections were studied in this dissertation. Nine tests were conducted to study these parameters experimentally. Past research and practice in related areas, as well as all concrete and all steel connections, were reviewed. Based on this review, as well as the observed behavior of the test specimens, the influence of axial load on columns, concrete strength, and reinforcement details inside and near the joint, are conservatively assessed. A design approach is developed in which both strength and stiffness requirements of the connections are considered.

In current practice, mixed systems are used primarily when wind forces govern the design. In this study, the performance of moment connections between steel beams and concrete columns under monotonic loading is of primary concern. Mixed systems, especially those combining steel beams with concrete columns or walls for the lateral load resisting subsystem, however, possess a great potential for seismic resistance when the connections are detailed adequately.

The scope of this study is limited to interior beam-column connections and the objectives are:

1. To investigate experimentally the behavior of moment connections between concrete columns and steel beams

with and without face bearing plates, primarily under monotonic lateral loads.

2. To assess, from past research and practice, the influence of secondary factors on the performance of such connections.
3. To develop a design model and formulate recommendations for the design of moment connections between steel beams and concrete columns.

Before describing the test series, a brief review of the past research and practice related to composite joints is presented in Chapter 2. The behavior of reinforced concrete beam-column joints and structural steel rigid connections and their design guidelines are summarized in Appendix A. The test series is described in chapter 3 and its results presented in chapter 4. Joint strength is evaluated in chapter 5 and a design model is proposed in chapter 6. Conclusions and design recommendations are summarized in chapter 7.

CHAPTER TWO

REVIEW OF PAST RESEARCH AND PRACTICES

2.1 Developments in the United States

There has not been any research reported in the United States at this time for moment connections between steel beams and reinforced concrete columns, as such. Some work on the behavior of embedded steel sections used as brackets, which might be relevant to this study, is presented here.

The Prestressed Concrete Institute (PCI) Committee on Connection Details [40, 41] presented design equations for the strength of structural steel sections embedded in reinforced concrete columns/walls to serve as brackets. These equations were based on conservative simplifying assumptions related to the forces shown in Fig. 2.1a. The concrete compression stress block was assumed to have a depth of $l_e/3$ and a width equal to beam width, b . The ultimate concrete bearing capacity, V_c , is given as Eq. 2.1a in Ref. 41 and as Eq. 2.1b in Ref. 40.

$$V_c = \frac{0.85 f'_c b l_e}{3 + 4 e/l_e} \quad (2.1a)$$

$$V_c = \frac{0.85 f'_c b l_e}{3.67 + 4 a/l_e} \quad (2.1b)$$

The two equations are similar in form except that the shear span, a or e , is defined differently.

The additional capacity of the bracket due to reinforcement welded to the structural steel section as shown in

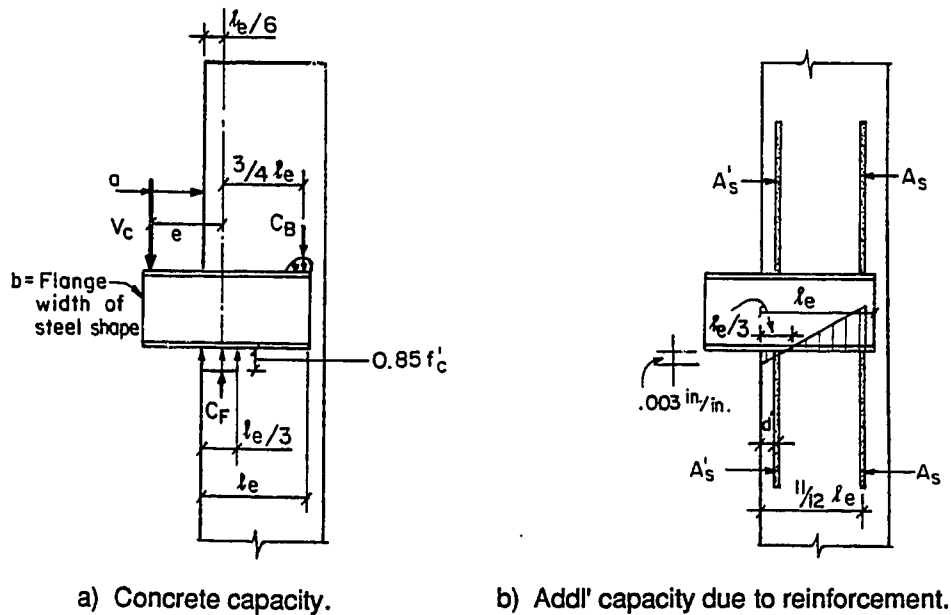


Fig. 2.1 Resistance of embedded bracket at ultimate (Ref. 44).

Fig. 2.1b is given by Eqs. 2.2a and 2.2b in Refs. 41 and 40, respectively.

$$V_r = \frac{3A'_s f'_s}{3 + 4 e/l_e} \quad (2.2a)$$

$$V_r = \frac{3A'_s f'_s}{3.67 + 4 a/l_e} \quad (2.2b)$$

where $f'_s = 87000 (1 - 3 d'/l_e) \leq f_y$ and f_y = specified yield strength of the welded bars. The sum of Eqs. 2.1 and 2.2 give the combined capacity, V_u . The reinforcement, A_s , if required, is calculated as:

$$A_s = 1/f_y [.85 f'_c b l_e/3 + A'_s f'_s - V_u] \quad (2.3)$$

Rath [44] examined the philosophy behind the PCI recommendations [40, 41] for the design of embedded steel sections used as bracket. The concept was believed to be conservative but adequate in the absence of research data. He also noted that holes (greater than 1 in. diameter) drilled through the web of the embedded wide flange section can ensure good concrete consolidation between flanges. Also, headed studs welded to the web should ensure bearing confinement of the concrete between the flanges as well as distribute bearing stresses over a width greater than the width, b , of the steel section.

Mattock and Gaafar [31] studied the behavior of embedded steel sections as brackets both analytically and experimentally. A total of five tests were conducted using 16-in. long steel sections which were embedded in one face of a 12 X 10 in. cross section reinforced concrete column. A typical test specimen is shown in Fig. 2.2. Rectangular steel sections of varying widths, I-sections with thick flanges, and a W4 section were used as brackets. The load was applied at a distance 4 to 6 in. from the face of the column. Concrete compressive bearing strains were recorded using strain gages, mounted on small mortar blocks which were epoxied to the steel section before placement in the forms. The gages were lost at ultimate load, however, the estimated strain for the W4 section was 0.012 under the web. The strain below the edge of the bottom flange was negligible until near the ultimate load when it increased to a maximum of about 0.005. This increase was attributed to a diagonal-strut action occurring in the concrete between the bottom flange and the faces of the

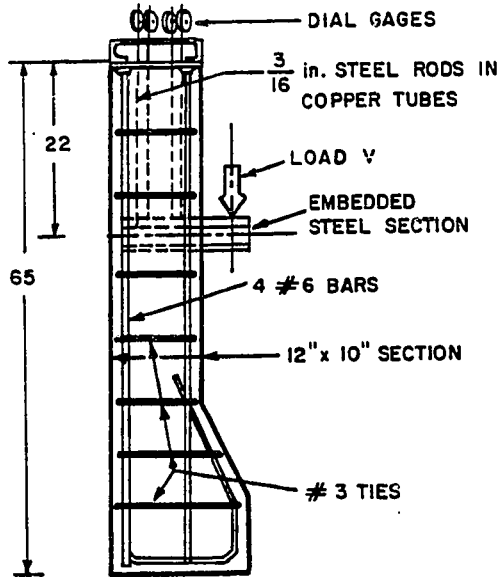


Fig. 2.2 Typical test specimen used by Mattock and Gaafar (Ref. 31).

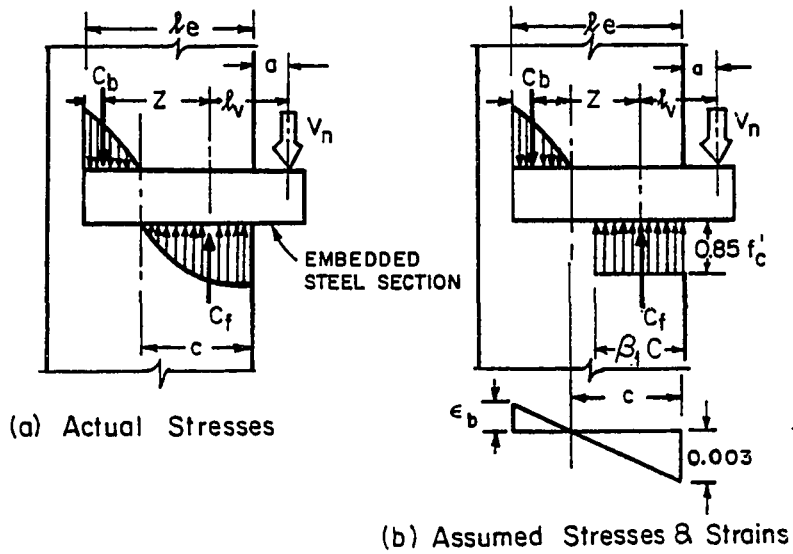


Fig. 2.3 Actual and assumed stresses and strains in concrete adjacent to embedded steel section (Ref. 31).

web of the W-section. The upper flange was not stiffened externally and thus resisted a very small bearing stress. The length of the compression zone, c , as shown in Fig. 2.3 was approximately 70% of the embedded length, l_e , for all five tests. The sum of the bearing stresses under the top and bottom flanges of the W4 section was approximately the same as that on the bottom of the solid rectangular section of the same width. The bearing stress, however, increased as the ratio of the width of the section, b , to the width of the column, b_c , decreased. The authors found the bearing stress, f_b , was

$$f_b = 0.85(b_c/b)^{0.66} f'_c \quad (2.4)$$

Other authors (21, 28, 60) found that concrete bearing strength under strip loading was proportional to the concrete tensile strength, f_{ct} , i.e. $\sqrt{f'_c}$, rather than the compressive strength, f'_c . Hence Mattock and Gaafar proposed that the bearing strength under the embedded section be calculated as:

$$f_b = 54 \sqrt{f'_c} (b_c/b)^{0.66} \quad (2.5)$$

Based on this relationship for f_b and keeping $c/l_e = 0.666$ and $\beta_1 = 0.80$, Mattock and Gaafar proposed the following formula for the design of the embedded bracket:

$$V_c = \frac{21 b l_e \sqrt{b_c/b} \sqrt{f'_c}}{(0.88 + a/l_e)} \quad (2.6)$$

Hawkins and Roeder [19] investigated the connections of steel beams to concrete columns through an embedded steel plate with headed shear studs. A total of 22 tests were conducted. These tests represent connections in which only a small moment is transferred and the shear transfer dominates. A typical test specimen is shown in Fig. 2.4. Shear spans, e , of only 3 in. to 12 in. were investigated. The loading simulated balanced gravity load moments i.e. the columns as well as joint panel were subjected to no shear or moment. The failure was due to yielding of the studs or pull-out from the concrete.

2.2 Research in Japan

A structural system consisting of structural steel members encased in reinforced concrete has been widely used in Japan since 1920 for the construction of medium to high-rise buildings. This structural system called, the Steel Reinforced Concrete (SRC) structural system, has gained popularity after buildings with this system performed better in the 1923 Kanto Earthquake. A typical subassembly of this system is shown in Fig. 2.5. The structural steel and reinforced concrete elements are typically proportioned so that there is a minimum stress transfer from one material to the other. The strength of the members, as well as the connections, are estimated using the method of superposition. In accordance with this philosophy, the Architectural Institute of Japan (AIJ), which is the specification writing body in Japan for steel, concrete, and composite structures, has required since 1958 that the ratio of the capacities of the structural steel elements in columns and beams should be between 0.5 and 2.0. That is:

$$0.5 \leq M_{sc}^u / M_{sb}^u \leq 2.0 \quad (2.7)$$

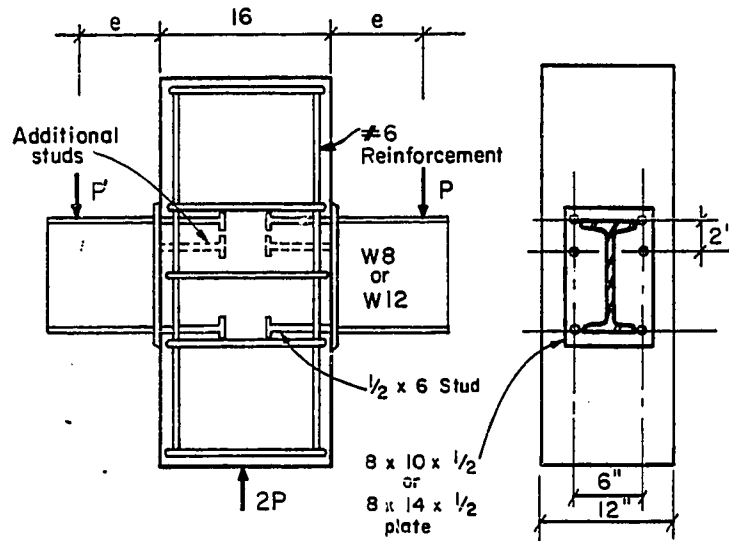


Fig. 2.4 Typical specimen used by Hawkins and Roeder (Ref. 19).

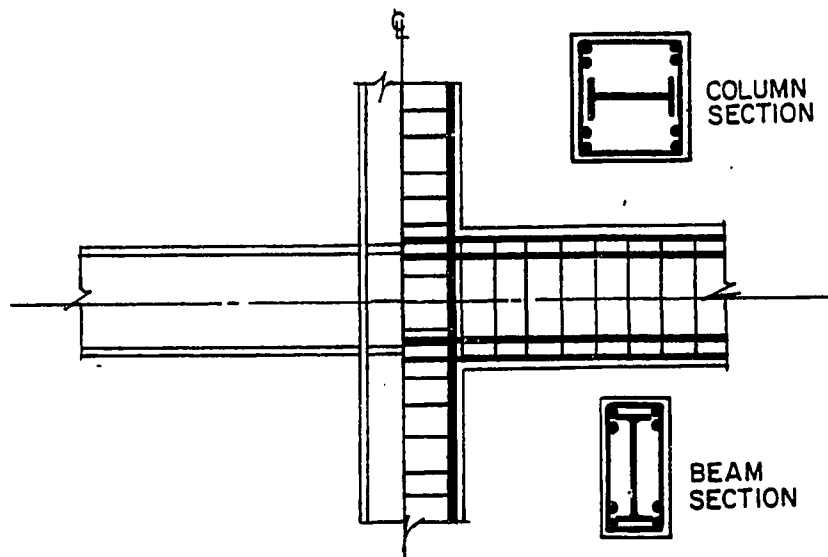


Fig. 2.5 Typical SRC assemblage (Ref. 10).

where M_{sc}^u and M_{sb}^u denote the flexural capacities of the steel part of columns and beams, respectively.

In the last decade or so there has been a natural shift towards using steel beams with SRC columns. This is generally termed a "Steel-SRC Mixed Structural System" or "Mixed System" and is especially popular for the prefabricated construction of buildings.

A large amount of research has been carried out in Japan to study beam-column joints for both SRC structures and Steel-SRC mixed structures. Unfortunately most of this data is not widely known because it has not been translated into English. Also, much of this research has been carried out by private construction companies and is not reported in the technical literature. A brief review of the available research is presented in the following.

In the period of 1950 to 1960, a number of research programs were carried out to study the behavior of SRC members and connections under various loadings. The findings of a few of these research programs are summarized by Wakabayashi in Ref. [51]. These studies were mainly conducted on composite structures consisting of fabricated open-web steel sections, connected with rivets and gusset plates and encased in a monolithically cast reinforced concrete structure. Shear failure of the connection panel was not recognized. Emphasis was placed on the gusset plate and other steel connection details. These research programs concluded that the strength of such connections can be estimated as the summation of the individual strength of the steel section and that of the ordinary reinforced concrete section.

In the period of 1960 to 1970 after rolling of wide-flange sections started in Japan, research on SRC members of full-web

type started. These research programs also concluded that the shear strength of the SRC connection panel can be estimated by summing up the strengths of steel and concrete panels within the depths of the steel beam and column. Wakabayashi, et al [62] proposed the following semi-empirical formula for the shear strength of connection panels such as shown in Fig. 2.6.

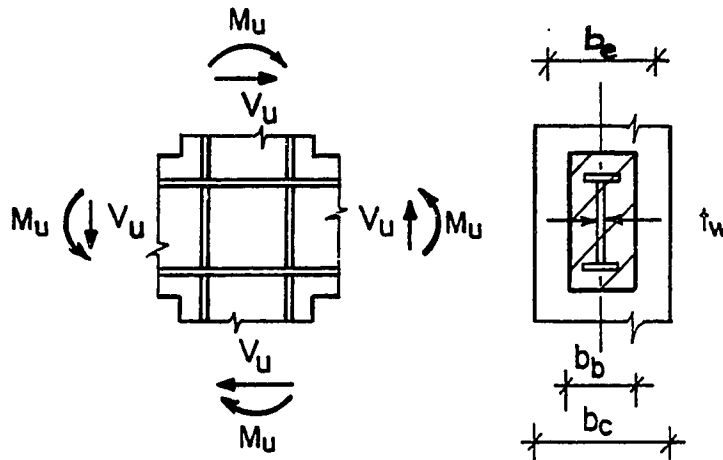


Fig. 2.6 SRC beam-to-column connection.

$$\frac{2M_u}{d_b'} - V_u = \frac{F_{yp}}{\sqrt{3}} t_{sp} d_c' + v f_c b_e d_c' \quad (2.8)$$

where t_{sp} = web thickness of steel connection panel,
 F_{yp} = yield stress of the web,
 b_e = effective width of concrete panel = $\frac{b_b + b_c}{2}$
 d_b' = c/c distance of flanges of beam,
 d_c' = c/c distance of flanges of column
 v = ratio of shear strength of concrete to f_c ,
 empirically given by

$$v = 1.08 - 0.0024 f_c \text{ (kg/cm}^2\text{)} \quad (2.9)$$

or may be safely assumed as

$$v = 0.56 \text{ for } f_c < 300 \text{ kg/cm}^2 \quad (2.10)$$

Most tests until 1970 were carried under monotonic loads or under a small number of cyclic loads. In the years after 1970 research interest was focused on hysteretic response of connections. Tests were also reported on Steel-SRC mixed connections. These tests were not conducted just to establish design standards for Steel-SRC mixed construction, but more importantly, to understand the stress transfer mechanism from steel to concrete, both in SRC construction and mixed construction. Aoyama et al. [10] carried out tests on two full size SRC connections. The structural steel portion of the members was substantial and was nearly identical for the beams and columns. They found that the joint shear is resisted not only by the concrete within the depth of the steel beam and column but by the entire concrete panel. They proposed the

following equation to estimate the joint shear strength:

$$2M_{bo} = \frac{(F_{yp}/\sqrt{3})\hat{V}_{sp}}{(1 - \frac{d'_c}{L} - \frac{d'_b}{H})} + \frac{(v_c + \rho_w f_{yw})\hat{V}_{cp}}{(1 - \frac{j_c}{L} - \frac{j_b}{H})} \quad (2.11)$$

where M_{bo} = beam moment at column center line.

d'_c, d'_b = distance between flanges of column and beam, respectively.

j_c, j_b = distance between centroids of tension reinforcement and compression stress block of column and beam, respectively.

L, H = beam span and floor height

ρ_w = web reinforcement ratio in the panel zone

\hat{V}_{sp} = volume of steel panel = $t_{sp} \cdot d'_c \cdot d'_b$

\hat{V}_{cp} = effective volume of concrete panel = $b_e \cdot j_b \cdot j_c$

b_e = average width of column and beam.

v_c = ultimate shear stress of concrete as in Eq. 2.12.

$$\begin{aligned} v_c &= (0.65 - 0.0014 f_c) f_c \quad \text{for } f_c < 232 \text{ kg/cm}^2 \\ &= 75.4 \text{ kg/cm}^2 \quad \text{for } f_c > 232 \text{ kg/cm}^2 \end{aligned} \quad (2.12)$$

Wakabayashi et al. [59] tested five 1/2 scale, cruciform shape specimens of steel beams and SRC columns to determine the shear strength of the connection. The size and strength of the steel part of the column was varied. The ratio of the flexural

strengths of steel column to RC column were 0.8, 0.4 and 0. They concluded that the shear in the connection is resisted by the steel panel and the concrete within the depth of the steel beam and column, and can be estimated by Eq. 2.8. However, they found the value of v to be 0.645 (concrete strength, $f_c = 300-350 \text{ kg/cm}^2$). For specimens with no steel column, the shear strength of the connection panel was found to be much lower. The authors attributed this reduction in strength to bond failure of main column reinforcing bars passing through the connection panel.

Naka et al. [36] also conducted tests on four, 1/3 scale Steel-SRC interior joints. Thickness of the steel panel and the size of the steel column were varied. The ratio of the flexural strength of steel column to steel beam was varied from 0.35 and 0.85. They also concluded that the shear strength of the connection panel can be estimated by Eq. 2.8, with b_e , the effective width of concrete panel, equal to $b_c/2$, i.e. half the column width. They found the shear strength ratio, v , to be more than 0.30.

Fujimoto et al. [16] investigated the behavior of connections in Steel-SRC system, with changing ratio of flexural strength of steel column to the total strength of the SRC column. They concluded that specimens with a ratio over 50% show good hysteretic performance.

Minami [34] and Wakabayashi et al. [58] reported tests on eight, 1/3 scale Steel-SRC exterior connections. Four specimens were tested with column axial load and four without axial load. The ratio of the flexural strength of the steel column to that of the SRC column varied from 0 to 1.0. Results showed no significant effect of axial load. As in Eq. 2.7, a minimum value of 0.50 was recommended for the ratio of the flexural capacity of the steel parts of the columns to that of the beams. The authors

presented a stress transfer mechanism called the "Lever Mechanism", shown in Fig. 2.7. Based on this mechanism and using a value of $2f_c$ for the stress in concrete bearing against a steel beam flange, the authors derived complicated formulae for predicting the ultimate strength of the assembly. These formulae need to be verified by more tests since most of the tests failed by flexural yielding of the beams.

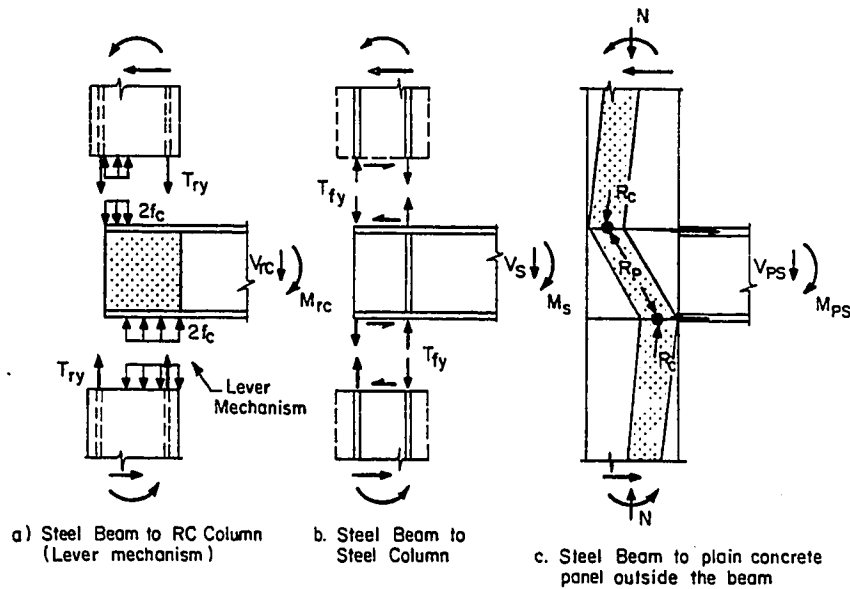


Fig. 2.7 Stress transferring mechanism in exterior joint (Ref. 34).

Kato et al [25] investigated the strength of Steel-SRC joints in which the steel beam flanges were connected to steel columns by high strength bolts using T-stubs. A total of six specimens were tested with the depth of concrete cover and the diameter of ties as variables. The effect of tie diameter was found to be insignificant. Maximum strength of the connections

was controlled by fracture of high strength bolts in tension. When the strong axis of the steel column was oriented in the plane of the joint, the depth of concrete cover had no influence on the maximum strength. On the contrary, the depth of cover had considerable influence when the column was oriented with its weak axis in the plane of the specimen. The authors derived formulas for estimating the strength of such connections which were based on yield line mechanisms for the flanges and web of the column near the bolted connections.

Tanaka et al. [50] studied the Steel-SRC connections with face bearing plates welded to the steel beams. Six, 1/2-scale, cruciform shape specimens with the weak axis of steel column in the bending plane, were tested under cyclic loads. Axial load was applied to three specimens. The ratio of the strength of steel column to that of SRC column was varied from 0.1 to 0.50. The authors found that only the concrete confined by the steel flanges and the steel face bearing plates is effective in resisting joint shear. Axial load had no significant effect. The size of the steel column had a considerable effect on the behavior and the authors recommended that the steel column develop at least 50% of the total SRC column strength.

Shimizu et al. [49] tested eight 1/2 scale specimens of steel beam-reinforced concrete column connections. All specimens had steel face bearing plates welded to the beams. In addition, the beams had reinforcing bars welded to the flanges to create a rough flange surface. Unfortunately the columns failed before the joint panels could reach capacity. Hence no conclusions could be drawn about the face bearing plates as well as the deformed flange surface of the beams.

Building structures in Japan are designed in accordance with standards published by Architectural Institute of Japan

(AIJ). These standards for SRC connections have been regularly revised. Wakabayashi has discussed the design formulas [52, 53, 54, 55, 56, 57]. The 1958 edition of AIJ standard gave no recommendations for the shear design of SRC connections. In the commentary of the 1963 edition, a design formula for the shear panel was presented which neglected the concrete panel. The commentary of the 1975 AIJ standard contained a method with formulas for design of the connection panel, which were based on the allowable stress design method. The 1985 edition contained additional formula for the ultimate shear strength of the connection panel. These formulae are discussed in Ref. 57.

It is apparent from the review of the Japanese research that the ultimate strength of the SRC connections, proportioned using Eq. 2.7, can be estimated conservatively. However, the behavior of steel-SRC mixed connections, especially with small steel column sections, is still not understood. As stated by Lu [29] and Wakabayashi [55], intensive research is urgently needed on (a) the mechanism of stress transfer from steel section to concrete at beam-to-column connections, and (b) methods for improving the anchorage capacity of the connecting elements.

2.3 Research in Australia

There has been some research in Australia for connections of wide flange structural steel beams (composite with slab) and wide flange structural steel columns encased in plain concrete.

Ansourian [8, 9] tested subassemblages of both exterior and interior connections. Fourteen structural subunits were tested to investigate connection shear. Comparison of the composite structure with bare steel joints showed the connection shear force for initial yielding almost doubled and the post-yielding stiffness was raised by a factor of six. Collapse of

most of the specimens occurred by plastic buckling of the beam and so the true ultimate strength in shear was not determined.

Analysis of the test results revealed three apparent regimes of connection zone behavior. In the first regime the column was uncracked and both steel and concrete were elastic. The entire column section was effective in resisting shear. The author commented that if the column and beam widths differ significantly, the average of the two widths perhaps should be considered for the concrete resisting shear. In the second regime the concrete in the column was cracked and only the steel web resisted joint shear. Yielding of the web marked the end of the second regime. A third regime existed in which the stiffness was provided only by strain hardening of the web and the elastic column flanges stiffened by the concrete cover over these flanges.

CHAPTER 3 EXPERIMENTAL PROGRAM

In the experimental study interior connections in plane frames were subjected to monotonic lateral loads. No axial load was imposed on columns. The prime variables were the thickness, width and configuration of face bearing plate and the thickness of steel panel.

3.1 Test Series Description

The test series consisted of a total of nine (9) tests (summarized in Table 3.1) in two groups. The first group included specimens 1 and 2, which were designed as pilot tests to establish the potential of the face bearing plates (FBP). The results of the pilot tests were used to design the remaining tests.

In a typical framed tube design, the depth of the prototype concrete columns, D_c , varies from 33 to 45 in. The beam depth, D_b , varies from 30 to 42 in. In ordinary frames, the column depth is anywhere from 24 to 36 in., and the beam depth 21 to 33 in. The aspect ratio of the connections, i.e. the ratio of column depth, D_c , to the beam depth, D_b , vary from 0.8 to 1.30. A ratio around 1.0 or slightly larger, is more likely for the framed tube and frames consisting of concrete columns and steel beams.

Pilot tests were intended to represent the prototype framed tube connections at 1/3 to 1/2 scale. A 15-in. square section for the column and a 12-in. deep W12x22 rolled steel section for the beams were used in specimens 1 and 2. The aspect ratio was 1.25. Tests 1 and 2 model an ordinary frame at 1/2 to

Table 3.1 Summary of Test Series

Specimen No.	Symbol	Column Depth D_c (in.)	Beam Depth D_b (in.)	Panel Thickness t_{sp} (in.)	Face Bearing Plate $t_p \times w_p \times d_p$	Purpose
1		15	12	1/4 (Gr. 50)	—	Plain beam
2		15	12	1/4 (Gr. 50)	7/16x4x11-1/2	FBP
3		20	17-1/2	1/4	—	Plain beam
4		20	17-1/2	1/4	3/8x8x16	Thin FBP
5		20	17-1/2	1/4	7/8x8x16 (Gr. 50)	Thick FBP
6		20	17-1/2	1-1/4 (Gr. 50)	3/8x8x16 w/styrofoam	Thick panel
7		20	17-1/2	1/4	7/8x12x16 (Gr. 50)	Wide FBP
8		20	17-1/2	1/4	7/8x25-1/2 (Gr. 50)	Extended FBP
9		20	17-1/2	—	7/8x8x16	No panel

NOTE: All material A-36 U.N.O.

MEMBER SIZES					
C O L U M N					
Specimen No.	Size (in. x in.)	f'_c psi	Reinforcement Vert	Ties	Beam Size
1 - 2	15 x 15	3500	8 - #9	#3 @ 4"	W12 x 22 (Gr. 50)
3 - 9	20 x 20	3500- 4500	12 - #10	#4 @ 8" #3 @ 8"	Built-up 3/4x8" Flg., Gr. 50 1/4x16" WEB, A-36

NOTE: For joint reinforcement see Figs. 3.8 and 3.9

2/3 scale. In specimen 1, a plain beam was embedded in the concrete column. No means were provided for the transfer of flange forces to the concrete panel. For specimen 2, Grade 50 face bearing plates of thickness, $t_p = 7/16$ -in., were welded to the beam in order to mobilize the concrete in the panel for improved joint shear resistance. The total width of the face bearing plates, w_p , was 4 in., i.e. equal to the flange width of the beam. The main features of specimens 1 and 2 are summarized in Table 3.1. In order to compare directly the results of the two specimens the geometry and reinforcement were identical except for the FBP.

Additional seven (7) tests were planned to evaluate the main parameters of the study. The member sizes were 1/2 to 2/3 scale for framed tube and 2/3 to full scale for ordinary frames. A 20-in. square section for columns and a 17-1/2-in. deep built-up section for beams were used, producing an aspect ratio of 1.14. These seven tests are listed as specimens 3 through 9 in Table 3.1. The hybrid beam section was proportioned with a weak web and relatively strong flanges. The web, made from A36 steel, was needed to furnish a greater difference in shear resistance between the steel and concrete panels. Grade 50 flanges were proportioned so that they were not excessively thick while at the same time providing adequate moment capacity to ensure connection failure.

Specimen 3 was similar to specimen 1, that is, a plain beam embedded in the column. It served as a reference specimen for specimens 4, 5 and 6. Specimens 4 and 5 were designed to study the effect of a face bearing plate and its thickness. A thin FBP ($t_p = 3/8$ -in.) was used in specimen 4 and a thick one ($t_p = 7/8$ -in.) in specimen 5. The width, w_p , was 8 in., equal to the flange width. All the other details were kept identical to

specimen 3 for better comparison. Test specimen 5 was a reference test for specimens 4, 7, 8 and 9.

A connection with a beam embedded in the concrete column resists the joint forces by a lever arm mechanism, as described in Chapter 1. The failure of such connections is controlled by either the shear capacity of the steel panel or concrete crushing against the compression flanges near the column faces. Specimen 6 was provided with a strong steel panel to find an upper bound on the lever arm mechanism. For this purpose a 1/2-in. thick doubler plate was welded on each side of the web in the joint zone. Face bearing plates, 3/8-in. thick, were also used to simulate the most realistic condition regarding the flange stiffness under concrete bearing. However, to isolate any transfer of flange forces through the FBPs to the concrete panel, a 3/8-in. thick styrofoam layer was placed on the inside of the FBPs before casting the specimens. The remaining details for specimen 6 were similar to those for specimen 3.

To study the effect of the width of the face bearing plates, specimen 7 was provided with 12-in. wide plates. Specimen 8 was designed to study the influence of the configuration of face bearing plates. The plates were extended 4 in. beyond the flanges, thereby giving a total depth of 25-1/2 in. for these FBPs. Support plates, 7/8-in. thick, were used on these plate extensions so that the extension had about the same stiffness as the plates between the flanges. The support plates were placed outside the column in order to have the same steel panel as the other tests. The remaining details for both specimens 7 and 8 were identical to specimen 5.

In order to clarify the influence of the steel panel on the extent to which the concrete panel can be mobilized for joint shear resistance, a 11-1/2 x 13 in. hole was cut into the steel

panel in specimen 9. The remaining details for this specimen were identical to specimen 5.

3.2 Specimen Design and Details

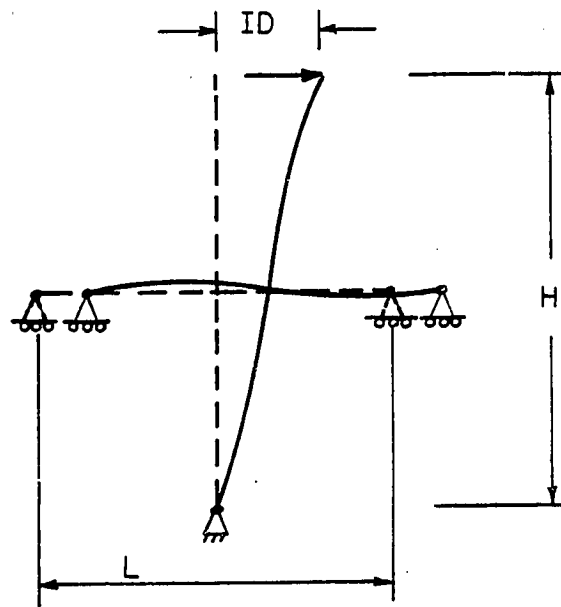
A beam-column assembly between the points of inflection of a frame subjected to lateral loads can be idealized as shown in Fig. 3.1(a). The displacement at the column top due to the lateral load, is equal to the inter-story displacement, ID . The same member and joint deformations can be achieved by modeling the beam-column assemblage as shown in Fig. 3.1(b) and loading the beam ends. The displacement at the beam ends, $\Delta/2$, is related to the interstory drift as follows:

$$\Delta = ID \times L/H \quad (3.1)$$

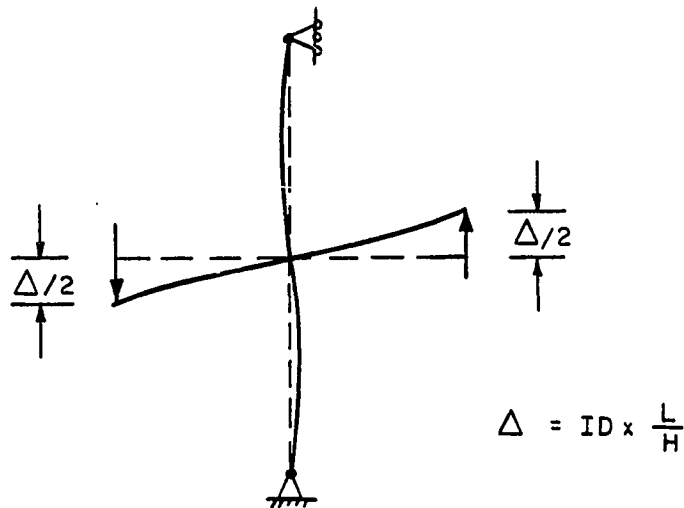
The test specimens were loaded as shown in Fig. 3.1(b) for convenience. No axial load was placed on the columns.

Dimensions of the specimen used in the pilot tests is shown in Fig. 3.2. The 15-in. square concrete column was 8 ft-10 in. high between reaction points. The W12 structural steel beam was 8 ft. between the load points. The dimensions of specimens 3 through 9 are shown in Fig. 3.3. The height of the 20-in. square concrete column was 12 ft-2 in. between the reaction points. The total beam length between the loading points was 16 ft. In order to reduce material costs, only a 6 ft-6 in. length of the 17-1/2 in. deep built-up steel beam was cast with the concrete column. Extension beams were spliced to each end of the built-up beam for loading purposes.

The specimens were designed to fail in the connection. Both columns and beams were adequately proportioned and reinforced to preclude any immature shear or flexural failure.



a) Idealized frame behavior.



b) Modelling for test specimen.

Fig. 3.1 Modelling of beam-column subassembly.

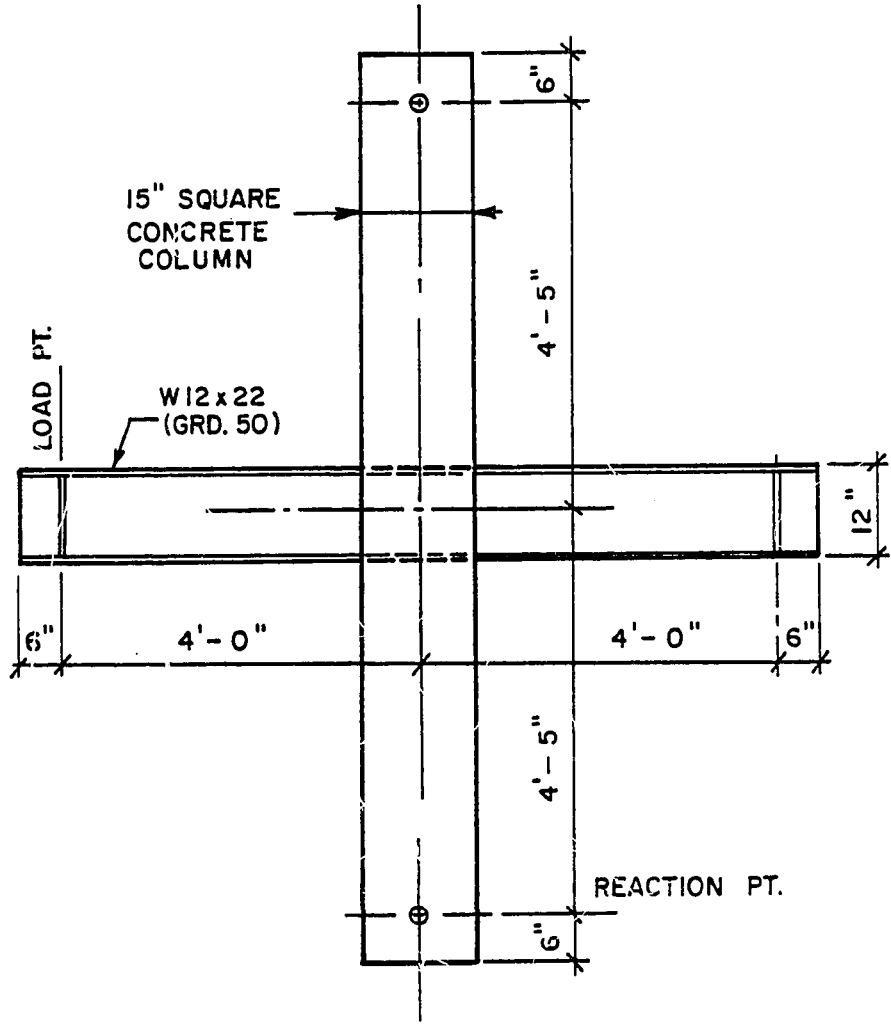


Fig. 3.2 Test specimens 1 and 2.

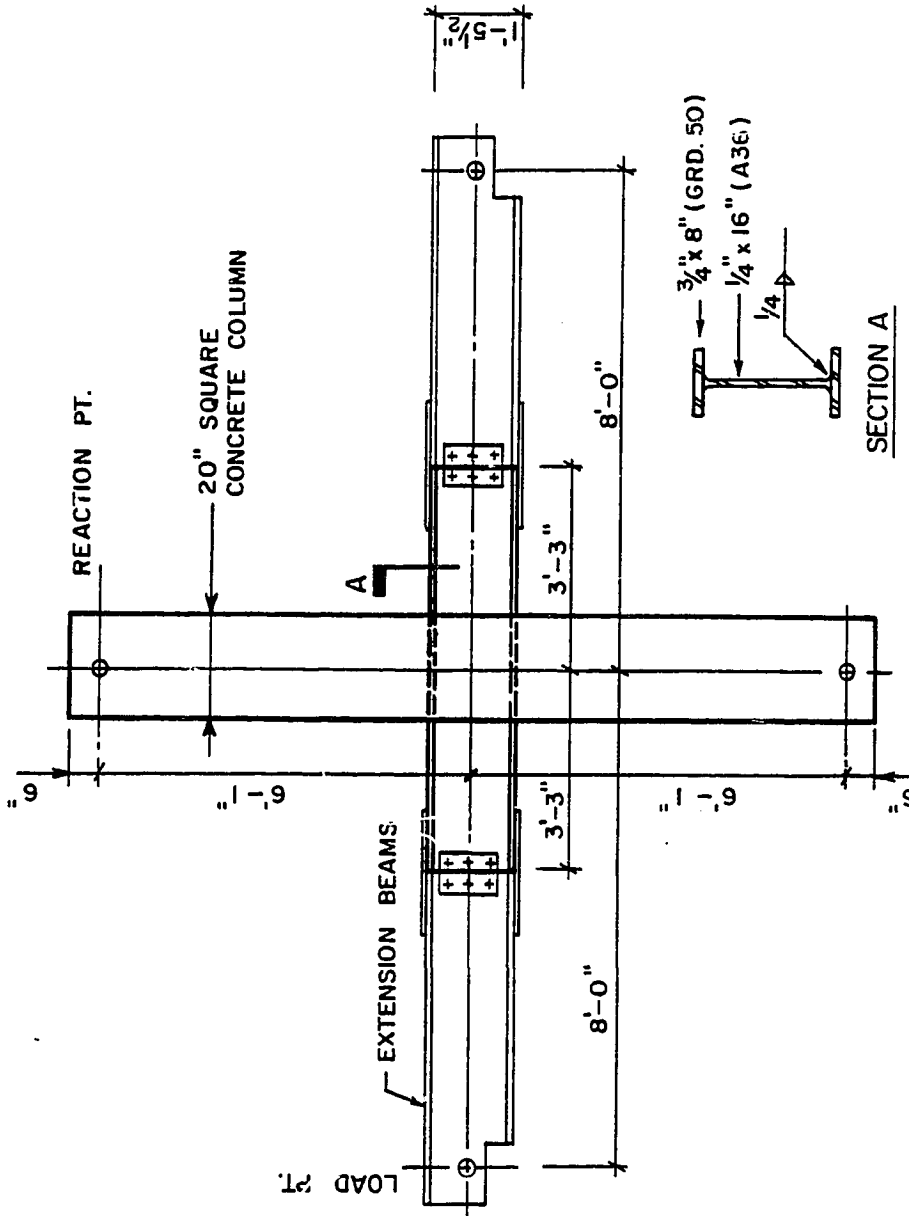


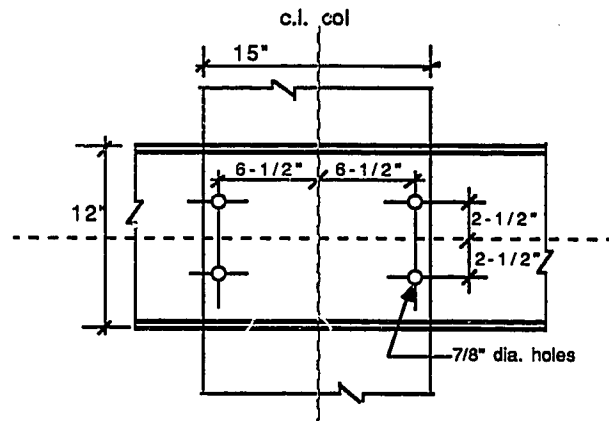
Fig. 3.3 Test specimens 3 thru 9.

The results of the research conducted by Mattock and Gaafar [31] on embedded brackets and by Wakabayashi et. al. [58, 59] and Naka et. al. [36] on SRC connections, as well as the pilot tests, were used to estimate the connection failure loads.

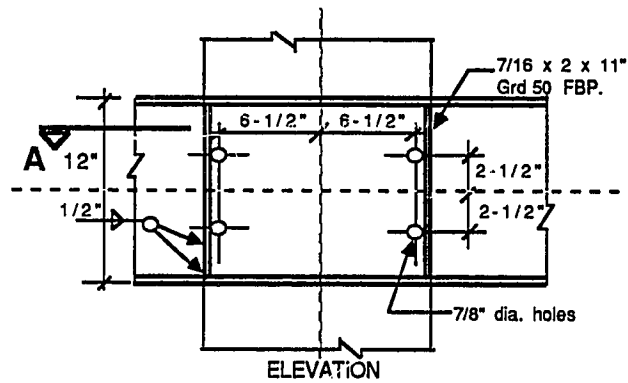
3.2.1 Beam Details. A W12x22, Grade 50 beam was used for specimens 1 and 2. The beam had a $b_f/2t_f$ ratio of 4.7 which is an average value for most rolled sections. The details in the joint area are shown in Fig. 3.4. Four 7/8-in. diameter holes were drilled in both specimens to accommodate U-shaped stirrups that formed perimeter hoops in joint area. For specimen 2, two pairs of 7/16 x 2 x 11-in., Grade 50 FBPs, fitting between the flanges at each side of the web, were welded flush with the faces of the concrete column. The width-to-thickness ratio, $w_p/2t_p$ for these plates was 4.7. A 1/4-in. fillet weld was used to develop the full capacity of the plates.

A 17-1/2-in. deep built-up hybrid section was used for specimens 3 through 9. This section had low panel shear capacity and high flexural capacity. The ratio $b_f/2t_f$ for the flanges was 5.33 which is an average value for most rolled steel sections. The beam details in the joint area for these specimens are shown in Figs. 3.5 through 3.7. Eight 15/16-in. diameter holes were drilled in each specimen to accommodate four pairs of U-shaped stirrups in the joint area.

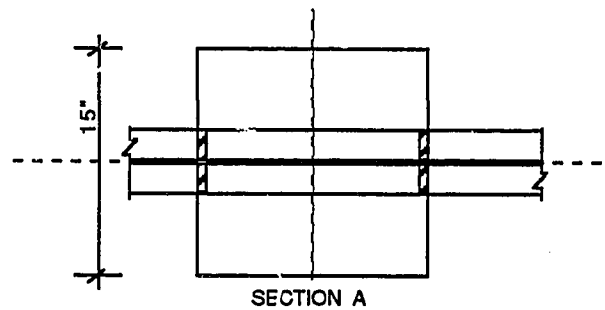
Specimen 3 contained a bare beam. Specimen 4 was designed with a thin face bearing plate. A pair of 3/8 x 4 x 16 in., A-36 plates were welded all around with a 1/4-in. fillet weld. The plates had a ratio, $w_p/2t_p$, of 10.67. A thick face bearing plate, as shown in Fig. 3.5(c) was studied in specimen 5 and it served as reference test for most tests. Four 7/8 x 4 x 16 in., Grade 50 plates were used, giving a $w_p/2t_p$ ratio of 4.57. These plates were welded to flanges using a 1/2-in. fillet



a) Specimen 1 elevation



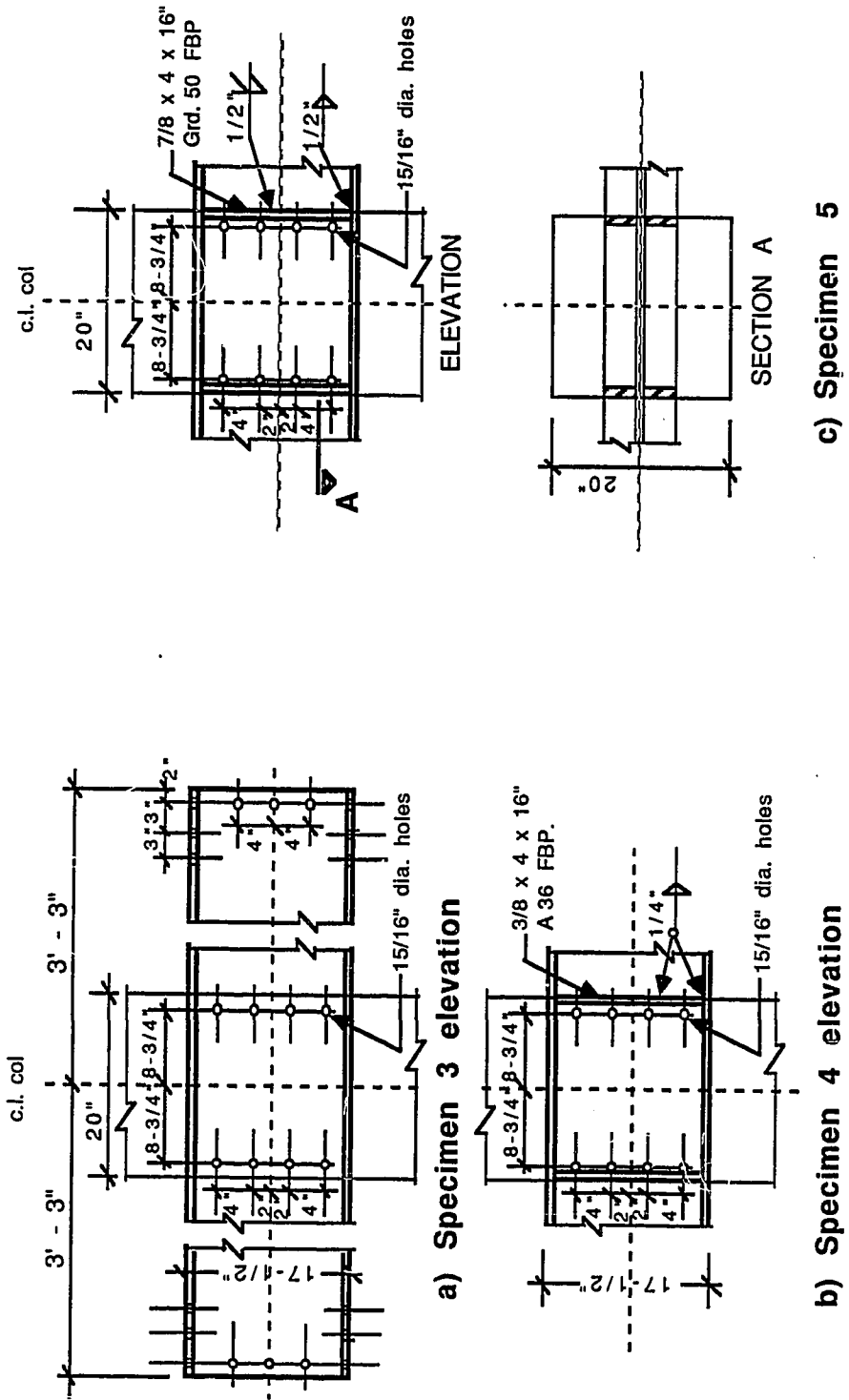
ELEVATION



SECTION A

b) Specimen 2

Fig. 3.4 Beam details in the joint area for specimens 1 and 2.

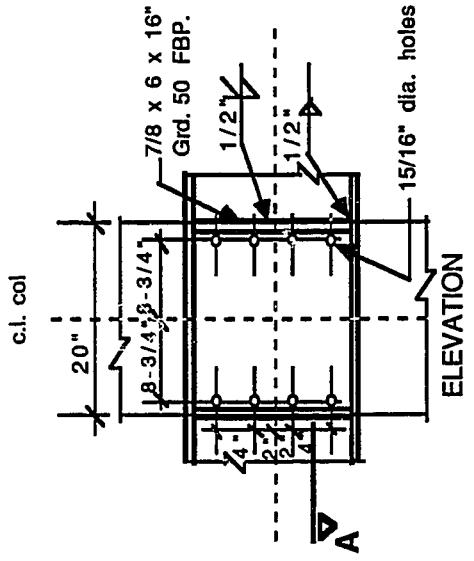


c) Specimen 5

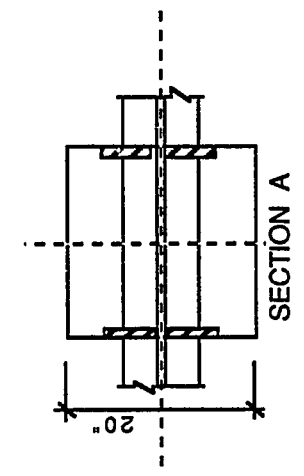
b) Specimen 4 elevation

a) Specimen 3 elevation

Fig. 3.5 Beam details in the joint area for specimens 3, 4 and 5.

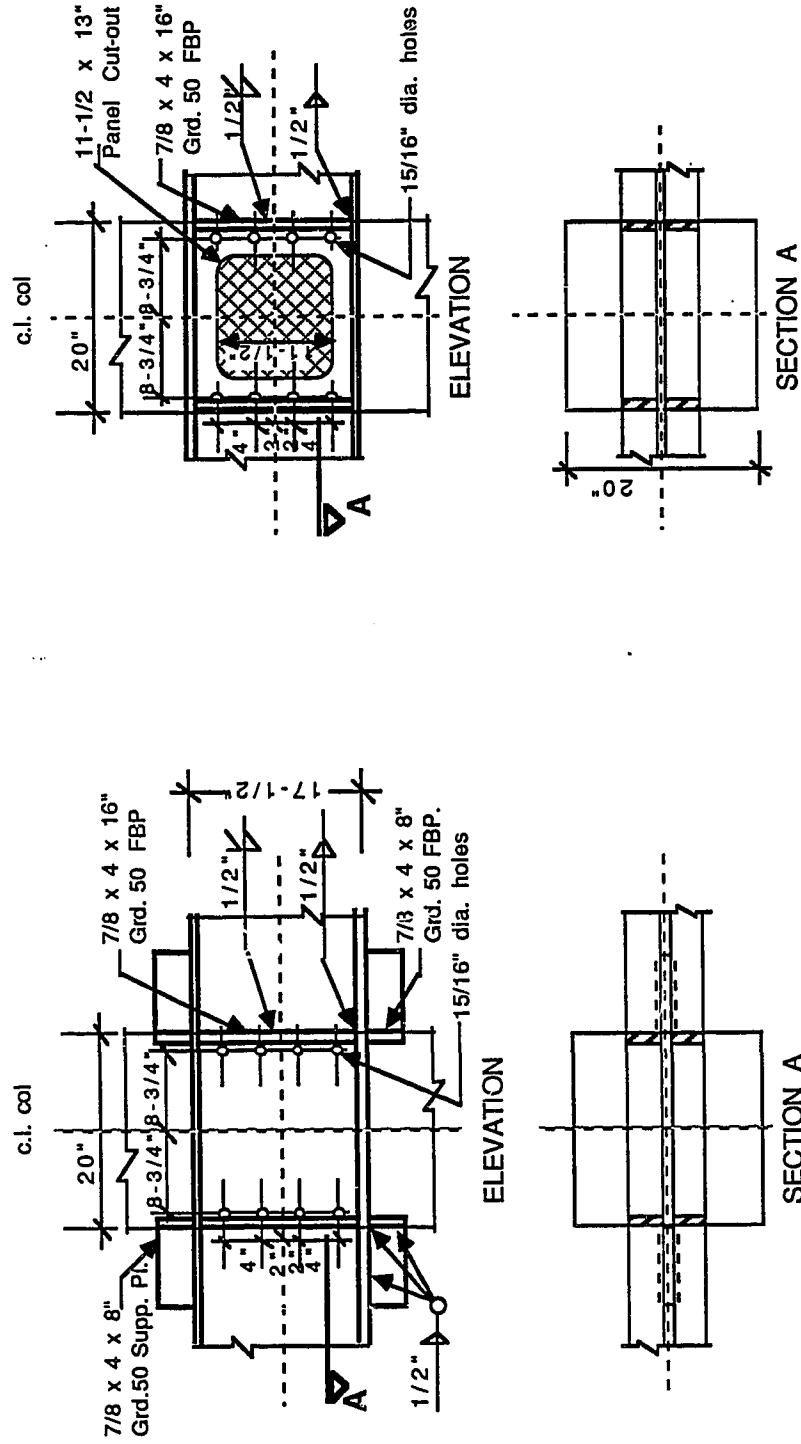


a) Specimen 6



b) Specimen 7

Fig. 3.6 Beam details in the joint area for specimens 6 and 7.



b) Specimen 9

a) specimen 8

Fig. 3.7 Beam details in the joint area for specimens 8 and 9.

weld. For the connection to the beam web, a partial penetration weld was used at the inside face of these plates, due to their proximity to the holes. At the outside face, however, a 1/2-in. fillet weld was used.

Details for specimen 6 with a thick steel panel are shown in Fig. 3.6(a). Four 3/8 x 4 x 16-in. A36 face bearing plates were welded first. Two 1/2 x 15-1/4 x 18-1/2 in. Grade 50 doubler plates were then fitted between the flanges and face bearing plates. A plug weld was used all around these plates to connect them to the web. In order to minimize the transfer of any flange forces to the concrete panel, a piece of 3/8 x 3-1/2 x 16-in. styrofoam was placed inside each FBP and a thin layer of grease was applied on each side of the steel panel, as well as inside faces of the flanges.

A wider face bearing plate was used in specimen 7. The beam details in the joint area are shown in Fig. 3.6(b). The 7/8 x 6 x 16 in. Grade 50 FBPs extended two inches beyond the flanges and the extension was 2.29 times the plate thickness. Welding details were identical to specimen 5.

The face bearing plates extended over a depth of 25-1/2 in. in specimen 8 as shown in Fig. 3.7(a). All the plate pieces used were of Grade 50 material. Four 7/8 x 4 x 16-in. FBPs were fitted between the flanges. Welding details for these plates were the same as those for specimen 5. Additional 7/8 x 4 x 8-in. plates were welded to the beam flanges to extend the FBP 4 in. beyond each beam flange. In order to function properly these additional face bearing plates required support plates which normally would be provided inside the joint, thus giving a clean external appearance. However, for better comparison with the other test results, the 7/8 x 4 x 8 in. support plates were welded outside the joint.

The details for specimen 9 with a weak steel panel are shown in Fig. 3.7(b). A 11-1/2 x 13-in. hole was cut out of the steel panel. The size of the face bearing plates and the welding details were exactly like those for specimen 5.

3.2.2 Column Details. Columns were sufficiently reinforced to prevent any shear or flexural failure outside the joint. Low concrete strength was chosen to increase the likelihood of failure in the connection. The column details as well as the concrete strength were kept as uniform as possible, within each group.

For specimens 1 and 2, eight #9 bars were used for vertical reinforcement. The shear reinforcement for the column consisted of #3 closed ties provided at 4-in. spacing. The transverse reinforcement in the joint area is shown in Fig. 3.8(a), and was provided in accordance with the ACI-ASCE Committee 352 recommendations for monolithic reinforced concrete beam-column joints [2]. Provisions for Type 1 joints, i.e. for non-seismic loads, were followed. The reinforcement provided is about 2/3 of the reinforcement required in Type 2 joints for seismic zones using Eqs. A.3 and A.4. Within the depth of the beam two pairs of U-shape ties were provided at 5-in. spacing. The first two ties below the beam soffit and above the top of the beam were spaced at 2-in. and then at 4-in. spacings. Concrete cover on the ties and aggregate size were scaled down as were all dimensions in the tests. Clear concrete cover on the outside of the ties was 3/4-in. and maximum 3/8-in. river gravel was used as coarse aggregate.

For specimens 3 through 9, twelve #10 rebars were used as vertical reinforcement. The shear reinforcement outside the joint area was comprised of sets of #4 and #3 ties placed at 8-in. spacings. The transverse reinforcement in and around the

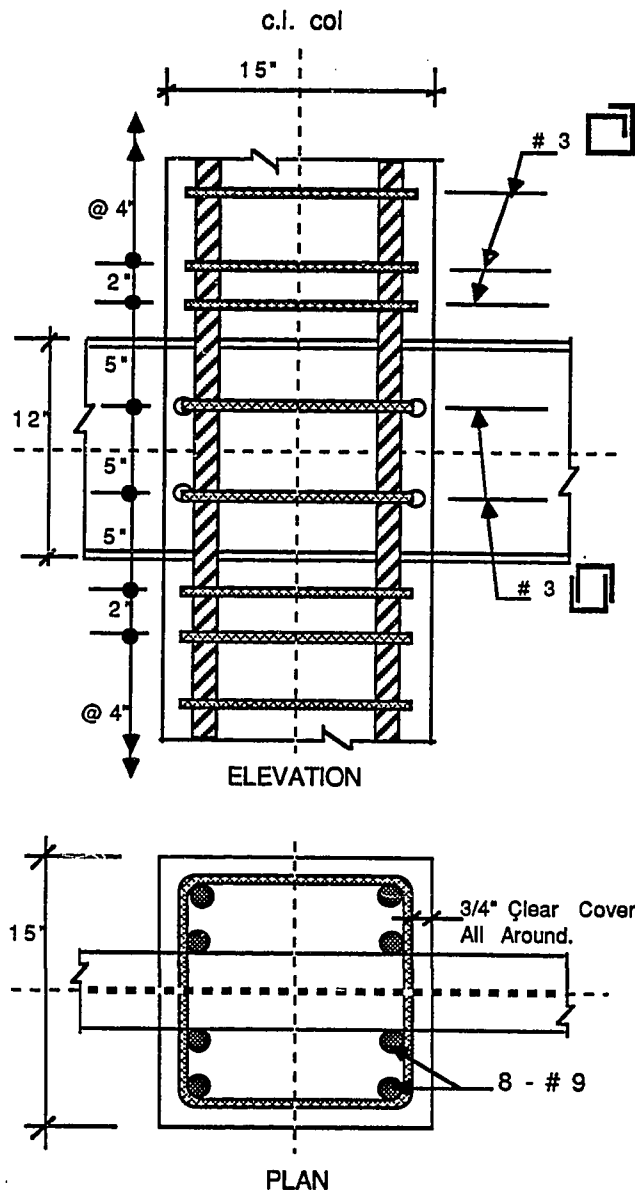


Fig. 3.8(a) Joint reinforcement for specimens 1 and 2.

joint is shown in Figs. 3.8(b) and 3.9. The reinforcement details were identical for all specimens, except for test 8, in which a few extra ties were provided near the extended face bearing plates. The amount of transverse joint reinforcement in the direction of shear in this group of tests was equal to the value recommended for seismic loads (Type 2 joints, Eq. A.3 and A.4) and was higher than that for specimens 1 and 2. The provided amount of transverse reinforcement in the direction normal to the beam axis was half the amount in the direction of shear. Sets of two U-shaped and two hairpin shape #3 ties were provided at 4-in. spacing within the depth of the beam. Extra #3 closed ties were placed above and below the beam as shown in Figs. 3.8(b) and 3.9. A clear concrete cover of 1 in. was maintained. Crushed stone of maximum 3/4-in. size was used as coarse aggregate for the concrete.

Details of the joint area of specimens 1, 5 and 8, are pictured in Figs. 3.10 through 3.12.

3.2.3 Specimen Fabrication. Column reinforcement cages were fabricated except for the ties in the joint area. The cages were erected and the beams positioned. The reinforcement in the joint area was then placed. A typical specimen is pictured in Fig. 3.13. For casting the specimens, wooden formwork with 3/4-in. thick plywood sheathing was used. Typically two specimens were cast from the same concrete batch. As pictured in Fig. 3.14, two windows were provided in the formwork to place the concrete in approximately 4-ft. lifts. A view of the concreting operation is pictured in Fig. 3.15. Two 2-in. diameter, needle type immersion vibrators were used for consolidating the concrete. A set of fifteen standard 6x12 cylinders were cast with the specimens. Two days after casting, the formwork was stripped and the specimens were left in exposed laboratory

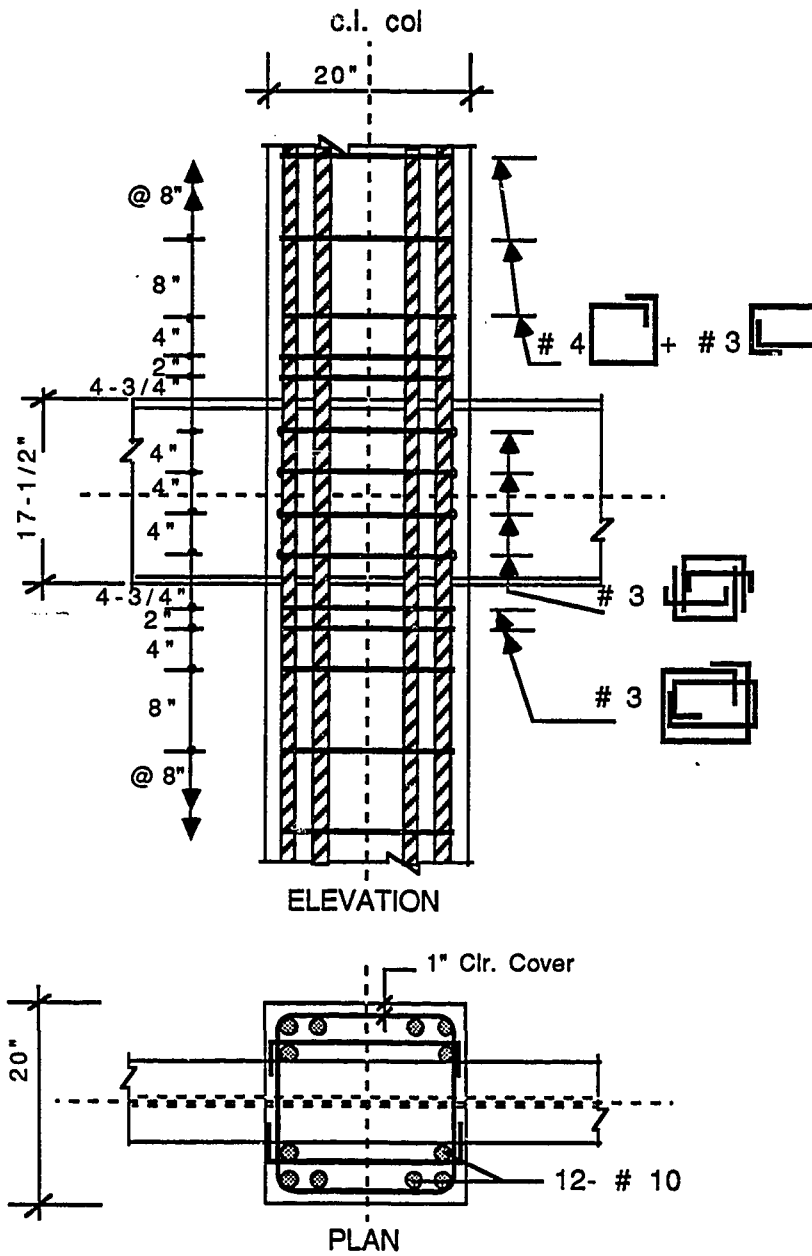


Fig. 3.8(b) Joint reinforcement for specimens 3 thru 7 and 9.

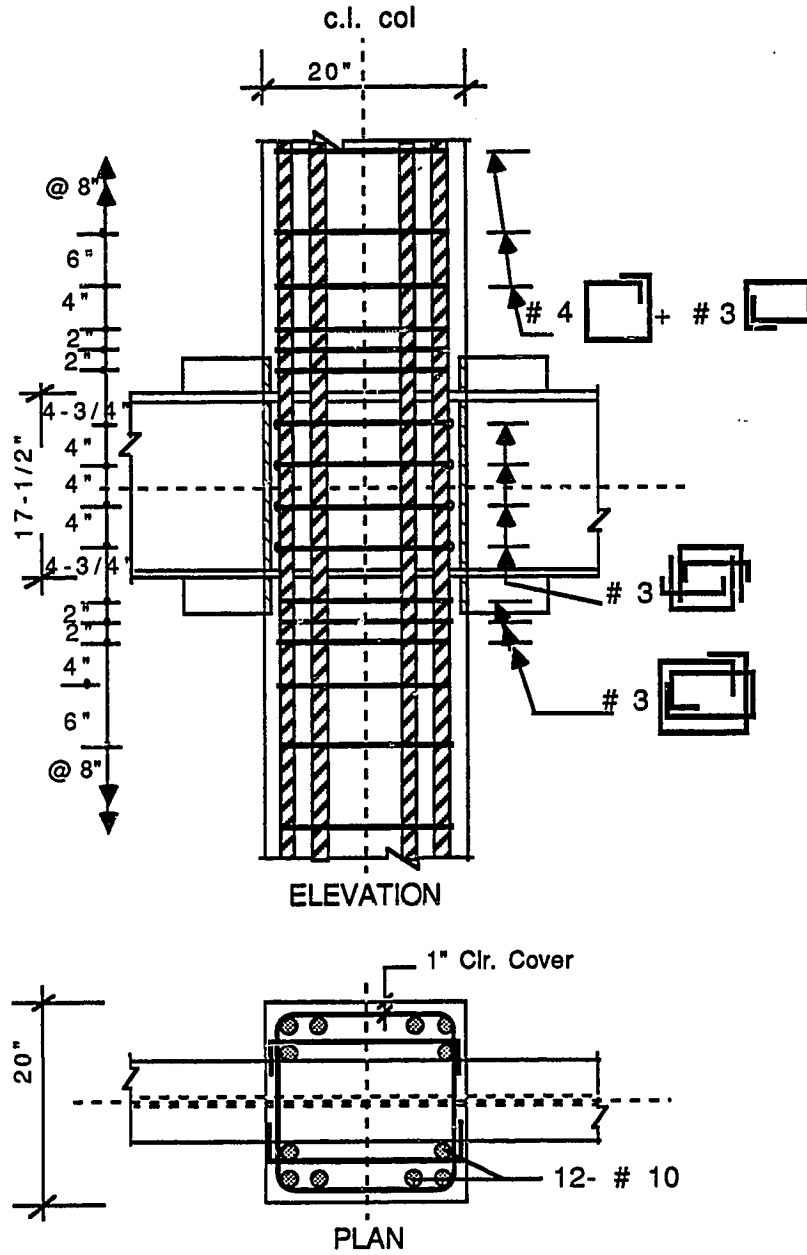


Fig. 3.9 Joint reinforcement for specimen 8.

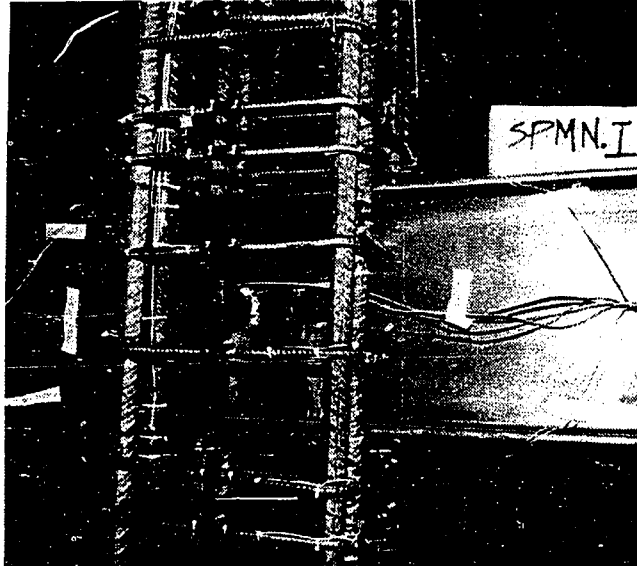


Fig. 3.10 A view of joint area of specimen 1.

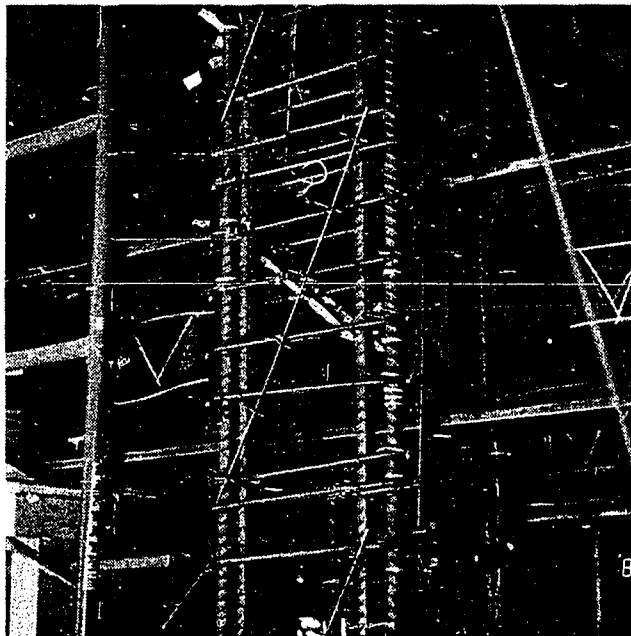


Fig. 3.11 Joint area of specimen 5.

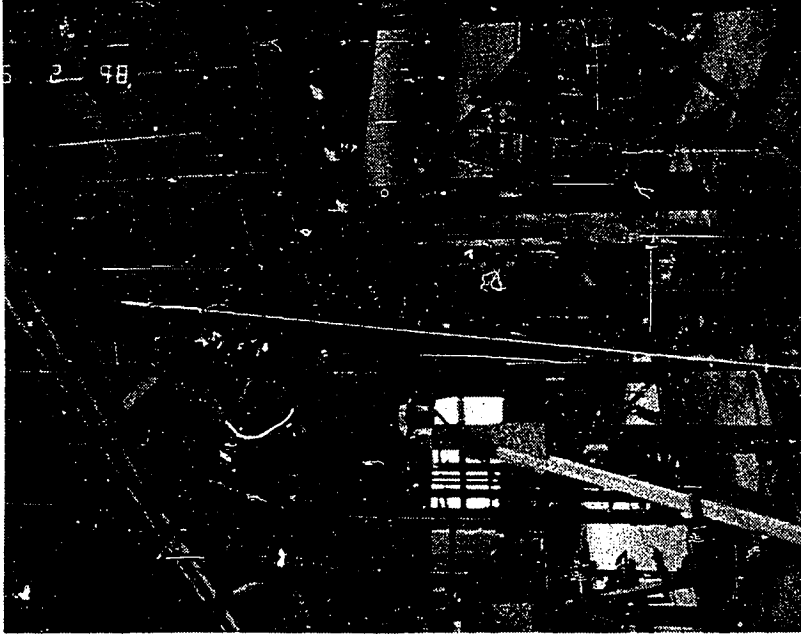


Fig. 3.13 A typical reinforcement cage.

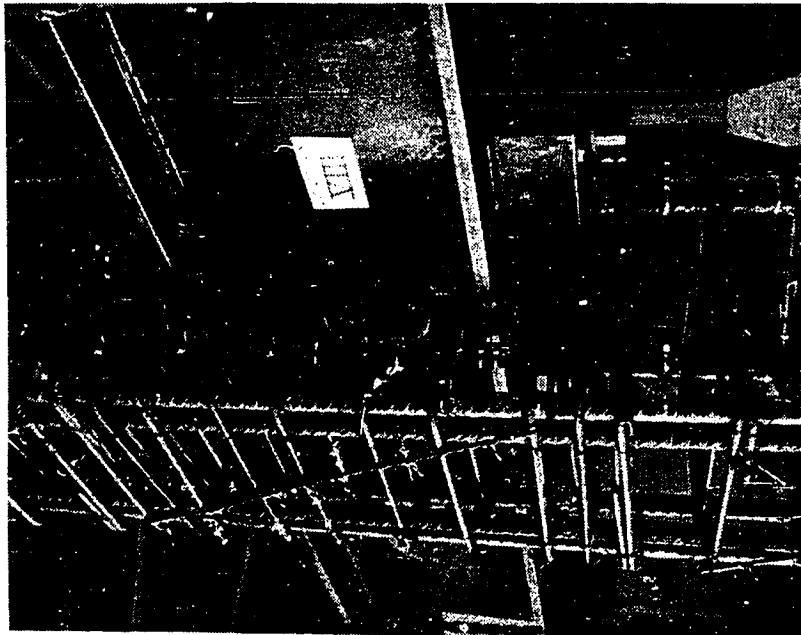


Fig. 3.12 Joint area of specimen 8.

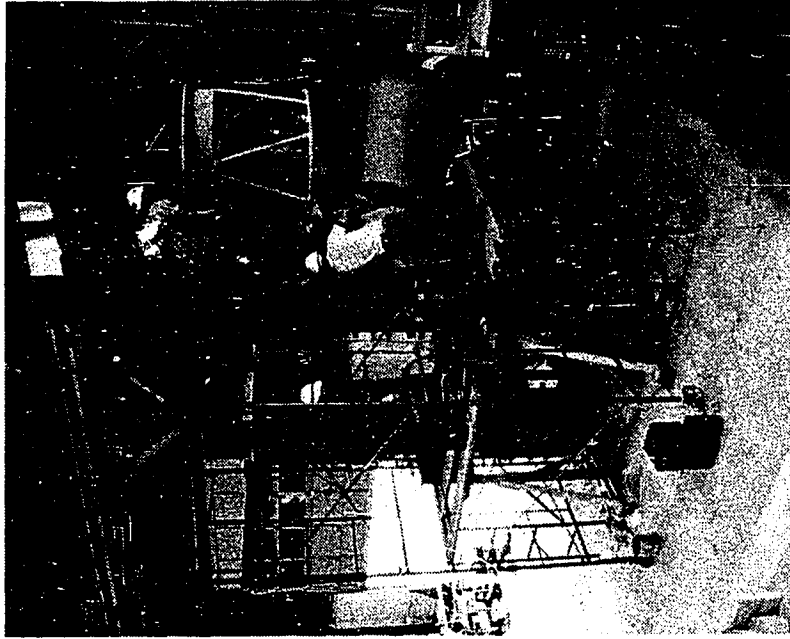


Fig. 3.15 Concreting operation.



Fig. 3.14 A view of formwork.

environment for curing. The cylinders were cured in the same manner.

3.3 Material Properties

As described in Sec. 3.1, the test series was planned such that only one parameter was varied in each test, so a clear evaluation of each parameter could be made. Structural steel beams for all specimens within a series were cut from one single length of beam. All column reinforcing bars of the same size for specimens within a series came from the same heat, except for specimens 8 and 9 which were from a different lot than those for specimens 3 through 7. Although an effort was made to keep the concrete strength uniform for the specimens within each series, it varied from 3550 to 4000 psi.

Tension coupons were tested to determine structural steel properties. These coupons were cut from the web and flanges of beams and face bearing plates. For the beam web, coupons were taken both in the longitudinal and the transverse direction, i.e. along the axis of the beam and perpendicular to it. Two coupons were tested for the material property desired at each location or direction. For better sampling, each of the two coupons were taken from a different specimen within the group and the results were averaged. The plate coupons were machined to the ASTM A370-77 specifications [7]. A 2-in. gauge length was used for all the coupons, except those for flanges of the beams in specimens 3 through 9, where an 8-in length was used. For the column reinforcing bars 36-in. long pieces were tested in tension with an 8-in. gauge length. These pieces were ordered with each lot of rebars and were from the same heat material.

A typical load-strain plot for a tension coupon is shown in Fig. 3.16. The static yield plateau was usually flat and was

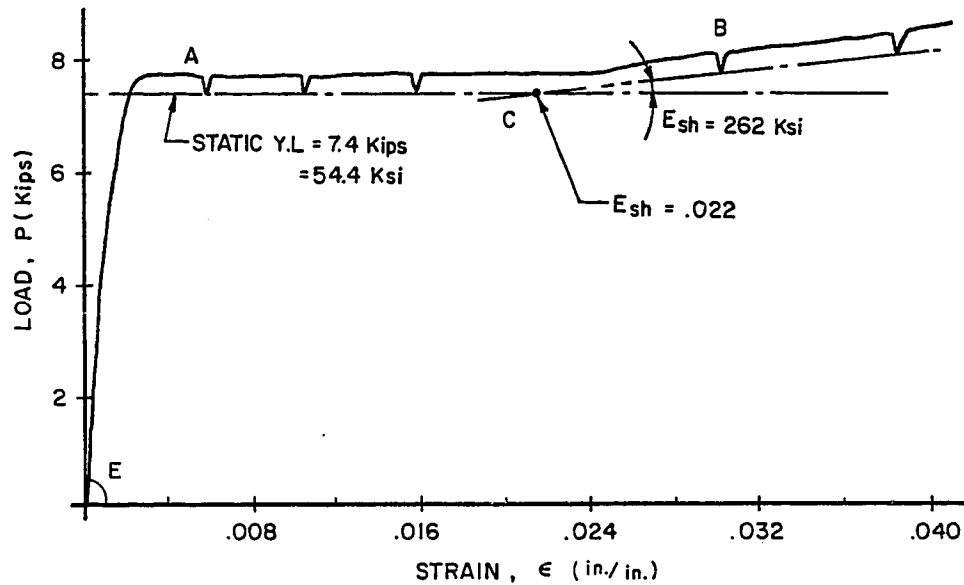


Fig. 3.16 Typical load vs strain plot for tension coupons.

determined by taking three static load points, A, on the yield plateau, at selected strain intervals. At each of these points the machine was stopped, thereby holding the deformation constant for five minutes before taking the load reading. The same procedure was used during the connection tests when a specimen began to lose its stiffness. The static yield load of the tension coupon was defined as the average of these readings. For the tension coupons from the beam webs, the strain hardening modulus, E_{sh} , as well as the strain at the onset of strain hardening, ϵ_{sh} , were also noted. Procedures outlined by Adams [32] were followed. A set of three readings were recorded at two points, B, at .005 to .010 strain apart. Again, the deformation

was held constant and the load was recorded each at time intervals of 2-1/2, 5 and 7-1/2 min. after stopping the machine. Thus, three values of modulus were calculated based on the two points B at 2-1/2, 5 and 7-1/2 min. The modulus of strain hardening, E_{sh} , was defined as the average of these three values. The strain at the onset of strain hardening, ϵ_{sh} , was estimated to be at point, C, obtained by intersecting the line joining the two B points at 5 min. with the static yield plateau. Strain was measured using a 2-in. or 8-in. extensometer capable of measuring strains with .0001 in./in. accuracy. The extensometer was removed after the readings at point B were recorded, and the specimen was loaded to ultimate. Percent elongation was then determined from the failed specimens using the pre-marked gauge length. A summary of the material properties both for structural steel and reinforcing bars are listed in Table 3.2.

The target concrete strength was 3500 psi for specimens 1 and 2 and 4000 psi for 3 through 9. The concrete strengths at 28 days after casting and on the day of testing, are listed in Table 3.3.

3.4 Test Set-Up

Simulated lateral loads were applied by loading the opposite beam ends upward and downward while permitting no displacement at the top and bottom of the column. The test set-up used for specimens 3 through 9 is pictured in Figs. 3.17 and 3.18. The set-up for specimens 1 and 2 was similar.

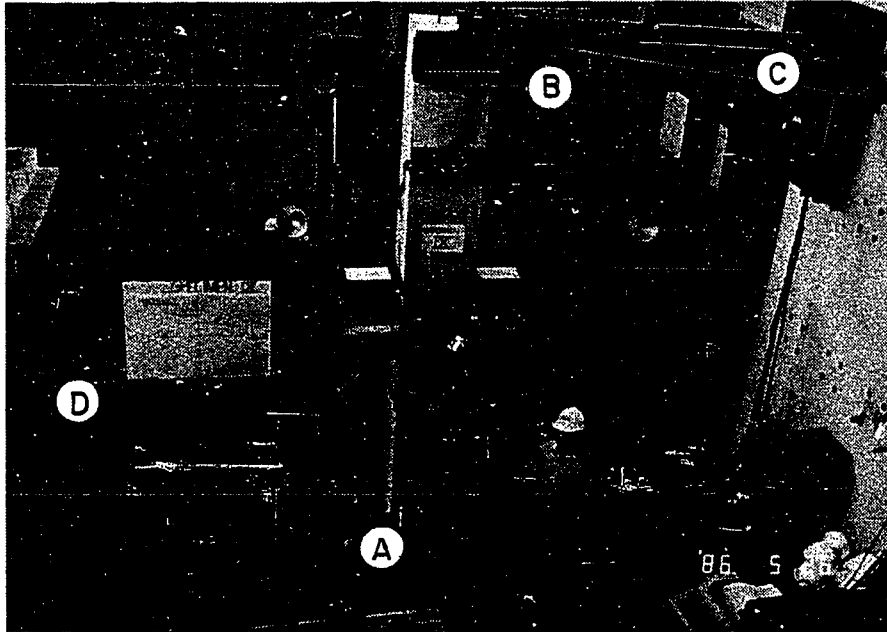
The test set-up prevented displacement in any direction at the column ends but permitted in-plane rotation at the column ends. A piece of 1-1/4-in. nominal diameter pipe was embedded in the concrete columns at 6-in. from the ends. A 1-1/4-in. diameter, A354 Grade BD stud was greased and placed through the

Table 3.2 Material Properties - Steel Coupons and Reinforcing Bars

Specimens	Description	Static Yield Stress (ksi)	Ult. Stress (ksi)	Gauge Length (in.)	% Elong.	Strain Hardening	
						E_{sh} (ksi)	ϵ_{sh} (in/in)
1 - 2	Long. Web	55.6	71.5	2	34.0	290	.024
1 - 2	Transv. Web	56.3	71.7	2	28.2	245	.020
1 - 2	Flange & FBP	44.5	66.3	2	37.7	—	—
3 - 9	Long. Web	36.5	56.5	2	40.5	335	.022
3 - 9	Transv. Web	35.9	56.1	2	33.1	27.0	.020
3 - 9	Flange	50.6	76.3	8	25.1		
3 & 6	3/8-in. FBP	43.4	68.5	2	38.0		
4, 5, 7-9	7/8-in. FBP	58.9	87.3	2	33.3		
1 - 2	#3 bars	62.1	92.1	8	17.0		
1 - 2	#9 bars	62.2	99.1	8	18.6		
3 - 7	#3 bars	65.0	101.8	8	15.3		
3 - 7	#4 bars	61.6	90.2	8	18.3		
3 - 7	#10 bars	65.7	104.2	8	16.1		
8 - 9	#3 bars	77.0	112.4	8	11.0		
8 - 9	#4 bars	60.0	101.8	8	11.6		
8 - 9	#10 bars	65.3	104.5	8	15.8		

Table 3.3 Concrete Cylinder Strength

Specimen	28-day Strength (psi)	Day of Testing	
		Age (days)	Strength (psi)
1	3300	93	3550
2	3300	106	3550
3	4400	42	4500
4	4100	48	4300
5	4100	56	4300
6	3900	74	4000
7	3900	81	4000
8	3600	28	3600
9	3600	39	3700



- A floor fixture
- B channel strut
- C angle brace
- D beam ram

Fig. 3.17 Test set-up for specimens 3 thru 9.



Fig. 3.18 A view of test set-up.

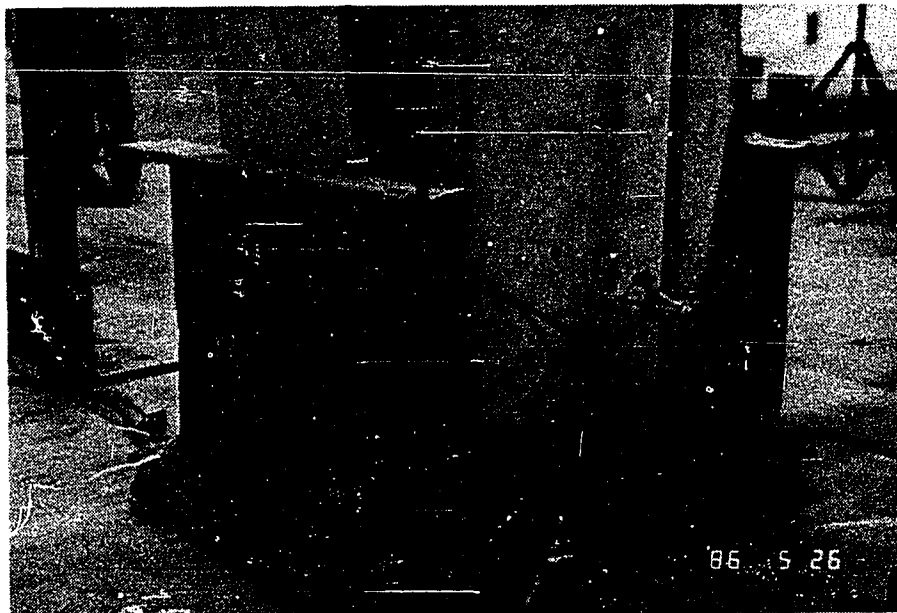


Fig. 3.19 Detail at the column base.

embedded pipes, and fastened to the base fixture at the bottom and to a channel strut at the top. The base fixture, shown in Fig. 3.19, was made with two 22-in. channels attached to a 1-1/4-in. thick plate which was tied to the floor slab. At the column top two 12-in. channels were used as a strut, tied to the reaction wall, as shown in Fig. 3.20. To prevent any lateral movement, an angle brace was used diagonally from the column top to the reaction wall, as shown in Fig. 3.17.

The specimens were loaded at the beam ends using two 50-ton, hydraulic rams as pictured in Fig. 3.21. The rams were tied to the floor through a pedestal and an eye bracket. The rod end of the hydraulic ram was connected to the beam at its centerline using a female rod clevis and a 2-1/2-in. diameter pivot pin. The beam web was reinforced by plates at the pivot pin to reduce the bearing pressure and to reduce the clearance between the web and the female clevis.

3.5 Load System

The lateral load on the beam-column assemblage was simulated by applying equal and opposite loads at the beam ends, i.e., an upward load at one end and a downward load of equal magnitude at the other end. Since the ram area in tension was less than that in compression, by the area of the piston rod, the tension ram required more hydraulic pressure than the compression ram for the same magnitude of load. The desired ratio of pressure in the two rams was controlled by using a multipressure load maintainer.

A schematic diagram of the loading system used is shown in Fig. 3.22. Hydraulic pressure was provided by a single electric pump, and a multipressure load maintainer was used to control the load applied by the hydraulic rams. The pump, load maintainer

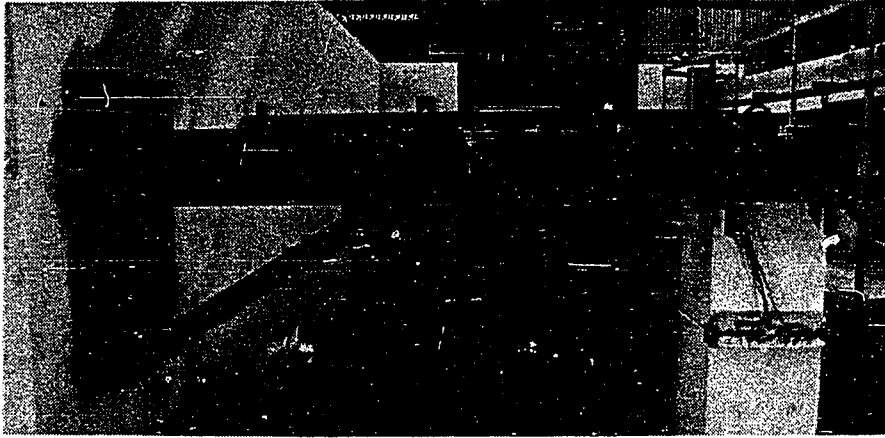


Fig. 3.20 Detail at the column top.

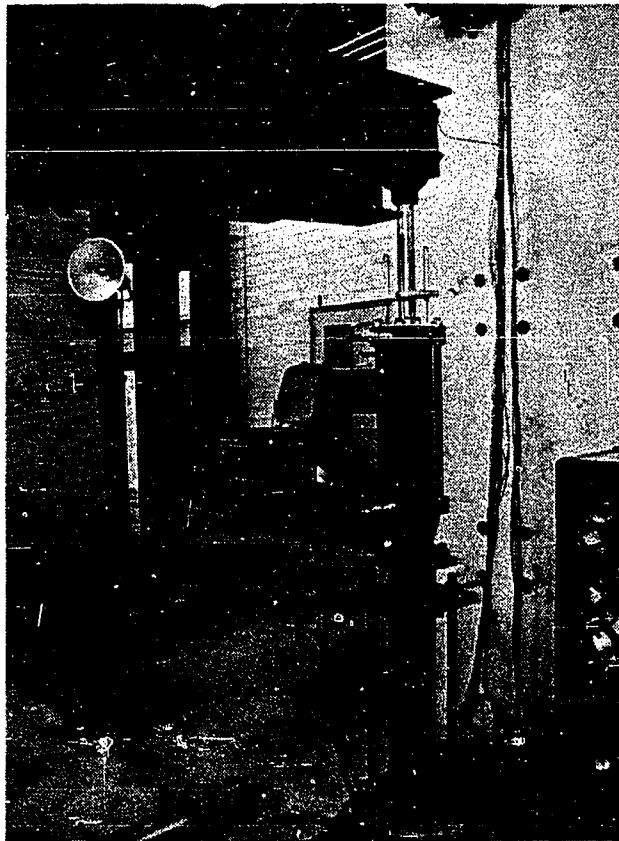


Fig. 3.21 Detail at the beam end.

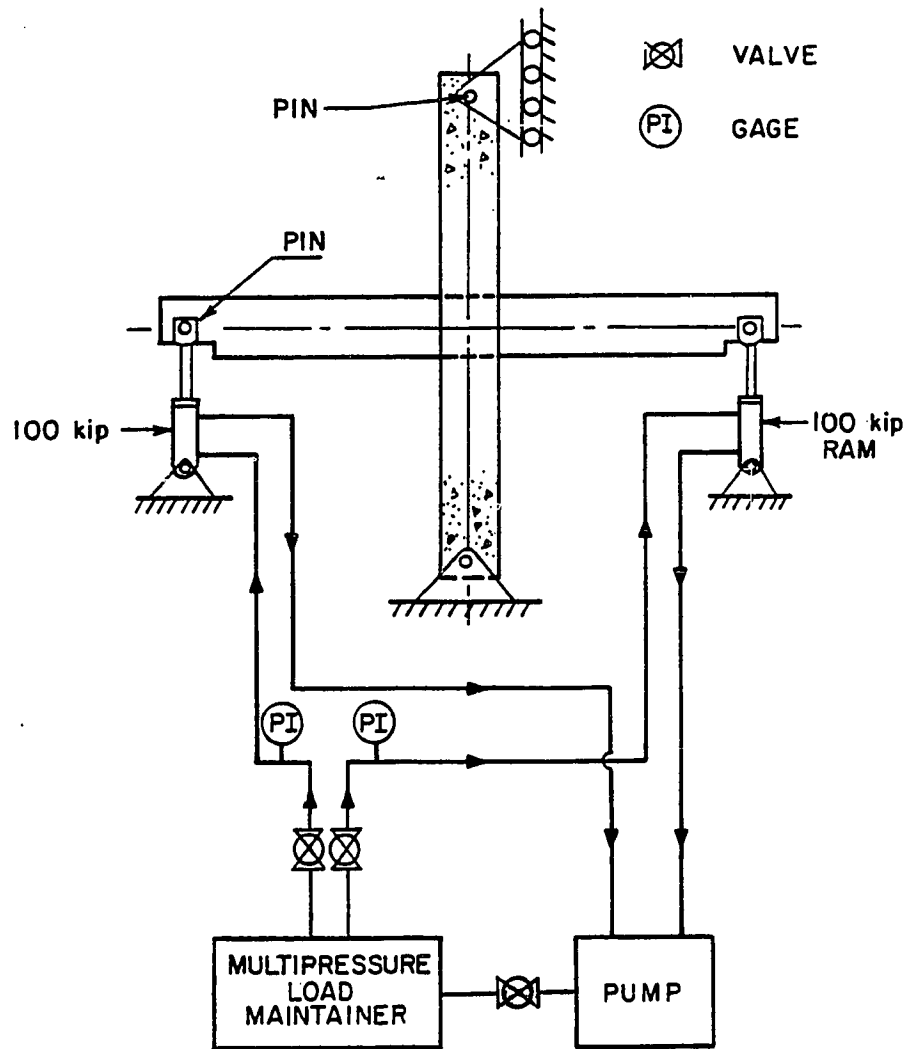


Fig. 3.22 Schematic of load system.

and rams were all connected using flexible pressure hoses. Oil shut off valves and dial gage pressure indicators, as shown in Fig. 3.22, were provided. In addition, two pressure transducers were installed in the pressure lines to electronically monitor the loads.

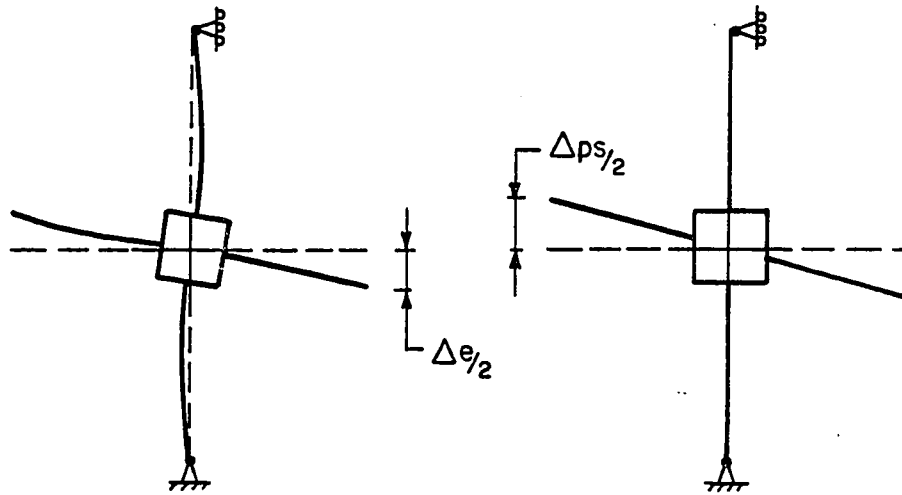
The multipressure load maintainer enabled the operator to manually control the rate of pressure increase, to maintain a fixed pressure, and to shut off the flow of oil into a ram. It also allowed the operator to increase the pressure to the two rams at a proportionate rate while maintaining the constant pressure ratio. It should be pointed out that this load system as well as the test set-up is in static equilibrium even when the magnitude of load in the two rams is not the same.

3.6 Instrumentation and Data Acquisition

To collect information regarding distortion in the joint area, to understand the stress transfer from the members to the connection panel, and to study the resistance mechanism of the panel, the following instrumentation was used.

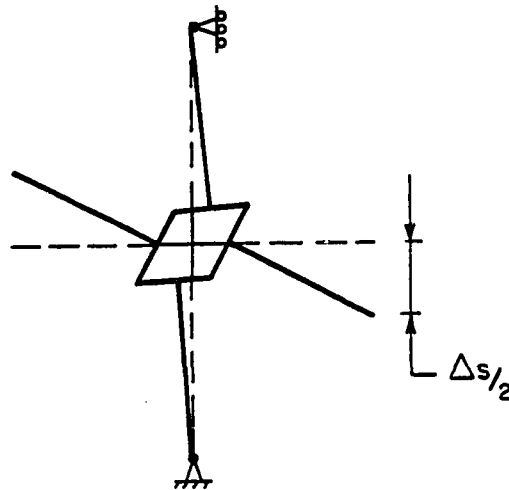
3.6.1 Joint Distortion, Drift and Load Measurements. In order to understand the stiffness deterioration of the connection, the three main components of interstory drift are identified as shown in Fig. 3.23. The first component is the elastic flexural deformation of the beam and column which can be estimated if the members are assumed to deform elastically. The second component is the panel separation which is the rigid body rotation of the steel beam with respect to the concrete column. The third component is the shear distortion of the connection panel or joint.

To measure the total drift of the beam-column subassemblage, linear voltage displacement transducers (LVDT) -



a) Beam and column elastic flexural deformation.

b) Panel separation.



c) Panel zone shear distortion.

Fig. 3.23 Components of beam deflection.

also termed as potentiometers - were used, as shown in Fig. 3.24. All the potentiometers had 2 in. stroke, except for potentiometers 1 and 2 which had a 6-in. stroke. Potentiometers 3 and 4 were necessary for specimens 3 through 9, to account for any slip in the beam splices. Potentiometers 5 and 6 were used in specimens 3 through 9 to monitor the panel separation.

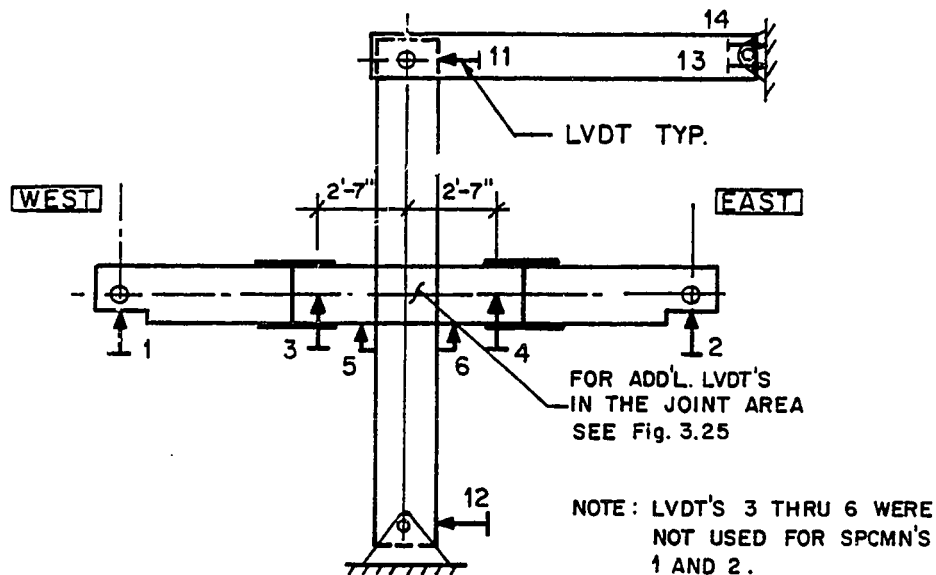


Fig. 3.24 Location of LVDTs - looking north.

It was anticipated that the shear distortion of the concrete panel, especially near the outside face, might not be equal in magnitude to that of the steel panel. This difference in the shear distortions of the steel and concrete panels, plus the panel separation, would almost be equal to the relative beam inclination (near the column) relative to the column centerline.

The relative beam inclination (RBI) was measured as shown in Fig. 3.25. A frame made with small angle sections was mounted on the beam 2-in. away from the column face, on each side of the joint. Four pointed screws were used to position the frame at the discrete location. Two potentiometers with 2-in. stroke were extended from each of these frames to measure the change in the distance to the column centerline. A view of this frame is pictured in Fig. 3.26.

A small electronic digital inclinometer, as shown in Fig. 3.27, was used to record absolute rotation at a few points. These readings were taken at the beam web and concrete faces near the joint. The locations are shown in Fig. 3.28.

The loads applied to the beam ends were monitored by measuring the hydraulic pressure of the loading rams. Dial gage pressure indicators as well as electronic pressure transducers were used.

3.6.2 Strain Measurements. The specimens were instrumented with strain gages at various locations in the connection. Two types of strain gages were used. Foil gages with 1/4-in. gauge length, in single, cross and rosette patterns, were used to monitor stresses in the structural steel and reinforcing bars. Resin impregnated, polyester mold, single gages with a 2-1/2-in. gauge length, were embedded in the concrete to monitor diagonal strut action of the concrete panel. The total number of strain gages varied from 30 in some specimens to 40 in others.

Typical locations for strain gages on column ties and vertical bars in the joint area are shown in Fig. 3.29 for specimens 1 and 2, and in Fig. 3.30 for specimens 3 through 9. Not all the gages shown in Fig. 3.30 were used in every specimen. For example, the six gages shown for vertical bars were mounted

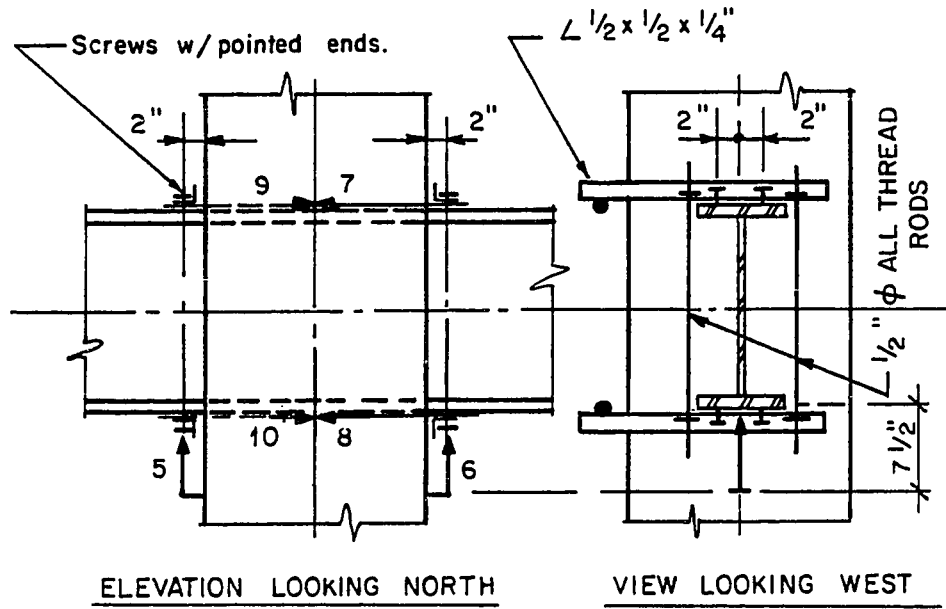


Fig. 3.25 LVDTs for joint distortion.

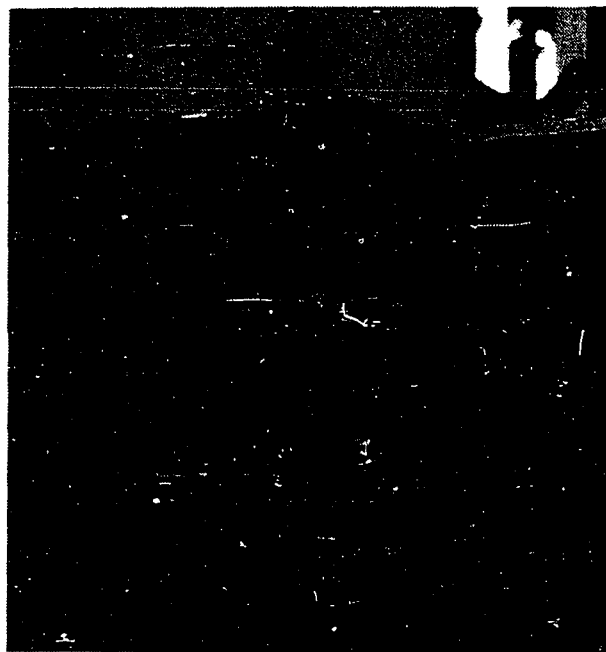


Fig. 3.26 Steel frame to measure joint distortion.

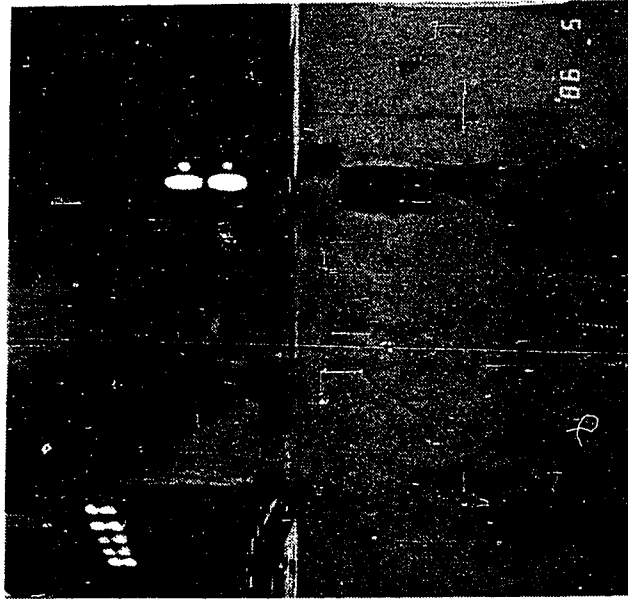


Fig. 3.27 Electronic digital inclinometer to measure the column face rotation.

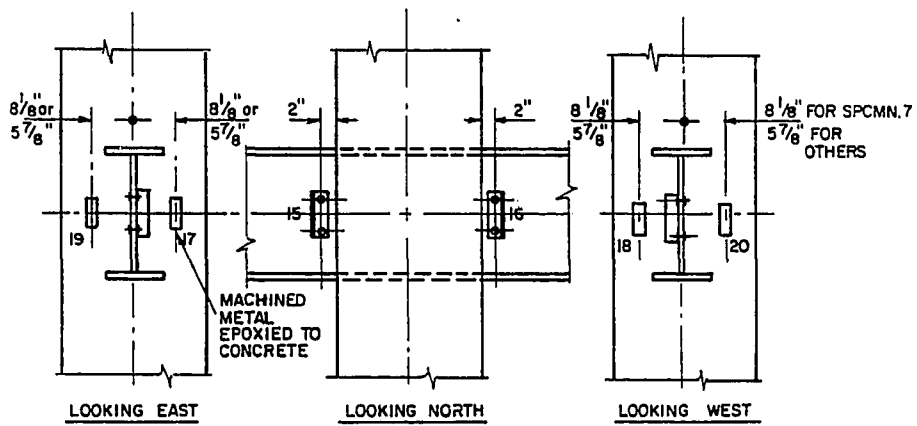


Fig. 3.28 Locations for rotation measurements with electronic inclinometer (specimens 3 thru 9 only).

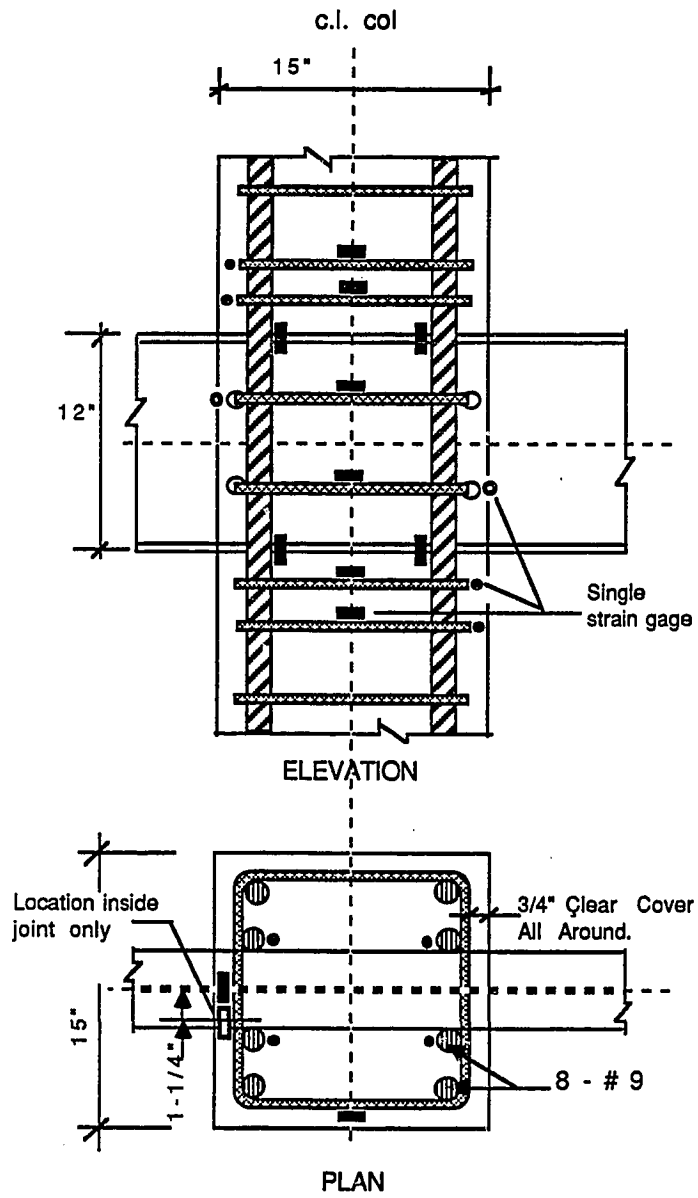


Fig. 3.29 Instrumentation on reinforcing bars for specimens 1 and 2.

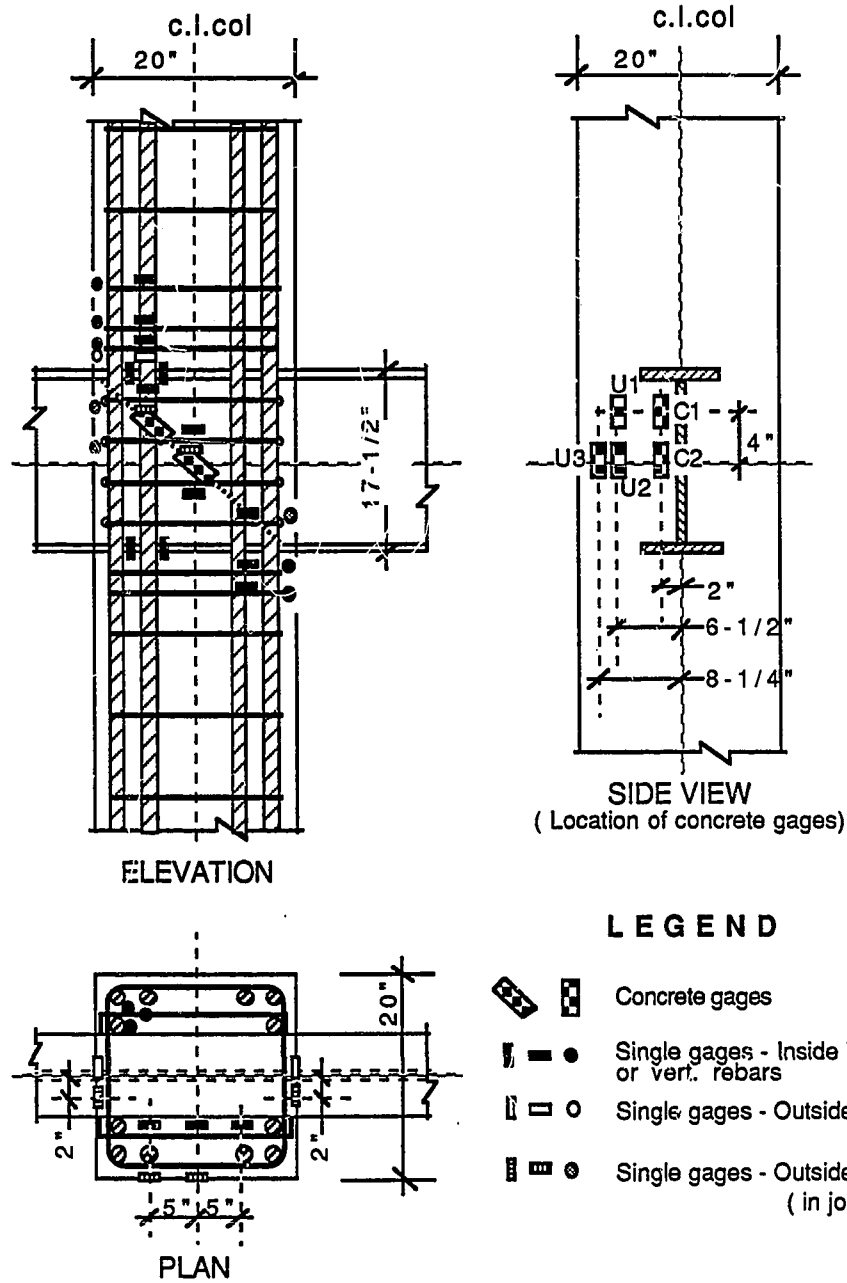


Fig. 3.30 Instrumentation on reinforcing bars and concrete -- specimens 3 thru 9.

only for specimens 3 through 5 and 8. Concrete strain gages were embedded in a few specimens. Typical locations are shown in Fig. 3.30. Concrete gages at locations C1, C2, U1, and U2 were used in specimens 5 and 9. One concrete gage at location C2 was embedded in specimens 6 and 8. Concrete gages at all five locations were used for specimen 7.

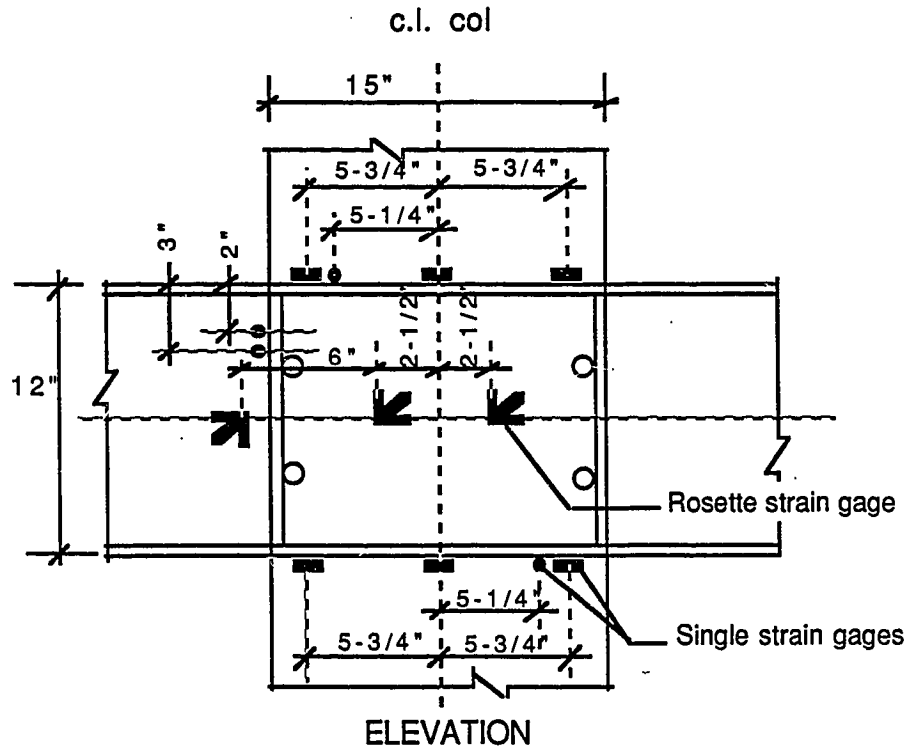
Single and cross strain gages were mounted on the steel beam in the joint area to monitor both transverse and longitudinal stresses in flanges and face bearing plates. Rosette gages were placed on the web to measure shearing stresses. A few gages were installed on the beam flange away from the joint to check the load applied by the hydraulic rams. Typical locations of these strain gages is shown in Fig. 3.31 for specimens 1 and 2, and in Fig. 3.32 for specimens 3 through 9.

3.6.3 Data Acquisition. The data from the pressure transducers, LVDT's and strain gages were processed using a data acquisition system. During the test the deflection at one end of the beam was continuously plotted against the ram load at that end using an X-Y plotter.

Prior to testing the specimens, steel beams were white-washed. Local yielding could then be visually identified as the white-wash flaked away from the steel with the brittle mill scale. Concrete cracks were marked throughout the loading history.

3.7 General Test Procedure

The same general test procedure was followed for almost all the test specimens. Before loading a specimen to ultimate load capacity, a low level load cycle, representing an approximate service load level, was applied in each direction. This service load level was kept at about half the anticipated



on FBP under Fig.
(specimen 2 only)

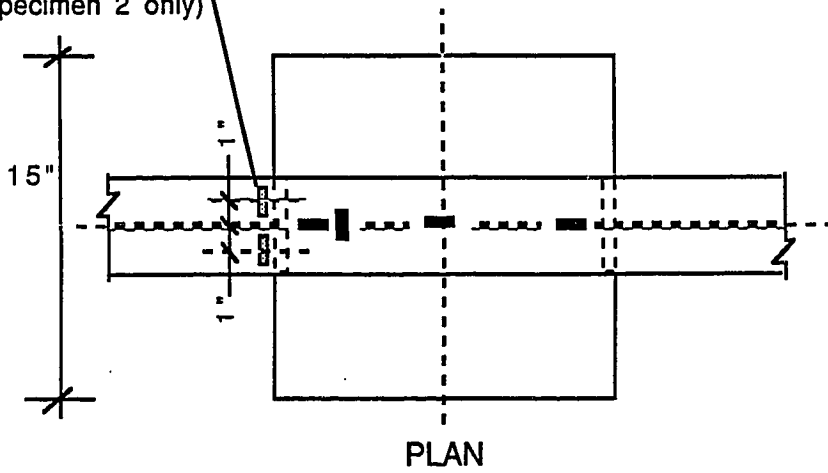


Fig. 3.31 Instrumentation on beam for specimens 1 and 2.

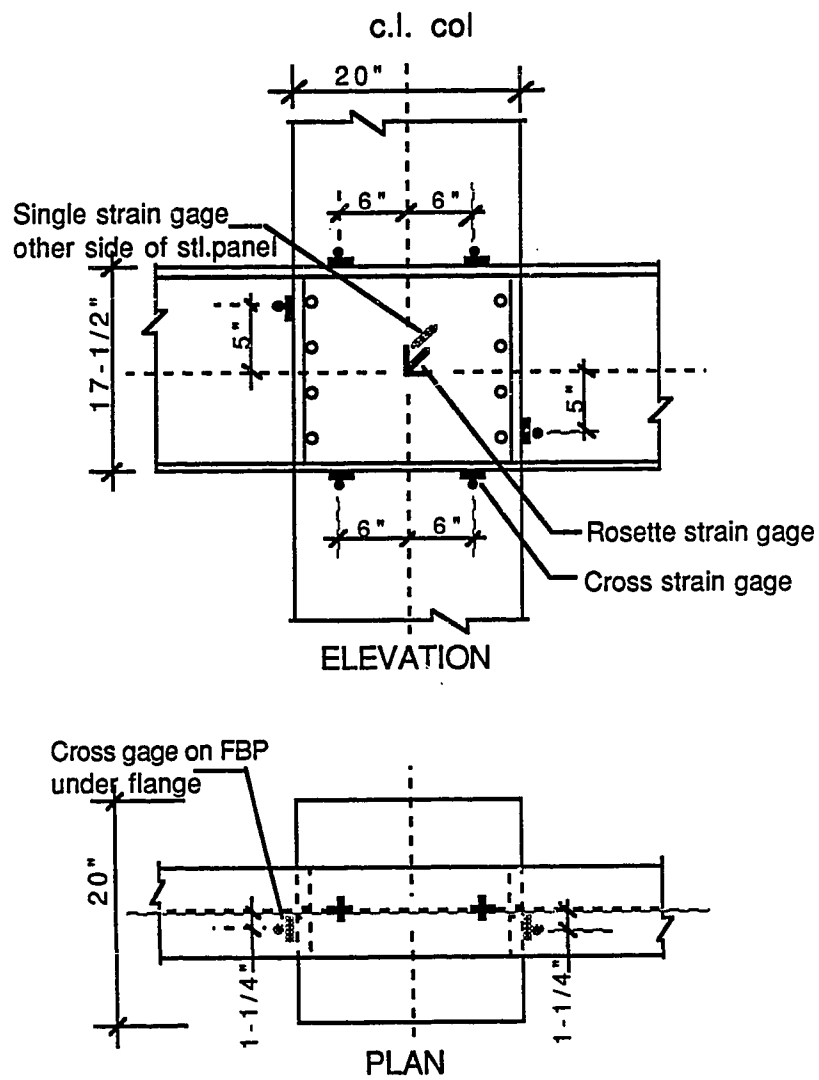


Fig. 3.32 Instrumentation on beam for specimens 3 thru 9.

ultimate load capacity of the specimen. This low level load cycle was skipped for specimens 5, 7 and 9, in order to retrieve more information from the embedded concrete gages that would otherwise have ceased to function due to concrete cracking.

Each specimen was eventually loaded to ultimate capacity in one direction. Loads were increased in small increments until the specimen started losing stiffness, at which point the loading was displacement controlled. Small increments of displacements were imposed at beam ends. At each of these incremental points, static loads were recorded in the same manner as described for the tension coupons. The oil flow from the load maintainer to the loading rams was shut off at the valve, preventing any further displacement and allowing the load to drop to its static value after few minutes. All the data were recorded at each of the incremental stages. The specimens were unloaded typically around 3 to 4% drift. The specimens were then loaded to failure in the other direction.

CHAPTER 4

EXPERIMENTAL RESULTS

The specimens were subjected to simulated lateral loads in which one end of the beam was loaded upward while the other downward as shown in Fig. 4.1. A typical loading curve is schematically shown in Fig. 4.2. For the presentation of the test results, the first half of the low level cycle, in the primary direction, is cycle L1. The second half, i.e. in the reverse direction, is cycle L2. Similarly, the first and second halves of the ultimate load cycle are U1 and U2, respectively.

During the test, data were collected at several stages. Each of these stages were identified by consecutive numbers. The concrete cracks were labelled with the stage numbers so as to trace their progression.

Under the loads as shown in Fig. 4.1, the beam flanges and column faces in diagonally opposite quadrants are subjected to the same kind of stresses, tension or compression. While describing the joint distress, the specimen orientation as well as the loading direction is identified by noting the type of stress in the particular flange or column face.

4.1 General Specimen Behavior

The specimen behavior is described by a plot of load vs. drift. An average of the loads at the two ends of the beam is plotted. The two loads were approximately equal until the specimen started losing stiffness beyond which the ram causing compression in the top flange carried more load. The drift of the specimen is calculated as the ratio of the total relative vertical displacement between a point on each beam, to the distance between the two points.

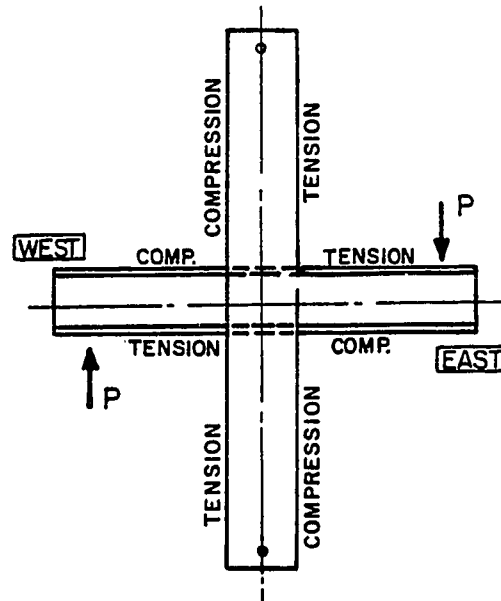


Fig. 4.1 Member stress zones under loading in the primary direction.

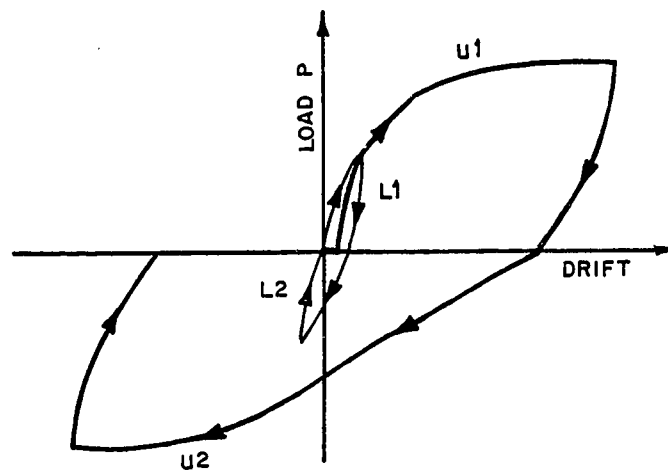


Fig. 4.2 Typical loading curve.

The critical concrete cracks are identified. These include diagonal shear cracks on the column sides and various cracks on the column faces as shown in Fig. 4.3. The following special cracking patterns are defined. Diagonal shear cracks, ds, started on the column sides in beam-column joint. Typically the first crack occurred close to the diagonal connecting corners of the joint and was followed by cracks parallel to it. As the load was increased, these cracks turned upward near the column compression faces. Cracks labelled tr radiated from the tension flanges. Typically first tr cracks originated from the tips of the tension flanges, followed by cracks initiating from the tension flange-web junction. Cracks td radiated downward at an angle, from the tip of the tension flange. As the load was increased, these cracks occasionally turned into flexural cracks. Cr cracks radiated from the compression flanges at a steep angle. First Cr cracks originated at the flange tips and in some cases were followed by cracks radiating near the compression flange-web junction.

The load points of importance for each specimen are listed in Table 4.1. To evaluate the joint rigidity the initial stiffness of the specimen as related to the joint moment is also listed. These values are not a direct measure of absolute joint stiffness, but they are useful for relative evaluation of different connection details and are calculated using the deformation at a load of 15 kips. Detailed description of each test is presented in the following.

Specimens 1 and 2. Pilot tests 1 and 2 were designed to investigate the potential value of face bearing plates. Figure 4.4 shows the load vs. drift plot for specimen 1 which had a plain W12 beam. In cycle L1, no distress was noted until a load of 11.8 kips was reached and cracks tr developed (Fig. 4.5). On

Table 4.1 Significant Load Points

Specimen No.	Init. Stiff. Related to Jt. Moment (K'/rad.)	1st Flex. Crack (kips)	1st Diag. Shear Crack (kips)	Yielding of Stl. Panel (kips)	Primary Direction at		Reverse Dir. at 2% Drift (kips)	1st Crushing Load Above Comp. (kips)	At Maximum Drift		
					1 % drift (kips)	2% drift (kips)			Load (kips)	Drift (")	
1	16,200	11.8-14.8	17.6	16.9	17.0	17.8	18.5	16.9	0.9	18.3	3.3
2	20,250	12.6	13.2	26.2	22.5	26.2	22.7	20.7	0.9	25.6	4.9
3	94,600	15.1	18.7	15.1	17.4	18.8	21.0	17.4	1.0	20.0	2.9
4	93,200	14.1	14.5	14.1	27.4	32.5	32.5	27.4	1.0	35.3	3.7
5	91,700	15.1	15.1	19.6	29.1	34.3	32.7	28.1	.9	34.2	4.5
6	110,400	16.1	24.0	---	36.7	45.3	36.7	38.7	1.1	44.6	5.0
7	111,800	15.7	15.7	18.6	34.6	41.2	36.7	33.1	.9	43.5	4.8
8	151,900	20.2	15.3	29.1	47.0	54.5	47.1	50.2	1.2	55.1	3.5
9	93,200	15.0	20.4	---	27.0	31.5	28.0	27.1	1.1	34.3	4.4

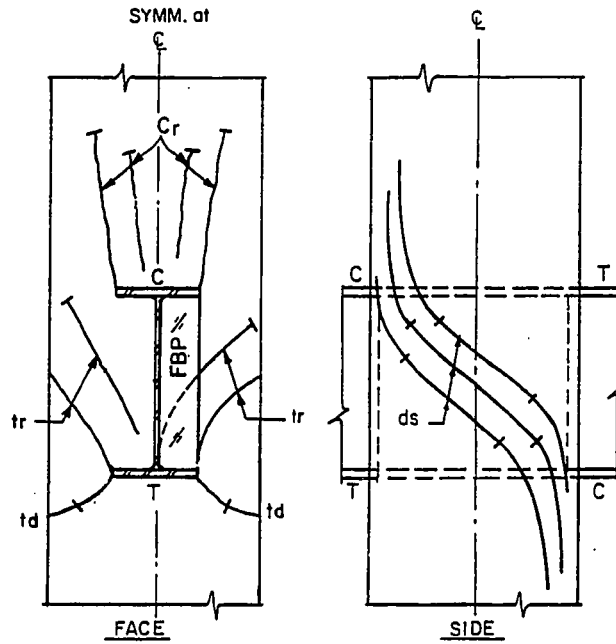


Fig. 4.3 Critical cracks in concrete column.
(Flange T is in tension)

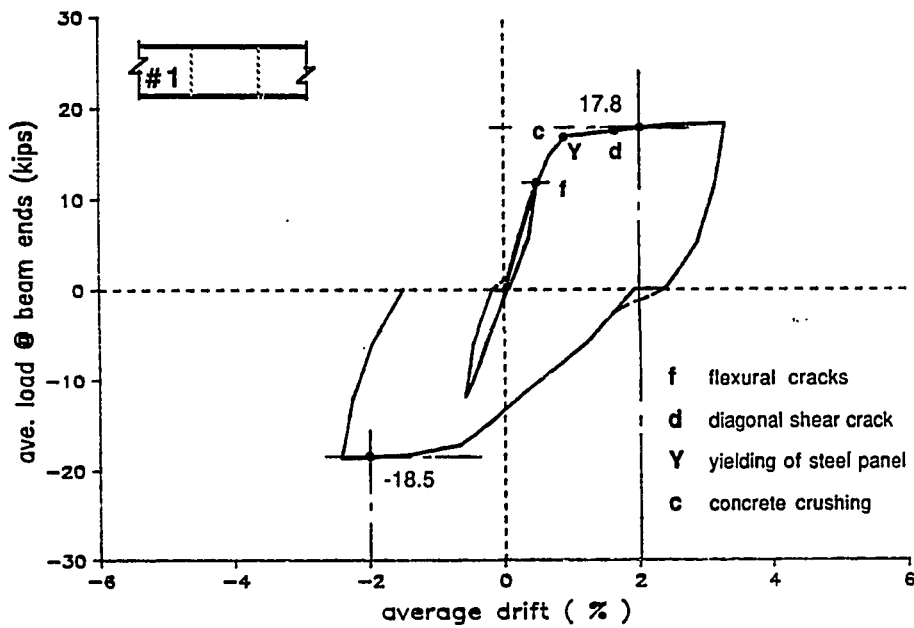


Fig. 4.4 Load-drift plot of specimen 1.

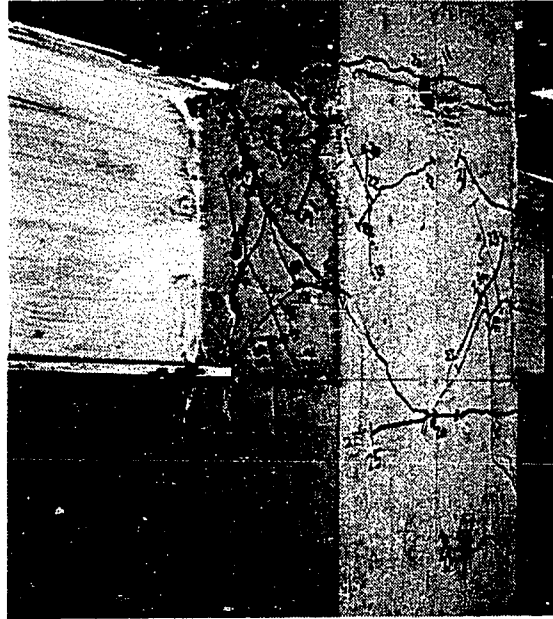


Fig. 4.5 A view of joint 1 after failure.
(Upper left flange in tension in cycles L1 and U1)

unloading there was no residual drift. The specimen was then loaded in the reverse direction to a load of 11.96k and unloaded. The behavior was similar to cycle L1, except that there was some residual drift which was recovered with negligible load application (Fig. 4.4). The loading curve in cycle U1 followed cycle L1. First flexural cracks appeared at the tips of the tension flanges at a load of 14.8k. Rosette strain gages showed yielding of the steel panel at 16.9 kips and consequently the specimen lost almost its entire stiffness. At a load of 17.6k, a few small diagonal shear cracks appeared away from the joint diagonal on the sides of the concrete column. Signs of concrete crushing on the compression flanges were noted and cracks Cr radiated from the tips of these flanges. The specimen carried

17.8 kips at 2% drift. Prior to reaching the ultimate load, local yielding of the flanges near the column was noted in the west beam which carried about 10-23% more load than the east beam. Also, concrete crushed against both compression flanges and a gap of about 3/16-in. was noted under (or above) the tension flanges. At the ultimate load of 18.3 k a drift of 3.3% was reached. Under loading in the other direction i.e. cycle U2, the specimen was less stiff. However, the cracking behavior was very similar to that in Cycle U1. The specimen carried slightly higher load in this cycle. The load-drift plot shows good energy dissipation.

Figure 4.6 shows the load-drift plot for specimen 2 in which a 7/16-in. FBP was used. In cycle L1, specimen 2 was slightly stiffer than specimen 1. Two flexural cracks appeared at this stage; one at the level of the tension flange and the other a few inches inside the joint (Figs. 4.7 and 4.8). In the other direction, cycle L2 there was almost no residual drift. As the load was increased in cycle U1, first diagonal shear cracks appeared at a load of 13.2k and cracks td initiated at the tips of the tension flanges. Cracks tr were noted at a load of 20.7k (Fig. 4.8). Some signs of concrete crushing against the top compression flange were also observed, followed by cracks Cr radiating from the tips of the compression flanges. At a load of 26.2k yielding was recorded in the steel panel and a few more Cr cracks developed near the compression flanges (Fig. 4.8). Near the ultimate load the beam loaded upward carried about 15% more load than the other. Concrete above the compression flanges was crushed and spalled and a 1/4-in. gap was noted under (or above) the tension flanges. A large permanent drift was observed upon unloading. The response of the specimen in cycle U2 was soft at first but it regained stiffness as the cracks closed. Pinching

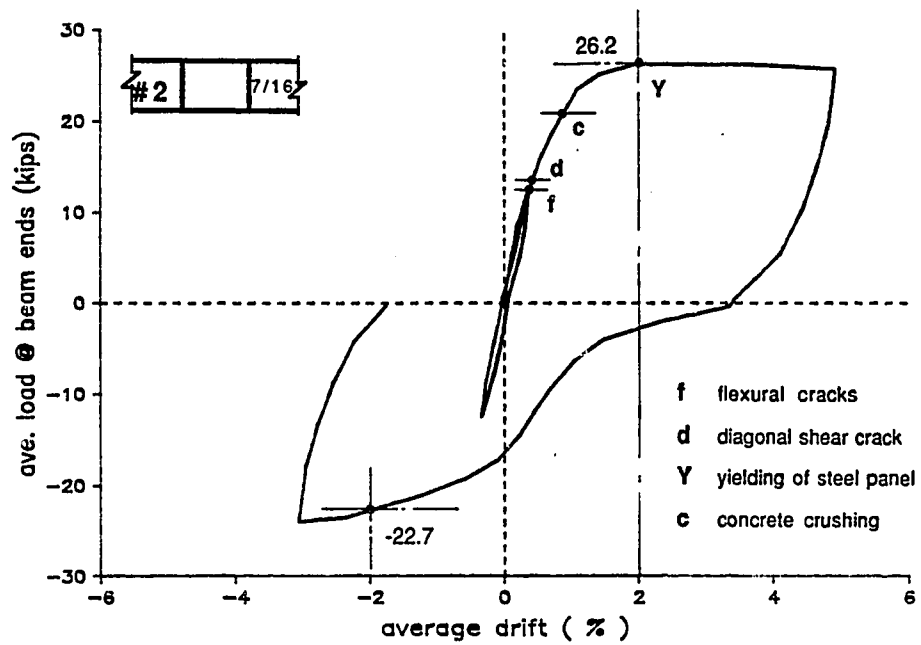


Fig. 4.6 Load-drift plot of specimen 2.

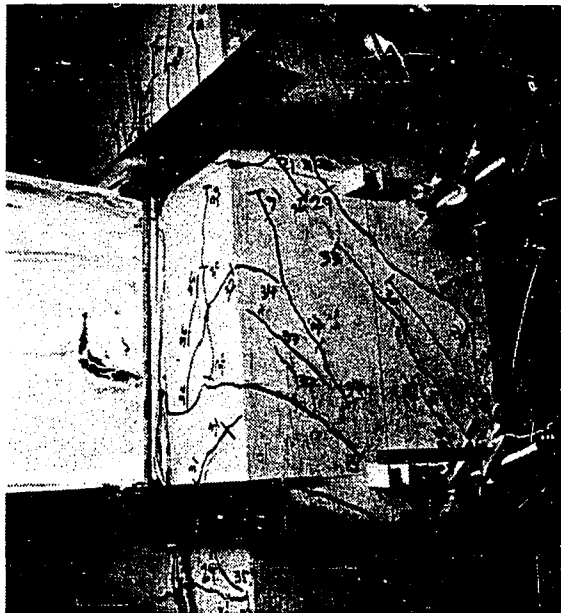


Fig. 4.7 A view of joint 2 after cycle U1.
(Upper left flange in compression)



Fig. 4.8 A view of joint 2 after failure.
(Top flange in compression in L1 and U1)

of the hysteresis loop can be seen in Fig. 4.5, however, the specimen still showed good energy dissipation. The specimen carried slightly lower load in cycle U2. Cracking behavior was pretty similar to that of cycle U1 resulting in a symmetrical cracking pattern.

Specimen 3. Specimen 3 was the first of the seven tests in the second group and had a plain steel beam embedded in the concrete column. The load-drift plot is shown in Fig. 4.9. In cycle L1 no distress was noted and the specimen showed almost no residual drift upon unloading. Unlike specimen 1, almost no residual drift was recorded after cycle L2. First flexural cracks appeared in cycle U1 at a load of 15.1k (Fig. 4.11). Yielding of the steel panel was recorded and subsequently the specimen lost substantial stiffness. At a load of 16.6k (.63%

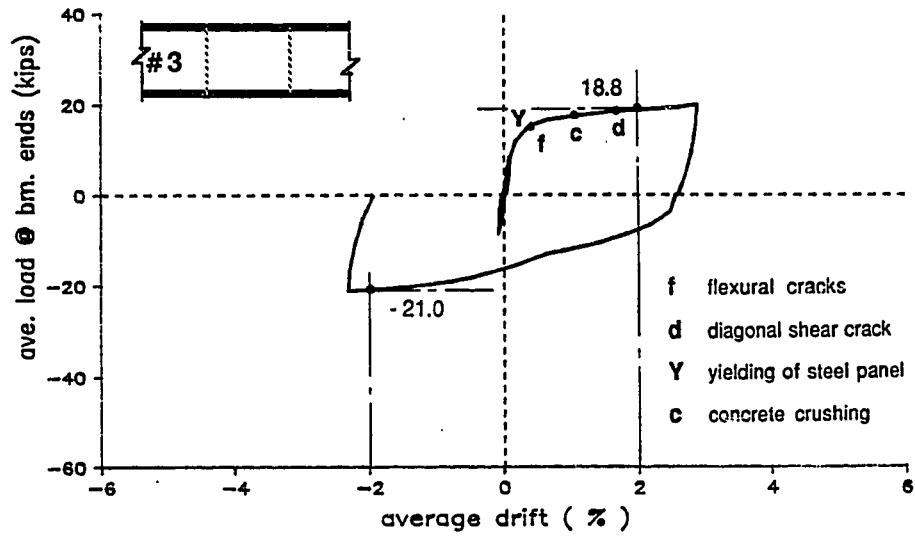


Fig. 4.9 Load-drift plot of specimen 3.

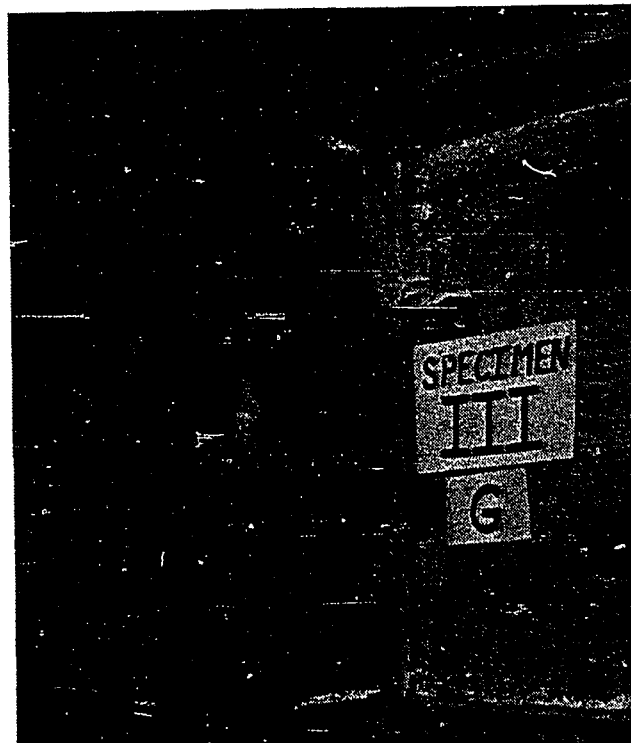


Fig. 4.10 A view of joint 3 after failure.
(Top flange in tension in L1 and U1)

drift), cracks tr originated from the tips of the tension flanges (Fig. 4.10). Crushing of the concrete against the compression flanges was noted at a load of 17.4k. A couple of small diagonal shear cracks (Fig. 4.11), were observed on each column side at a load of 18.7k. The specimen carried an average load of 18.8k at 2% drift. A few small yield lines near the flange-web junction outside the joint were noted both in the flanges and the web at a load of 19.1k (Fig. 4.10). Crushing of the concrete was more pronounced at this stage and a gap of about 3/16-in. was noted under (or above) the tension flanges. The specimen exhibited greater stiffness in the post-yield regime compared to specimen 1. This could be attributed to thicker beam flanges in specimen 3. Near the ultimate load, the beam loaded upward carried about 28% more load than the other beam. Upon unloading, the specimen showed large residual drift. In cycle U2, a load of 21.0 kips was reached at 2% drift. Cracking was essentially the same as in cycle U1. The load-drift plot indicates large energy dissipation characteristics.

Specimens 4 and 5. Specimens 4 and 5 were designed to study the effect of face bearing plates and their thickness. Figure 4.12 shows the load vs. drift plot for specimen 4 which had a thin, 3/8-in. A36 FBP. In cycle L1 the specimen was loaded to 14.5k when first diagonal shear crack appeared on the joint diagonal (Fig. 4.13). A small tr crack also radiated from the tension flanges as shown in Fig. 4.15. The initial stiffness of the specimen was almost the same as that of specimen 3. In cycle U1, the specimen was less stiff than in cycle L1. Yielding in the steel panel was recorded at a load of 14.1k. Flexural cracks near the tension flanges were also noted at this load level. At a load of 24.3k old tr cracks progressed further and new tr and td cracks appeared on the column faces (Fig. 4.15). A few ds

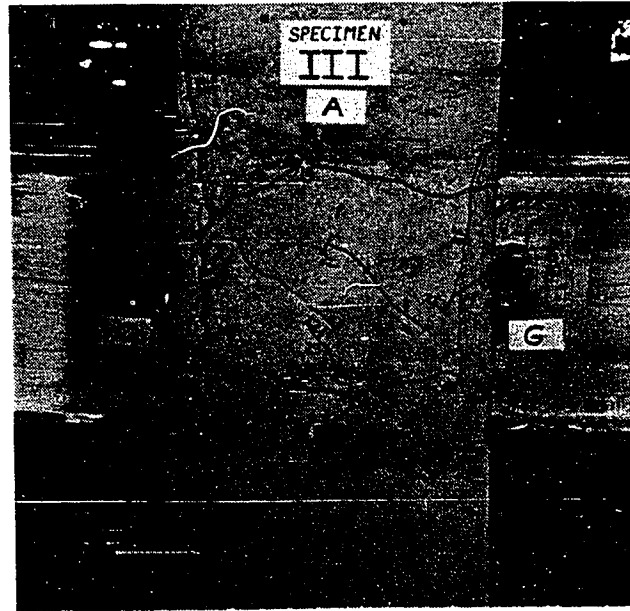


Fig. 4.11 Joint 3 after failure.
(Left beam loaded upward in L1 and U1)

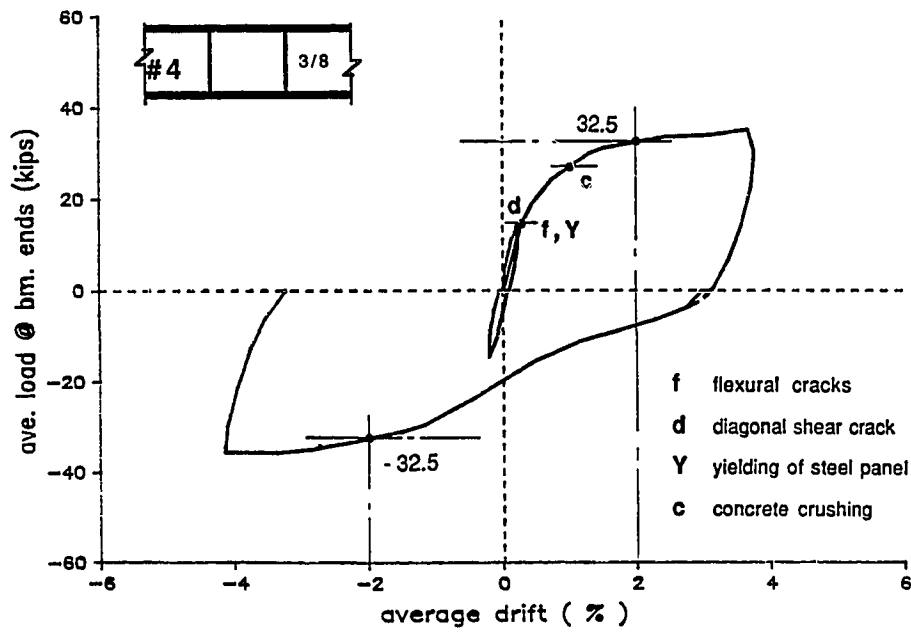


Fig. 4.12 Load-drift plot of specimen 4.

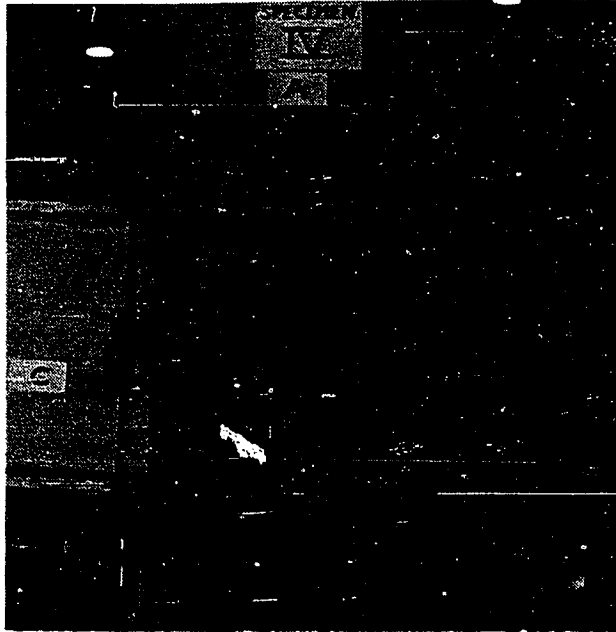


Fig. 4.13 Joint 4 after cycle U1.
(Upper left flange in compression)

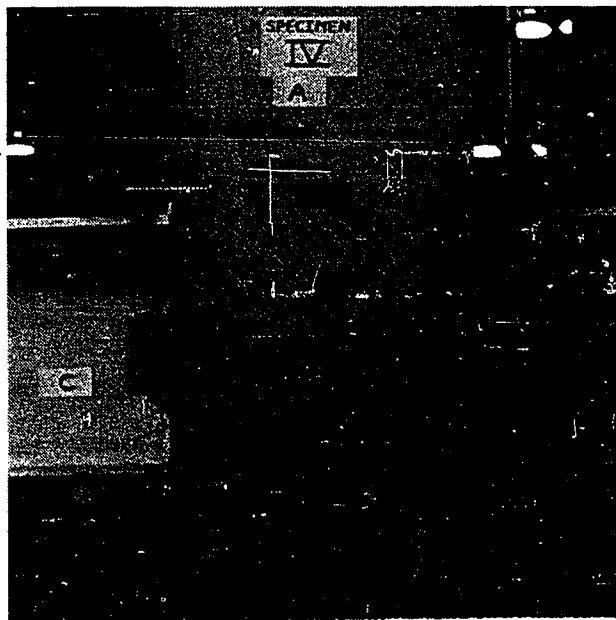


Fig. 4.14 Joint 4 after failure.
(Left beam loaded upward in L1 and U1)

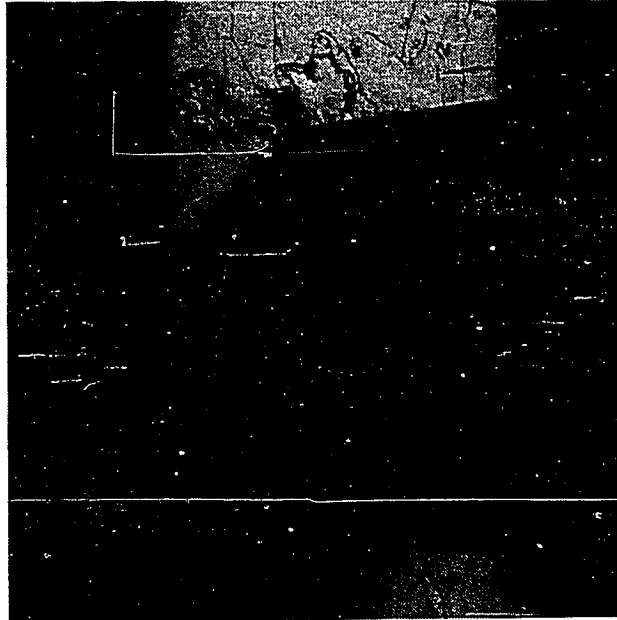


Fig. 4.15 Joint 4 after failure.
(Top flange in compression in L1 and U1)

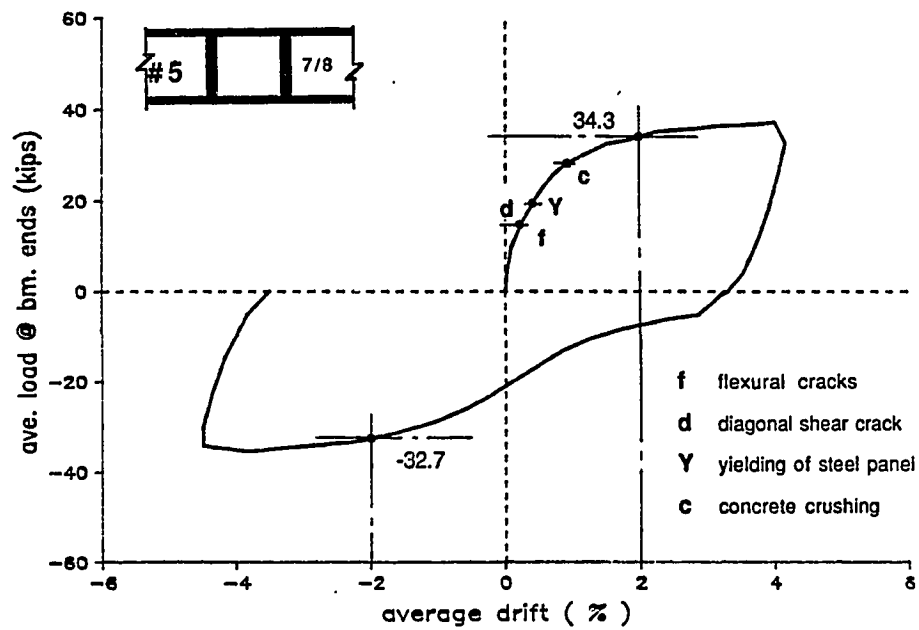


Fig. 4.16 Load-drift plot of specimen 5.

cracks were also noted on column sides. Concrete crushing against the compression flanges was noted. The specimen carried average 32.5 kips at 2% drift. Yielding was noted in the FBP located in the beam loaded upward which was confined near the compression flange at the weld toe and is pictured in Fig. 4.15. Upon further loading these FBPs were noticeably bent at the weld toe. Also, yield lines were noted in the web outside the joint, for the beam loaded upward only (Fig. 4.15). At a load of 35.3k, cracks Cr arose from the tips of the compression flanges and concrete crushing was eminent against these flanges. At the ultimate, upward load was about 23% higher than the downward load. A 5/16-in. gap was noted near (or above) the tension flanges. In the reverse direction, cycle U2, the stiffness of the specimen increased as the cracks closed. The specimen carried 32.5 kips at 2% drift, the same load as in cycle U1. The cracking and yield-lines pattern were pretty symmetrical as pictured in Fig. 4.14.

A thick, 7/8-in. FBP of Grd. 50 material was used in specimen 5. Figure 4.16 shows the load-drift plot for this specimen. The low level load cycle was omitted in this test. The cracking pattern as well as the general specimen behavior was very similar to that of specimen 4. However, no yielding or distress was noted in the FBPs. Diagonal shear cracks and flexural cracks appeared at about the same load level as in specimen 4. The web yielding, however, was recorded at a higher load, 19.6 kips. Figures 4.17 and 4.18 show the crack patterns. At 2% drift the load was 34.3 kips, slightly higher than specimen 4. Web yielding outside the joint for the beam carrying a higher load, started at a load of 30.1k and was more prominent than in specimen 4 (Fig. 4.18). The ultimate load was 37.3k. Beam

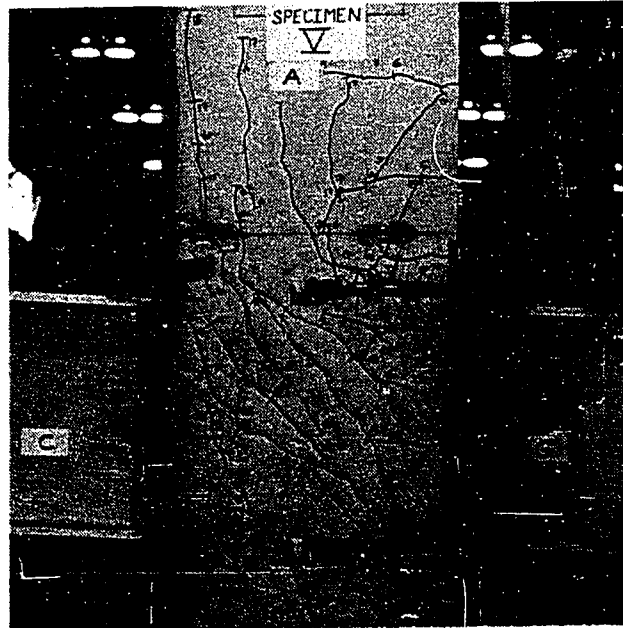


Fig. 4.17 Joint 5 after cycle U1.
(Upper left flange in compression)

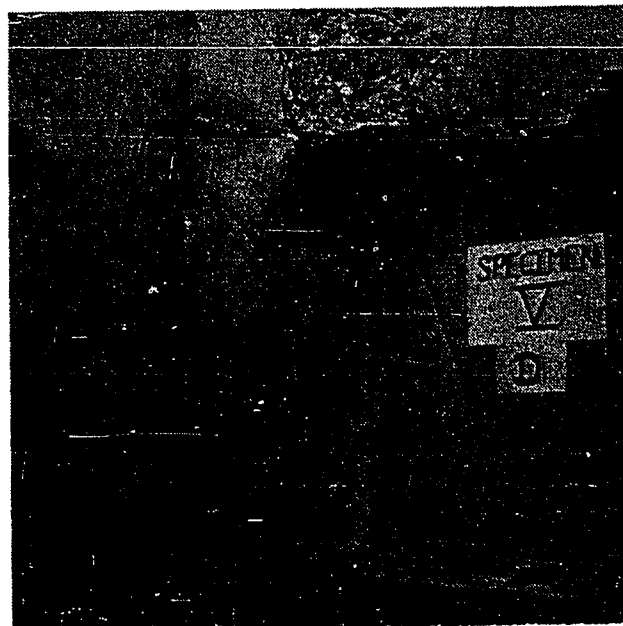


Fig. 4.18 Joint 5 after failure.
(Top flange in compression in L1 and U1)

loaded upward, carried about 30% higher load than the other beam. A 3/8-in. gap was recorded under (or above) the tension flanges.

Specimen 6. Specimen 6 was designed to study the effect of the steel panel, strengthened with doubler plates. Styrofoam was placed inside the FBPs to preclude transfer of flange forces to the concrete panel through them. The load-drift plot is shown in Fig. 4.19. The initial stiffness was slightly higher than specimen 5. First flexural cracks appeared at a load of 16.1k. In cycle U1, the initial stiffness was lower than in cycle L1. First, diagonal shear cracking was noted at a load of 20.6k, away from the joint diagonal (Fig. 4.20). At a load of 34.8k more ds cracks appeared near the joint diagonal. Cracks tr and td also radiated from the tips of the tension flanges. Signs of concrete crushing against the top compression flange were observed at a load of 38.7k and the stiffness dropped substantially. Yield lines in the web and the compression flange, adjacent to the joint were noted in both beams. These yield lines appeared earlier than expected, perhaps due to the residual stresses caused by welding and flame cutting of the plates. Yield lines were also noted in the so called FBPs, perhaps due to the compressive stresses and can be seen in Fig. 4.21. At 41.9k cracks Cr appeared from the tips of the compression flanges. A flat plateau was reached at an average load of 45.3 kip at 2% drift. At ultimate load, the upward load was about 20% higher than the downward load. A gap of about 1/2-in. was noted under (or above) the tension flanges. Crushing of concrete against the compression flanges was severe (Fig. 4.22), hence the specimen was unloaded. In cycle U2 almost the entire residual drift was recovered before the stiffness increased. The resulting S-shaped hysteresis loop indicated a reduction in energy dissipation

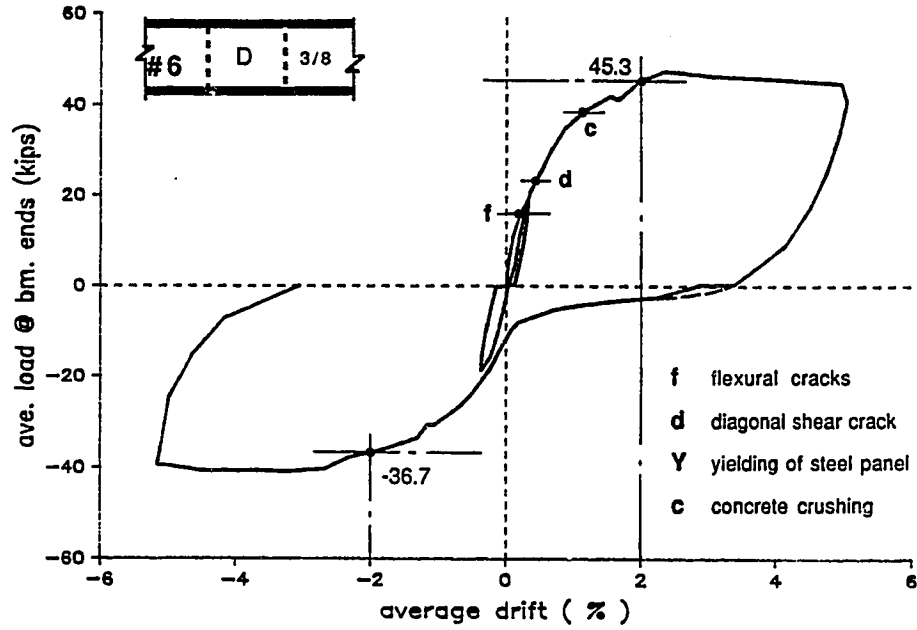


Fig. 4.19 Load-drift plot of specimen 6.

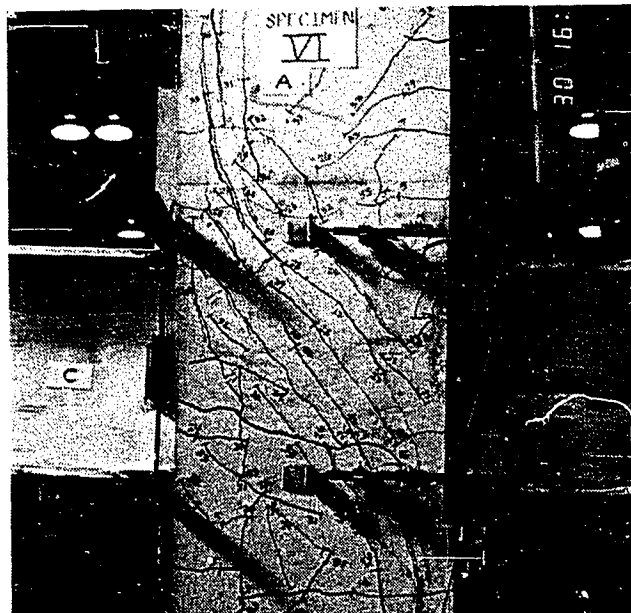


Fig. 4.20 Joint 6 after cycle U1.
(Upper left flange in compression)

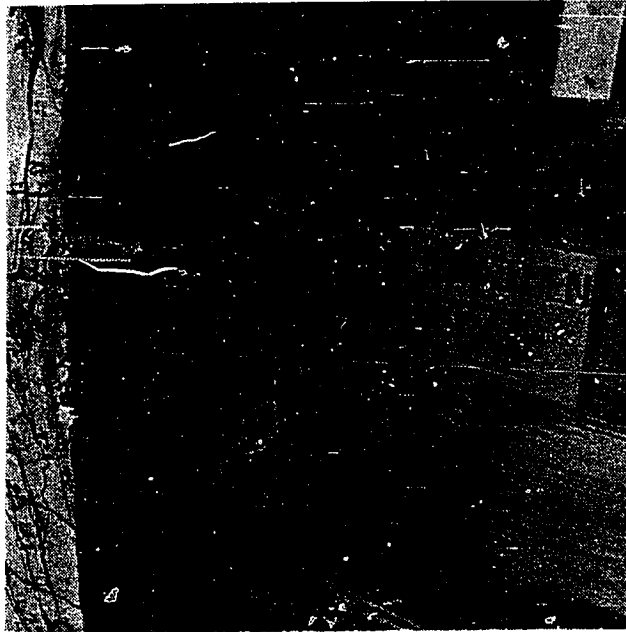


Fig. 4.21 Joint 6 after failure.
(Top flange in compression in L1 and U1)

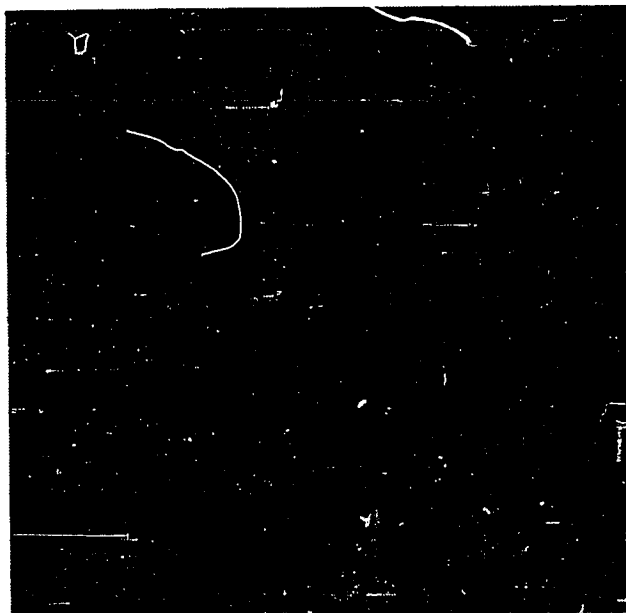


Fig. 4.22 Joint 6 after failure.
(Top flange in compression in L1 and U1)

capacity of the specimen. The specimen carried substantially less load in cycle U2, 36.7 kips at 2% drift.

Specimen 7. A 12-in. wide, 7/8-in. thick, face bearing plate was used in this specimen. The load-drift plot is shown in Fig. 4.23. Load cycle L1 was omitted in order to avoid damaging the embedded concrete strain gages. The initial stiffness of the specimen was the same as that of specimen 6. First ds and flexural cracks appeared at a load of 15.7k (Figs. 4.24 and 4.25). Yielding of the steel panel was recorded at 18.6 kips. As the load was further increased, more flexural cracks appeared between the flanges and away from the joint. Cracks radiating from the tension flanges were absent except for cracks td, arising from near the flange tips, which were noted at a load of 36.2k. Concrete crushing against the compression flanges was also seen at this stage. The load was 41.2 kips at 2% drift. Yield lines were noted in the web and the compression flange (Fig. 4.25). Yield lines were also seen in the FBPs near the tips of the compression flange of the beam loaded upward (See Fig. 4.25). At a load of 42.4k cracks Cr extended from the tips of the FBPs (not the tips of the compression flanges) and penetrated to the column edges (Fig. 4.26). Near the ultimate load, the beam loaded upward carried about 20% more load than the other beam. A 3/8-in. gap was measured under (or above) the tension flanges. The behavior of the specimen in cycle U2 was similar to that of specimens 4 and 5. The specimen carried an average 36.7 kips at 2% drift, which was slightly less than the corresponding load in cycle U1.

Specimen 8. Face bearing plates extended 4 in. above and below the beam in this specimen. The load - drift plot is shown in Fig. 4.27. The initial stiffness was much higher than the other specimens. First diagonal shear cracks appeared at a

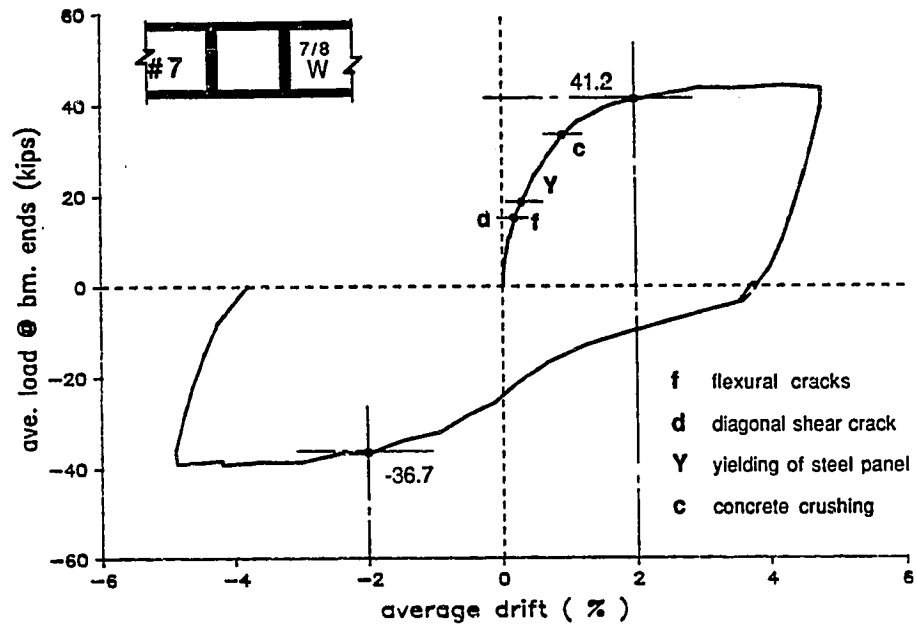


Fig. 4.23 Load-drift plot of specimen 7.



Fig. 4.24 Joint 7 after cycle U1.
(Upper left flange in compression)

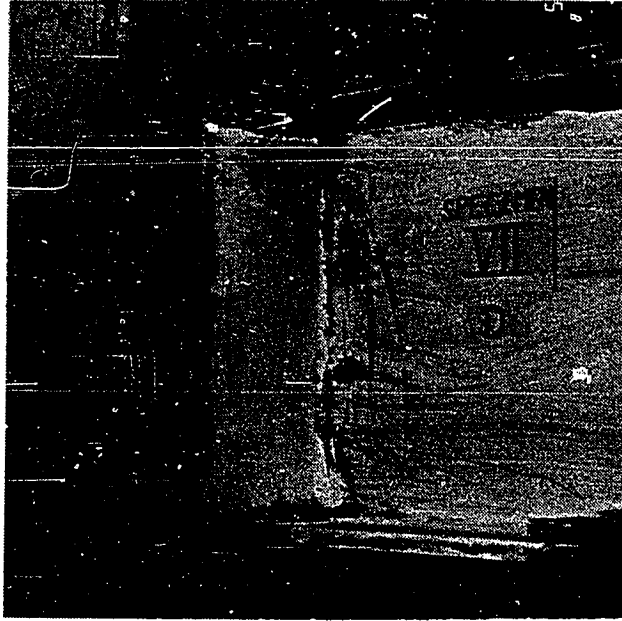


Fig. 4.25 Joint 7 after failure.
(Top flange in compression in L1 and U1)

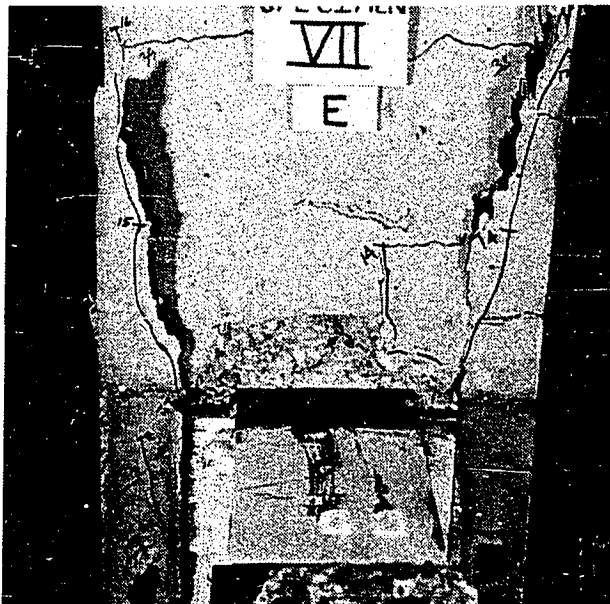


Fig 4.26 Joint 7 after failure.
(Top flange in compression in L1 and U1)

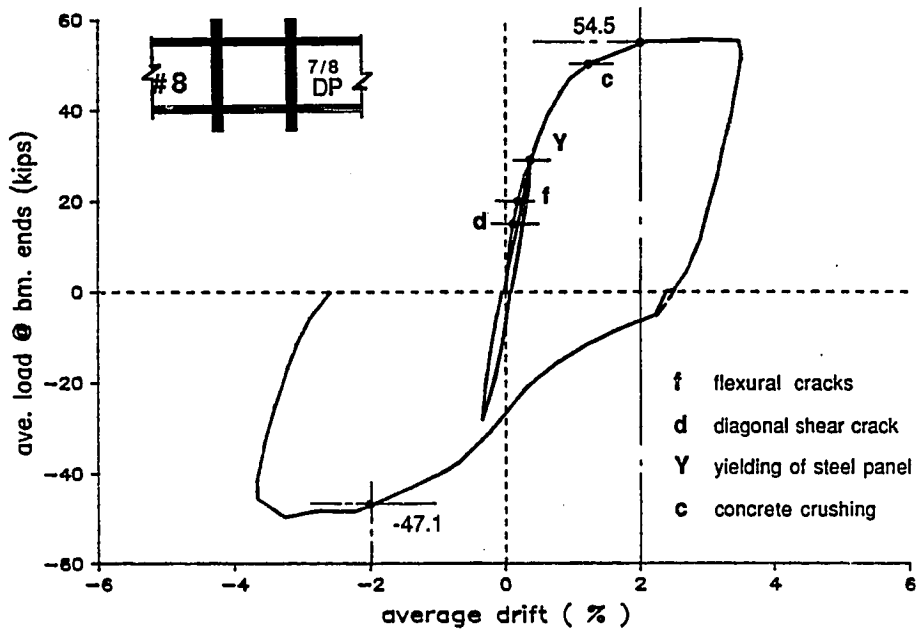


Fig. 4.27 Load-drift plot of specimen 8.

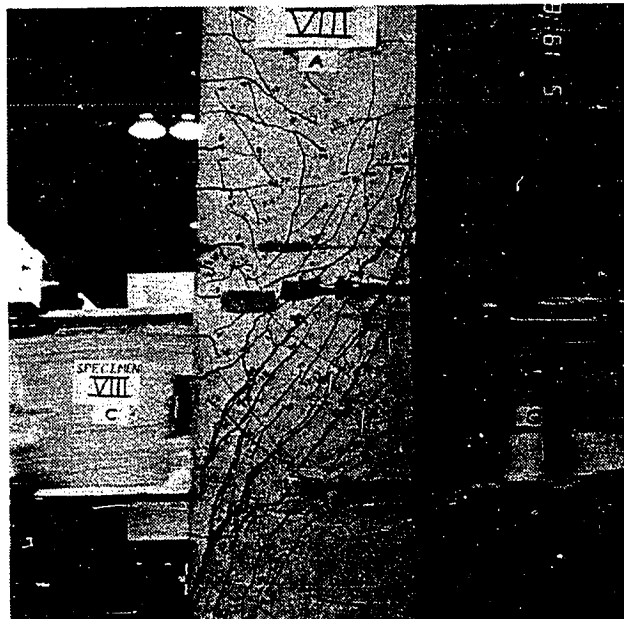


Fig. 4.28 Joint 8 after cycle U1.
(Upper right flange in compression)

load of 15.3k. Flexural cracks were noted at a load of 20.2k at the tips of the extended FBPs near the tension flanges. At a load of 25.4k cracks originated from the tips of the tension flanges as seen in Fig. 4.30. In cycle U1, steel panel yielded at a load of 29.1 kips. Upon further loading, more ds and flexural cracks appeared on the column sides and faces (Fig. 4.28). Crushing of the concrete near the compression flanges was noted at a load of 50.2k when the specimen started losing its stiffness. At 2% drift, the specimen was carrying 54.5 kips load. Near the ultimate, the beam loaded upward carried about 20% higher load than the beam loaded downward. Yield lines on the web and compression flanges outside the joint were extensive (Figs. 4.30 through 4.32). The built-up beams reached almost 90% of their flexural capacity in this test. Extended face bearing plates near the compression flanges also showed yield lines which can be seen in Fig. 4.31. A vertical movement of 1/4-in. was recorded for the extended FBPs near the tension flanges. The specimen was unloaded when severe crushing and spalling of concrete near the compression flanges was noticed. The specimen carried considerably less load in cycle U2, 47.1 kips at 2% drift.

Specimen 9. An 11-1/2 x 13-in. hole was cut into the beam web to weaken the steel panel in Specimen 9. The load-drift plot for the specimen is shown in Fig. 4.33. Cycle L1 was omitted in this test. The initial stiffness of the specimen was the same as in specimen 5. First flexural cracks appeared near the tension flanges at a load of 15.0k. Cracks propagated from the tips of the tension flanges at a load of 18.0k (Fig. 4.35). First diagonal shear cracks appeared on the joint diagonal at a load of 20.4k. More cracks appeared as the load was increased (Fig. 4.34). Concrete crushing near the

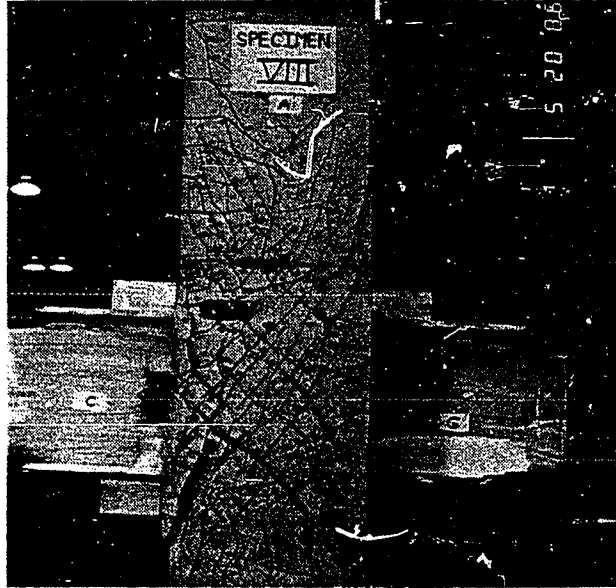


Fig. 4.29 Joint 8 after failure.
(Upper right flange in compression in L1 and U1)

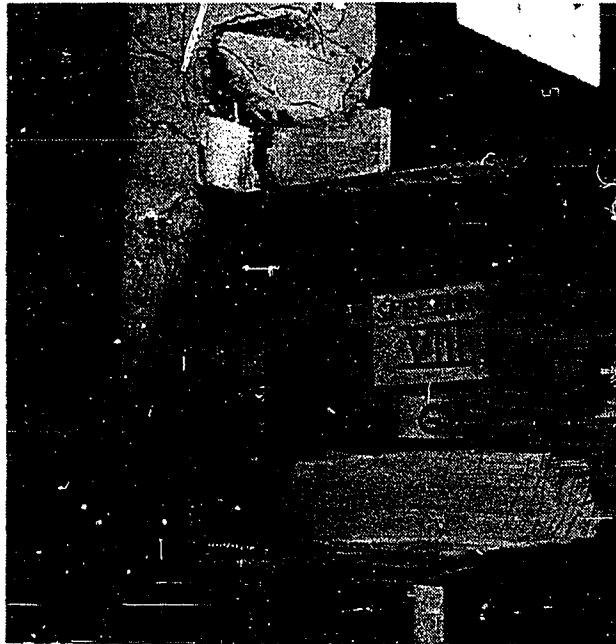


Fig 4.30 Joint 8 after failure.
(Top flange in compression in L1 and U1)

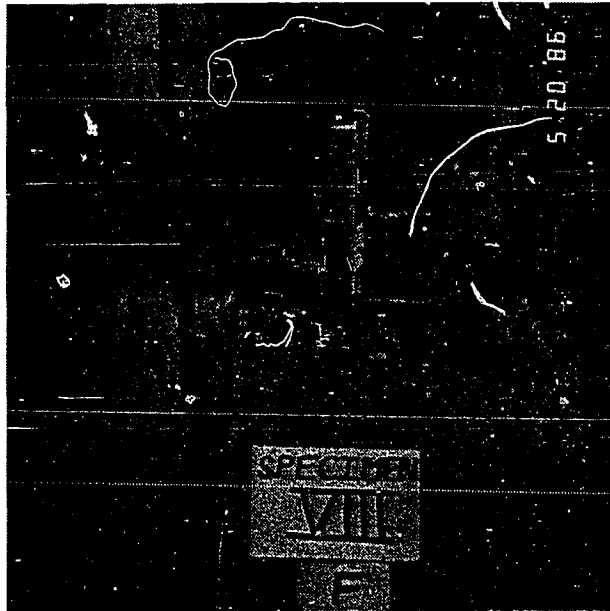


Fig. 4.31 Joint 8 after failure.
(Bottom flange in compression in L1 and U1)

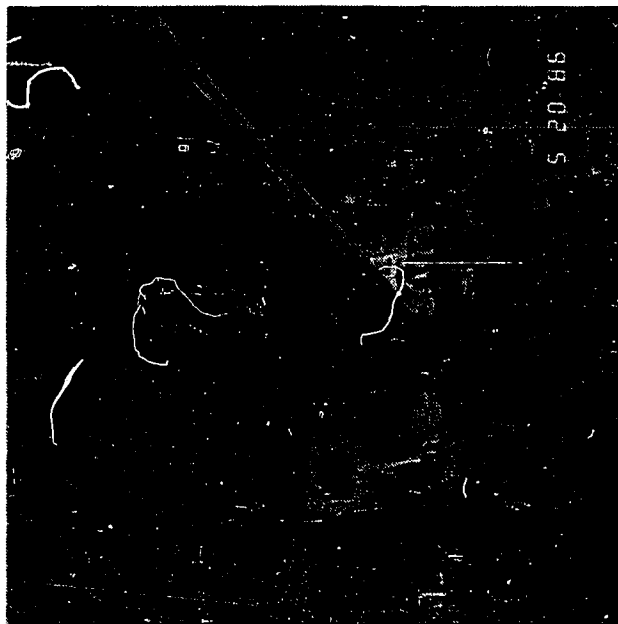


Fig. 4.32 Joint 8 after failure.
(Top flange in compression in L1 and U1)

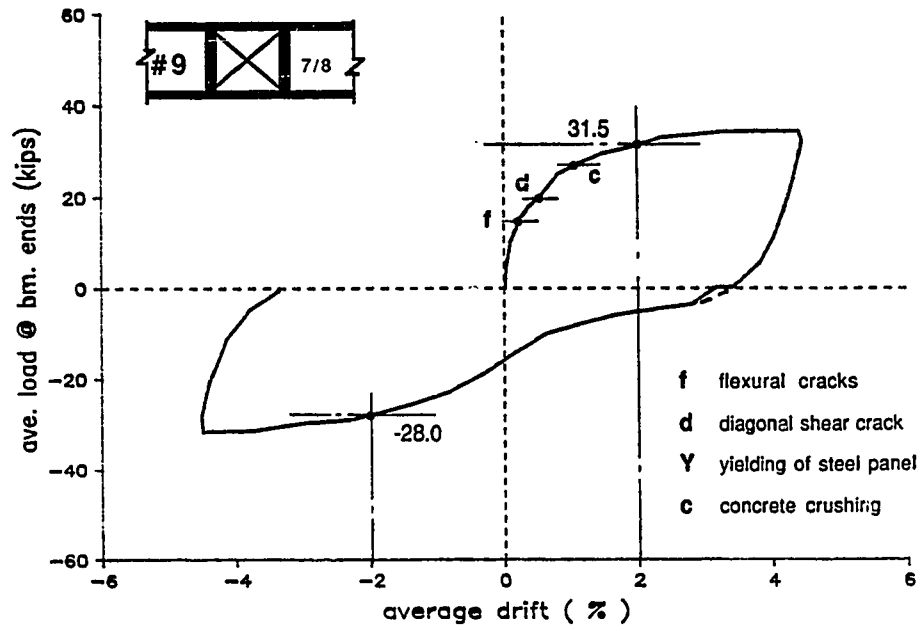


Fig. 4.33 Load-drift plot of specimen 9.

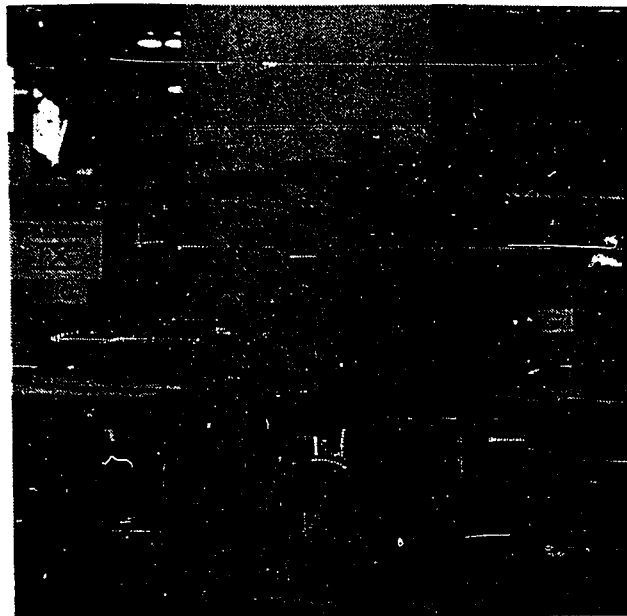


Fig. 4.34 Joint 9 after cycle U1.
(Upper left flange in compression)

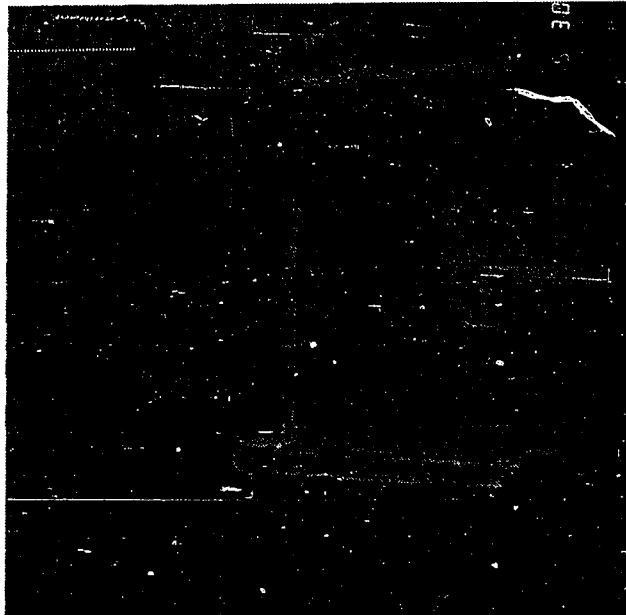


Fig. 4.35 Joint 9 after failure.
(Top flange in compression in L1 and U1)

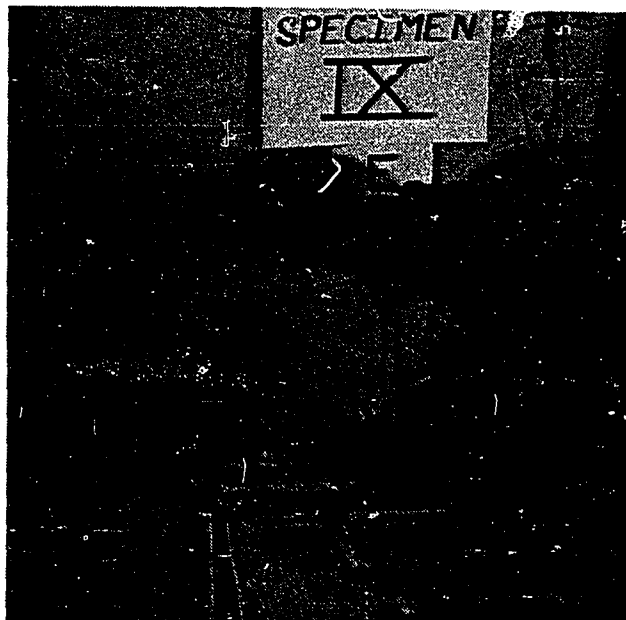


Fig. 4.36 Joint 9 after failure.
(Top flange in compression in L1 and U1)

compression flanges was noted at a load of 27.1k. At a drift of 2%, the specimen carried average 31.4 kips. Cracks Cr radiated from the tips of the compression flanges to the column edges (See Fig. 4.36). Near the ultimate load the beam loaded upward carried about 26% more load than the other beam. A gap of 3/8-in. was recorded under (or above) the tension flanges. Yield lines were noted in the web outside the joint (Fig. 4.35). The stiffness characteristics of the specimen in cycle U2, were similar to specimen 5. At 2% average drift, the specimen carried 28.0 kips, about 90% of that in cycle U1.

4.2 Stiffness Characteristics

In order to evaluate the stiffness characteristics of the steel beam to concrete column connections, the relationship between joint shear and joint distortion need to be studied. The joint distortion and its various components were measured directly. However, shear forces must be computed from the forces transmitted to the joint by the adjoining members, as shown in Fig. 1.8(b), assuming mechanism of transfer of flange forces to the concrete panel is known. For the purposes of comparison, the stiffness characteristics are presented in terms of load vs. joint distortion. This relationship should be qualitatively similar to the shear vs. joint distortion diagram and is not dependent on shear force computations.

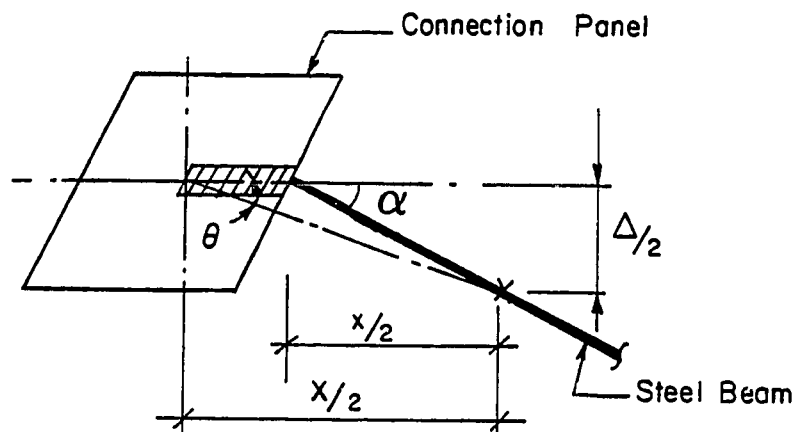
4.2.1 Components of Joint Distortion. The beam deflection or drift is due to the elastic flexural deformation of members and to joint distortion. The total distortion in the joint is comprised of steel panel separation and shear distortion of the connection panel. Due to strain incompatibility of steel and concrete panels, the shear distortion of the two panels is

not the same. A definition of the terms used here is given in the following.

- a) Drift - ratio of the total relative vertical movement (Δ) between a point on each beam, located at an equal distance from the column centerline, to the distance between these two points (X). It is calculated as a percentage and related directly to the interstory lateral drift in buildings.
- b) Member Contribution - contribution of the elastic flexural deformation of the beams and columns, as shown in Fig. 3.23(a), to drift.
- c) Total Joint Distortion (TJD) - total distortion in the joint due to panel separation and panel shear.
- d) Panel Separation (PSep) - drift caused by the rigid body motion of the steel beam (or panel) with respect to the column, as shown in Fig. 3.23(b).
- e) Panel Zone Distortion (PZD) - shear distortion of the connection panel. Since the shear distortion in the steel and concrete panels differ in magnitude, PZD is considered equal to the greater of the two.
- f) Steel Panel Distortion (StlPD) - shear distortion of the steel panel in the joint.
- g) Concrete Panel Distortion (ConcPD) - shear distortion of the concrete panel in the joint.
- h) Relative Beam Inclination (RBI) - inclination of the steel beam just outside the joint relative to the centerline of the concrete column at the joint.

As defined above, the TJD, consisting of panel separation and steel panel shear distortion, causes drift in

excess of the member contribution. Whereas, the drift caused by the P-Sep is not influenced by the size of the joint, that caused by the StlPD does. As illustrated in Fig. 4.37, the StlPD will be smaller as the joint size decreases, i.e. ratio X/x , increases. To account for this effect, the TJD as well as the StlPD as computed from the measured drift were corrected for the joint size, as indicated in Fig. 4.37. However, this correction could not be made for specimens 1 and 2, because the instrumentation was not the same as in specimens 3-9.



Corr. Distortion, $\alpha = \theta \frac{X}{x}$

Fig. 4.37 Joint size correction for shear distortion.

The total joint distortion in the test specimens was calculated as follows:

$$TJD = (\text{Drift} - \text{Member Contribution} - \text{PSep}) X/x + \text{PSep} \quad (4.1)$$

where member contribution was computed as described in Sec. 4.2.2 and panel separation was measured by the LVDT's near the faces of the concrete column as described in Chapter 3. The TJD as computed by Eq. 4.1 compared well in general with that measured using the electronic digital inclinometer. The steel panel shear distortion was then computed as follows.

$$StlPD = TJD - \text{PSep} \quad (4.2)$$

Again, this computed value compared very well with that measured using the electronic digital inclinometer.

The relative beam inclination (RBI) for the test specimens was measured using a frame mounted on the beam near the joint, as shown in Fig. 3.25 and described in Chapter 3. The RBI includes the panel separation and the difference in the shear distortions of the steel and concrete panels. Hence the concrete panel distortion at the centerline of the column sides was computed as

$$\text{ConcPD}(\text{CL}) = TJD - \text{RBI} \quad (4.3)$$

The concrete panel distortion was also determined at the faces of the concrete column by measuring the absolute rotation of these faces using the digital inclinometer. The ConcPD(face) was then computed by deducting the column rotation at the joint due to its

elastic flexural deformation. These measurements and computations were not made for specimens 1 and 2.

As mentioned above, the total joint distortion was computed from the measured drift by subtracting the member contribution. Since the member contribution was a small part of the drift, the TJD should be quite accurate. However, the same may not be true for its components, especially at early loading when the magnitudes of distortion were small. The panel separation, which was a key in determining other components, may not be so accurate the way it was measured. Figure 4.39 shows the typical arrangement used for measuring panel separation. There were two sources of error in this arrangement; a) flexural deformation of column under the beam, and b) steel panel distortion. The flexural tension cracks and the flexural compressive strains in the concrete column between points A and the beam soffit (See Fig. 4.39) overestimate the panel separation. The relative magnitude of error is large when the distortions are small. For instance, a 0.01-in. wide flexural tension crack would cause 0.001 rad. (i.e. 0.1%) excess panel separation. The second source of error was the steel panel distortion. As shown in Fig. 4.39, St1PD increases measured P_{Sep} and results in a smaller St1PD (as per Eq. 4.2). The magnitude of error perhaps ranged from 20 to 35% of the St1PD. Due to these inaccuracies, the composition of TJD in quantitative terms may be misleading, and hence this data is presented in a qualitative form only.

4.2.2 Member Contribution. The Member Contribution here refers to the drift caused by the elastic flexural deformation of the beams and columns. The members of the test specimens were over-designed to force the failure in the joint. Hence, there was almost no inelastic flexural deformation in

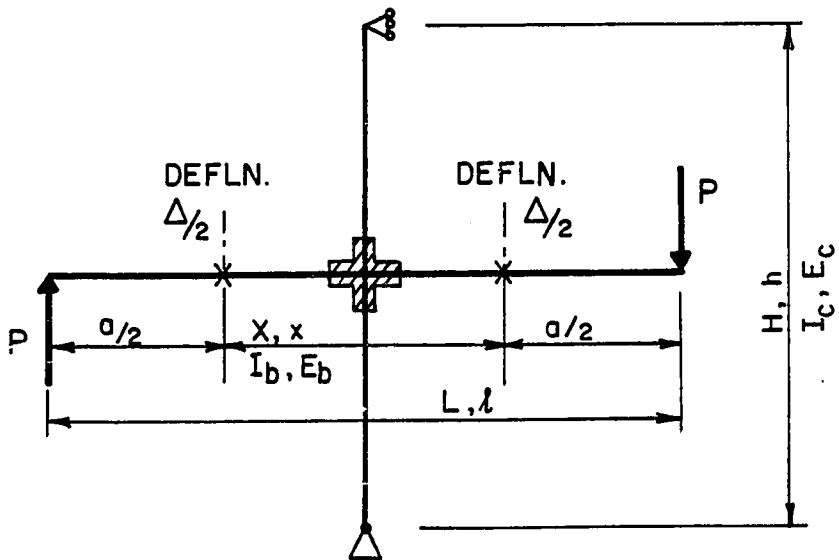


Fig. 4.38 Schematic diagram of the test specimen.

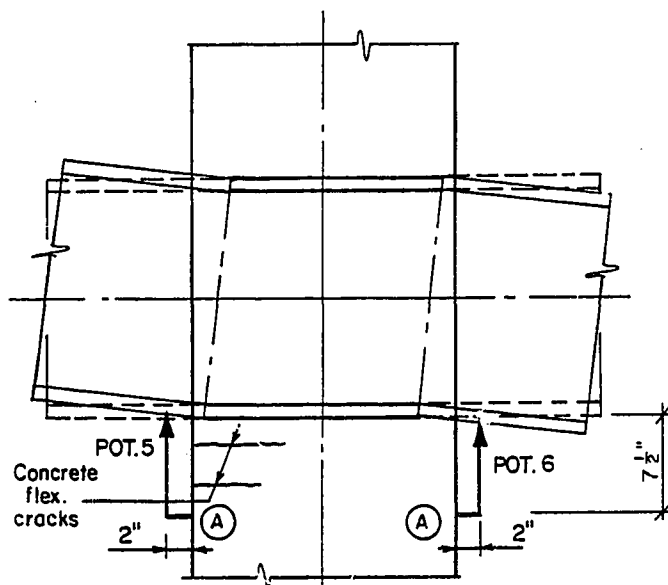


Fig. 4.39 Sources of error in panel separation and steel panel distortion.

these members. However, the column concrete was cracked due to flexural tension at an early load in most of the specimens. Hence, the gross concrete area was not effective in providing stiffness. Also, column reinforcing bars in the joint area slipped in most tests causing additional drift which is recorded as part of panel separation. Member contribution to drift was very small as compared to the overall drift of the test specimens.

A typical test specimen is shown schematically in Fig. 4.38. For the purpose of calculating member contribution, the joint is assumed infinitely rigid. Equal and opposite loads P are applied at the beam ends, a distance L apart. The distance between the two points where deflection is measured, is indicated as X . Height of the column between reaction points is shown as H . These distances in lower case, i.e. l , x and h , represent the corresponding distances after deducting the joint size.

A simple analysis of this sub-assembly would show that the total vertical deflection, Δ , between the two points at a distance X apart, would be

$$\Delta = \frac{PhXL}{12 E_c I_c} \left(\frac{h}{H}\right)^2 + \frac{Px^3 (1 + 1.5 a/x)}{12 E_b I_b} \quad (4.4)$$

and, the corresponding drift would be

$$\Delta/X = \frac{PhL}{12 E_c I_c} \left(\frac{h}{H}\right)^2 + \frac{Px^2(1+1.5 a/x)}{12 E_b I_b} \frac{x}{X} \quad (4.5)$$

The concrete compressive strength, f'_c , for specimens 1 and 2 was 3550 psi at the day of testing. Using the ACI recommendations, the modulus of elasticity, E_c , is equal to $57000\sqrt{f'_c}$, i.e. 3396 ksi. The moment of inertia of the gross transformed section of the column is 6210-in^4 and that of the cracked transformed section is 3260-in^4 . The load at the beam end when the column concrete in flexural tension reaches its modulus of rupture of $7.5\sqrt{f'_c}$ is 8.7 kips. Hence for the purpose of calculating member contribution, the effective moment of inertia, I_c , for the column section in specimens 1 and 2 was taken as 3500-in^4 .

For specimens 3 through 9, the concrete strength, f'_c , on the average was 4000 psi, yielding a modulus of elasticity, E_c , of 3605 ksi. The moment of inertia of the gross transformed section of the column is $18,790\text{-in}^4$ and that of the cracked transformed section is $10,000\text{-in}^4$. The load at the beam end, when the concrete in flexural tension reaches $7.5\sqrt{f'_c}$, is 10.5 kips. Hence, effective moment of inertia, I_c , for the column section was taken as $13,000\text{-in}^4$ for specimen 3 and $10,500\text{-in}^4$ for specimens 4 through 9.

The drift of specimens 1 and 2 was based on the deflections measured at the beam ends, i.e. $X = L$, while that of the specimens 3 through 9 was based on the deflections measured at the two points, distance $X = 5\text{ ft}-2\text{ in.}$ apart. Using the values of E_c and I_c as mentioned above, the member contribution to drift for any load P at the beam ends, was calculated based on Eq. 4.5, as follows

$$\text{Specimens 1 \& 2 : Member Contribution} = P/66\% \quad (4.6a)$$

$$\text{Specimen 3 : Member Contribution} = P/183\% \quad (4.6b)$$

$$\text{Specimens 4 through 9 : Member Contribution} = P/159\% \quad (4.6c)$$

4.2.3 Load vs. Joint Distortion Relationship. In this section the total joint distortion (TJD) and its various components are described. Since specimen 5 was designed as a reference test for the evaluation of most parameters, its results are presented first, followed by specimens 4, 3 and 6 through 9. The results of pilot tests 1 and 2 are presented last. The composition of joint distortion for each test is summarized in Table 4.2 for better comparison

Specimens 5 and 4. Figure 4.40 shows plots of total joint distortion and its two main components, panel separation and steel panel distortion, for specimen 5 in which a thick FBP was used. A comparison of TJD in Fig. 4.40 and drift in Fig. 4.16 clearly show the similarity of two plots due to a small member contribution. This similarity was noted in all the specimens. The joint in specimen 5 was extremely rigid in the beginning but started softening as the load was increased above 10 kips, presumably due to breaking bond between the steel beam and concrete and bending of FBPs. Upon further loading the steel panel yielded at 19.6 kips when the TJD was 0.29%. The joint gradually started losing stiffness as more and more diagonal shear cracks appeared on the concrete panel. It reached a load of 34.1 kips at 2% TJD. Upon further loading more cracking and crushing was noted. However, the joint not only maintained its strength but showed a small increase, before the specimen was unloaded at 4.25% TJD.

Panel separation accounted for almost the entire TJD at the low levels of load but soon dropped to 80%. After the steel panel yielded the contribution of P_{Sep} further dropped to 60% and stayed almost constant thereafter. Steel panel distortion, thus, contributed about 40% to the TJD. Figure 4.41 shows plots of

Table 4.2 Summary of Joint Distortion (Cycle U1)

Specimen No.	Init. Stiff. Related to Joint Moment (K'/rad.)	Panel Separation (% of TJD)		Stl. Panel Distortion (% of TJD)		Conc. PD (cL) (% of TJD)		Conc. PD (face) (% of TJD)	
		upto $\frac{1}{2} P_{max}$	$\frac{1}{2} P_{max}$ to P_{max}	upto $\frac{1}{2} P_{max}$	$\frac{1}{2} P_{max}$ to P_{max}	upto $\frac{1}{2} P_{max}$	$\frac{1}{2} P_{max}$ to P_{max}	upto $\frac{1}{2} P_{max}$	$\frac{1}{2} P_{max}$ to P_{max}
1	25,400	—	—	—	—	0	0	—	—
2	38,500	—	—	—	—	25	25	—	—
3	149,000	80	80-40	20	20-60	0	0	0	0-60
4	146,200	60	60	40	40	25	12	45	45
5	143,400	80	80-60	20	20-40	0	20	40	40
6	193,500	100	90	0	10	0-10	10-55	40-45	45-55
7	197,800	100-80	80-60	0-20	20-40	0-20	20-40	40	40-25
8	369,700	100	100-60	0	0-40	30	30-80	80	80
9	146,200	55	55	45*	45*	0-20	20-35	45	45

*Out-out steel panel

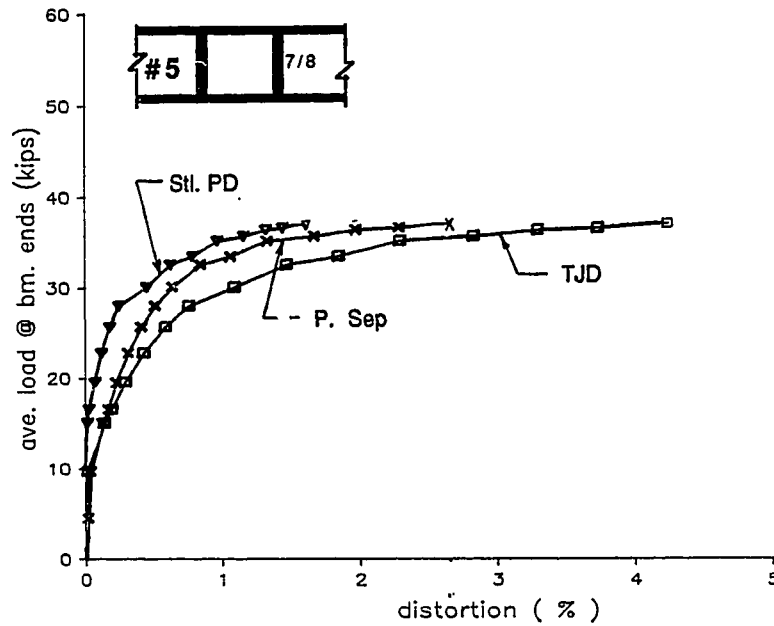


Fig. 4.40 Composition of joint distortion in specimen 5

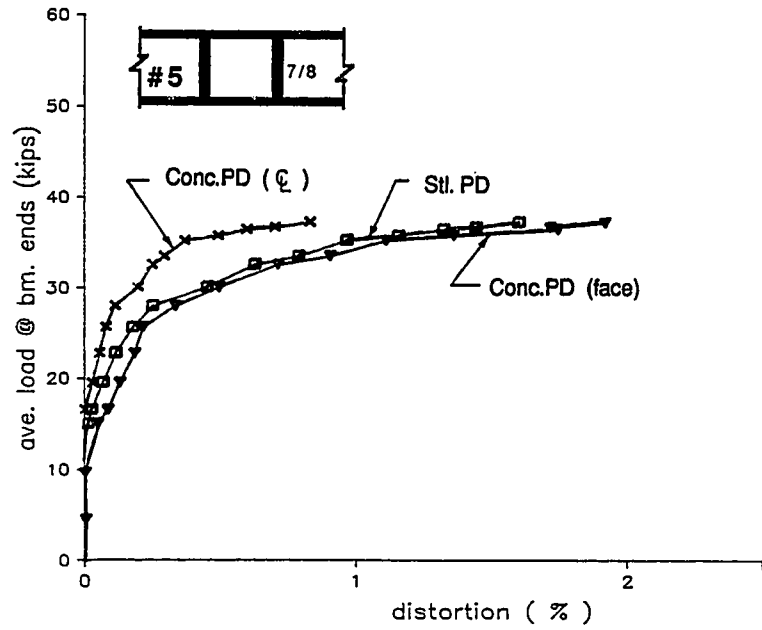


Fig. 4.41 Comparison of distortion in steel and concrete panels of specimen 5.

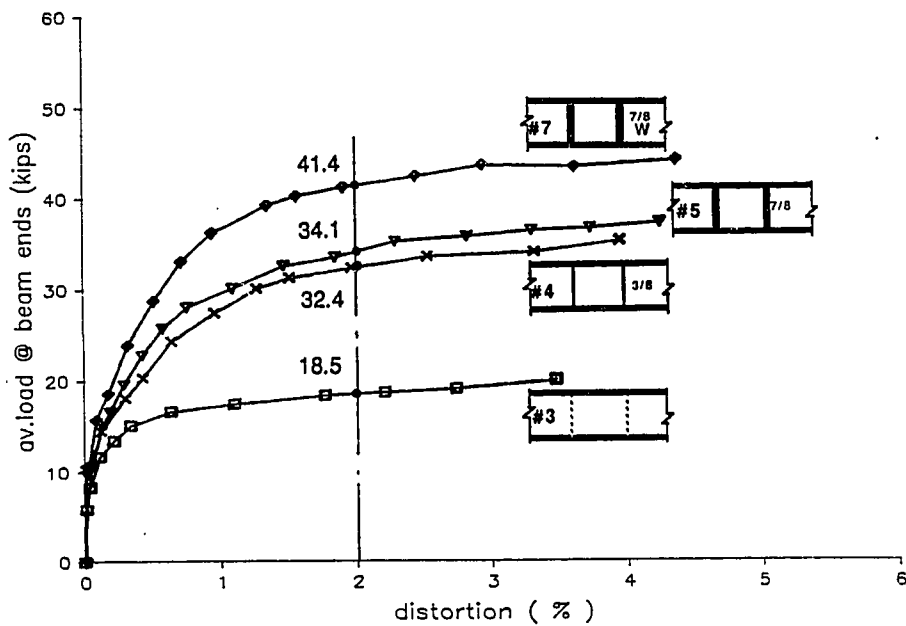


Fig. 4.42 Load vs TJD plot for specimens 3, 4, 5 and 7.

steel panel distortion and the concrete panel distortions as measured at the centerline of column side and at its faces. The ConcPD(CL) was almost zero in the beginning but after the concrete started cracking (around 20 kips load) it increased to about 20% of TJD and stayed at this level through the remaining load history. The ConcPD(face) was 40% of TJD. The concrete panel exhibited the same distortion as steel panel at the faces but lagged behind at the column centerline.

The TJD in specimen 4 which employed a thin FBP, is plotted in Fig. 4.42. Like specimen 5, the joint was initially quite rigid. The stiffness changed at around 5 kips, perhaps due to bending of thin FBPs. The joint stiffness was comparable to that of specimen 5.

The total joint distortion was composed of P_{Sep} and St₁PD, accounting for about 60% and 40% of TJD, respectively. Concrete panel distortion at the column faces was a little bit greater than the St₁PD, about 45% of TJD. ConcPD(CL) was about 25% of TJD up to 20 kips load but thereafter steadily dropped down to about 12% of TJD, thereby demonstrating a distortion lag similar to specimen 5.

Specimen 3. The plot of TJD for specimen 3 which contained a plain beam, is shown in Fig. 4.42. Initial stiffness of the joint, like other specimens, was almost perfectly rigid. However, as the bond between the steel beam and concrete broke at a load of about 5k, stiffness dropped rapidly. Once the steel panel yielded at about 15 kips, the joint had very low stiffness.

The components of TJD, P_{Sep} and St₁PD, accounted for 80% and 20% of TJD, respectively, up to 10 kips. The contribution of P_{Sep} beyond this load steadily dropped to 40% at ultimate load. ConcPD (face) was less than St₁PD and was almost nil up to 15 kips, whereafter, it gradually increased to 60% of TJD at

ultimate load. ConcPD(CL) was zero through the entire load history.

Specimen 6. In specimen 6 doubler plates were used to prevent shear yielding of the steel panel. The TJD for the specimen is plotted in Fig. 4.43. The initial stiffness was about 30% greater than the corresponding stiffness in specimens 4 and 5. Around 0.7% TJD and 35 kips, the concrete started crushing against the compression flanges and the joint stiffness dropped further. The joint reached its peak strength, i.e. 46.8 kips at 2% TJD. With further loading, the joint strength dropped slightly, a characteristic of this specimen only. Perhaps this was due to extensive concrete crushing.

The measured panel separation was about 90% of TJD in the primary direction of loading and about 110% in the reverse direction. However, in view of the accuracy of these measurements, it can be assumed that the P_{Sep} accounted for nearly all of TJD. ConcPD (face) was recorded 45 to 55% of TJD

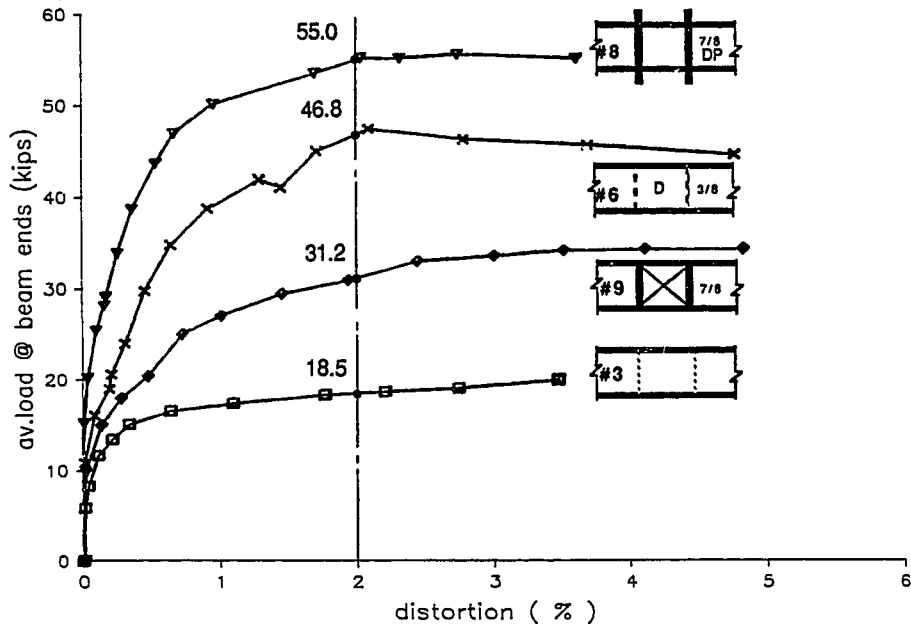


Fig. 4.43 Load vs TJD plot for specimens 3, 6, 8 and 9.

through the entire load history of the specimen. ConcPD(CL) was almost nil up to 20 kips but increased linearly to 30% of TJD at peak load and to about 55% of TJD, thereafter.

Specimen 7. A wider face bearing plate was investigated in specimen 7. The plot of load vs. total joint distortion is shown in Fig. 4.42. The stiffness characteristics of the joint were almost the same as that of specimen 6, 30% greater than the corresponding value in specimens 4 and 5.

The panel separation accounted for about 80% of TJD initially, but as the load exceeded 30 kips, P_{Sep} dropped to about 65%. The remaining joint distortion was due to the St1PD. The ConcPD (face) was a little higher than St1PD, around 40% of TJD. However, as the load reached ultimate, the ConcPD (face) dropped below St1PD. Contrary to the other tests, ConcPD(CL) in this test was almost exactly the same as St1PD, which may mean the concrete panel was mobilized more effectively. Also it is interesting that the magnitude of ConcPD(CL) in this test was the same in as in specimen 6.

Specimen 8. A plot of TJD for specimen 8 which had extended FBPs is shown in Fig. 4.43. The joint showed almost no distortion up to 15.0 kips. Upon further loading stiffness reduced slightly but was almost two and a half times that of specimens 4 and 5. At 29.1 kips, when the steel panel yielded, the joint showed 0.17% TJD. The joint stiffness started deteriorating at 50 kips average load as the concrete crushed against the compression flanges. The joint reached its ultimate strength at 55.0 kips at 2% TJD and maintained it until 3.61% TJD, when it was unloaded.

Panel separation, as measured, accounted for almost 100% of TJD until 40.0 kips and dropped down almost linearly thereafter to about 60% at ultimate load and beyond. Concrete

panel distortion at the columns faces was 80% of TJD almost through the entire loading history, and was significantly larger than the StlPD. ConcPD(CL) was about 30% of TJD until 30 kips and then increased almost linearly to about 80% near ultimate load.

Specimen 9. The total joint distortion in specimen 9 in which the steel panel was cut out, is plotted in Fig. 4.43. The stiffness characteristics of the joint were similar to specimens 4 and 5. The magnitude of load carried by the specimen was also close to that in specimens 4 and 5. The TJD composition was 55% panel separation and 45%, so called StlPD, almost through the entire load history. ConcPD (face) was equal to the StlPD. However, typical of most specimens, ConcPD(CL) lagged behind the distortion at column faces. It was zero up to 20 kips, and ranged from 20% of TJD to 35% at ultimate.

Specimens 1 and 2. Specimens 1 and 2 were designed as pilot tests to investigate the potential of FBPs. The plots of total joint distortion for the two tests are shown in Fig. 4.44. It should be pointed out that the member proportions in these tests were entirely different from those in remaining seven tests. Hence, while a particular load at the beam ends would cause identical joint shear in specimens 1 and 2, it would correspond to entirely different joint shear in the remaining tests. Therefore, the results of these two tests cannot be compared directly with those of other tests.

A distinct feature of the TJD plot for the two specimens is the absence of initial rigidity of joint which was observed in specimens 3 through 9. The joint stiffness of specimen 1 was fairly constant up to 15.0 kips and .50% TJD. As the steel panel yielded at 16.9 kips, the joint had almost no stiffness.

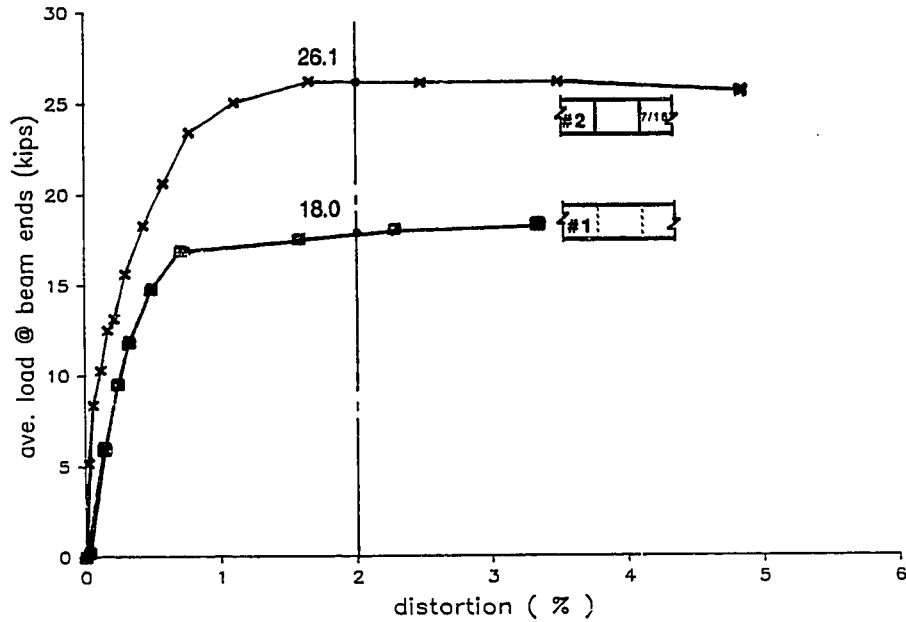


Fig. 4.44 Load vs TJD plot for specimens 1 and 2.

ConcPD(CL) was almost zero through the entire load history. Other components of distortion were not measured.

The initial joint stiffness in specimen 2 was around one and a half times that of specimen 1. The joint lost some stiffness around 16.0 kips when the TJD was 0.30%. As the concrete above the compression flanges started crushing, the joint lost substantial stiffness at 23.5 kips and 0.77% TJD. ConcPD(CL) was about 25% of TJD over the entire load history.

4.3 Flange and Face Bearing Plate Stresses

The forces resisted by the steel and the concrete panels of the joint are shown in Fig. 4.45. The individual contributions to the overall joint resistance depends on the

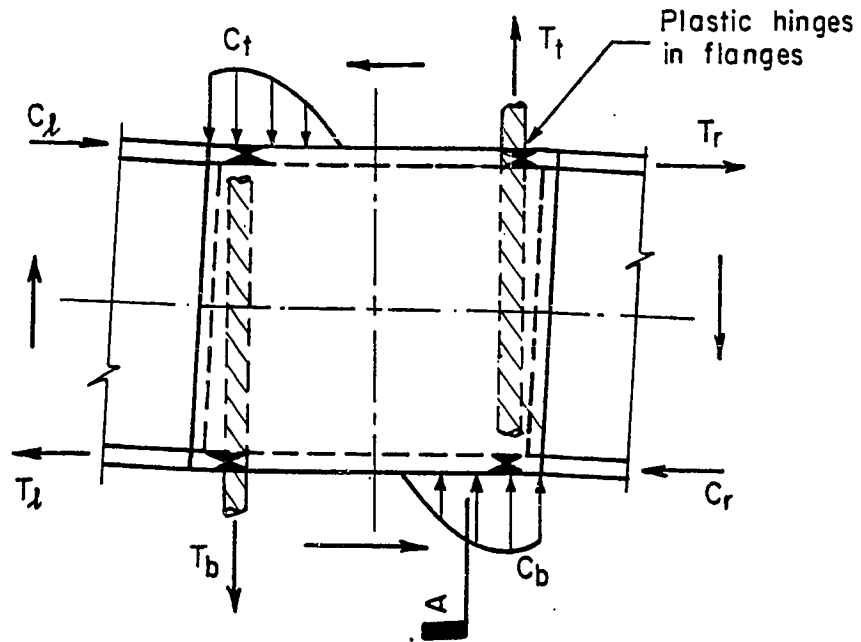


Fig. 4.45 Forces on a typical joint.

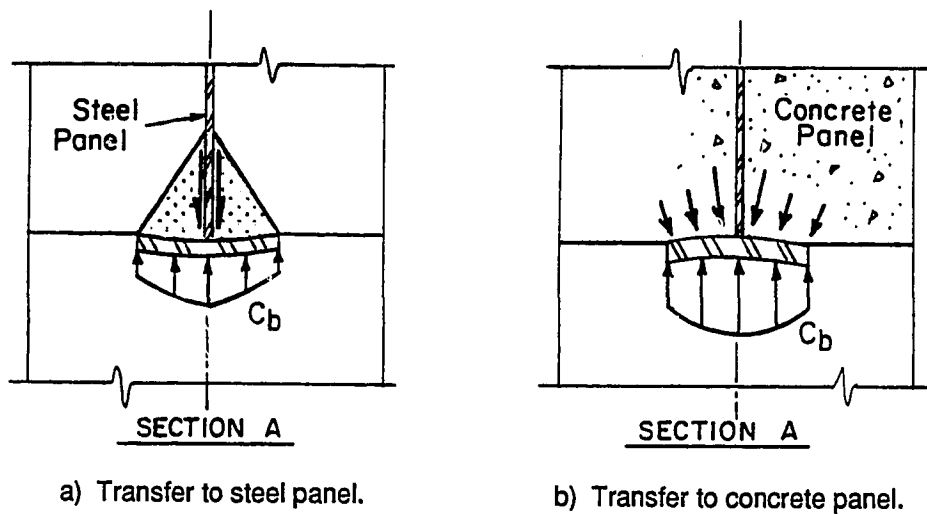


Fig. 4.46 Transfer of column flexural compression to the connection panel.

connection details, i.e. face bearing plates, the relative stiffness of the two panels, etc. To get information on internal distribution of forces within the panel, the strains in the beam flanges inside the joint and in the face bearing plates were monitored at a few locations. The data were recorded as strains and later converted into stresses by multiplying with the modulus of elasticity, E_s , with a due consideration for poisson's effect. Therefore, the calculated stresses, as presented in the following, were only correct until the material reached its elastic limit, i.e. measured yield strength, F_y . Reader should exercise caution while interpreting these data beyond stress F_y .

4.3.1 Transverse and Longitudinal Flange Stresses.

Cross pattern gages were used to monitor the surface strains at the flange centerline in the longitudinal and transverse directions. Typically a gage was 4 inches inside the face of the column on the flanges subjected to compression under the primary loading defined in Fig. 4.1. The longitudinal stress history in the two flanges of specimen 5 (thick FBP), shown in Fig. 4.47, are similar. The longitudinal flange stresses calculated at the face of the column using simple beam theory are shown for reference. As expected the flange stresses are lower than the calculated stresses at the column face at low load levels. As the ultimate load was approached, the compressive flange stress increased rapidly. This was unexpected since the compressive stress at the gages should reduce when the force from the tension flange of the other beam is transferred to the FBP, once the steel web panel is yielded. The large compressive stress near the ultimate load indicate that perhaps the stress is not uniform across the flange width. The surface stresses could be affected by bending of the flanges about their own axis. After the steel panel yields in shear, additional resistance is furnished by the

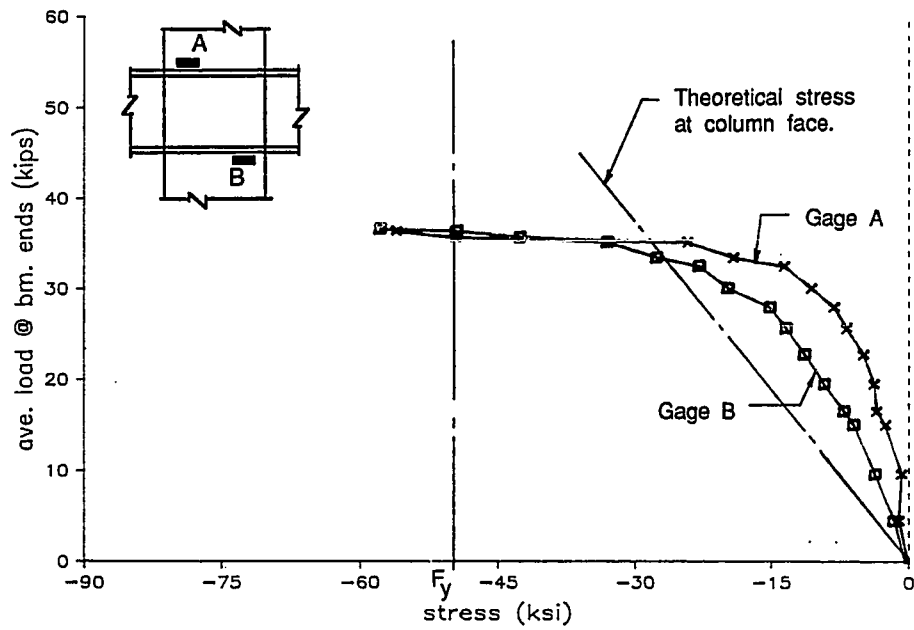


Fig. 4.47 Longitudinal stress in flanges of specimen 5.

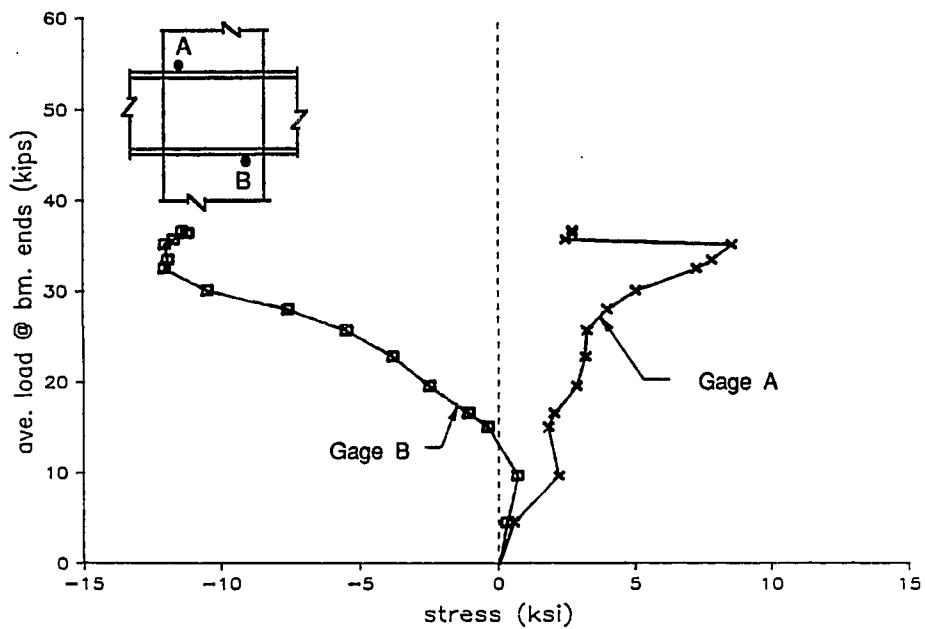


Fig. 4.48 Transverse stress in flanges of specimen 5.

bending strength of the flange plates until plastic hinges form near four corners, as shown in Fig. 4.45. In future studies strains should be measured on both surfaces of the flange so that the average flange stress can be determined and local flange bending stresses eliminated.

The transverse flange stresses at the two gage locations of specimen 5 are plotted in Fig. 4.48. Because of the gage locations and loadings, the stress histories were expected to be similar, and they were in most specimens, but in specimen 5 they were very different. Gage B indicated a slight tension until 15 kips when the direction changed to compression and the stress increased to 12 ksi near the ultimate load. The stress history at this gage was a better representation of what was noticed at both gage locations of most specimens. The initial tension was presumably due to the transverse bending of the flanges caused by bearing forces as shown in Fig. 4.46(a). A major part of this bearing force was transferred to the steel panel through the flanges and the concrete wedged between them and the steel panel, as shown in the figure. However, after the steel panel yielded in shear more of this bearing force was transferred to the concrete panel causing the reverse bending of the flanges as shown in Fig. 4.46(b), thus indicating compressive stress at Gage B beyond 15 kips. On the contrary, Gage A indicated tension through the entire load history. The stress increased to 9 ksi at 35 kips before dropping to about 3 ksi at 36 kips, when the gage ceased functioning. A different stress history at Gage A is hard to explain. One can only speculate that it is perhaps because of the unsymmetrical nature of concrete panel caused by the entrapped air and vertical consolidation of concrete constituents under the flanges, as shown in Fig. 4.49.

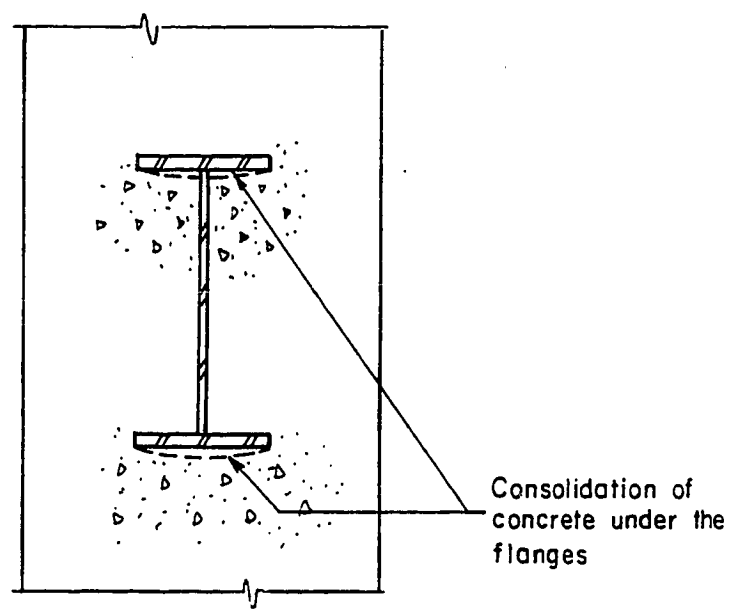


Fig 4.49 Diagrammatic representation of concrete settlement under flanges.

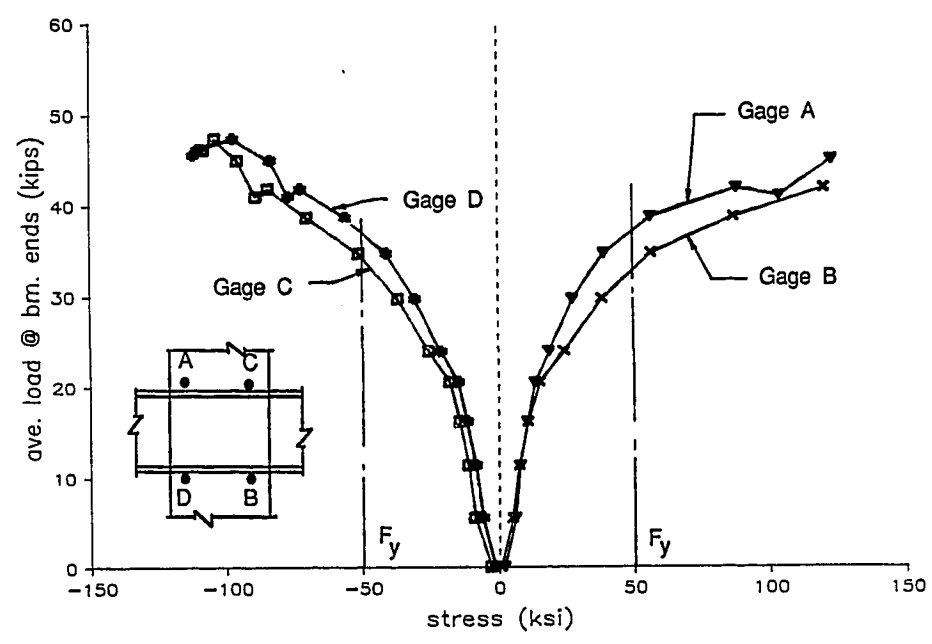


Fig. 4.50 Transverse stress in flanges of specimen 6.

The transverse stress history in the flange of specimen 6 (with doubler plates) is plotted in Fig. 4.50. Four cross pattern gages, one on each flange, were installed. The stress history at the compression flanges, gage A and B, was symmetrical to that at the tension flanges, Gages C and D. Since the steel panel did not yield, Gages A and B indicated surface tension due to transverse bending as shown in Fig. 4.46(a), through the entire primary loading. The flanges at Gages C and D were bent in the opposite direction. The stress at all four locations increased slowly and reached yield stress at a beam load of 40 kips. It is not clear if thicker flanges would have increased the specimen strength since the steel panel did not reach its shear capacity. The symmetry of stress history at the tension and compression flanges indicate that a significant part of the column flexural forces were transferred to the steel panel through the tension flanges.

4.3.2. Transverse and Vertical Stresses in Face Bearing Plates. Cross pattern strain gages were mounted on the FBPs in most of the specimens. Typically two gages were used, one each on the west and the east FBPs. Their location is given in Fig. 3.32.

The history of transverse stress at the two gage locations in specimen 5 (thick FBP) is plotted in Fig. 4.51. The surface stress was compressive in nature through the entire primary loading, and was due to transverse bending of FBPs under the bearing pressure. As the load was increased, the stress increased at an accelerated rate, reaching a maximum value around 40 ksi. Gage A, located on the west FBP, typically showed a slightly higher stress since the west beam, loaded upward, carried more load compared to the other beam.

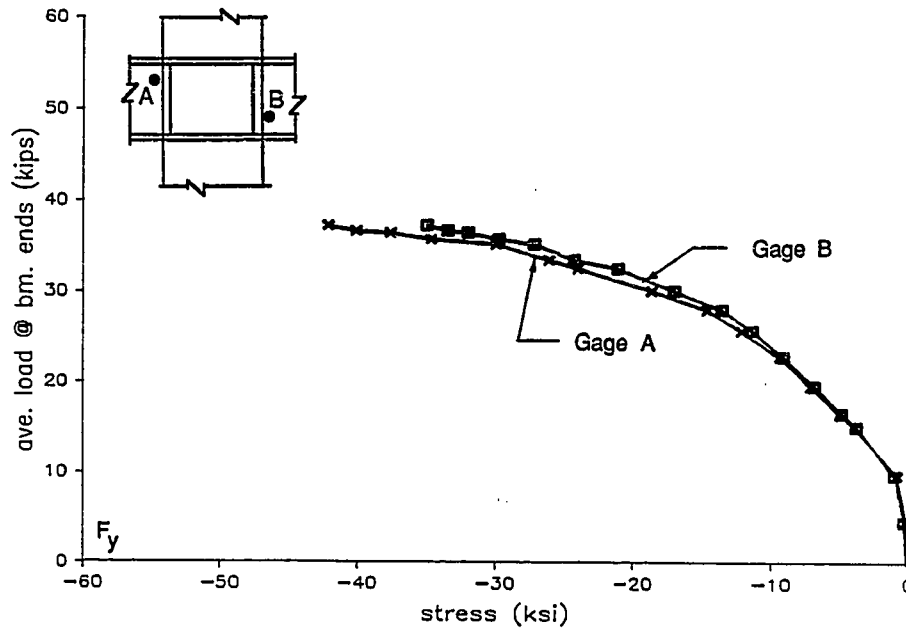


Fig. 4.51 Transverse stress in face bearing plates of specimen 5.

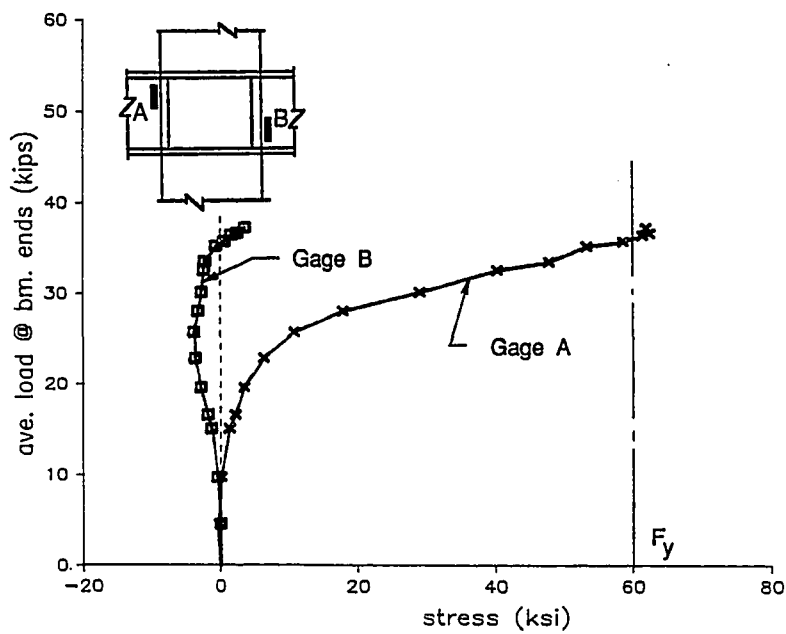


Fig. 4.52 Vertical stress in face bearing plates of specimen 5.

The vertical stress at the two gage locations of specimen 5 are plotted in Fig. 4.52. As stated earlier, because of the symmetrical locations and loading, the stresses were expected to be similar, but the two gages typically showed a significantly different stress history. Gage B of specimen 5 indicated a small magnitude of stress which was compressive in nature until near ultimate load when it changed to tension. In contrast, Gage A indicated a small tension at low loads which increased quickly and reached yield. A high tensile stress at Gage A was noted in most specimens, though not quite as high in other specimens. It is not clear why the vertical stress history differed so much at the two locations. Perhaps it could be attributed to the consolidation of concrete under the flanges, causing unsymmetric concrete panel properties as stated earlier and shown in Fig. 4.49. The tensile vertical stress in the FBPs could be due to the transfer of tension force of the column vertical bars to the diagonal compression strut through friction at the FBPs, as shown in Fig. 4.53.

The vertical stress in the FBP of specimen 6, in which only one cross pattern gage was installed, is plotted in Fig. 4.54. The stress increased almost steadily in compression, reaching a maximum of 30 ksi at the peak load. As the plates were isolated from concrete, they had almost no bending stresses. The entire stress was due to the distribution of bearing pressure from the compression flanges to the steel panel as shear. The stress history shows the effectiveness of the FBPs in distributing bearing forces on the flanges.

4.4 Reinforcing Bar Behavior

Research conducted on reinforced concrete beam-column joints has indicated the bond characteristics of column vertical

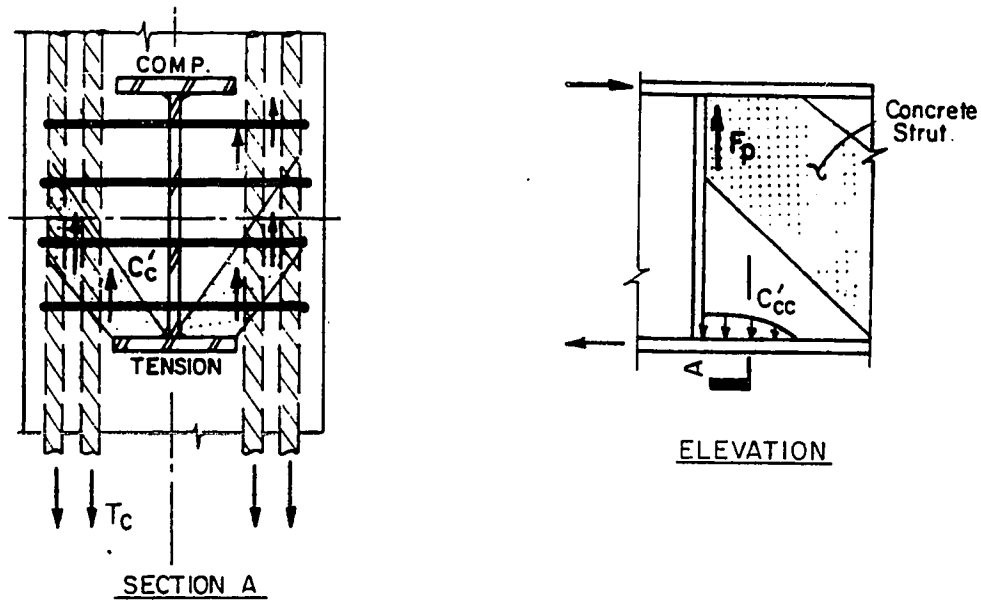


Fig. 4.53 Transfer of vertical bar tension to the concrete strut through friction.

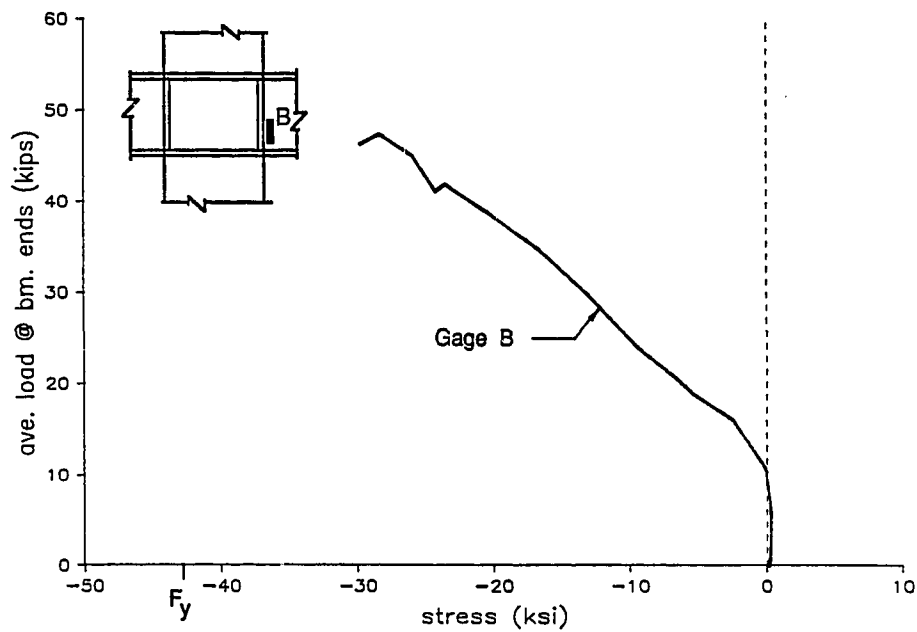


Fig. 4.54 Vertical stress in face bearing plate of specimen 6.

bars are especially important for the stiffness of the joint. Also the transverse reinforcement in the joint enhances concrete shear capacity by providing confinement. To evaluate the performance of joint reinforcement, a few of the vertical bars and ties were instrumented in the test specimens. Selected data from this instrumentation are presented in this section. As mentioned in the last section, the data from these instrumentation were recorded as strains and later converted into stresses. Therefore, the calculated stresses, as presented here, were only correct until the material reached its elastic limit. Reader should exercise caution while interpreting these data beyond measured yield strength, F_y .

4.4.1 Column Vertical Bars. The strains in the vertical bars were monitored in specimens 1 through 5 and 8. In specimens 1 and 2, four bars closest to the steel beam were instrumented while in other specimens vertical bars in one corner were gaged. The gage locations are given in Chapter 3.

The stresses indicated by the gages located at the bottom flange level for specimen 5 (thick FBP) are plotted in Fig. 4.55. The stresses in the same bars at the top flange level are plotted in Fig. 4.56. Gage labelled AT malfunctioned and is therefore not plotted. Stresses in the bars calculated at the gage locations, based on the cracked transformed section properties, are plotted for reference. The stress obtained by strain gages AB, BB and CB, located in the flexural tension zone under primary loading, compared reasonably well with the calculated stress as shown in Fig. 4.55. The stresses indicated by the gages were slightly lower than the computed values in the early part of loading, but as the concrete cracked the stresses gradually increased to the computed value. Strain gage AB malfunctioned around 33 kips. Gages BT and CT, located in the

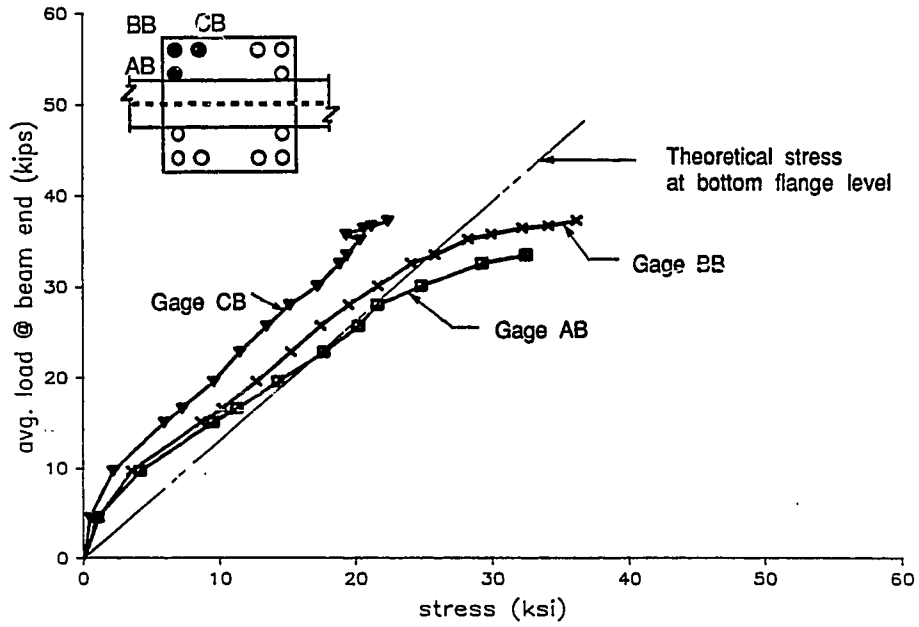


Fig. 4.55 Stress in vertical bars of specimen 5 near bottom flange.

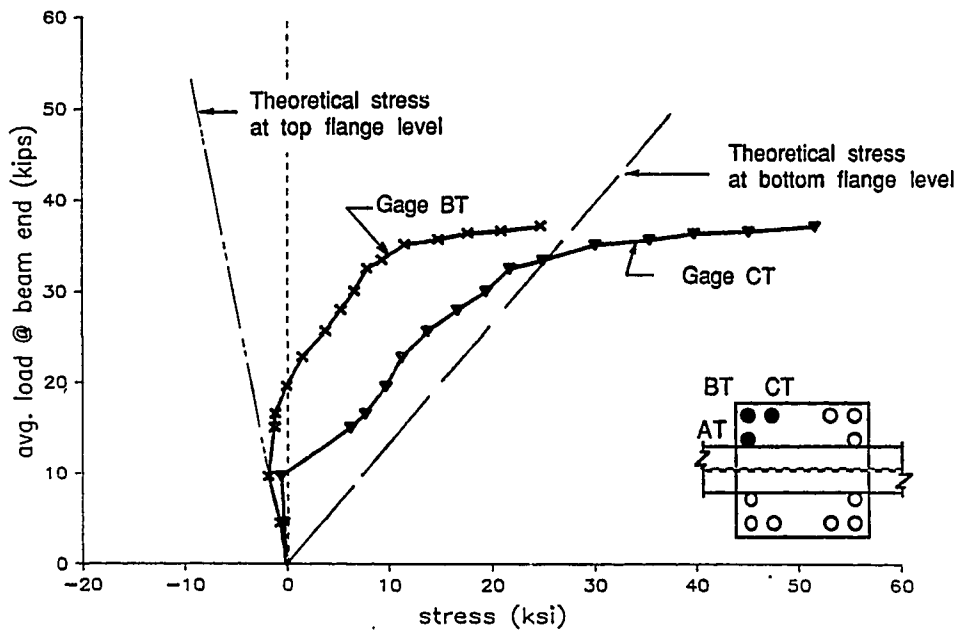


Fig. 4.56 Stress in vertical bars of specimen 5 near top flange.

flexural compression zone under primary loading, indicated a small compression in the early part of loading, but soon changed direction to tension which increased with load, as shown in Fig. 4.56. The tension at each gage was lower than the stress at the corresponding gage at the bottom flange level, except near the ultimate load when the stresses sharply increased. These stress histories indicate that during early part of loading, the tension in these reinforcing bars at bottom flange level was transferred to the concrete through bond within the beam depth, as shown in Fig. 4.57(b), therefore gages BT and CT indicated a small compression. However, as the steel panel yielded in shear and the bond with concrete deteriorated, a part of the vertical bar tension was anchored in the compression block above the top flange, as shown in Fig. 4.57(b), thus Gages BT and CT indicated tension. Near the ultimate load some readjustment of stress at the top flange level took place and Gage BT indicated a stress lower than the corresponding Gage BB while Gage CT indicated a stress higher than the corresponding Gage CB. It will be incorrect for this specimen to compare the average stress of two functioning gages at top flange level to the average of three gages at bottom flange level. Similar comparison for other specimens, where all the gages functioned, indicate the average stress at the top flange level to be close to the average value at the bottom flange level near ultimate indicating that there was little transfer of stress from bars to concrete over the beam depth. The readjustment of stress among the bars near ultimate load could not be rationalized with the available data.

The stress history at gages located in the flexural tension zone under primary loading of specimen 8 (extended FBP) is plotted in Fig. 4.58. Gage labelled CB malfunctioned, and is therefore not plotted. The stresses indicated by the strain

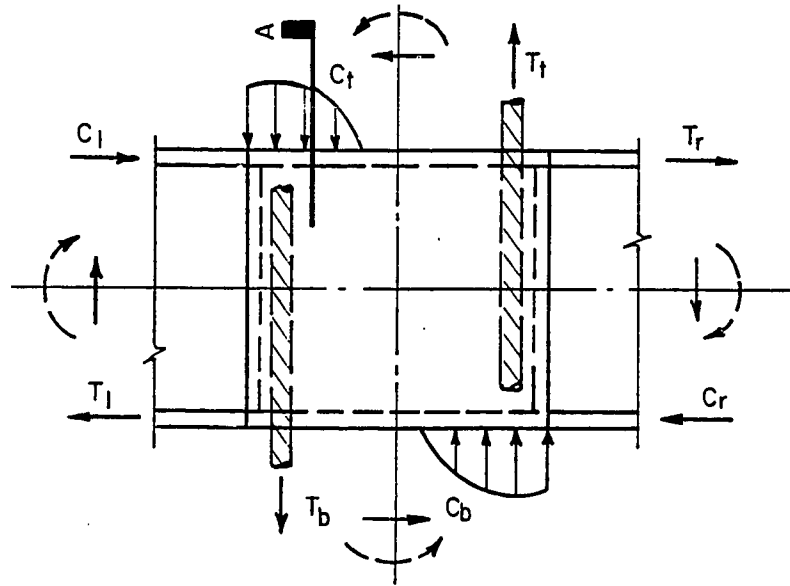
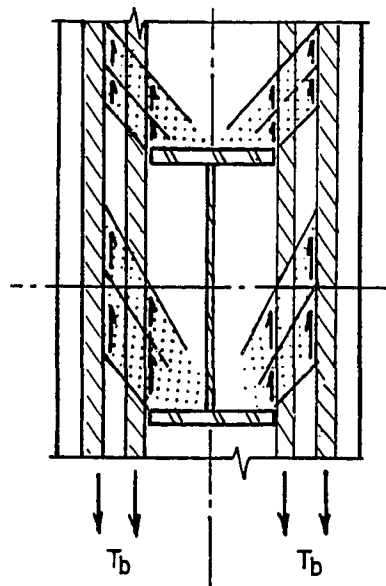
a) TYPICAL JOINTb) SECTION A

Fig. 4.57 Flexural forces on a typical joint.

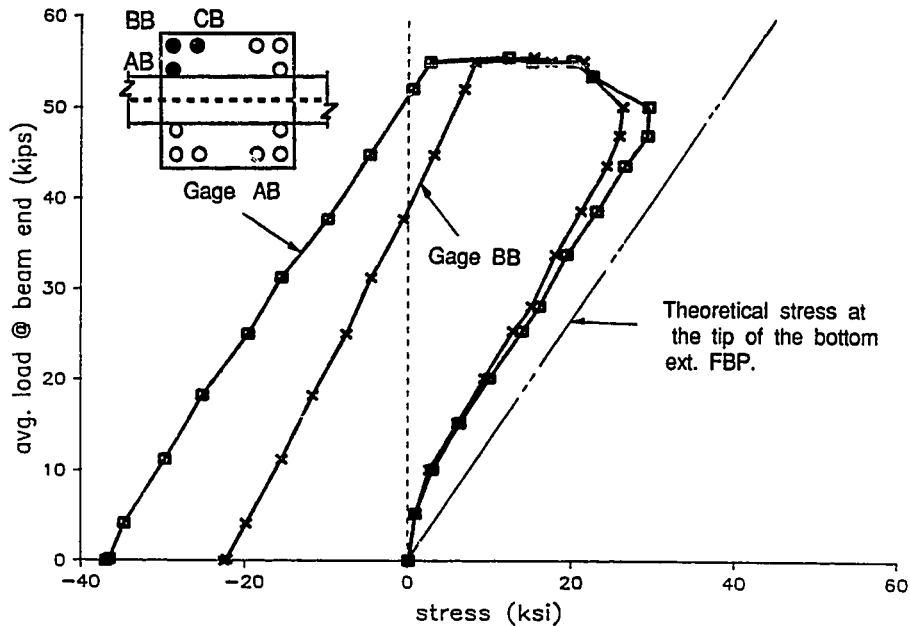


Fig. 4.58 Stress in vertical bars of specimen 8 near bottom flange.

gages were slightly lower than those calculated based on the cracked transformed section properties of column at the tip of the extended FBP. As the load exceeded 47 kips, the stress at both gages sharply dropped. Perhaps the bars were bent about their own axis, causing the net surface stress at the gage location to reduce while still maintaining the net tension across the area of the bar. Bending of the bars could be due to the transfer of part of the flange forces, C_b and T_b , to the diagonal compression strut through the mechanism shown in Fig. 4.59(b). Part of this force was transmitted on the bars located across the column depth and returned back to the diagonal compression strut

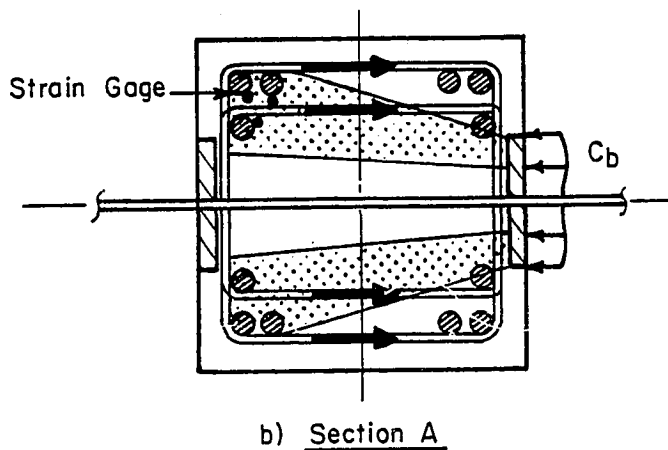
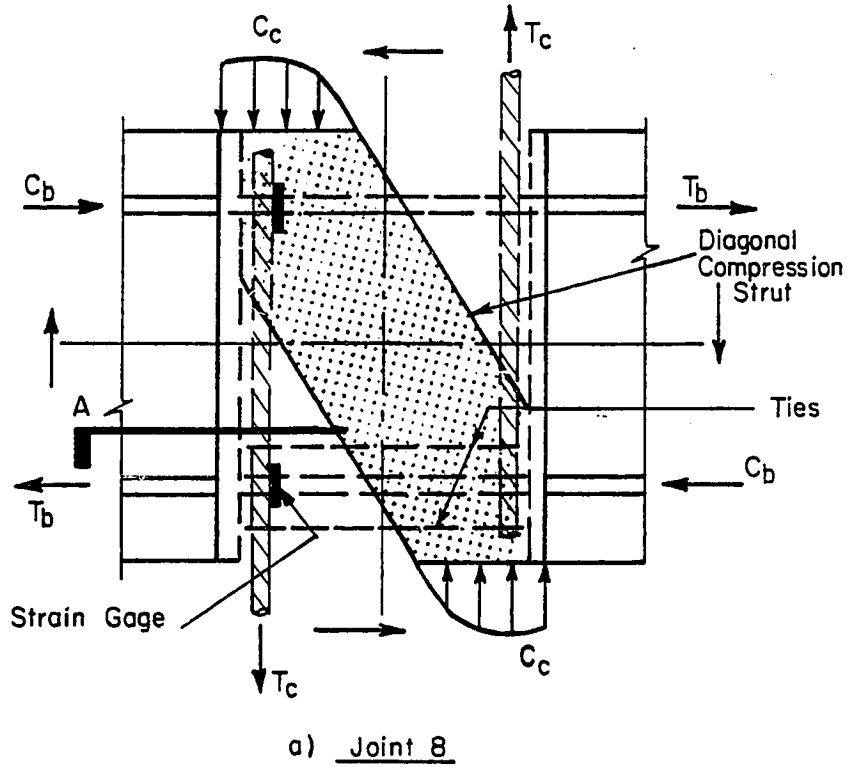


Fig. 4.59 Mechanism of transfer of partial flange forces to the diagonal compression strut.

via tension in the ties as indicated in Fig. 4.59(b). The stress history at the gages located in the flexural compression zone of the column is shown in Fig. 4.60. The initial load range in which the stress was compressive in nature was higher than in other specimens. Also, the magnitude of tension beyond this range was relatively small, although the specimen carried almost 1-1/2 times the load recorded for specimen 5, for instance. This lower tension could be due to the longer bar development length available within the beam depth. It should be pointed out that the effective depth of the steel beam due to the extended FBPs was almost 50% more in this specimen. Near ultimate, like in other specimens, the tension in all the three gages sharply increased, reaching yield (65 ksi) in AT, 48 ksi in BT and 19 ksi in CT, giving an average stress of 44 ksi which compared very well with the calculated value at the tip of the bottom Ext. FBP. This means the vertical bars were debonded within the beam depth at the ultimate load.

4.4.2 Joint Ties. The strains in the ties within the beam depth and in a few ties located above and below the beam were monitored in all the specimens. The gage locations are given in Chapter 3.

The gages located within the beam depth typically recorded strains after the diagonal shear cracks appeared and increased almost linearly to yield near the ultimate load. Since there were no diagonal shear cracks in specimens 1 and 3, the joint ties in these specimens showed hardly any strain. The ties near the mid-depth typically yielded early and were strained higher than others. Figure 4.61 shows the stress history in the ties across the column depth located in the top half of the joint in specimen 5 (thick FBP). High stress and yielding of both, ties across the column depth, and those across its width,

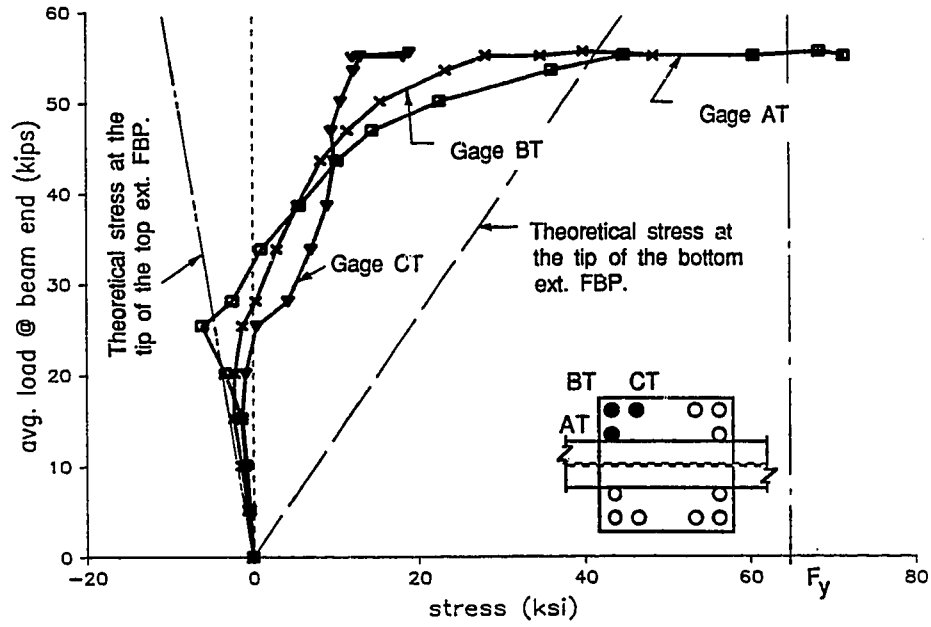


Fig. 4.60 Stress in vertical bars of specimen 8 near top flange.

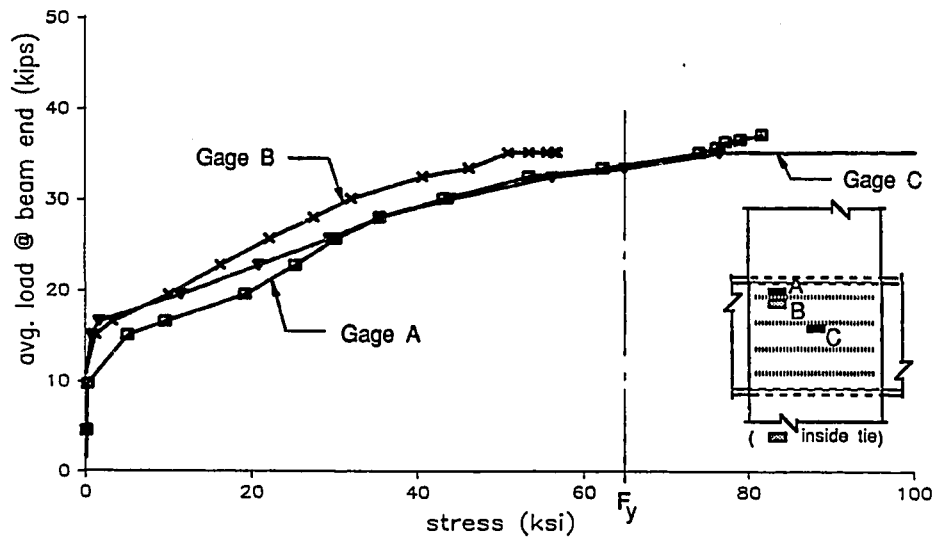


Fig. 4.61 Stress in ties located within beam depth of specimen 5.

indicate their effectiveness in confining the diagonal compression strut.

Outside the joint, the two sets of instrumented ties across the width of column face in compression, typically indicated a very small stress until near ultimate load when the stress increased sharply to yield as the concrete started crushing. Ties inside the joint reached yield earlier than those outside, and were strained more. The outside ties were effective in holding the concrete together under high bearing stress thereby improving bearing strength. The two sets of instrumented ties across the column depth, located above the top flange, were strained after the concrete started cracking which increased with the load and reached yield in some specimens. The outside tie of the first set was typically stressed highest, followed by the inside tie of this set. The stress history of these gages in specimen 4 (thin FBP) is shown in Fig. 4.62. The higher stress, typical in the outside ties, was perhaps due to the mechanism described earlier and shown in Fig. 4.59.

4.5 Connection Panel Behavior

4.5.1 Steel Panel Behavior. The shear stress in the steel panel was monitored with a single rosette strain gage at the center of the panel in specimens 3 through 8. In specimens 1 and 2 two rosette strain gages were installed at one third points on a line at mid-depth of the beam. The strain data from these rosettes were analyzed using Mohr's strain circle and maximum shear strain was calculated. The maximum shear stress was then calculated using this strain at each load point. Whereas the strain calculations were valid through the entire load history or until the gage malfunctioned, the calculated maximum shear stress was only correct until the material reached its elastic limit.

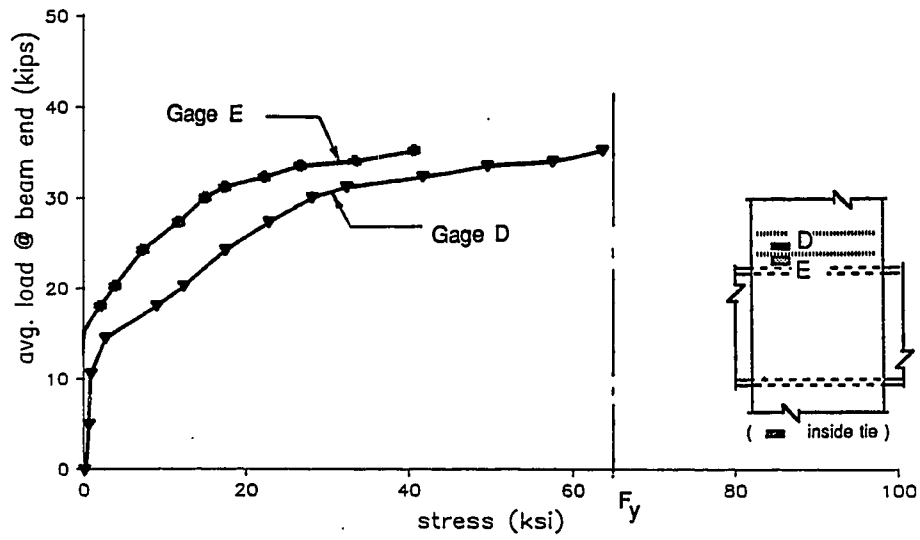


Fig. 4.62 Stress in ties located above beam of specimen 5.

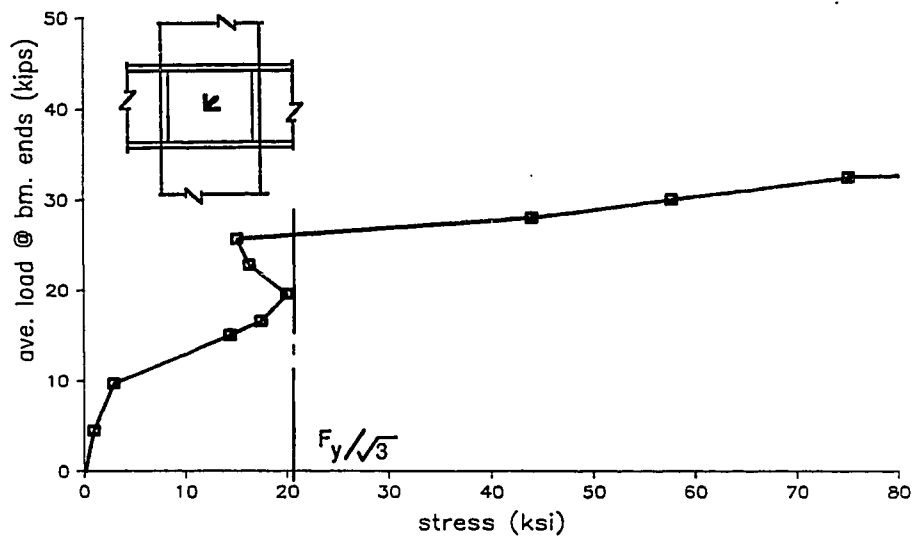


Fig. 4.63 Maximum shear stress in the steel panel of specimen 5.

The steel panel was considered to have yielded when the maximum shear stress reached a stress value of $F_y/\sqrt{3}$, according to the Von Mises's yield criteria, where F_y is the measured yield strength of the steel panel material, 36 ksi for specimens 3 through 8 and 56 ksi for specimens 1 and 2. The doubler plates in specimen 6 were 50 ksi.

The gages typically did not indicate much shear in the steel panel until adhesive bond between the steel beam and concrete was overcome (at a load of around 10 kips). The shear stress then increased with load until it reached yield. The load corresponding to the yield stress for each specimen is listed in Table 4.1 at the beginning of this chapter. As planned, the steel panel in specimen 6 did not yield. As the load was further increased, in most specimens the maximum shear strain increased sharply. Figure 4.63 shows the plot of maximum shear stress at the gage location in the steel panel of specimen 5 (thick FBP). The shear reached yield stress at 20 kips. Unlike most specimens, the maximum shear strain reduced slightly then rapidly increased again at 26 kips. It is not clear why the strain dropped after reaching yield, perhaps the shear was redistributed from the steel panel to the concrete panel. Nevertheless, almost the entire joint shear due to load above 26 kips was resisted by the concrete panel. Some resistance was provided by bending of the flanges about their own axis.

4.5.2 Concrete Panel Behavior. The concrete panel in a few specimens was instrumented with resin impregnated, 2-1/2 in. gauge length, embedded strain gages. The location of these gages in each specimen is described in Chapter 3. Typically the gages were placed along the diagonal between the west-top and east-bottom corners of the connection panel at the quarter-point and mid-point. The gages placed in the confined zone within the

flange width were labeled as C1 and C2. The gages located in the less confined zone outside the flange width, were labelled as U1, U2 and U3.

The data from these gages, like others, were recorded in terms of strain. Due to the non-linear stress-strain relationship for concrete, these results are presented as such. The relationship between stress and strain of concrete depends very much on whether it is confined or unconfined. Figure 4.64 shows typical stress-strain curves for both confined and unconfined concretes. The stress is shown in terms of the compressive cylinder strength of concrete, f'_c . The curve shown for unconfined concrete represents fairly well the stress-strain relationship for concrete strengths between 3000 and 6000 psi. The peak stress may not be exactly at .002 strain but lies very close to it. The stress-strain curve for confined concrete, however, is typical only in shape. The magnitude of the peak stress, $f_{c \max}$, as well as the slope of the descending branch, α , are very heavily dependent on the amount of confinement. For the concrete confined by spiral or hoop reinforcement, the stress $f_{c \max}$ may range from f'_c to $2 f'_c$. However, if the concrete is confined by closed structural steel sections, i.e. circular or rectangular tubes, the stress $f_{c \max}$ may be several times higher. The exact magnitude of $f_{c \max}$ for the portion of concrete panel confined by the steel beam flanges and FBP in this series of tests is impossible to determine. However, the concrete panel outside the width of flanges, which was perhaps confined only by the joint ties, may be well represented by the stress-strain curve for confined concrete in Fig. 4.64.

The strains in the concrete panel of specimen 5 (thick FBP) as recorded by gages C1, C2, U1 and U2, are plotted in Fig. 4.65. Gages U1 and U2 recorded about half the strain of C1 and

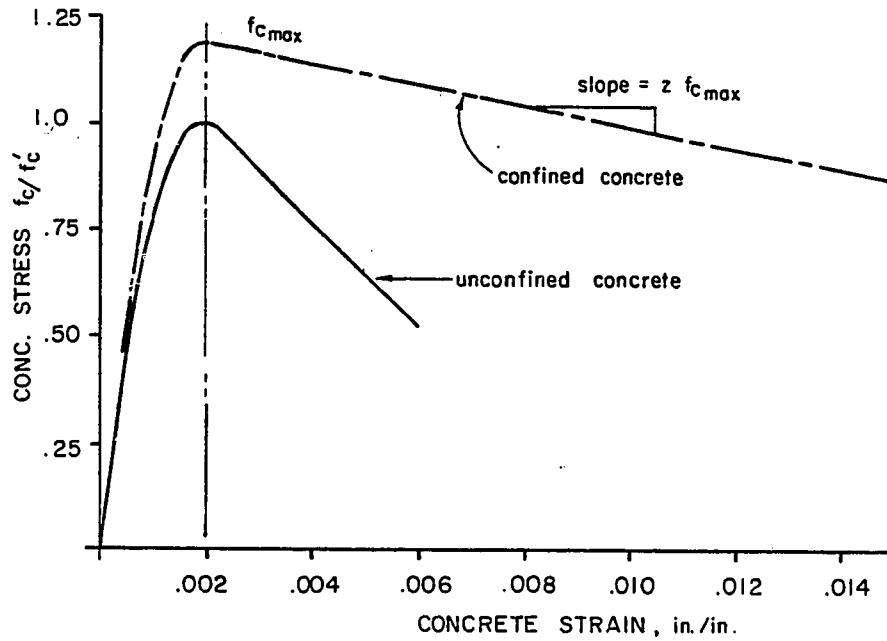


Fig. 4.64 Concrete stress-strain curve in uniaxial compression.

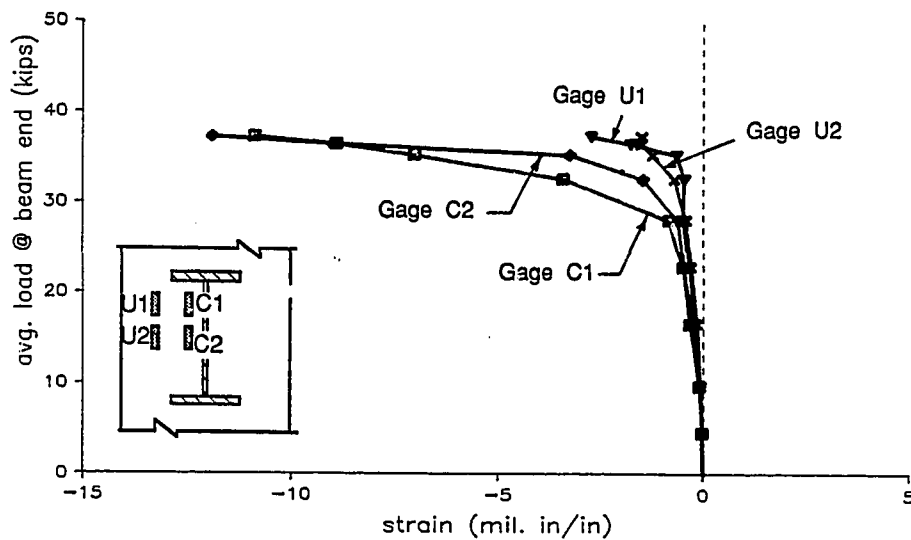


Fig. 4.65 Strain in the concrete panel of specimen 5.

C2 up to a load of about 25k. Upon further loading the strain in gages C1 and C2 increased much faster. At ultimate load C1 and C2 recorded 0.011 and 0.012 strains, respectively and U1 and U2 0.0027 and 0.0015 strains, respectively. This large lag in strain between the C and U gages, suggest that the concrete panel within the flange width may be separated from the concrete panel outside the flange width. This leads to the hypothesis that the diagonal compression strut of the concrete panel was perhaps confined within the widths of flanges and FBPs near the ultimate load. The stress in this diagonal strut was at least equal to or greater than f'_c . The width and depth of this strut could not be determined from these data.

In specimen 6 doubler plates were welded on the steel panel and a styrofoam layer was placed behind the FBPs to prevent any participation of the concrete panel in resisting the joint shear. A single concrete gage C2 was used to measure the shear in the concrete panel. A maximum strain of 0.00008 in./in., which correspond to a stress of 290 psi, was recorded at 40 kips before the gage malfunctioned. This small stress clearly shows the concrete panel resisted almost no joint shear. Nevertheless, the pattern of diagonal cracks on the concrete panel as shown in Fig. 4.20 and described in Sec. 4.1 was very similar to that of specimens 5 and 7. Perhaps the diagonal cracking of the panel was due to the tension transferred from the column vertical bars in flexural tension, and due to the fact that the nature of the applied loads is such that shear distortion is imposed on the concrete panel.

Five strain gages were embedded in the concrete panel of specimen 7 (wide FBP). The strain history of all five gages is plotted in Fig. 4.66. The strains recorded by gages C2 and U1 are perhaps lower than the actual magnitudes since they indicated

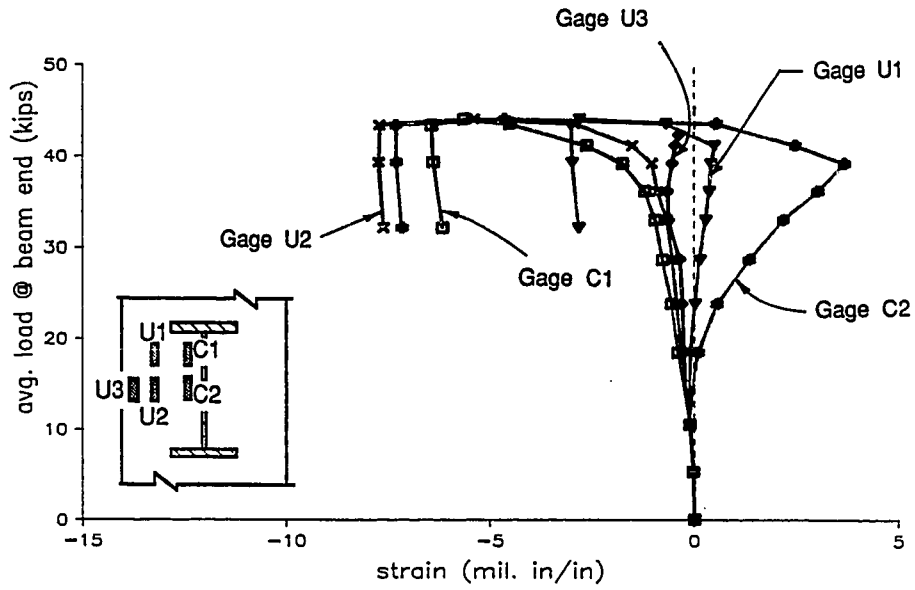


Fig. 4.66 Strain in the concrete panel of specimen 7.

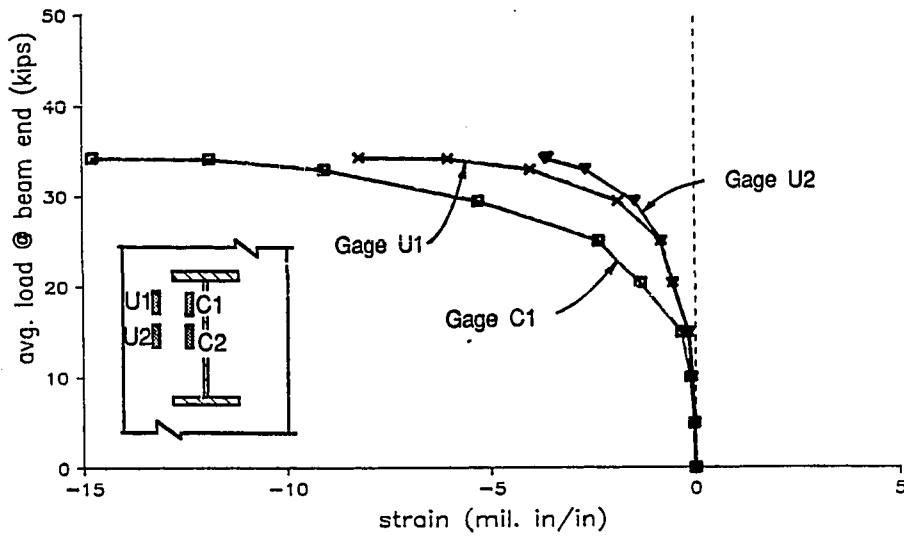


Fig. 4.67 Strain in the concrete panel of specimen 9.

tensile strain at low loads, perhaps due to cracks in the vicinity. The gage U3 which was at 8-1/4 inches off the web, recorded strains smaller than .0007 in./in. up to 42 kips load when it ceased functioning. It is clear that the strain lag between gage C1 and U1 and between C2 and U2, was much smaller than what was noticed in specimen 5. It should be pointed out that the gages U1 and U2 were located 6-1/2 in. from the web, almost the same distance as the edge of the FBPs. Gage U3 which was outside the FBP, showed a large lag in strain compared to the other gages. The diagonal compression strut of the concrete panel may have been confined by the FBPs.

In specimen 9 the effect of an extremely weak steel panel (hole cut in web) on the performance of the concrete panel was studied. Almost the entire joint shear was carried by the concrete panel. Four concrete gages, C1, C2, U1 and U2, were embedded, but gage C2 did not work. The strain history of the remaining three gages is plotted in Fig. 4.67. At ultimate load gages C1, U1 and U2 recorded strains of .015, .008 and .0035 in./in., respectively. Comparison of strains in gages C1 and U1 indicate much smaller strain lag than in specimen 5. The maximum strains in gages U1 and U2 were almost two to three times the corresponding maxima in specimen 5. This comparison clearly indicates the diagonal compression strut in this specimen extended beyond the width of flanges and FBPs since the specimen carried almost the same load as Specimen 5 even though the steel panel was cut-out.

C H A P T E R 5
EVALUATION OF JOINT STRENGTH

In this chapter, the test data are synthesized into a behavioral model for joint strength. Different mechanisms for the transfer of flange forces to the concrete panel are identified and the possible failure modes of the joint are discussed. The effect of face bearing plates on the joint stiffness and strength is evaluated in greater detail.

5.1 Failure Criteria

In many of the tests a maximum load was not reached. The tests were terminated when gross joint distortion occurred. Specimen 3, for instance, supported a load of 16 kips at 0.6% drift and 20 kips at 3%, when the loading was discontinued. Thus, the determination of a "failure load" is somewhat arbitrary. In addition to strength, the deformation of the joint both at service load level and over-load (ultimate load) should be considered in determining the failure load. Excessive deformation near ultimate load may cause large second order (P- Δ) effects which can affect the strength. It is also important that the joint maintains a substantial part of its strength, even at excessive deformations, to avoid sudden and brittle failure and to provide ductility.

In current design, the lateral drift under service wind loads is limited to 0.2 - 0.5% (Ref. 12). The lateral drift is the result of member deformation and joint distortion. In all-steel frames, particularly for tall buildings, it is customary to recognize the shear distortion of the connection panel, in one form or the other. Usually the frames are analyzed by ignoring the connection size and considering centerline dimensions of the

framing members rather than clear spans. It is assumed that for most structures the longer span compensates for the loss of stiffness due to shear distortion of the steel connection panel (Ref. 14). Some designers analyze frames considering finite but rigid joints and later add the estimated drift caused by shear distortion of the panel zone. Contacts with structural engineers indicate that joint distortion may contribute from 10 to 35% to the overall lateral drift of the steel frame. In the design of all-concrete building frames, joints often are considered rigid and shear distortion is ignored altogether despite the fact that test data indicate substantial joint distortion. Tests on reinforced concrete beam-column subassemblages conducted by Meinheit [32] indicate a total joint distortion at service load level of 0.20 to 0.35%.

How much joint distortion should be permitted at failure is a difficult question to answer. For the purpose of defining the useful ultimate strength of the steel beam-to-concrete column joints, a value of joint distortion at the failure load equal to 8 to 10 times that at service load may be adequate. The average value of distortion in steel beam-to-concrete column joints at service load levels may realistically be limited to about 0.20 to 0.25%, i.e. the same as the value measured in reinforced concrete beam-column joint tests. With joint distortion at failure as 8 to 10 times a value of 0.2 to 0.25%, the failure load can be defined at 2% total joint distortion and is the value used in this study.

5.2 Summary of Test Results

Failure load for each of the nine test specimens is listed in Table 5.1. The initial joint stiffness as related to the joint moment is also tabulated for comparison of connection

TABLE 5.1 Summary of Test Results

Specimen No.	Concrete Strength f'_c (psi)	Init. Stiff. Rel. to Joint Moment (k'/rad.)	Failure Load (2% TED) P (kips)	Remarks
1	3550	26,400	18.0	Plain beam
2	3550	38,500	26.1	FBF
3	4500	149,000	18.5	Plain beam
4	4300	146,200	32.4	Thin FBF
5	4300	143,400	34.1	Thick FBF
6	4000	193,500	46.8	Thick Stl. Panel
7	4000	197,800	41.4	Wide FBF
8	3600	369,700	55.0	Extended FBF
9	3700	146,200	31.2	No Stl. panel

details. These values are for the primary direction of loading. Due to severe damage of the joint during this loading, response under loads in the reverse direction was not used to determine joint capacity. The test results show that face bearing plates substantially enhanced joint strength. Variations in the thickness of these plates, did not affect the joint capacity. This capacity, however, was increased 20% by increasing the width of the FBP from 8 to 12 in. Extending the FBPs above and below the beam was most effective and increased the joint strength by 60% of that with unextended FBPs.

The comparison of joint stiffness for specimens with and without FBP indicate that while the FBP increased the stiffness by about 45% in pilot specimens, it did not affect the stiffness of specimens 4, 5 and 9. This difference in behavior cannot be explained by the test data available. However, the wider FBP in specimen 7 and the thick steel panel in specimen 6 increased the joint stiffness by about 30%. The extended FBP of specimen 8 enhanced the stiffness by 150%. The total joint distortion was typically composed of 50 to 60% panel separation with the remaining due to steel panel distortion. Specimen 6, which had a thick steel panel, was an exception and derived its entire TJD from panel separation.

In addition to flexural cracks, two basic types of concrete cracks were noticed: a) those radiating from the tension and compression flanges on the column faces, and b) the diagonal shear cracks on the sides. Diagonal shear cracks were present irrespective of whether or not the diagonal compression strut was mobilized in the connection panel. These cracks appeared as a result of shear distortion imposed on the connection panel due to the nature of loading.

The column vertical bars passing through the joint were substantially debonded near the ultimate load in all the specimens except specimen 3. These bars transferred their tension to the connection panel through the compression block above the compression flanges.

The strain gages embedded in the concrete panel demonstrated a large strain lag near the ultimate load between the concrete panel within the width of flanges and FBPs (whichever is more) and that outside this width. It seems the two parts of concrete panel were separated near the peak load. This effect was minimal in specimen 9, which had the steel panel cut out.

5.3 Mechanisms for Resisting Joint Forces

The concrete in the joint area was mobilized to carry more joint shear by the addition of face bearing plates. The transfer of beam flange forces and the column vertical bar tension to the connection panel and the resistance provided by steel and concrete panels is detailed in this section.

The forces transmitted by the beams and columns on a typical connection are shown in Fig. 5.1. The forces from each beam are considered to be of equal magnitude. Also, due to the determinate nature of the test specimens, the forces transmitted by the top and bottom columns are of equal magnitude. For simplicity, the entire beam moment is resolved into the flange forces, C_b and T_b . The column moment is resolved into vertical bar tension, T_c , and a compressive stress block, C_c . The nature of the stress block C_c differs substantially from the familiar parabolic stress blocks in flexural or axial compression, and in reality is a high intensity bearing pressure acting on a width narrower than the actual column width. In most specimens this

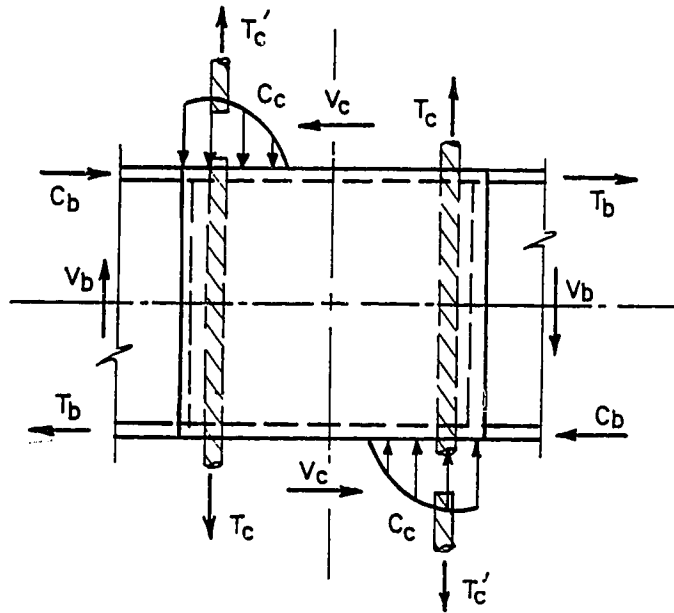


Fig. 5.1 Forces on a connection.

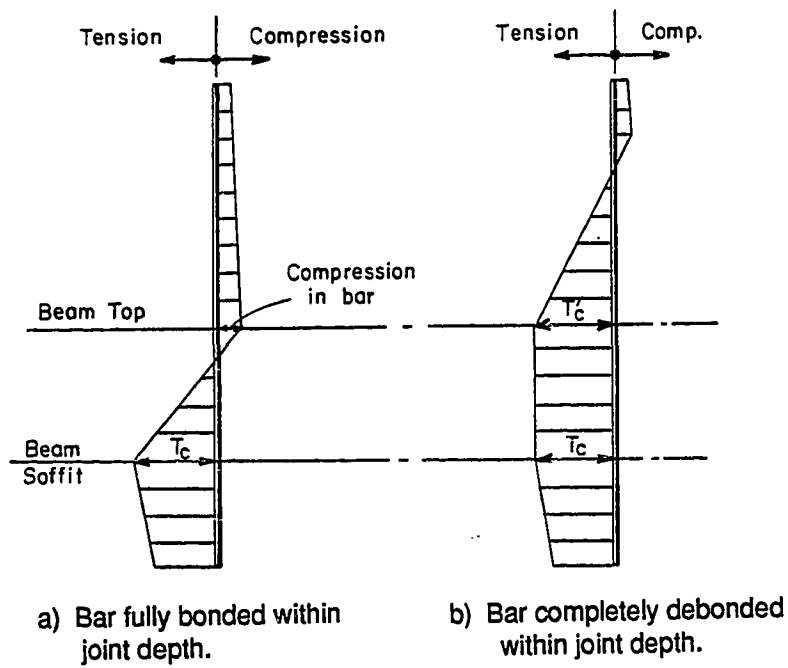


Fig. 5.2 Stress in column vertical bars.

width is equal to the beam flange width, and is discussed later in further detail. The magnitude of this stress block C_c depends on the state of the bond of the vertical bars within the joint, and must satisfy the following relationship

$$C_c = T_c + T'_c \quad (5.1)$$

by summation of vertical forces at a column section near top flange. Figure 5.2 shows the stress profiles of a column vertical bar under two extreme bond conditions. When the bar is fully bonded within the depth of the joint, it is in compression near the top of beam, resulting in a stress block C_c of magnitude smaller than the tension T_c . When the bars are completely debonded, the stress block C_c is equal to twice the tension T_c . However, when the bars are partially debonded as in the test specimens, the magnitude of stress block C_c is between T_c and $2T_c$. The difference between tensions T_c and T'_c must transfer to the connection. It is transferred partly to the concrete panel as bond force, F_b , and remaining on the tension flange as stress block C'_c , as shown in Fig. 5.3. A part of this stress block, C'_c , is transferred to steel panel and is labelled as C'_{cs} in Fig. 5.4(a). The remainder, C'_{cc} , is transferred to the concrete panel through friction against FBPs, F_p , as shown in Fig. 5.4(b).

In order to segregate the steel panel and the concrete panel mechanisms of joint resistance, each of the external forces, shown in Fig. 5.1, are split into two components as shown in Fig. 5.5. The forces which are apportioned to the steel panel are shown in Fig. 5.5(a) and carry an extra subscript, 's', with them. Similarly, the other part of these forces assigned to concrete panel are shown in Fig. 5.5(b) with an extra subscript, 'c'.

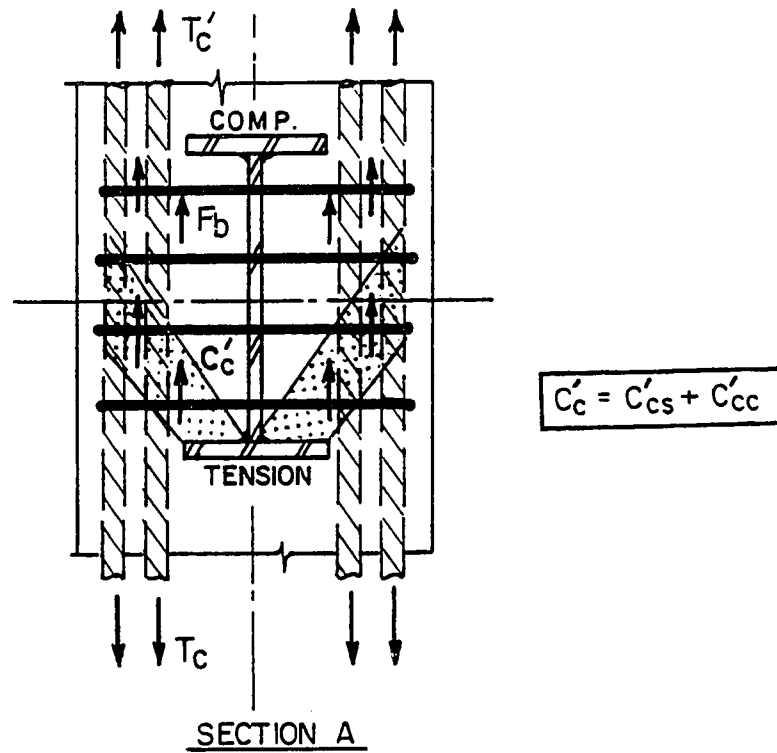


Fig. 5.3 Vertical bar forces inside the joint.

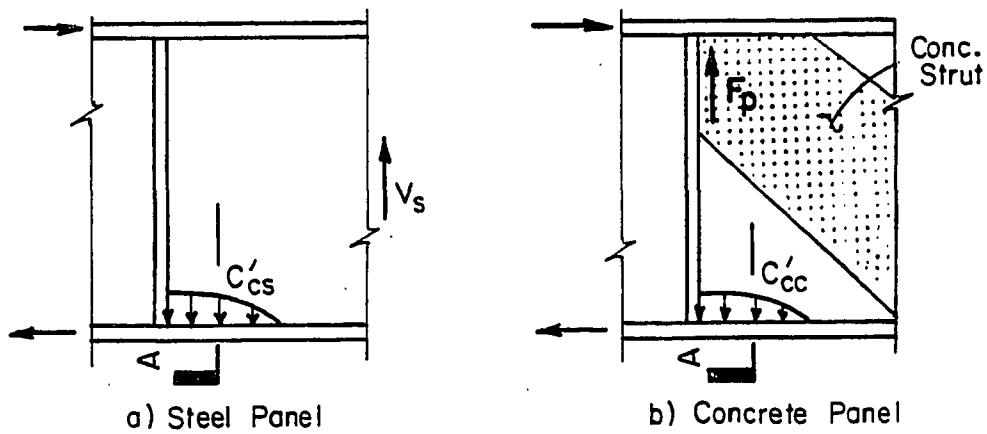


Fig. 5.4 Assignment of force C_c' to steel and concrete panels.

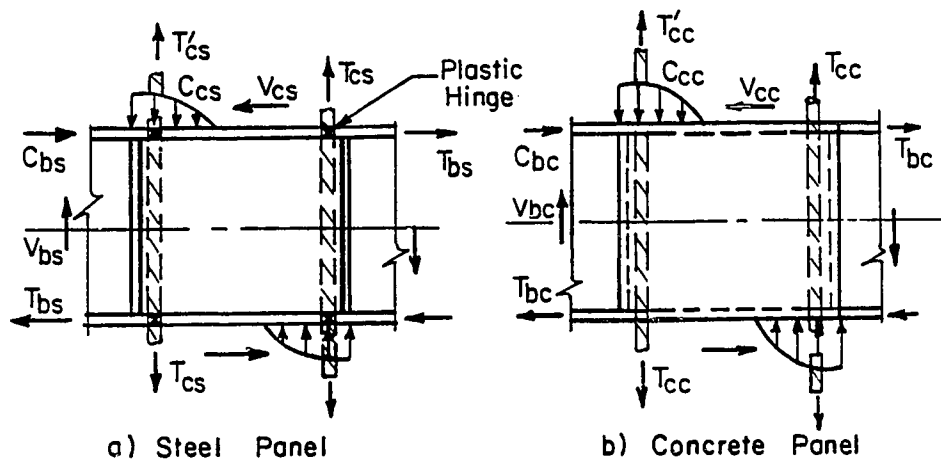


Fig. 5.5 Assignment of external forces to steel and concrete panels.

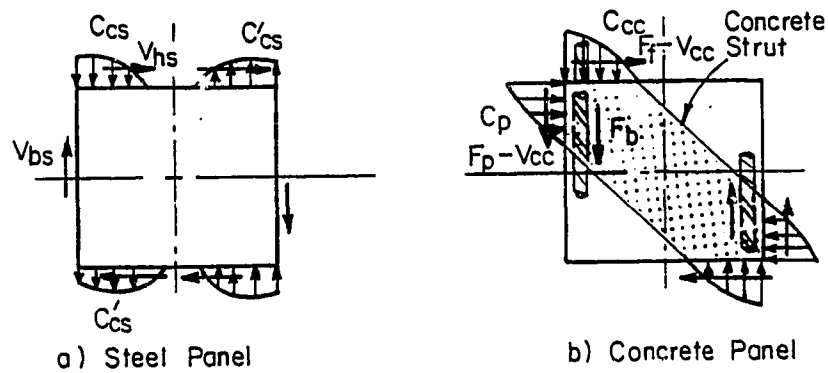


Fig. 5.6 Forces at the panel boundaries.

The forces acting on the boundary of the steel panel are shown in Fig. 5.6(a). The steel panel provides resistance to the joint forces by virtue of panel shear. The horizontal shear force, V_{hs} , is transmitted by the flange forces and may be calculated by summing the horizontal forces on a flange [refer to Figs. 5.5(a) and 5.6(a)], as follows:

$$V_{hs} = C_{bs} + T_{bs} - V_{cs} \quad (5.2)$$

The vertical shear force, V_{vs} , is caused by the stress blocks C_{cs} on the compression flange and C'_{cs} on the tension flange, as explained earlier and shown in Figs. 5.3 and 5.4(a). The stress block C_{cs} accounts for a major portion of shear. Summation of vertical forces on the left half panel shown in Fig. 5.6(a), gives the vertical shear force as

$$V_{vs} = C_{cs} + C'_{cs} - V_{bs} \quad (5.3)$$

The steel panel provides resistance to the joint forces by virtue of panel shear. After the shear strength of the steel panel is exhausted, additional shear resistance is provided by the bending of beam flanges about their own axis until plastic hinges are formed at the four locations shown in Fig. 5.5(a).

The concrete panel provides resistance to the joint forces by the familiar diagonal compression strut mechanism. The forces on the strut are shown in Fig. 5.6(b). The beam flange forces are transmitted to the strut, a) through FBPs as bearing stress block C_p and b) as friction force F_f under the compression flanges. The tension in the vertical bars is transferred to the concrete strut, partly as friction behind the FBPs, F_p , and by direct bond transfer, F_b . The majority of this bar tension,

however, reaches the concrete strut via the stress block C_{cc} which also includes flexural compression of the column. The net horizontal shear force in the concrete panel as per Fig. 5.6(b) is therefore,

$$V_{hc} = C_p + F_f - V_{cc} \quad (5.4)$$

The net vertical shear force in the concrete panel is equal to

$$V_{vc} = C_{cc} + F_b + F_p - V_{bc} \quad (5.5)$$

It should be noted here that the friction forces F_p and F_f can only be mobilized in the presence of the respective compression stress blocks C_p and C_{cc} . Furthermore, the equilibrium considerations require both horizontal forces C_p and F_f and vertical forces C_{cc} , F_p and F_b to be acting simultaneously in order to form the concrete strut. It is unlikely that the concrete panel will be effectively mobilized without face bearing plates or other means of direct stress transfer. The test results of specimens 1 and 3 reinforce this concept.

In the above description the general behavior of a steel beam-to-concrete column moment connection is outlined. Various components of forces at the boundaries of both steel and concrete panels are identified. Whereas each of these component forces are important from the behavioral aspect, only a few may be important for determining the joint strength at failure. As described in Chapter 4, the vertical bars in most specimens were significantly debonded at ultimate load. Hence the forces C'_{cs} , F_p and F_b were small. With the available test data it may not be possible to quantify these forces. Therefore, in the subsequent evaluation of the test results, their contribution will be

ignored. The steel and concrete panel are analyzed for the forces shown in Fig. 5.7.

5.4 Joint Shear

In order to determine the magnitude of the forces in Fig. 5.7 and thus shear force in the joint, the distribution of the forces $C_c (= C_{cs} + C_{cc})$ and C_p need to be known. In the absence of this information, further assumptions are made to estimate these forces. As shown in Fig. 5.8, the resultant of the compression block C_c is assumed at the centroid of the tension reinforcement. The resultant of the compression block C_p and friction force F_f is assumed at the centroid of beam flanges. Based on these assumptions, the tension force in the vertical bars, T_c , net compression force C_c and the total horizontal shear V_h at the failure load were calculated for each test specimen and are given in Table 5.2. The horizontal shear force carried by the steel panel, for those specimens in which shear yield was reached is estimated as,

$$V_{hs} = \frac{F_y}{\sqrt{3}} Z_c t_{sp} + \frac{4 M_p}{d_b} \quad (5.6)$$

- where
- F_y = measured yield strength
 - t_{sp} = thickness of steel panel
 - Z_c = distance between the centroids of the tension reinforcements.
 - M_p = plastic moment capacity of flanges based on the actual material strength, and
 - d_b = center-to-center distance between flanges.

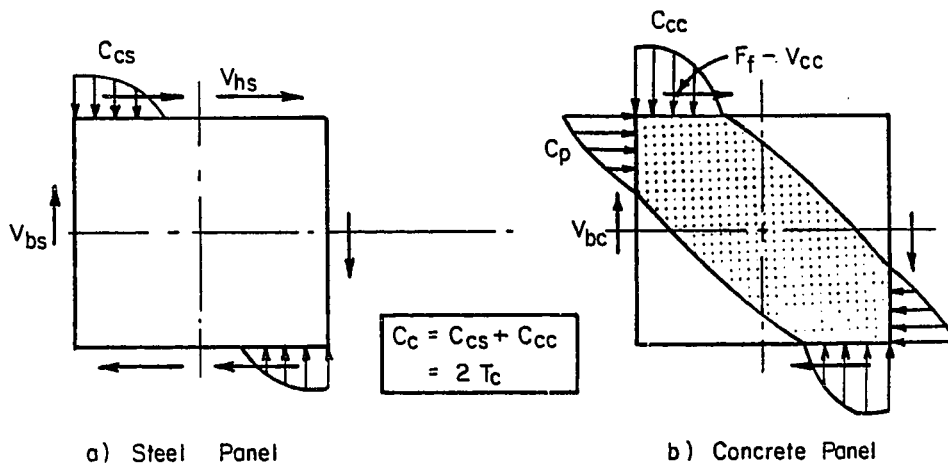


Fig. 5.7 Forces on the connection panel at failure load.

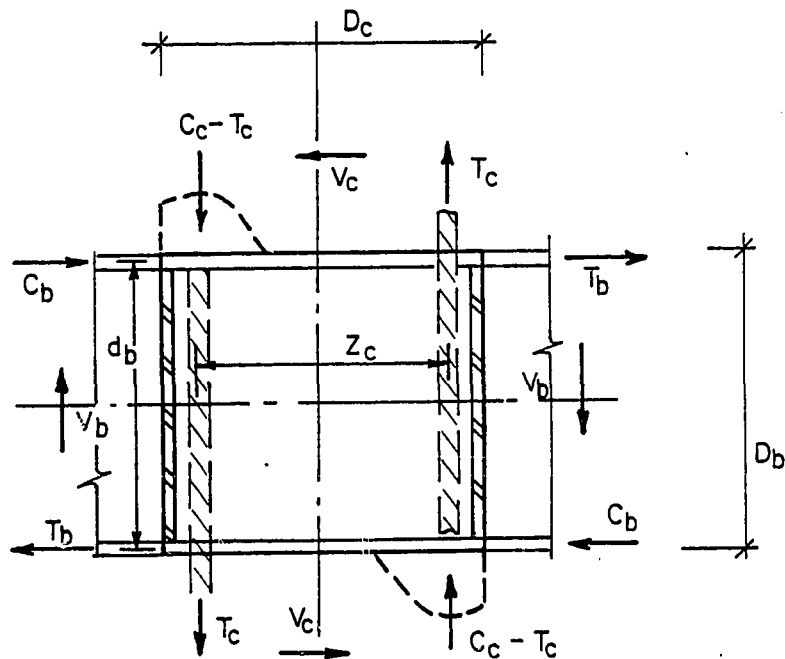


Fig. 5.8 Simplified analysis of joint.

Table 5.2 Estimated Joint Shear

Specimen No.	Panel Material Strength		Shear Cap. of Steel Panel V_{SP} (kips)	Failure Load (2% TUD) P (kips)	Rebar Tension T_c (kips)	Comp. Block $C_c=2T_c$ (kips)	Total Horiz. Shear V_h (kips)	Shear in Stl. Panel V_{hs} (kips)	Shear in Conc. Panel V_{hc} (kips)	Norm. Shear Stress γ	Remarks
	f'_c (ksi)	F_y (ksi)									
1	3550	56	98	18.0	66.4	133	106	98	8	2.2	Plain beam
2	3550	56	98	26.1	96.3	193	154	98	56	15.7	FBP
3	4500	36	92	18.5	107.7	215	165	92	73	6.8	Plain beam
4	4300	36	92	32.4	188.7	377	288	92	196	18.7	Thin FBP
5	4300	36	92	34.1	198.6	397	303	92	211	20.1	Thk. FBP
6	4000	36/50	510	46.8	272.5	545	416	372	e4	4.3	Doubler P
7	4000	36	92	41.4	241.1	482	368	92	276	18.2	Wide FBP
8	3600	36	92	55.0	320.3	641	489	92	397	41.4	Ext. FBP
9	3700	36	25	31.2	181.7	363	278	25	253	26.0	Hole

† Based on the measured shear stress = 20.5 ksi

For specimen 6, the horizontal shear in the steel panel is estimated based on the measured shear stress, F_s , as

$$V_{hs} = F_s Z_c t_{sp} \quad (5.7)$$

For specimen 9 in which the steel panel was cut out, the shear resistance due to the frame action of the remaining panel is estimated based on the plastic moment capacity of the T-sections.

The horizontal shear carried by the concrete panel is also listed in Table 5.2 and is calculated as the difference of V_h and V_{hs} ,

$$V_{hc} = V_h - V_{hs} \quad (5.8)$$

In order to normalize the concrete shear, the thickness of the concrete panel which was effective in providing shear resistance must be established. The data from the concrete gages indicated a large strain lag between the concrete panel within the width of beam flanges and FBP (whichever is larger) and that outside this region. Also the equilibrium considerations of the concrete strut require that it receive both vertical force C_{cc} and horizontal force C_p at its ends. Therefore the thickness of the concrete panel, t_{cp} , is assumed to be equal to the beam flange width, b_f or the width of FBP, w_p , whichever is larger.

$$t_{cp} = \max[b_f, w_p] \quad (5.9)$$

However, with this definition there should be a limit on the width of the FBP projecting beyond the flange width. The limit is addressed in the next chapter.

Based on the thickness of the concrete panel as defined in Eq. 5.9., the normalized shear stress,

$$\gamma = \frac{V_{hc}}{t_{cp} D_c \sqrt{f'_c}} \quad (5.10)$$

is also listed in table 5.2. For specimens 1, 3, and 6, in which any direct transfer of beam flange forces to the concrete panel was precluded, the magnitude of concrete shear stress was small and varied from $2.2 \sqrt{f'_c}$ in specimen 1 to $6.8 \sqrt{f'_c}$ in specimen 3. The relatively high value in specimen 3 was perhaps due to two factors, a) more transverse reinforcement in the joint, and b) low tension in the vertical bars resulting in less bond deterioration within the joint depth.

For specimens 4, 5, and 7, in which FBPs were used, the concrete shear stress varied from $18\sqrt{f'_c}$ to $20\sqrt{f'_c}$. However, specimen 2 carried only $15.7\sqrt{f'_c}$. It is not clear if the failure load of this specimen was controlled by the shear strength of the concrete panel. Specimen 9, with a hole in the steel panel, carried concrete shear stress of $26\sqrt{f'_c}$. This higher magnitude of shear stress, as well as the concrete strain gage data suggest a relatively wider concrete strut is mobilized in the presence of a weak steel panel. Specimen 8, which had extended FBPs, carried the highest magnitude of concrete shear stress, $41.4\sqrt{f'_c}$. Again, the higher concrete shear in Specimen 8 indicates that a wider concrete strut can be mobilized when the stiffness of the steel panel is low compared to the effective stiffness of the concrete panel, which is obvious from the joint stiffness and from the fact that the steel panel yielded at a high load for specimen 8.

5.5 Modes of Failure

Before the main parameters chosen for this study are evaluated, the possible modes of failure of the connection will be discussed. The following failure modes have been identified: shear failure of the panel zone, concrete crushing against the beam compression flange, concrete crushing against the face bearing plates, shear fracture of the face bearing plates, and transverse bending failure of the flanges and face bearing plates. Due to the limited number of tests it may not be possible to determine the load related to every mode of failure.

Connection Panel Shear. The connection panel consists of a steel panel and a concrete panel. In the absence of any direct means of stress transfer from beam flanges to the concrete panel, such as a FBP, almost the entire shear resistance is provided by the steel panel. However, when such means are provided, both steel and concrete panels resist the joint shear. Initially, the major part of the shear resistance is provided by the steel panel until it yields. Subsequently, the concrete panel is mobilized and furnishes the additional resistance without any noticeable change in joint stiffness and response. The connection is considered to have reached failure when the horizontal joint shear is equal to the total shear capacity as follows:

$$V_h = V_{sp} + V_{cp} \quad (5.11)$$

where V_{sp} and V_{cp} are the steel and concrete panel horizontal shear capacities, respectively.

Concrete Crushing Against Compression Flanges. As described earlier, the flexural forces from the concrete column including a substantial part of vertical bar tension is

transferred to the connection panel as a compression stress block C_c as shown in Fig. 5.1 and 5.8. This high intensity stress can best be termed "bearing stress" and acts on an area with a width equal to the thickness of the concrete panel, t_{cp} , as defined in Eq. 5.9, or the flange width, b_f , when FBPs are not provided. The extent of this area, as well as the actual distribution of the force C_c cannot be determined in the present scope of work. However, it is clear that if this force is too high and distributed on a narrow area, the connection may fail due to crushing of concrete under high bearing stress, similar to the failure of specimen 6.

Concrete Crushing Against the Face Bearing Plates. It was explained in the last chapter that the beam flange forces are transferred to the concrete panel by friction F_f under the flanges and by the bearing stress block C_p acting against the FBPs as shown in Fig. 5.6(b). Although the magnitude of each of these forces was not determined experimentally, the sum of the two forces should be approximately equal to the shear force in the concrete panel, V_{hc} . Also, the distribution of the force C_p cannot be determined with the available test data. Under certain conditions the bearing stress may exceed the crushing strength of the concrete in the connection panel, resulting in a premature failure of the connection. In the series of tests conducted in this study none of the specimens appeared to fail in this mode.

Shear Fracture of Face Bearing Plates. The transfer of flange forces to the concrete panel through the FBP can adversely affect the steel beam and the FBP. Forces on the flanges and the FBP are shown in Fig. 5.9. Equilibrium requires that the following relationship be satisfied.

$$C_p + F_f = C_{bc} + T_{bc} - V_{cc} \quad (5.12)$$

The distribution of force C_p across the depth of the FBP depends on the thicknesses of the steel web, steel panel and FBP. The intensity of bearing stress would be maximum near the beam flanges and the shear in the FBP along a-b-c, as shown in Fig. 5.9 would be equal to the total force C_p . The FBP should be thick enough to preclude shear fracture along a-b-c. For beam sections with a thin web and steel panel, the shear transferred along line b-c may be controlled by the capacity of the steel web in compression just outside the joint and that of the steel panel in tension inside the joint.

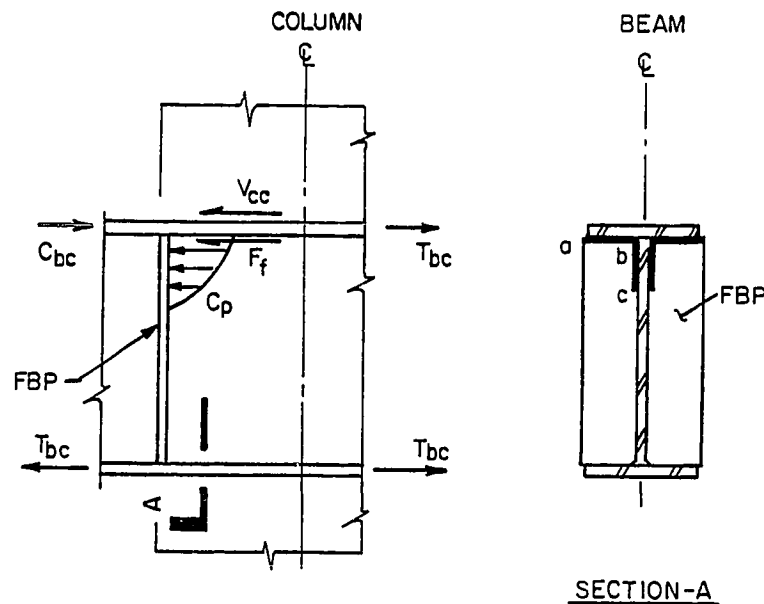


Fig. 5.9 Forces on face bearing plates.

The connection failure in this mode was not experienced in any of the nine tests. However, if this failure mode controlled, it would have occurred in specimen 4, since it had 3/8-in. FBPs with measured yield strength, F_y , of 43.4 ksi and ultimate strength, F_u , of 68.5 ksi. Calculations indicate that beam web yielding rather than FBP fracture would control along side b-c. Assuming length b-c equal to one quarter the clear beam depth, i.e. 4 in., the force C_p at shear fracture of the FBP is

$$\begin{aligned}
 C_p &= \frac{F_y}{\sqrt{3}} 2 l_{ab} t_p + F_{yw} 2 l_{bc} t_w & (5.13) \\
 &= \frac{68.5}{\sqrt{3}} \times 2 \times 3.75 \times .375 + 36.5 \times 2 \times 4 \times .26 \\
 &= 111.2 + 75.9 = 187.1 \text{ kips}
 \end{aligned}$$

Hence, the maximum force C_p in specimen 4 is 187 kips. A lower-bound estimate for the shear in the concrete panel of the specimen, at failure is 196 kips (Table 5.2). This comparison reinforces the assumption that at least a part of the flange force was transferred to the concrete panel as friction force F_f . Strain hardening of the beam web along b-c could also explain the higher strength but extensive yielding of the beam web was not observed so the friction component seems more plausible.

Transverse Yielding of Flanges and Face Bearing Plates.

As stated in Section 5.2, the transfer of column flexural force C_{cs} to the steel panel causes the beam flanges to bend inward. The two flanges are stiffened by the concrete wedged between them and the steel panel, as shown in Fig. 4.51(a). However, if the

flanges are too thin to support the force C_{CS} , required to yield the steel-panel in shear, the flanges will yield in transverse bending. This may be followed by a premature crushing of concrete bearing above the flanges. The effective width of the flanges supporting C_{CS} may decrease when the beam flanges are wide and thin. This mode of failure should be guarded against when a thick steel panel is provided since this produces a large potential force C_{CS} . It is worth noting that a substantial portion of the strength of the concrete panel may not be mobilized until after the steel panel yields in shear as the distortion of the steel panel becomes different in nature from that of the concrete panel.

The behavior of the FBP in transferring the flange forces to the concrete panel as bearing force C_p , is similar to that of the beam flanges described above, except that the stiffening effect of the concrete wedges is not present. Therefore, when the FBPs are wide and thin, their entire width may not be effective in supporting the force C_p , resulting in premature crushing of concrete bearing against these plates.

5.6 Thickness of Face Bearing Plates

The results of this test series show that the face bearing plates substantially enhance the connection strength by effectively mobilizing the concrete in the joint area. The plot of total joint distortion for pilot specimens 1 and 2 in Fig. 4.47 show a 45% increase in both strength and stiffness of the joint due to the FBPs. The plot for specimens 3, 4, and 5, shown in Fig. 4.45, indicate the FBPs increased the joint strength by 75 to 85%; however, they did not change the stiffness.

One of the main parameters chosen in this study was the thickness of the FBP. A 3/8-in. thick, A36 plate with width-to-

thickness ratio, $w_p/t_p = 10.7$ was used in specimen 4, while a 7/8-in. thick, Grd. 50 plate with $w_p/t_p = 4.6$ was employed in specimen 5. The results of the two specimens, shown in Fig. 4.45, indicate the thickness of the FBP had no appreciable effect on strength or stiffness of the joint.

The strain gages mounted on the FBPs of specimen 4 indicate yielding occurred near the weld toe. Yielding of those plates was also observed when flakes of mill scale separated from the plates. The strain gages of specimen 5 showed almost the same magnitude of stress but no yielding of the Grd. 50 FBP. These results indicate that the bearing force C_p on the FBPs was concentrated near the web and flanges, more so on the thin plate of specimen 4 than the thick plate of specimen 5.

The face bearing plates of specimen 4 appear to give realistic data on which to select the thickness of the FBP.

5.7 Width of Face Bearing Plate

To evaluate the effect of FBP width, a 12-in. instead of an 8-in. wide FBP was used in specimen 7 which was otherwise similar to specimen 5. A comparison of the test results for the two specimens, plotted in Fig. 4.45, indicate a 20% increase in strength and about 35% increase in the stiffness of the joint.

The data from the strain gages mounted on the FBPs of specimen 7 indicated the bending stress at the weld toe reached yield (60 ksi) at ultimate load. In comparison, the stress in specimen 5 reached a maximum of 40 ksi. The bearing force C_p was high and distributed over a wider FBP in specimen 7. Also, the results of the strain gages embedded in the concrete panel (Sect. 4.5.2) indicate a wider concrete diagonal strut was mobilized in specimen 7. As analyzed in Sec. 5.4, the wider FBPs of specimen 7 effectively increased the thickness of the concrete panel to 12

in. How far the FBPs can be extended beyond the flange width without reducing their effectiveness still needs to be determined.

5.8 Configuration of Face Bearing Plates

A FBP between the two flanges of the beam is not the most efficient configuration for transferring the flange forces to the concrete panel. At the expense of some added cost, the efficiency of FBPs may be improved by extending them above and below the beam. This configuration was studied in specimen 8, which was otherwise similar to specimen 5.

The results of specimens 5 and 8, shown in Fig. 5.10, indicate the extended FBPs increased the joint strength by 60% and the stiffness by more than 150%. Since the two specimens had identical steel panels, the entire increase in joint strength came from mobilizing a larger volume of concrete in the connection panel. As shown in Table 5.2, the shear capacity of the concrete panel in specimen 8 was more than double that of specimen 5. Also, the compression force C_c bearing on the compression flanges was 18% higher than specimen 6, which failed by crushing of the concrete against the compression flanges. This means the crushing strength of concrete bearing on the compression flanges was enhanced due to the additional confinement provided by the extended FBPs.

The maximum stress recorded by the strain gages mounted on the portion of FBPs fitting between the top and bottom flanges of specimen 8 was about 20 ksi, i.e. almost half of what was recorded in specimen 5 at the peak load. The gages on the extended portion of FBPs indicated the stress near the weld toe was less than 20 ksi prior to reaching ultimate load at which point the stress increased rapidly to yield (60 ksi). This shows

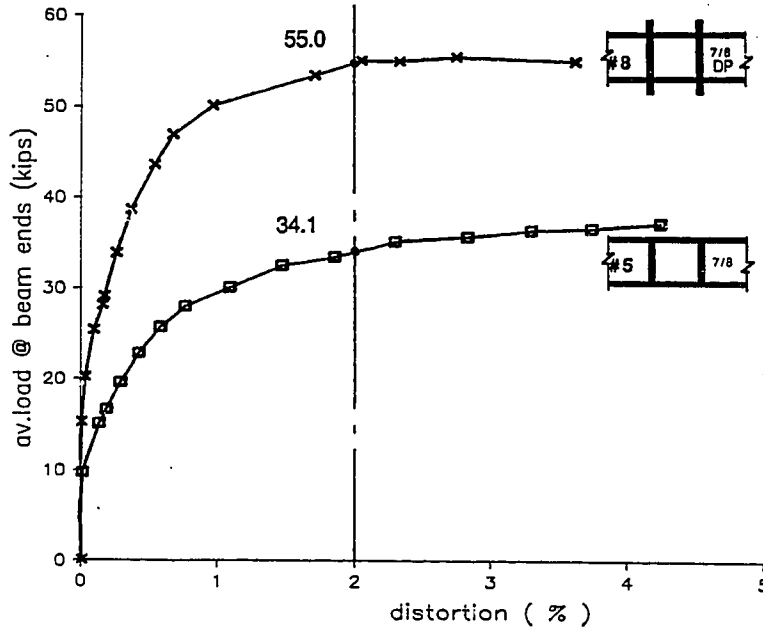


Fig. 5.10 Load vs TJD plot for specimens 5 and 8.

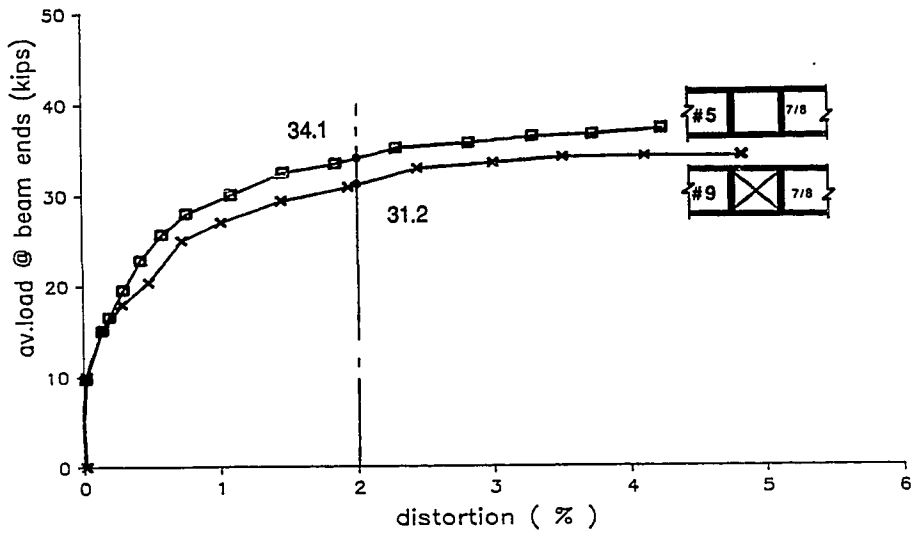


Fig. 5.11 Load vs TJD plot for specimens 5 and 9.

that the extended portion of FBPs transferred a substantial part of the flange forces to the concrete panel, thus mobilizing the concrete more efficiently.

5.9 Thickness of Steel Panel

The steel panel was varied in thickness from 1/4-in. in most specimen to 1-1/4-in. in specimen 6 to almost zero in specimen 9, in order to examine the influence of the steel panel strength on connection capacity.

The response of specimens 3 and 6 are plotted in Fig. 4.46. While the thicker steel panel of specimen 6 enhanced joint strength to almost 2.5 times that in specimen 3, the joint stiffness was improved by only 30%. As planned, the mode of failure of the connection was changed from connection panel shear in specimen 3 to concrete crushing against the compression flanges in specimen 6. This gave information regarding the bearing strength of the concrete on the compression flanges. The strain gage data for specimen 6 indicate yielding of flanges at the centerline due to bending in the transverse direction at 3/4 of the maximum load. It is not clear how much this might have influenced the concrete bearing strength, certainly the results yield a lower-bound value.

The results of specimens 5 and 9, as shown in Fig. 5.11 and analyzed in Table 5.2, show that the absence of the steel panel in specimen 9 increased the shear capacity of the concrete panel by about 30%, compared to that in specimen 5 which had a 1/4-in. thick steel panel. The overall stiffness of the joint was not affected. The data from the strain gages embedded in the concrete panel suggest a relatively wider diagonal concrete strut was mobilized in specimen 9.

CHAPTER 6

DESIGN RECOMMENDATIONS

In this chapter a design approach is formulated for proportioning and detailing the moment connections between steel beams and concrete columns. The approach is developed for connections in moment resisting plane frames or framed tubes, primarily for non-seismic loads and is confined to interior connections. The approach can be extended to exterior connections; however, corner or knee connections are excluded. The formulation is based on the results of this experimental data discussed in chapters 4 and 5.

In current practice a moment connection between steel members is designed according to the AISC Load and Resistance Factor Design (LRFD) Specifications, September 1986 [6] or the AISC Specifications, November 1978 [5]. A moment connection between concrete members is designed according to the ACI-ASCE Committee 352 recommendations [15]. The design philosophy for the moment connections in non-seismic zones differs in the two specifications. While LRFD specifications require the connections to be designed for the adjoining member forces due to factored loads, ACI-ASCE Recommendations require them to resist the actual flexural strength of the adjoining beams, based on the specified strength of concrete and reinforcing steel. The calculated flexural strength of the reinforced concrete beams does not differ substantially from the beam forces due to factored loads since reinforcement is provided for strength only.

It seems appropriate that the connections between steel beams and concrete columns should be designed based on the forces due to factored loads similar to that required by the LRFD specifications. This would eliminate an unnecessary premium on

connection costs and details when the sizes of the structural members are controlled by stiffness and drift requirements and not by the strength considerations. However, the importance of strong and stiff joints cannot be emphasized enough. Joint distortion at service load and factored loads must be controlled to ensure the integrity of the joint and the column, thus minimizing the consequences of inaccuracies in the structural analysis which may result due to flexibility of joints, inelastic flexural deformation of members, etc. Also, under creep and shrinkage, the induced forces due to relative axial movement of columns and the second order effects may exceed those considered in normal structural analysis. Therefore, the connections in this design approach are recommended to be designed for 120% of the adjoining member forces resulting from factored loads, even when these amplified forces exceed the member strengths. This additional factor of safety is in line with the AISC design philosophy which provides a F.S. of 2.0 for sudden and brittle failures, e.g. material fracture or member buckling and a F.S. of 1.67 for gradual and ductile failures like material yielding and flexural plastification of members.

6.1 Parameters Governing Design

As discussed in Chapter 5, the most important parameters controlling various failure modes of a moment connection between a steel beam and a concrete column are the bearing strength of concrete against the compression flanges and the face bearing plates, the size and configuration of the FBPs, and the shear capacities of the steel and concrete panels. Other considerations which need to be included in these design recommendations are flange size, joint aspect ratio, joint reinforcement, bond conditions, and joint stiffness. These later

parameters, which have not been investigated in this experimental program, are included in these recommendations in an implicit form, based on the past research and practice, as well as, the observed behavior of the test specimens.

6.2 Proposed Model for Joint Forces

Figure 6.1 shows a typical interior connection between a steel beam and a concrete column, subjected to forces from the adjoining members due to lateral loads. When the connection reaches capacity or fails, these forces are resolved as shown in Fig. 6.2. The column vertical bars are considered to be completely debonded and the bearing force C_c is considered to be acting on an area having length a_c and effective width, b_e , with uniform bearing stress $\lambda_c f'_c$, where λ_c is the coefficient of bearing stress against the compression flange. The effective width, b_e , is equal to the thickness of the concrete panel, t_{cp} , as defined in Chapter 5. That is,

$$b_e = \max[b_f, w_p] \quad (6.1)$$

where b_f is flange width and w_p is width of the FBP. Summing up all the vertical forces shown in Fig. 6.2 at a column section near the top flange,

$$C_c = 2T_c = \lambda_c f'_c b_e D_c \left(\frac{a_c}{D_c} \right) \quad (6.2)$$

Summation of moments due to these forces yields,

$$M_c = 0.5 C_c D_c \left(1 - \frac{a_c}{D_c} \right)$$

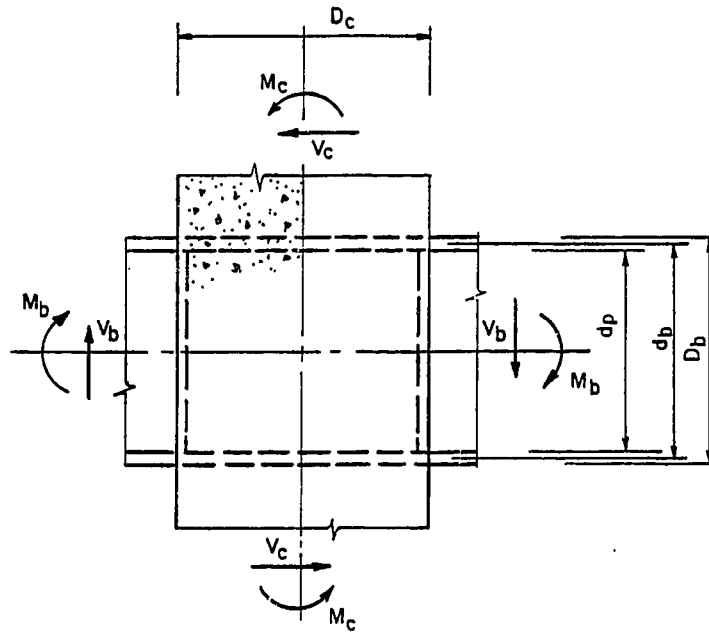


Fig. 6.1 Forces on a steel beam-to-concrete column connection due to lateral loads.

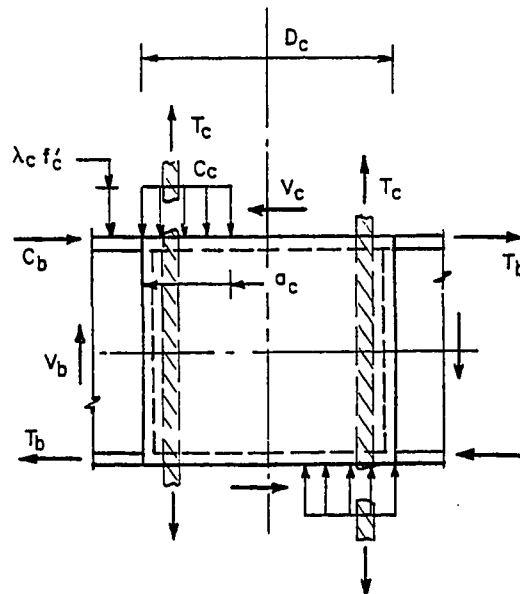


Fig. 6.2 Modelling of external forces on the joint.

$$= 0.5 \lambda_c f'_c b_e D_c^2 \left[\frac{a_c}{D_c} \left(1 - \frac{a_c}{D_c} \right) \right] \quad (6.3)$$

The joint shear resistance is furnished by both steel and concrete panels as shown in Fig. 6.3. The steel panel provides resistance by virtue of pure shear strength and the concrete panel by diagonal compression strut strength. The total horizontal shear capacity of the joint is thus equal to

$$V_h = V_{sp} + V_{cp} \quad (6.4)$$

where V_{sp} is the steel panel capacity and V_{cp} is the concrete panel capacity mobilized after the steel panel has reached its capacity.

The flange forces are considered to be transferred to the concrete panel entirely as bearing force C_p against the FBPs, on an area having width w_p and depth a_p . For the distribution of this bearing force C_p triangular as well as rectangular bearing blocks were considered. Triangular distribution may better model the actual behavior but a rectangular bearing block results in less complicated computations. Hence, the bearing forces C_p is considered to be distributed with a uniform bearing stress $\lambda_p f'_c$, where λ_p is the plate bearing stress coefficient. The joint forces exerted on the beam are shown in Fig. 6.4. As was shown in Figs. 5.5(b) and 5.6(b), the transfer of flange forces T_{bc} to the concrete panel through the FBP cause tension in both flanges. Summation of horizontal forces shown in Fig. 6.4 at a beam section adjacent to the FBP gives,

$$C_p = 2T_{bc} = \lambda_p f'_c w_p d_p \left(\frac{a_p}{d_p} \right) \quad (6.5)$$

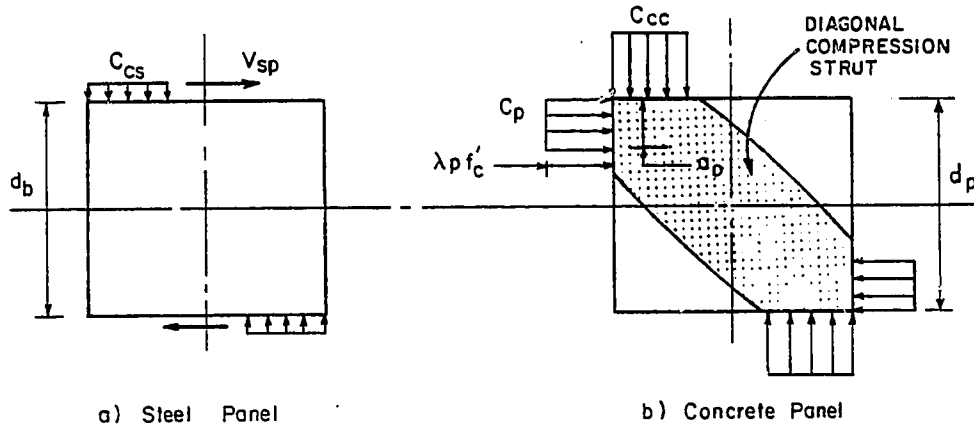


Fig. 6.3 Modelling of forces on the connection panel.

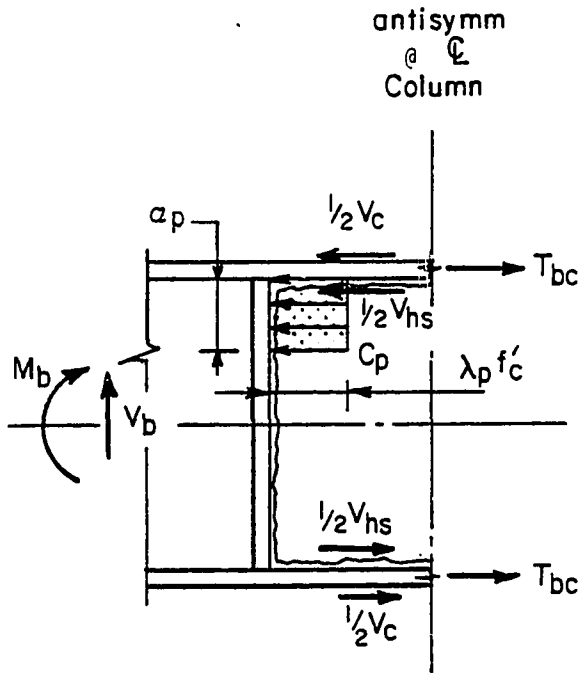


Fig. 6.4 Forces on steel beam.

The summation of the moments due to these forces must be equal to the beam moment,

$$\begin{aligned}
 M_b &= 0.5 C_p d_p \left(1 - \frac{a_p}{d_p}\right) + 0.5 V_{hs} d_b + 0.5 V_c D_b \\
 &= 0.5 \lambda_p f'_c w_p d_p^2 \frac{a_p}{d_p} \left(1 - \frac{a_p}{d_p}\right) + 0.5 V_{hs} d_b + 0.5 V_c D_b
 \end{aligned}
 \tag{6.6}$$

Also, horizontal shear across the concrete panel shown in Fig. 6.3(b) can be expressed as:

$$V_{hc} = C_p = \lambda_p f'_c w_p d_p \frac{a_p}{d_p}
 \tag{6.7}$$

The proposed model, as described here, can be used to estimate the ultimate strength of a steel beam-to-concrete column connection as a function of the values chosen for the bearing stress coefficients λ_c and λ_p and the ratios a_c/d_c and a_p/d_p . The evaluation of these coefficients and ratios, as well as the horizontal shear capacity of the joint, are presented in the following section.

6.3 Explicit Considerations

6.3.1 Bearing Block Size and Intensity

a) Bearing against compression flanges (a_c, λ_c). The values for the depth of the bearing block, a_c , and the bearing stress coefficient, λ_c , should be chosen such that the failure of the connection due to crushing of concrete against compression flanges is prevented. Specimen 6 (with doubler plates) was forced to fail in this mode, hence the results of this test are

used to evaluate a_c and λ_c . For specimen 6, Eqs. 6.2 and 6.3 indicate that a value of 0.3 for the ratio a_c/D_c and 3 for the coefficient λ_c satisfy both column moment (M_c) and joint shear. In almost all the test specimens, irrespective of the failure mode, crushing of concrete against the compression flanges was noted as the drift increased. The failure was similar in behavior to that of an under-reinforced concrete section in flexure where concrete crushes at eventual failure. Therefore, the design philosophy is kept similar to that of under-reinforced concrete sections in flexure. A constant value of 3 is recommended for λ_c , with the ratio a_c/D_c varying from 0 to a maximum value of 0.3. That is, for the connections where a FBP is provided between the flanges only,

$$\lambda_c = 3 \quad (6.8a)$$

and

$$a_c/D_c \leq 0.3 \quad (6.8b)$$

The effective width of the bearing block is equal to b_e , as defined in Eq. 6.1.

b) Bearing against Face Bearing Plates (a_p, λ_p). The values for the depth of the bearing block, a_p , and the bearing stress coefficient, λ_p , should be chosen to prevent crushing of concrete against the face bearing plates. In the series of tests conducted in this research program, none of the test specimens failed in this mode. However, specimen 9 (with a cut-out steel panel) had the highest bearing stress against FBPs. An analysis of test results of this specimen according to Eqs. 6.5 and 6.6 yield a bearing stress coefficient, λ_p , of 3 when the depth of the bearing block, a_p , is equal to $0.25 d_p$. Hence, the maximum values for the coefficient λ_p and ratio a_p/d_p are conservatively

taken as 3 and 0.25, respectively. In a design approach the bearing force could be distributed in one of the following two ways. Either the stress intensity, i.e. λ_p could be kept constant while varying the depth a_p , similar to the way a bearing force on the compression flange is handled, or the depth a_p could be kept constant while varying the stress intensity λ_p according to the magnitude of the total force. For concrete bearing against the FBP, the latter approach is adopted. It has the advantages of simpler computations and better represents the behavior at low loads. Hence, a constant value of 0.25 is recommended for the ratio a_p/d_p with the coefficient λ_p varied from 0 to a maximum of 3. That is, for the connections where a FBP is provided between the flanges only,

$$a_p/d_p = 0.25 \quad (6.9a)$$

and

$$\lambda_p \leq 3 \quad (6.9b)$$

The effective width of the bearing block is equal to w_p , the width of the FBP.

6.3.2 Face Bearing Plate Size and Configuration

a) Width: Face bearing plates enhance the capacity of a steel beam-to-concrete column connection by mobilizing the concrete panel for the resistance of joint shear. With a minimal additional cost, the connection capacity is further increased when a FBP wider than the flange width is used. This increase is taken into account by considering (a) the effective width, b_e , of the bearing forces C_c and C_p and (b) the effective thickness of the concrete panel, both equal to the width of the FBP. It is, however, certain that the width of the FBP cannot be projected

too far beyond the flange width without adversely affecting its function. In the absence of any experimental data, it is arbitrarily recommended that such projection be limited to 2.5 times the plate thickness. That is

$$w_p \leq b_f + 5t_p \quad (6.10)$$

where t_p is the thickness of the FBP.

b) Depth: The beam flange forces can be transferred to the concrete panel much more efficiently by extending the FBP above and below the beam. This extension of the FBP also enhances the crushing strength of concrete against compression flanges by providing additional confinement. An analysis of the results of specimen 8 yield a bearing stress coefficient λ_c of 3.8 when the ratio $a_c/D_c \leq 0.3$ is used. Due to a lack of test data it is recommended that a conservative value of the coefficient λ_c be taken as 3.5 where the FBP is extended above and below the beam, i.e.

For extended FBP

$$\lambda_c = 3.5 \quad (6.11)$$

In the previous section, the depth of the bearing block, a_p , and the bearing coefficient λ_p were defined for connections where the FBP is provided between the two flanges. The bearing force C_p on the FBP extended a distance e_p above and below the beam is diagrammatically shown in Fig. 6.5. If the depth of the FBP, d_p , is defined as shown in Fig. 6.5, the expressions for the force C_p moment M_b and shear V_{hc} , as given in Eqs. 6.5 through 6.7 would still be valid provided the flange thickness, t_f , is small compared to the FBP depth, d_p . It seems reasonable to assume that for any substantial increase in connection strength, the FBP should be extended at least a distance $d_p/4$ or $b_f/2$.

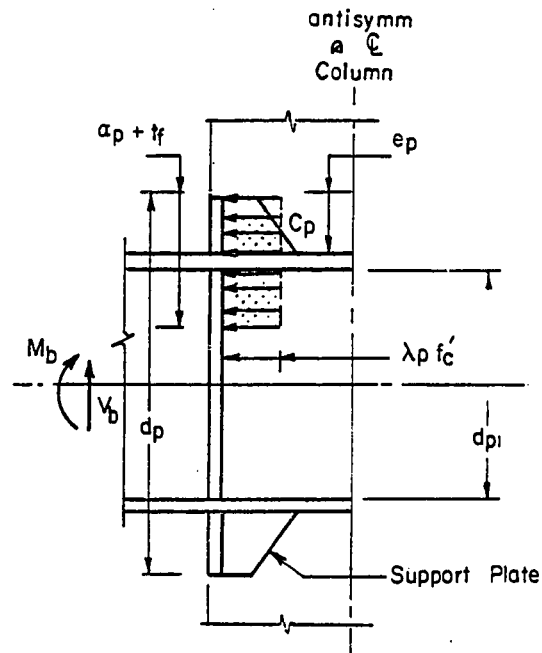


Fig. 6.5 Forces on extended face bearing plate.

Also, the FBP portion near the flanges, steel panel and the support plate would be the stiffest part and hence bear most of the force C_p . Therefore, for the connections where the FBP is extended above and below the beam, the depth of the bearing block, a_p , is recommended as

$$a_p = 0.25d_{p1} + e_p \leq 0.5 d_{p1}$$

or

$$a_p/d_p = 0.25 d_{p1}/d_p + e_p/d_p \leq 0.5 d_{p1}/d_p \quad (6.12)$$

For the bearing stress coefficient λ_p , it is recommended that the value given in Eq. 6.9(b) be taken. The support plate should be

designed as a bracket for the bearing force resisted by the extended FBP, i.e. $\lambda_p f'_c W_p e_p$.

c) Thickness. The thickness of the FBP should be proportioned to prevent shear fracture and flexural yielding under the bearing force C_p . Referring to Fig. 5.9 and as mentioned in Sec. 5.5, the shear transferred along b-c is controlled by either a) the capacity of the steel web in compression at one side of the FBP and in tension at the other, or b) the ultimate shear capacity of the FBP itself. Assuming the length b-c is equal to $b_f/2$, the bearing force C_p , when the FBP reaches shear fracture [case (a)], may be expressed as

$$C_p = \frac{1}{\sqrt{3}} F_{ub} b_f t_p + F_{yw} b_f t_w \quad (6.13)$$

Since the bearing force C_p is equal to the shear force in the concrete panel, V_{hc} , the thickness of the FBP may be given as

$$t_p = \frac{\sqrt{3} (V_{hc} - b_f t_w F_{yw})}{b_f F_{ub}} \quad (6.14)$$

where F_{ub} is the tensile strength of the FBP material and F_{yw} is the yield strength of the beam web outside the joint.

In case (b) when the shear capacity of the FBP controls shear transfer along the entire length a-b-c, the bearing force C_p at shear fracture may be written as:

$$C_p = \frac{2}{\sqrt{3}} F_{ub} b_f t_p \quad (6.15)$$

which gives the following expression for the thickness of the FBP.

$$t_p = \frac{\sqrt{3} V_{hc}}{2 b_f F_{ub}} \quad (6.16)$$

To prevent shear fracture of the FBP, its thickness should be equal to the larger of the two values given by Eqs. 6.14 and 6.16.

The FBP should also be thick enough to provide the bending strength needed to support the bearing force C_p (Fig. 5.9). Since the exact distribution of the bearing force C_p is not known, the flexural forces in the plate cannot be determined accurately. Therefore, based on the test results of specimen 4 in which a 3/8-in. thick FBP was used, an empirical equation is developed for the thickness of the FBP. If a uniform bearing pressure of intensity $C_1 V_{hc}/(w_p d_p)$ is assumed on the FBP (Fig. 6.4), the FBP moment may be estimated as:

$$\text{FBP Moment} = C_2 \left(\frac{C_1 V_{hc}}{w_p d_p} \right) w_p^2 \quad (6.17)$$

where C_1 and C_2 are constants. The flexural resistance of the FBP can be written as

$$\text{FBP Capacity} = C_3 t_p^2 F_{yb} \quad (6.18)$$

Equating Eqs. 6.17 and 6.18, the expression for FBP thickness can be written as

$$t_p = C_4 \left(\frac{V_{hc} w_p}{F_{yb} d_p} \right)^{0.5} \quad (6.19)$$

From the test results of specimen 4, the constant C_4 is determined to be about 0.2. Hence, to prevent flexural yielding of the FBP, its thickness is recommended as

$$t_p = 0.20 \left(\frac{V_{hc} w_p}{F_{yb} d_p} \right)^{0.5} \quad (6.20)$$

Also, from the stiffness standpoint, the width-to-thickness ratio of the FBP is recommended to be kept less than 22

$$w_p/t_p \leq 22 \quad (6.21)$$

6.3.3 Steel Panel Capacity. The steel panel resists the joint shear until it yields. After complete yielding some additional resistance is furnished by frame action of the flanges bent about their own axis. This additional resistance is ignored in this design approach. The horizontal shear capacity of the steel panel is recommended to be taken as:

$$V_{sp} = \frac{1}{\sqrt{3}} F_{yp} t_{sp} D_c \left(1 - \frac{a_c}{D_c} \right) \quad (6.22)$$

where F_{yp} is yield strength and t_{sp} the thickness of the steel panel.

6.3.4 Concrete Panel Size and Capacity. The concrete panel provides resistance to joint shear through a diagonal compression strut mechanism. A substantial part of this resistance is mobilized only after the steel panel has yielded. Tests have demonstrated that the effective thickness of the concrete panel is equal to b_e , as defined in Eq. 6.1. With this definition for the size of the concrete panel, the horizontal shear capacity of the concrete panel can be expressed as follows:

$$V_{cp} = \gamma \sqrt{f'_c} b_e D_c \quad (6.23)$$

where f'_c is the compressive strength of concrete in psi and γ is a shear strength factor for the concrete panel.

To evaluate γ , the test results are reanalyzed in Table 6.1 using the proposed model for the joint forces described in Section 6.2. The bearing block depths a_c and a_p and the bearing stress coefficients λ_c and λ_p are defined in Eqs. 6.8, 6.9, 6.11 and 6.12. The horizontal shear in the steel panel V_{hs} , is calculated as:

$$V_{hs} = \frac{2M_b}{d_b} - V_c \leq V_{sp} \quad (6.24)$$

where V_{sp} is the horizontal shear capacity of the steel panel which for the purpose of this analysis is given by Eq. 6.22, to which the additional shear due to plastic hinging of the flanges is added. This gives a lower-bound value for shear in the concrete panel. For specimen 6, in which the steel panel did not reach its shear capacity, the horizontal shear V_{sp} is limited to the value, estimated based on measured shear stress in the steel panel. For specimen 9 in which the steel panel was cut-out, the shear capacity V_{sp} is estimated as the shear resistance due to the frame action of the remaining panel based on the plastic moment capacity of the T-sections. The horizontal shear in the concrete panel, V_{hc} , is calculated using Eqs. 6.6 and 6.7, i.e.

$$V_{hc} = \frac{(2M_b - V_{hs}d_b - V_c D_b)}{d_p \left(1 - \frac{a_p}{d_p}\right)} \quad (6.25)$$

Table 6.1 Revised Analysis of Test Results

Specimen No.	Panel Material		Failure Load P (kips) (4)	Column Moment M_c (k-in) (5)	Beam Moment M_b (k-in) (6)	λ_g (6)	a_c/D_c (7)	V_{cs} (kips) (9)	V_{co} (kips) (10)	λ_p (11)	a_p/d_p (12)	$V_{uc}/b_e D_c f'_c$ (13)	Failure Mode (14)
	f'_c (ksi) (2)	F_y (ksi) (3)											
1	3550	56	18	764	729	3.0	.20	103	3	—	0	.8	Panel shear
2	3550	56	26.1	1108	1057	3.30	.30	89	89	2.19	.25	24.9	Crush on Flange/ Panel Shear
3	4500	36	18.5	1562	1591	3.0	.08	112	54	—	0	5.0	Panel Shear
4	4300	36	32.4	2735	2786	3.0	.16	101	260	1.89	.25	24.8	Panel Shear
5	4300	36	34.1	2878	2933	3.0	.17	100	283	2.06	.25	27.0	Panel Shear
6	4000	36/50 (20.5)	46.8	3950	4025	3.0	.29	367*	49	—	0	4.8	Crush on Flange
7	4000	36	41.4	3495	3560	3.0	.14	101	372	1.94	.25	24.5	Panel Shear
8	3600	36	55	4643	4730	3.84	.30	79	390	1.69	.31	40.6	Crush on Flange/ Panel Shear
9	3700	—	31.2	2634	2683	5.0	.18	25	352	2.97	.25	36.2	Panel Shear

* based on actual stress in steel panel

This value of V_{hc} is listed in column 10 of Table 6.1. The shear strength factor, γ , is calculated in column 13. The probable mode of failure for each specimen is listed in column 14.

The analysis of test results presented in Table 6.1 shows the connection in specimen 6 failed due to crushing of concrete against the compression flanges. Failure of specimens 2 and 8 was either due to crushing of concrete against the compression flanges or shear in the connection panel. The remaining specimens clearly failed in shear at the connection panel.

The calculated values of the shear strength factor, γ , for the concrete panel of the test specimens are listed in column 13 of Table 6.1. Two distinct ranges of values are noticed. For specimens with FBP placed between the flanges, γ varied from 24.5 to 27.0. For the specimen having a cut-out steel panel and that with extended FBP, γ ranged from 36.2 to 40.6. It is clear that if the effective thickness of the concrete panel, b_e , is defined by Eq. 6.1, the shear strength factor, γ , is a function of (a) the relative stiffness and strength of the steel panel and (b) whether the FBPs are extended above and below the beam or not. The ratio of concrete panel shear capacity to that of steel panel for specimen 9, which had a cut-out steel panel, was approximately 14.0. However, it is unlikely that the shear capacity of the concrete panel would have changed much if this ratio was somewhat lower. There is a certain ratio of concrete and steel panel shear capacities, beyond which a higher value of shear strength factor, γ , could be used. This ratio is arbitrarily chosen equal to 10.0, i.e.

$$V_{cp}/V_{sp} > 10.0 \quad (6.26)$$

Substituting Eqs. 6.22 and 6.23, this condition may be written as,

$$\frac{\sqrt{3} \gamma \sqrt{f'_c} b_e}{F_{yp} t_{sp} \left(1 - \frac{a_c}{D_c}\right)} > 10.0 \quad (6.27)$$

Substituting $\gamma = 36$, $a_c/D_c = 0.30$ and $b_e = b_f$, Eq. 6.27 may be expressed as

$$t_{sp} < \frac{9 \sqrt{f'_c} b_f}{F_{yp}} \quad (6.28)$$

Hence, the following values of γ are recommended for calculating the shear strength of the concrete panel per Eq. 6.23.

- (i) When the FBPs are extended above and below the beam with a minimum extension, e_p , equal to $b_f/2$ or $d_{p1}/4$, whichever is smaller, or when the thickness of the steel panel,

$$t_{sp} \leq \frac{9 \sqrt{f'_c} b_f}{F_{yp}} \quad (6.29a)$$

$$\gamma = 36$$

- (ii) For other connections with FBP

$$\gamma = 24 \quad (6.29b)$$

6.4 Other Considerations

A few selected parameters were investigated experimentally in this test program and were incorporated in the design recommendations discussed in the previous section. Some other important parameters are considered in this section which are based on observed behavior of the test specimens, and past research and practice in the related areas.

6.4.1 Flange Size. As described in Section 6.2, and shown in Fig. 6.3, a part of the bearing force C_c labelled as C_{cs} , is transferred to the steel panel through the beam flanges, causing shear in the panel. The flanges are stiffened by the FBPs, as well as the concrete wedged between flanges and the steel panel as depicted in Fig. 4.46(a). It is important that the flanges be strong enough to support the bearing force C_{cs} , required to yield the steel panel in shear, since most of the shear strength of the concrete panel cannot be mobilized until after the steel panel has yielded. It is, however, difficult to know the exact distribution of the bearing force C_{cs} , and thereby determine the true nature of stresses in the flanges. Therefore, the flange thickness, t_f , required to support the force C_{cs} , is determined empirically from the test results of specimen 6 in which transverse stress in the flanges reached yield near the ultimate load. The expression for t_f is derived as follows:

Assuming the force C_{cs} is distributed uniformly on the flange, as shown in Fig. 6.6, the bearing pressure, p_b , may be expressed as follows:

$$p_b = C_5 \frac{C_{cs}}{b_f D_c} \quad (6.30)$$

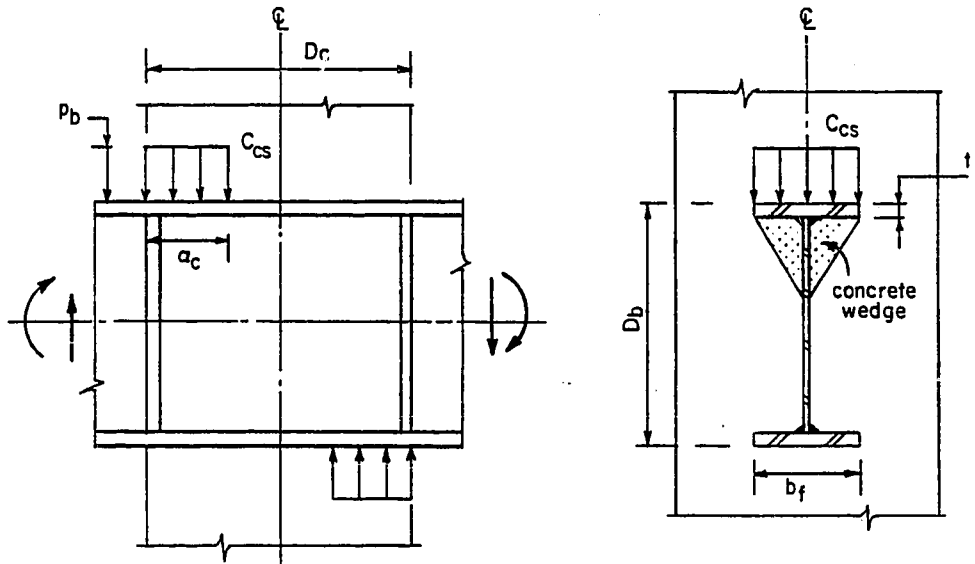


Fig. 6.6 Transfer of forces on the flanges to the steel panel.

where C_5 is a constant. The moment in the flange due to this bearing pressure may be written as

$$\text{Flg. Moment} = C_6 p_b b_f^2 \quad (6.31)$$

and the flexural resistance of the flange can be written as

$$\text{Flg. Capacity} = C_7 t_f^2 F_{yf} \quad (6.32)$$

where C_6 and C_7 are constants and F_{yf} is the yield strength of the flange material. Equating 6.31 and 6.32 and substituting Eq. 6.30, the thickness of the flange, t_f , may be expressed as follows:

$$t_f = C_8 \left(\frac{C_{CS} b_f}{D_c F_{yf}} \right)^{0.5} \quad (6.33)$$

C_8 is a constant. The bearing force C_{CS} required to yield the steel panel, may be taken approximately equal to $(F_{yp}/\sqrt{3})t_{sp}D_b$. Therefore, equation 6.33 may be written as

$$t_f = C_9 \left(\frac{b_f D_b t_{sp} F_{yp}}{D_c F_{yf}} \right)^{0.5} \quad (6.34)$$

Based on the test results of specimen 6, the constant C_9 is calculated as 0.3. Hence, the minimum flange thickness required to support the bearing force C_{CS} which would yield the steel panel in shear is recommended as:

$$t_f = 0.3 \left(b_f t_{sp} \frac{D_b F_{yp}}{D_c F_{yf}} \right)^{0.5} \quad (6.35)$$

6.4.2 Beam Embedment and Aspect Ratio. Aspect ratio of a connection or joint is defined as the ratio of column depth, D_c , to beam depth, D_b . In the tests conducted in this study, this ratio varied from 1.14 to 1.25. If the aspect ratio is too small or too large, as compared to the range of values studied, the connection behavior may differ from what was observed and concluded from these tests. The aspect ratio may influence the distribution of bearing forces C_c on the compression flanges, and affect the shear strength of both steel and concrete panels. The proposed design recommendations should be used with caution when the aspect ratio of a steel beam to concrete column connection does not fall between 0.75 and 1.5.

6.4.3 Joint Reinforcement. A large amount of research has been carried out to study the influence of transverse reinforcement on reinforced concrete beam-column joints. While different codes and design recommendations disagree on the contribution of transverse reinforcement to joint shear capacity, especially for the seismic design, there is general agreement that a minimum amount of transverse reinforcement is required for confinement of the joint concrete and the transmission of column axial load.

In steel beam-to-concrete column connections, joint reinforcement between the top and bottom flanges is needed and some transverse reinforcement may be needed above the compression flanges to strengthen the concrete subjected to bearing stresses. Due to the limited number of tests in this study, the effect of the amount of transverse reinforcement in the joint could not be evaluated. In the tests the transverse reinforcement was proportional as recommended by ACI-ASCE Committee 352 [2] (Eqs. A.3 and A.4).

Strain gage data indicated that joint ties within the beam depth, particularly those located near mid-depth were effective in providing confinement to the concrete panel. Ties above the compression flanges, especially those normal to the beam axis improved bearing strength of the concrete. It is recommended that the area of transverse reinforcement in the direction of shear should be at least equal to that given by Eqs. A.3 and A.4. That is,

$$A_{sh} = 0.3 \frac{S_h D_c f'_c}{f_{yh} A_c} \left(\frac{A_g}{A_c} - 1 \right) \quad (6.36)$$

but not less than

$$A_{sh} = 0.09 \frac{S_h D_c f'_c}{f_{yh}} \quad (6.37)$$

The area of transverse reinforcement in the direction normal to the beam axis may be reduced to half that given by above equations, if the joint is subjected to no shear in this direction. The vertical spacing of ties within the beam depth should not exceed six inches. In addition, at least two sets of ties spaced not more than three inches apart should be provided above and below the steel beam.

6.4.4 Bond Conditions. Bond deterioration of column vertical bars reduces joint stiffness and increases story drift. In the design of steel beam-to-concrete column connections, it may not be practical to completely eliminate bond deterioration of vertical bars. However, similar to the approach adopted by ACI-ASCE Committee 352 [2], the diameter of the column vertical bars passing through the joint should be restricted so that bond deterioration is not excessive at expected drift levels. The ACI-ASCE Committee 352 recommendation that the diameter, d_{bar} , of the column vertical bars meet the following requirement

$$D_b/d_{bar} (col) \geq 20 \quad (6.38)$$

is suggested as a guide for proportioning column bars in steel beam-concrete column connections.

6.4.5 Joint Stiffness. In the design of a moment connection between steel beams and concrete columns, not only the strength but also the stiffness should be considered. Failure criteria defined in Sec. 5.1 include stiffness considerations. Test results indicate that joint distortion at service load level

are of the same magnitude as observed for reinforced concrete beam-column joints. A connection designed according to the recommendations outlined in this chapter may exhibit a total joint distortion up to 0.25% at service loads. However, since all the joints in a frame are generally not stressed to their capacity, the joint distortion would probably result in drift much less than 0.25%. It is suggested that if even higher joint rigidity is required, the connections should be designed more conservatively by keeping the shear stress in the concrete panel as well as the bearing stresses on the compression flanges and FBP lower than those recommended.

6.5 Design Approach

The design formulation developed so far does not include the strength reduction factor, ϕ , for the connection strength in various failure modes. It is important to use an appropriate value of ϕ which is consistent with applicable load factors and satisfies the AISC-LRFD Specifications [6] or ACI Building Code [4].

In the following, the design recommendations are synthesized into a ten-step procedure. The strength reduction factor, ϕ , is included in the previously developed equations. Notations used in the formulation are as indicated in Figs. 6.1 through 6.3. A design example is presented in Appendix B.

1. Select proportions: Check to see if aspect ratio of the joint is within limits, i.e.

$$0.75 < D_c/D_b < 1.5 \quad (6.39)$$

Choose face bearing plate (FBP) configuration.

2. Check bearing on comp. flanges: Find a_c/D_c by solving the following equation

$$\frac{a_c}{D_c} \left(1 - \frac{a_c}{D_c}\right) = \frac{2M_c}{\phi \lambda_c f'_c b_e D_c^2} \quad (6.40)$$

where ϕ for bearing on concrete = 0.60, $b_e = \max[b_f, w_p]$ and for connections where FBP is provided between the flanges only,

$$\lambda_c = 3.0$$

and for extended FBP

$$\lambda_c = 3.5$$

The calculated ratio a_c/D_c should not exceed 0.30.

3. Calculate shear in steel panel, V_{hs} :

$$V_{hs} = \frac{2M_b}{d_b} - V_c \leq V_{sp} \quad (6.41)$$

where shear capacity of the steel panel

$$V_{sp} = \phi \frac{1}{\sqrt{3}} F_{yp} t_{sp} D_c \left(1 - \frac{a_c}{D_c}\right) \quad (6.42)$$

and ϕ for steel panel shear = 0.90

4. Check shear in concrete panel, V_{hc} :

$$V_{hc} = \frac{2M_b - V_{hs} d_b - V_c D_b}{d_p \left(1 - \frac{a_p}{d_p}\right)} \quad (6.43)$$

where for connections with FBP between flanges only, $a_p/d_p = 0.25$. For connections with FBP extended a distance e_p above and below the beam,

$$\frac{a_p}{d_p} = 0.25 \frac{d_{p1}}{d_p} + \frac{e_p}{d_p} \leq 0.5 \frac{d_{p1}}{d_p}$$

The calculated shear V_{hc} should not exceed the shear capacity of the concrete panel,

$$V_{cp} = \phi \gamma \sqrt{f'_c} b_e D_c \quad (6.44)$$

where ϕ for concrete panel shear = 0.85 and γ is defined as follows:

(i) when the face bearing plates (FBPs) are extended above and below the beam with a minimum extension e_p equal to $b_f/2$ or $d_{p1}/4$, whichever is smaller, or when the thickness of the steel panel,

$$t_{sp} \leq \frac{9\sqrt{f'_c} b_f}{F_{yp}} \quad (6.45a)$$

$$\gamma = 36$$

(ii) For other connections with FBP

$$\gamma = 24 \quad (6.45b)$$

5. Check bearing on face bearing plate: Calculate the coefficient of bearing stress against FBP, λ_p , and check to see if it is within limits, i.e.

$$\lambda_p = \frac{V_{hc}}{\phi f'_c w_p a_p} \leq 3.0 \quad (6.46)$$

where ϕ for bearing on concrete = 0.60.

6. Calculate face bearing plate thickness: Thickness t_p of FBP must satisfy the largest of the following:

For shear fracture ($\phi = 0.75$),

$$t_p = \frac{\sqrt{3}(V_{hc} - b_f t_w F_{yw})}{\phi b_f F_{ub}} \quad (6.47a)$$

or

$$t_p = \frac{\sqrt{3} V_{hc}}{2\phi b_f F_{ub}} \quad (6.47b)$$

For flexural bending ($\phi = 0.90$),

$$t_p = 0.2 \left(\frac{V_{hc} w_p}{\phi F_y b d_p} \right)^{0.5} \quad (6.47c)$$

but $w_p/t_p \leq 22$ and the width w_p of the FBP,

$$w_p \leq b_f + 5t_p$$

7. Design support plate as a bracket to resist the bearing force on the extended FBP = $\lambda_p f'_c w_p e_p$
8. Check flange thickness: To avoid plate bending, the flange thickness, t_f , must satisfy

$$t_f \geq 0.3 \left(\frac{b_f t_{sp} D_b F_{yp}}{\phi D_c F_{yf}} \right)^{0.5} \quad (6.48)$$

where ϕ for plate bending = 0.90.

9. Calculate joint reinforcement: The area of transverse reinforcement in the direction of shear should be at least equal to

$$A_{sh} = 0.3 \frac{S_h D_c f'_c}{f_{yh}} \left(\frac{A_g}{A_c} - 1 \right) \quad (6.49a)$$

but not less than

$$A_{sh} = 0.09 \frac{S_h D_c f'_c}{f_{yh}} \quad (6.49b)$$

The area of transverse reinforcement in the direction normal to the beam axis may be reduced to half that given by above equations, if the joint is subjected to no shear in this direction. The vertical spacing, S_h , should not exceed six inches. In addition, at least two sets of ties spaced not more than three inches apart should be provided above and below the steel beam.

10. Check size of column vertical bars: The diameter of the column vertical bars, d_{bar} , should be such that

$$D_b/d_{bar(col)} \geq 20 \quad (6.50)$$

6.6 Limitations of Design Approach

Several limitations to the proposed design approach must be noted. The design recommendations presented here are applicable to connections with face bearing plates (FBP) only and not include other means of stress transfer which may very well

prove to be efficient. Another consideration is the presence of axial load on the column, which could not be included in the scope of this study. Tests on steel beam-to-SRC column connections, conducted by Minami [34] and Tanaka et al. [50] have shown no significant effect of axial load on the connection capacity. For reinforced concrete connections, ACI-ASCE Committee 352 report [2] has also concluded that the axial load on columns have no significant effect on the connection capacity. New Zealand Concrete Design [38], however, considers the influence of axial compression as beneficial. For structural steel connections, experimental evidence [26] has shown that almost all the column axial force is transferred to the column flanges in the joint once the panel zone has yielded in shear. It is anticipated that in steel beam-to-concrete column connections, most of the column axial force would be transmitted through the concrete outside the beam width and the influence of axial load on the connection capacity should range from insignificant to beneficial. It is, therefore, conservative to ignore the column axial load in this design approach. However, caution should be exercised when the columns are subjected to axial loads greater than half the crushing capacity.

Another limitation is that the procedure is derived for interior beam-column joints only. While similar equations can be written for exterior joints, special attention should be given to the transfer of tension flange forces to the concrete panel. The beam should be extended to the far face of the concrete panel and FBPs provided at both faces of the concrete column. Also, the shear capacity of the concrete panel in exterior connections may be lower than in interior connections. For reinforced concrete exterior beam-column connections, ACI-ASCE Committee 352 [2] permits a joint shear of 75 to 80% of that in interior

connections, thereby recognizing the reduced confinement of the concrete panel in exterior connections. Although the confinement conditions in steel beam-to-concrete column connections may not differ substantially from interior to exterior connections, it is still suggested that the shear in the concrete panels of exterior connections be limited to $3/4$ the recommended value, until additional test data is available to justify a higher value. Reader should note that the terms "interior" and "exterior" connections in this test differ from those used in ACI-ASCE Committee 352 report [2]. While the connections in this test series (beams framing into two opposite faces of columns) are termed "interior" in this text, they would be classified as "exterior" according to ACI-ASCE Committee 352. Similarly, the connections with beam framing into one face of the column only are termed "exterior" in this text, but would be classified as "corner" as per ACI-ASCE Committee 352.

One last limitation, which must be pointed out, pertains to the concrete strength in the joint area. The use of high strength concrete, ranging from 8000 to 14,000 psi and readily available at a very competitive price, is rapidly gaining popularity, especially for the construction of tall buildings. It must be pointed out that the proposed design recommendations are based on tests conducted with concrete strengths ranging from 3500 to 4500 psi. The characteristics of high strength concrete may differ from those of medium strength concrete. Therefore, the application of the proposed design recommendations to concrete strengths higher than 6000 psi should be carried out with caution.

6.7 Comparison with Test Results

The recommended design formulations are compared to the capacity of the test specimens in Table 6.2. Although these design recommendations require a face bearing plate (FBP) in all connections, the formulation is still valid for connections without FBP, provided the flanges are adequate in strength and stiffness to support the bearing force required to yield the steel panel. Therefore, all the tests in this program and a few others with sturdy beam flanges are included in this comparison. In Table 6.2, shear capacities of the steel and concrete panels are calculated using Eqs. 6.42 and 6.44. For this comparison a strength reduction factor, $\phi = 1.0$, is used. The concrete panel capacity, as controlled by crushing of concrete against the FBPs,

Table 6.2 Comparison of Design Approach with Test Results

Specimen No. (1)	Stl. Panel Shear Cap. V_{sp} (kips) (2)	Conc. Panel Cap. V_{cp} (kips)		Predicted Load P (kips)		P_{design} (kips) (7)	P_{test} (2% TJD) (kips) (8)	$\frac{P_{test}}{P_{design}}$ (9)
		Shear (3)	Crushing on FBP (4)	Based on Panel Cap. (5)	Based on Crushing on Flg. (6)			
1	101	0†	—	17.2	23.6	17.2	18.0	1.047
2	88	86	122	25.5	23.6	23.6	26.1	1.106
3	99	0†	—	11.1	53.9	11.1	18.5	1.666
4	91	252	413	30.5	51.5	30.5	32.4	1.062
5	90	252	413	30.4	51.5	30.4	34.1	1.122
6	480	0 [‡]	—	54.0	47.9	47.9	46.8	.977
7	93	364	576	39.8	71.8	39.8	41.4	1.040
8	76	346	683	53.2	53.6	53.2	55.0	1.034
9	0	350	355	28.6	44.3	28.6	31.2	1.091
WR1 [J14]	310	0†	—	32.9	27.5	27.5	25.0	.909*
WR2 [J14]	465	0†	—	49.4	39.1	39.1	29.0	.742*
MS000 [J3]	103	0†	—	20.7	20.3	20.3	15.5	.764*
TMS10 [J6]	53	70	86	16.0	15.03	15.03	17.25	1.148*

† FBP not provided

‡ FBP ineffective

* Tests conducted under repeated cyclic loads.

is calculated as per Eq. 6.46 and is tabulated in Col. 4. The capacity of the specimens, listed in Col. 7 is based on the smaller of a) the panel capacity per Eq. 6.43, or b) concrete crushing against the compression flanges, Eq. 6.40. The measured capacity is listed in column 8. The ratio of the two capacities is tabulated in column 9. For the nine specimens tested, the ratio $P_{\text{test}}/P_{\text{design}}$ vary from 0.97 to 1.13, except specimen 3 for which this ratio is 1.67. The high ratio for specimen 3 is due to a) the additional shear carried by the frame action of the flanges, and b) the participation of concrete panel through bond between steel beam and concrete. Specimen 6, for which the connection capacity is controlled by the concrete crushing against the flanges, indicate the lowest ratio, being 0.97. However, this ratio is 1.106 for specimen 2 for which the design strength was controlled by the same mode.

In addition to the nine tests conducted in this research program, four more tests found in the literature are compared in Table 6.2. All four specimens were tested under reversed cyclic loads ranging from 20 to 30 cycles at various deflection levels. Since the monotonic envelope was not obtained, the comparison of these tests with the design formulations based on monotonic loading may not be entirely valid. Tests labelled WR1 and WR2, reported by Wakabayashi et al. [59] carried a constant axial load of 157 kips (1.12 ksi) on the columns in addition to the cyclic lateral loads. The axial load is ignored in calculating the predicted capacity. Test labelled MS000 is reported by Minami [34] and was conducted on an exterior connection. Test TMS10 is reported by Tanaka and Nisigaki [50] and was carried out on connections with face bearing plates. A small size steel column ($d = 6.7"$, $b_f = 3.9"$, $t_w = 1/4"$, $t_f = 3/8"$) with its weak axis in the plane of the joint, was also present, which is again

ignored in this analysis. The dimensions for each of these four specimens are listed in Table 6.3. The computations of predicted load (columns 5 and 6 of Table 6.2) indicate that the capacity of all four specimens was controlled by concrete crushing against the flanges, although the panel capacity for specimens MS000 and TMS10 was close to the crushing capacity. The ratio P_{test}/P_{design} for these tests vary from 0.74 to 1.15. As stated earlier, their low strengths were due to the repeated cyclic nature of loading and does not warrant any concern for monotonic wind type loads.

In the final analysis, the design recommendations presented here can adequately predict the strength of steel beam to concrete column connections detailed within the limitations outlined.

Table 6.3 Salient Features of Japanese Tests

Ser. No.	Description	WR1 [J14]	WR2 [J14]	MS000 [J3]	TMS10 [J6]
1	Specimen Capacity, P (kips)	25	29	15.5	17.25
2	Column Axial Load, kips (ksi)	157 (1.12)	157 (1.12)	---	---
3	Conc. Strength, f'_c (psi)	3420	4870	4200	2550
4	Stl. Panel Strength, F_{yp} (ksi)	47.2	44.5	40.1	46.9
5	Beam span, L (in.)	108	108	44	89
6	Column Height, H (in.)	95	95	88	57
7	Column width, B_c (in.)	7.87	7.87	9.84	11.81
8	Column depth, D_c (in.)	17.72	17.72	8.86*/9.84	11.81
9	Beam depth, D_b (in.)	9.84	9.84	7.87	9.84
10	Flange width, b_f (in.)	3.94	3.94	3.94	4.92
11	Flange thickness, t_f (in.)	1.417	1.417	.748	.354
12	Stl. Panel Thickness, t_{sp} (in.)	.866	1.26	.63	.236
13	FBP size (w_p , d_p , t_p)	---	---	---	4.92x9.13x5/8
14	Connection type	interior	interior	exterior	interior

*beam embedment

CHAPTER 7
CONCLUSIONS AND RECOMMENDATIONS

7.1 Summary

In recent years mixed steel-concrete structural systems have gained popularity for the construction of tall buildings. Although these systems are termed "mixed", the structural members within a subsystem, i.e. gravity load subsystem or lateral load resisting subsystem, are made of single material, steel or concrete. These systems traditionally make use of simple shear connections between steel beams and concrete columns. As a result, there is minimum interaction between the two materials. The efficiency of mixed systems can be substantially enhanced by combining members of both structural steel and reinforced concrete within a subsystem. This would require a moment connection between steel beams and concrete columns. Currently there is no information available for the design of such connections.

Several methods are available for the transfer of steel beam flange forces to the connection panel. The lever mechanism and face bearing plates (FBP) were investigated experimentally in this study. The steel panel thickness, and the width, configuration, and thickness of FBP were chosen as variables. Nine, 1/2 to 2/3 scale steel beam-concrete column subassemblages representing interior connections were tested under simulated monotonic lateral loads. The specimens were instrumented to examine both strength and stiffness.

7.2 Conclusions

The test results show that face bearing plates (FBP) substantially enhanced joint strength by effectively mobilizing

the concrete panel. Variations in the thickness of these plates did not affect the joint capacity. This capacity, however, was increased 20% by increasing the width of the FBP from 8 to 12 in. Extending the FBPs above and below the beam was most effective and increased the joint strength by 60% and stiffness by 150%. The data from strain gages embedded in the concrete panel indicate that only the concrete panel within the width of flanges and FBP was mobilized, except when the steel panel was very weak, in which case a wider concrete panel was effective.

Based on the test data a design model for the connection zone was developed to determine joint capacity, which identified principal forces on the connection panel. The resistance to joint shear is provided by a) the steel panel in pure shear, and b) the concrete panel through diagonal compression strut. Checks are made to ensure that bearing forces on the compression flanges and on the FBPs do not produce crushing of the concrete. Other modes of failure - shear fracture of FBPs, flexural yielding of FBPs and flanges - are identified and formulations developed to size the thickness of the FBPs and flanges. A comprehensive design approach was presented which can be used to determine the strength of interior connections between steel beams and concrete columns employing face bearing plates.

7.3 Future Research Needs

1. Other means of panel zone stress transfer - steel erection columns, shear studs, rods/bars - need to be investigated.
2. The influence of steel beam width and joint aspect ratio on the connection capacity should be studied.
3. Exterior connections: Test data are needed to examine exterior connections.

4. Axial load: The influence of column axial load on the connection capacity should be investigated, especially in connections where wide steel beams are used.
5. Joint reinforcement: The amount of joint reinforcement required within the beam depth for shear and confinement, and above and below the beam to confine the concrete under high bearing stresses should be examined.
6. High strength concrete: Concrete strengths ranging from 8000 to 14,000 psi are rapidly gaining popularity, especially for the construction of tall buildings. Work is needed to determine modifications required in the proposed design recommendations for high strength concrete.
7. Seismic loads: These tests were conducted primarily under monotonic loads; however, one complete load cycle at large deformations was applied. The test results showed large energy absorbing capacity, especially by the steel panel in shear, which indicate a good potential for the use of such connections in the seismic zones as well. Work is needed to establish hysteretic characteristics of connections under repeated cyclic loads.

A P P E N D I X A

A.1 Review of Reinforced Concrete Beam-Column Joints

Until recently, the typical connection of reinforced concrete members was assumed to be a noncritical component. The design of joints was often limited to satisfying anchorage requirements. Numerous structural failures pointed to connection inadequacies as a contributing factor in undesirable structural performance especially where lateral forces due to strong wind or earthquakes are significant. A large amount of research has been carried out in the last 10 to 15 years and it has become obvious that the joint can be a weak link in the structure. Based on this research, design recommendations have been made but they vary substantially from one study to another. There is disagreement as to the basic mechanism controlling the transfer of forces across a joint, as well as to the relative importance of the parameters to be used in design.

The joint should be designed for the interaction of the multi-directional forces which the members framing into it transfer to the joint. A free-body diagram of a planar beam-column joint with the forces at the boundaries is shown in Fig. A.1. There are three considerations associated with the design of these joints, namely; (a) shear resistance across the joint, (b) anchorage of the main longitudinal bars of the beams and columns passing through the joint, which may be in tension on one side of the joint and compression on the other, and (c) transmission of the column axial load through the joint region.

Shear force across the horizontal section of the joint, as shown in Fig. A.1, may be calculated as

$$V_j = T_r + C_l + C'_l - V_t \quad (A.1)$$

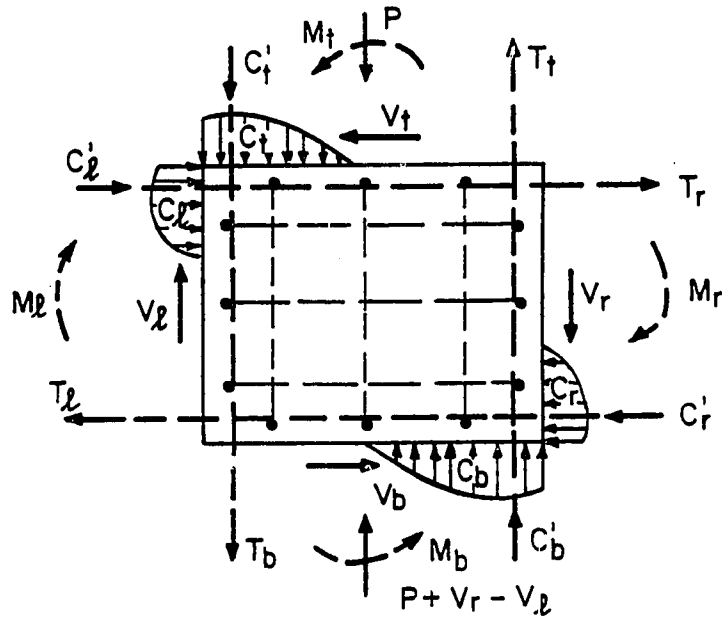
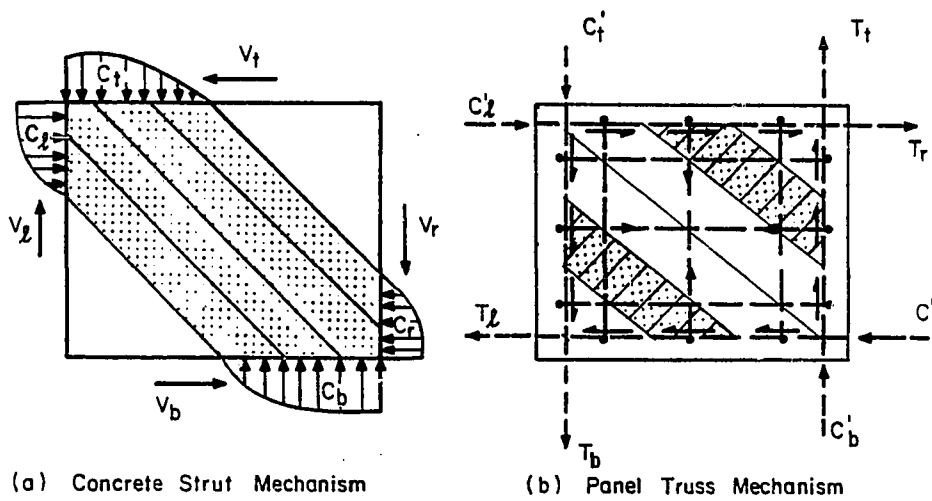


Fig. A.1 Forces on a beam-column joint.



(a) Concrete Strut Mechanism

(b) Panel Truss Mechanism

Fig. A.2 Mechanism for joint core shear resistance.

assuming the joint panel is adequately reinforced with both horizontal and vertical ties and there is absolutely no bond slip of the main longitudinal bars of the beams and columns, there are two mechanisms of joint core shear resistance which satisfy the equilibrium requirements of the joint core. These mechanisms are:

1. A diagonal compression strut mechanism carrying the concrete compressive forces across the joint, as shown in Fig. A.2a.
2. A panel truss mechanism of joint core reinforcement carrying the longitudinal bar forces across the joint, as shown in Fig. A.2b

The differences in design philosophies stem from the emphasis given to these two joint core shear resistance mechanisms and the anchorage requirements of the main longitudinal bars of the beams and columns. In the U.S. and Japan, shear strength is based on the compression strut mechanism and anchorage requirements are not severe. In the New Zealand and European approach shear is based on the panel truss mechanism and anchorage requirements are strict. To elaborate these differences, the recommendations for the design of reinforced concrete beam-column joints as given by ACI-ASCE Committee 352 and the New Zealand Concrete Design Code are presented and compared in the following.

A.1.1 ACI-ASCE Committee 352 Recommendations. First recommendations for the design of the beam-column joints in monolithic reinforced concrete structures were reported by ACI-ASCE Committee 352 in 1976 [1]. The recommendations were substantially revised in ACI 352 R-85 [2]. The revised design recommendations are as follows.

Joints are required to be designed for forces calculated from the flexural strength of the beams. In seismic zones the flexural strength is required to be increased by at least 25% to account for the yield strength of the reinforcement exceeding specified values and for the strain hardening. The entire shear resistance is considered to be provided by the concrete. No reinforcement is required for shear, however, minimum horizontal transverse reinforcement is required for the confinement of the joint concrete and for transmission of column axial load. Calculated shear in the joint must not exceed V_j , where

$$V_j = \phi \gamma \sqrt{f'_c} b_j D_c \quad (\text{A.2})$$

where b_j = average width of the beam and the column.

D_c = depth of the column

ϕ = strength reduction factor = 0.85

In seismic zone of high risk,

γ = 20, 15 and 12 for interior, exterior and corner joints, respectively.

In non-seismic zones

γ = 24, 20 and 15 for interior, exterior and corner joints, respectively

f'_c = concrete cylinder compressive strength (psi) but not more than 6000 psi.

For transverse reinforcement, at least two layers of reinforcement (consisting of the same ties as provided for the column) are required to be provided between the top and bottom layers of the longitudinal reinforcement of the deepest beam. The spacing between these layers should not exceed 6-in. In seismic zones, however, the area of this transverse reinforcement should be at least equal to:

$$A_{sh} = 0.3 \frac{S_h h'' f'_c}{f_{yh}} \left(\frac{A_g}{A_c} - 1 \right) \quad (A.3)$$

but not less than

$$A_{sh} = 0.09 \frac{S_h h'' f'_c}{f_{yh}} \quad (A.4)$$

In seismic zones when spiral transverse reinforcement is used, the volumetric ratio, ρ_s , should be:

$$\rho_s \geq 0.12(f'_c/f_y) \quad (A.5)$$

where S_h = spacing of hoops (in.)
 h'' = depth of the column (in.)
 A_g = gross area of the column (in.²)
 A_c = confined area of the column (in.²)
 A_{sh} = total area of transverse reinforcement (in.²)
 f_{yh} = yield strength of transverse reinforcement (psi)

In addition, the column vertical bars extending through the joint are required to be well distributed around the perimeter of the column core for seismic design.

Where beams of substantial width frame into two opposite faces of the joint, transverse reinforcement in the direction of the beam may be omitted in non-seismic zones. In seismic zones reinforcement must be provided but may be reduced by 50% in direction of the beam.

For joints in seismic zones, the diameter, d_{bar} , of all the main beam and column bars passing through the joint must satisfy

$$D_c/d_{bar} \text{ (beam)} \geq 20$$

and

$$D_b/d_{bar} \text{ (col)} \geq 20$$

where D_c and D_b are the depths of column and beam respectively.

A.1.2. The New Zealand Standard. The New Zealand concrete design code [38] gives a procedure only for seismic design of reinforced concrete beam-column joints. Like the ACI-ASCE Committee 352 recommendations, this code requires the joints to be designed for forces calculated using the actual flexural strength of the beams. These forces are required to be further increased by 25% for 40 ksi reinforcing steel and by 40% for 55 ksi steel.

The contribution of the diagonal compression strut mechanism to the shear strength varies as a function of the magnitude of the axial load on the column and on the location of plastic hinging in the beam (adjacent to the joint or away from it). The shear carried by the diagonal compression strut is calculated as follows:

- 1) When plastic hinging in the beam occurs at the column face,

$$V_{ch} = 0 \quad \text{when } P_e \leq 0.1(f'_c/C_j)A_g \quad (A.6)$$

$$V_{ch} = (1/80)\sqrt{[(C_j P_e/A_g) - (f'_c/10)]} b_j D_c \quad (A.7)$$

$$\text{when } P_e > 0.1 (f'_c/C_j)A_g$$

- 2) When plastic hinging in the beam is forced to occur at a distance away from the column face:

$$V_{ch} = 0.5(A'_s/A_s) V_{jh} [1 + (C_j P_e)/(0.4 A_g f'_c)] \quad (A.8)$$

$$3) V_{cv} = (A'_{sc}/A_{sc}) V_{jv} [0.6 + (C_j P_e)/(A_g f'_c)] \quad (A.9)$$

where V_{jh} , V_{jv} = horizontal and vertical design joint shear, respectively

V_{ch} , V_{cv} = shear capacity of diagonal compression strut in the horizontal and vertical direction, respectively

$C_j = V_{jh}/(V_{jx} + V_{jy})$ where V_{jx} , V_{jy} are the horizontal design joint shear in the two principal directions.

b_j = b_c or $b_w + 0.5 h_c$, whichever is smaller

b_c , b_w = width of column and beam web, respectively

D_c = overall depth of the column in the direction being considered

P_e = minimum axial compressive column load

A_g = gross area of column cross-section

f'_c = concrete compressive cylinder strength

A_s , A'_s = area of tension and compression reinforcement of the beam, respectively

A_{sc} , A'_{sc} = area of tension and compression reinforcement of the column, respectively.

When the joint shear is greater than the concrete capacity, shear reinforcement is required. The total area of horizontal shear reinforcement required to be placed between the top and bottom reinforcement of the beam is

$$A_{jh} = (V_{jh} - V_{ch})/f_{yh} \quad (A.10)$$

and the total area of vertical shear reinforcement required to be placed as intermediate column bars on the side faces of the column is

$$A_{jv} = (V_{jv} - V_{cv})/f_{yv} \quad (A.11)$$

where f_{yh} and f_{yv} are the yield strength of the horizontal and vertical shear reinforcement, respectively.

The code requires the total horizontal shear strength in either principal direction to be limited to

$$V_{jh} \leq 18\sqrt{f'_c} b_j D_c \quad (A.12)$$

For confinement of the joint core, the recommendations require the total area of horizontal transverse steel in each principal direction to be at least equal to:

$$A_{sh} = 0.3 S_h h'' [(A_g/A_c) - 1] (f'_c/f_{yh}) [0.5 + 1.25 (P_e/\phi f'_c A_g)] \quad (A.13)$$

but not less than

$$A_{sh} = 0.12 S_h h'' (f'_c/f_{yh}) [0.5 + 1.25 (P_e/\phi f'_c A_g)] \quad (A.14)$$

where S_h = spacing of hoop

h'' = depth of the column

A_c = confined area of the column

A_{sh} = total area of horizontal transverse reinforcement

However, if the joint has beams framing into all four column faces and plastic hinging occurs away from the column face, this transverse reinforcement may be reduced to one-half.

The diameters, d_{bar} , of the beam and column bars passing through the joint are required to satisfy the following:

- (1) beam bars: when plastic hinging occurs at the column face $D_c/d_{\text{bar}} \geq 25, 35$ for 40 ksi and 55 ksi bars, respectively. When plastic hinging is forced to occur away from the column face, $D_c/d_{\text{bar}} \geq 20, 25$ for 40 ksi and 55 ksi bars, respectively.
- (2) column bars: $D_b/d_{\text{bar}} \geq 15, 20$ for 40 and 55 ksi bars, respectively.

where D_b, D_c = overall depths for beams and columns, respectively.

A.1.3 Comparison of the Two Methods. The comparison of the two recommendations can only be made for seismic design of the beam-column joints. The Committee 352 recommendations rely almost entirely on the diagonal strut mechanism and consider the joint shear strength insensitive to both joint shear reinforcement and axial compression. The New Zealand code relies heavily on the panel truss mechanism, thus requiring substantial shear reinforcement, and considers the influence of axial compression as beneficial.

The design philosophy of Committee 352 is based on tests conducted on beam-column joints without vertical shear reinforcement. It was observed in these tests that after diagonal cracks propagate in the joint, bond of the main bars of the beam and column deteriorates. The tension in these bars is anchored partly in the diagonal strut and partly in the beam/column compression block across the joint. This increases the intensity of stress in the compression block thereby transferring the entire tension force of the reinforcing bar to the diagonal strut. This new force system is shown in Fig. A.3.

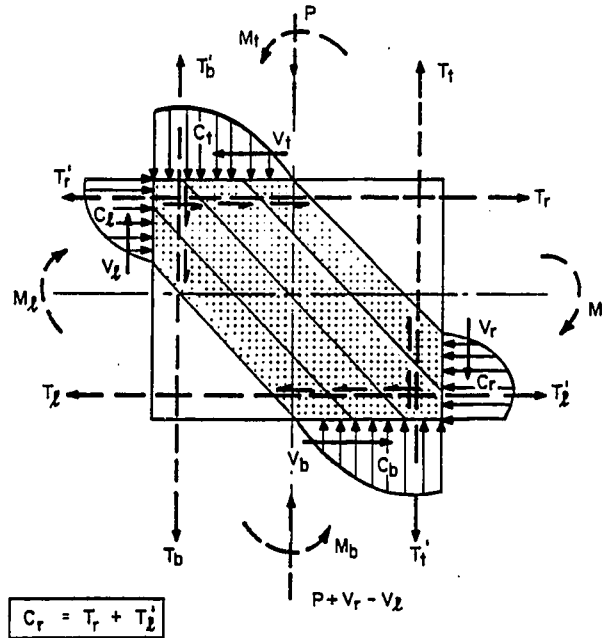


Fig. A.3 Forces on a joint after bond slip.

However, due to loss of bond, the joint loses stiffness. It is also noted in these tests that the joint maintains a substantial portion of its strength after repeated cycling even when plastic hinging of the beam occurs adjacent to the joint.

Park [38] argues for the New Zealand philosophy saying, "The diagonal strut mechanism will not be effective if full depth cracking occurs in the beam at the column face due to cyclic flexure." It appears, the New Zealand philosophy is based on tests where the beams were subjected to severe plastic hinging adjacent to the joint under cyclic reversals. The committee 352 states in its report [2], "The New Zealand approach is based on the performance of statically determinate beam-column

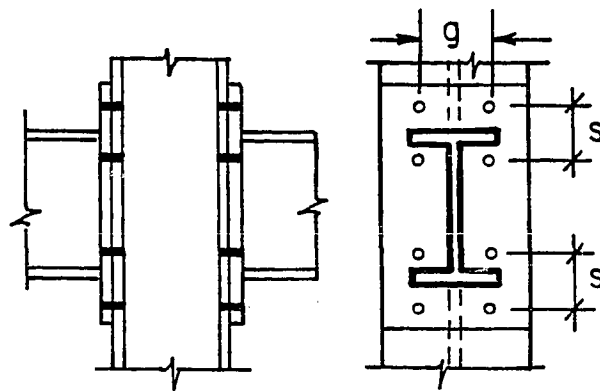
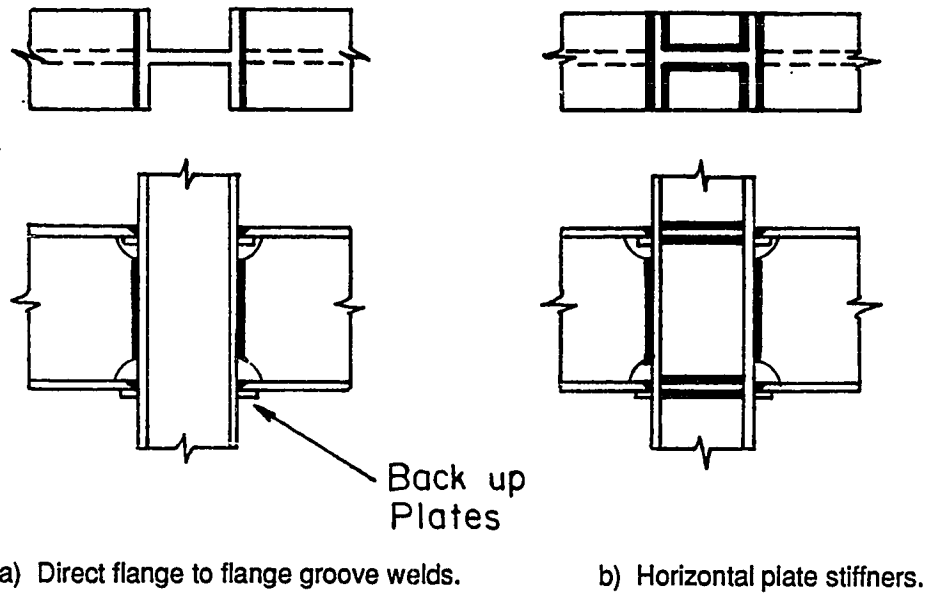
subassemblies at very large deformation reversals which would correspond to excessive drift values in frame structures."

This controversy, however, should not affect the design approach formulated in this study for the steel beam-to-concrete column connections, as it is confined to monotonic, i.e. wind type loads.

A.2 Review of Structural Steel Beam-Column Connections

In steel construction typically "rigid connections" (moment connections) are made by attaching beams to each side of the column which in itself is a continuous member. The orientation of the column can be such that the beams frame either into the column flanges, i.e. the column is subjected to moment about its strong axis, or the beams are attached to each side of the column web, thereby subjecting the column to moments about its weak axis. For the purpose of this study, only connections where the column is bent about its strong axis are presented. Also, as was pointed out earlier, this study is restricted to interior connections only.

Rigid connections are intended to provide a full transfer of moment and little or no relative rotation of members within the joint. For this purpose, beams can be attached in a variety of ways, a few of which are shown in Fig. A.4. The design of these connections involve providing sufficient stiffening material so that the connection will transmit moment from beams to columns and vice versa, without undesirable deformations. Some columns are sturdy enough to carry the beam moment without stiffening. Other columns require stiffening of their webs or flanges to aid in transmitting the concentrated forces from the flanges of the connected beams.



c) Welded end plates.

Fig. A.4 Continuous beam-to-column connections (Ref. 48).

The design of a beam to column rigid connection in structural steel requires that (a) beam flange compression and tension forces are transferred to the column web, and (b) shear resistance of the panel zone is adequate.

A.2.1 Transfer of Flange Forces. When the forces in beam flanges are transmitted to column flanges, horizontal stiffeners as shown in Fig. A.4(b) may be required. Such stiffeners prevent web crippling and the overall web buckling when the beam flange forces are compressive. For the transfer of beam flange tension, the stiffeners may be required to prevent a premature fracture of the column web and excessive deformation of the column flange which could result in fracture of welds connecting the beam flange to the column flange.

Consider a beam flange transmitting the force P_{bf} to a column as shown in Fig. A.5. When the maximum strength of the

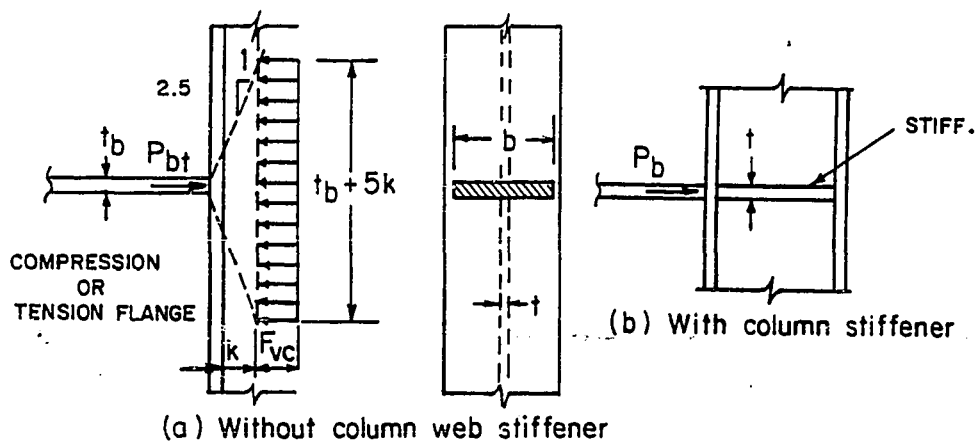


Fig. A.5 Strength of column web (Ref. 48).

column web is reached, AISC - 1.15.5.2 [5] assumes the load is distributed along the base of the fillet (k from the face of flange) on a 1:2.5 slope. Thus, the minimum column web thickness, t , required to prevent the crippling or premature yielding of the web is:

$$t \geq \frac{P_{bf}}{(t_b + 5k)F_{yc}} \quad (A.15)$$

where t_b = thickness of flange or moment connection plate delivering concentrated force, inches.

k = distance between outer face of column flange and web toe of its fillet, inches.

F_{yc} = column yield stress, ksi

P_{bf} = computed force delivered by the flange or moment connection plate multiplied by the proper load factor, or the capacity of flange ($A_f F_{yb}$) if plastic hinging of the beam is required, e.g. when moment redistribution is considered for gravity loads or when it is part of a moment resisting frame in earthquake zones.

In addition, vertical buckling of the web plate under the compressive flange force must also be avoided. Based on the buckling solution of a plate subjected to equal and opposite concentrated loads in its plane, AISC-1.15.5.3 [5] gives a semiempirical expression for web buckling,

$$\frac{d_c}{t} < \frac{4100 t^2 \sqrt{F_{yc}}}{P_{bf}} \quad (A.16)$$

where d_c is the clear depth of column web.

In order to avoid excessive deformation of the column flanges under the beam flange tension force, as shown in Fig. A.6, the resistance of the flanges must be known. The thick

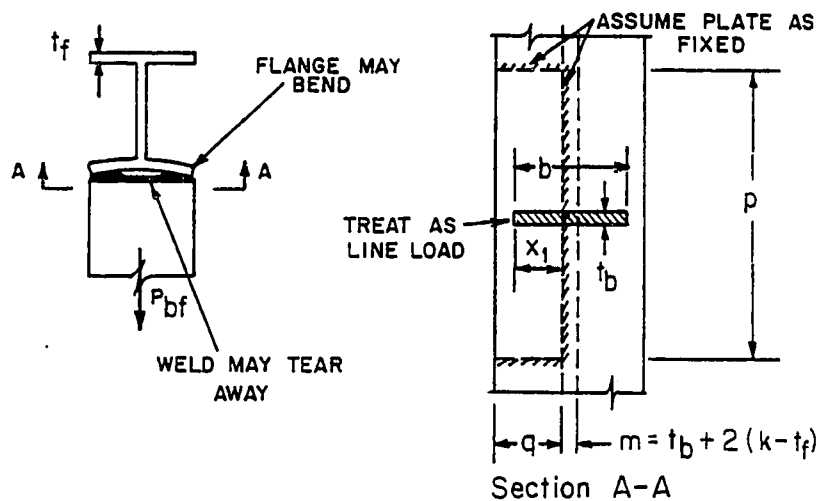


Fig. A.6 Strength of column flange in tension region of connection (Ref. 48).

central portion of width, m , may be assumed to resist the beam flange force as if it were rigid. Thus the column flange direct resistance,

$$P_{\text{direct}} = F_{yc} t_b m \quad (\text{A.17})$$

The remainder of the column flange resistance is due to plate bending of the projecting portion of the flange. A yield-line

analysis shows the column flange bending resistance of the form,

$$P_{\text{bending}} = C_1 F_{yc} t_f^2 \quad (\text{A.18})$$

Where C_1 is a coefficient depending on the column flange width, q , its length, p , the projected beam flange width, x_1 , and the boundary conditions. Hence, the total resistance of the column flange is,

$$P_{\text{flange}} = 2C_1 F_{yc} t_f^2 + F_{yc} t_b m \quad (\text{A.19})$$

AISC-1.15.5.3 [5] assumes the column flange length, p , equal to $12 t_f$. Additional conservative assumptions regarding the relative dimensions of beams and columns are made to simplify Eq. A.19 so that

$$P_{\text{flange}} = 6.25 F_{yc} t_f^2 \quad (\text{A.20})$$

Using Eq. A.20, AISC- 1.15.5.3 [5] requires the column flange thickness to be at least equal to

$$t_f \geq 0.4 \sqrt{P_{bf}/F_{yc}} \quad (\text{A.21})$$

to prevent excessive deformation of the flange. When either of Eqs. A.15 or A.16 is not satisfied, a stiffener must be provided on the column opposite the compression flange of the beam. And when either of Eqs. A.15 or A.21 is not satisfied, a stiffener must be provided on the column opposite the tension flange of the beam. The expression for the required area of the stiffener, A_{st} , as given in AISC-1.15.5, is

$$A_{st} = \frac{P_{df} - F_{yc} t(t_b + 5\kappa)}{F_{yst}} \quad (A.22)$$

where F_{yst} is the yield stress of the stiffener material.

In addition to satisfying Eqs. A.15 through A.22, the stiffener geometry must also comply with the empirical rules of AISC-1.15.5.4 which are as follows:

1. The width b_s of each stiffener plus 1/2 the thickness t of the column web shall not be less than 1/3 of the width b of the flange or moment connection plate delivering the concentrated force P_{df} ,

$$b_s + t/2 \geq b/3 \quad (A.23)$$

2. The thickness t_s of stiffener shall not be less than $t_b/2$ and the local buckling requirements for compression elements must be satisfied. Thus

$$t_s \geq t_b/2 \quad (A.24)$$

and

$$b_s/t_s \leq 95/\sqrt{F_y} \quad (A.25)$$

3. When the concentrated force P_{df} occurs at only one flange of a column, the stiffener length need not exceed 1/3 of the column depth.
4. The weld joining stiffeners to the column web shall be sized to carry the force in the stiffener caused by unbalanced moments on opposite sides of the column.

Popov et al [43] recently studied the behavior of large beam-column assemblies under cyclic loading. They found that after the formation of plastic hinges in the beams adjacent to the connection, the beam flanges strain harden which result in yielding and/or buckling of the stiffeners. They concluded that the design of stiffeners based on the nominal yield of the beam flanges is unconservative.

Miller [33] has outlined the design recommendations for rigid connections in the Load and Resistance Factor Design (LRFD) Specifications [6]. Nominal strength for web yielding overall web buckling, as well as local flange bending are the same as discussed above. However, the nominal strength must be multiplied by a resistance factor, ϕ , to obtain the design strength. The resistance factors, ϕ , are as follows:

Web yielding	1.0
Overall web buckling	0.90
Local flange bending	0.90

A.2.2 Shear in Panel Zone. The connection panel in the beam-column rigid connection should be designed to resist the forces transmitted from the members framing into it. A typical joint, subjected to the moments and shears from the beams and columns due to the antisymmetrical loading that could be caused by wind or earthquake is shown in Fig. A.7. This loading results in large shearing forces in the connection panel, m-n-o-p. The net shearing force across the depth of the column web can be resolved as:

$$V_u = C_g + T_r - V_t \quad (A.26)$$

The connection panel not only should have the strength to resist this large shearing force, but should be stiff enough to avoid

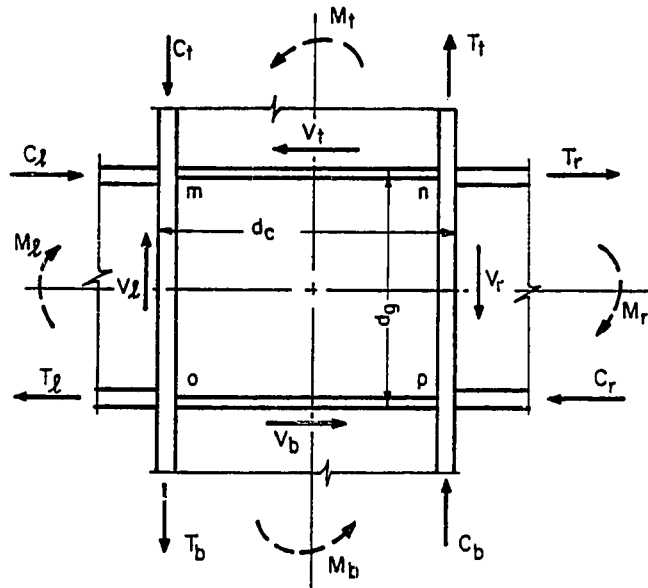


Fig. A.7 Forces on a typical rigid connection.

excessive story drift due to joint distortion which could cause large $P-\Delta$ effects and hence jeopardize the stability of the frame.

AISC Specifications [5] in the commentary of Sec. 2.5 limit the shearing stress in the connection panel to $F_y/\sqrt{3}$ as per Von Mises yield criteria. Assuming the distance between centroids of column flanges as $0.95d_c$, the following formula for the shearing strength of the panel is given:

$$V_{\max} = 0.55 F_y d_c t \quad (\text{A.27})$$

where d_c is the overall column depth, t is the panel thickness and F_y is the web yield strength. In Eq. A.27, the loss in shear capacity due to the axial load on the column is not considered. If the axial load on the column is considered, Eq. A.27 is modified and becomes

$$V_{\max} = 0.55 F_y d_c t \sqrt{1 - (P/P_y)^2} \quad (\text{A.28})$$

where P is the axial load on the column and P_y is its capacity at yield. However, experimental evidence [26] has shown that after the panel zone yields in shear, almost all of the axial force in the column is transferred to the column flanges in the joint. Clearly this is true only for columns in which the flanges have the necessary capacity. Hence, in most cases, it may not be necessary to include the effect of axial load.

There have been questions regarding the distribution of shear stress within the panel. Elastic solutions show that the distribution is a parabolic variation from a constant stress at the corners of the panel. However, measured strains [14] indicate that the elastic shear strain distribution is more nearly uniform than parabolic.

In the last few years research [14, 15, 26, 27, 43] indicates that the behavior of connection panels in shear is bilinear. A linear elastic response was exhibited until the panel yields completely in shear. The panel stiffness in the linear region is

$$K_e = A'G \quad (\text{A.29})$$

where A' is the effective area of web in shear and is equal to $(d_c - t_f) t$, where t_f is the thickness of column flange, and G is

the shear modulus of the panel. Post-yielding response is approximately linear, with decreased stiffness, over a wide range of deformation. Until recently, linear post-yielding behavior was attributed to strain hardening. Research [14, 26, 27, 43] has indicated this behavior is due to the flexural rigidity of the flanges at the connection panel boundaries as shown in Fig. A.8.

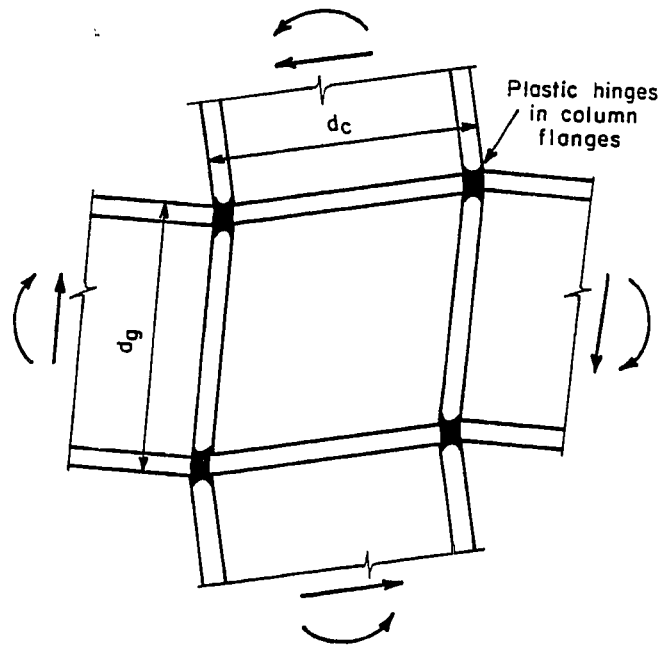


Fig. A.8 Connection panel at ultimate shear capacity.

Fielding and Chen [14] have given the following formula for the stiffness of the connection panel in the post-yielding region.

$$K_p = 24EI_f/d_g^2 \quad (\text{A.30})$$

where d_g is the depth of the girder and I_f is the moment of inertia of the column flange = $(b_f t_f^3)/12$. They consider the ultimate shear capacity of the panel is reached when the web panel completely yields and plastic hinges form in the column flanges as shown in Fig. A.8. The following equation is given for the ultimate shear capacity of the panel.

$$V_{\max} = (F_y/\sqrt{3}) A' + 4M_{pf}/d_g \quad (\text{A.31})$$

where $M_{pf} = F_y(b_f t_f^2/4)$ in the absence of axial load on the column. More correctly, M_{pf} should be calculated taking into consideration the flange axial tension or compression due to column moment.

Krawinkler [26] has approximated the post-elastic stiffness of the web panel by springs at the four corners of the panel.

$$K_p = \frac{1.095 b_f t_f^2 G}{d_g} \quad (\text{A.32})$$

or

$$\frac{5.0EI_f}{d_g t_f}$$

He defines the ultimate shear capacity of the panel as the shear at the total angle of distortion of four times the distortion at shear yield, and proposes

$$V_{\max} = K_e \gamma_y + 3 K_p \gamma_y \quad (\text{A.33})$$

$$= 0.55 F_y d_c t \left[1 + \frac{3.45 b_f t_f^2}{d_g d_c t} \right]$$

The studies reviewed show that there is a large margin of reserve strength in the connection panel beyond shear yield. However, it is achieved at a large distortion of the panel. Therefore, the connection design should be based on the required connection rigidity rather than on the criteria defining connection yielding.

For seismic design Krawinkler and Popov [25, 27] recommend that the joints should be permitted to dissipate energy through limited inelastic deformations. This can be accomplished by considering the post elastic shear strength of the joint and would eliminate unnecessarily thick doubler plates.

In view of this research, the LRFD Specification [6] gives the following nominal strength for the panel zone in shear

$$R_n = 0.7 F_y d_c t \quad (A.34)$$

However, this needs to be multiplied by the resistance factor ϕ of 0.90 to get the design strength. It is, however, ironic that Popov, et al. [43], based on their more recent tests on large beam-column assemblies, find the current code provisions for panel shear somewhat unconservative for seismic design. They write:

"There is a very delicate balance as to how much inelastic rotation must be taken by the beams and how much may be permitted to be taken by the panel zones.

A modest increase in panel zone thickness over the currently stipulated code provisions improves the ductility of joints by forcing the development of inelastic rotation in the beams."

APPENDIX B

Design Example

This design example is presented for a typical connection at the lower stories of a 40-story framed-tube structure.

Data Given

Column shear due to wind (working loads),

$$V_c = 200 \text{ K}$$

$$M_c = 900 \text{ K}'$$

$$V_b = 200 \text{ K}$$

$$M_b = 875 \text{ K}'$$

Column Size: 39-in. x 39-in.

$$f'_c = 5000 \text{ psi}$$

Vert. Reinf.: 28 - #14

Beam Size: W36 x 160

$$F_y = 36 \text{ ksi}$$

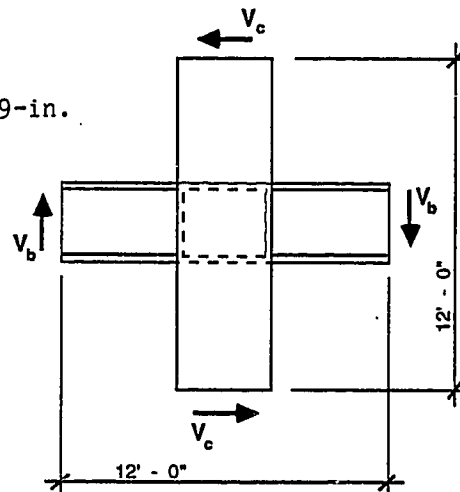
$$F_u = 58 \text{ ksi}$$

$$b_f = 12.0''$$

$$D_b = 36.01''$$

$$t_f = 1.02''$$

$$t_w = 0.65''$$



Solution

Forces due to factored loads:

LF for wind = 1.30

Additional amplification factor for connections = 1.20

$$V_c = 1.2 \times 1.3 \times 200 = 312 \text{ kips}$$

$$M_c = 1.2 \times 1.3 \times 900 = 1404 \text{ k-ft}$$

$$V_b = 1.2 \times 1.3 \times 200 = 312 \text{ kips}$$

$$M_b = 1.2 \times 1.3 \times 875 = 1365 \text{ k-ft}$$

1. Select proportions:

$$\text{Aspect ratio, } D_c/D_b = 39/36 = 1.083$$

$$0.75 < 1.083 < 1.5 \quad - \text{OK}$$

Let us try FBP fitting between the flanges only. Keep

$$w_p = b_e = 12.0''$$

2. Bearing on compression flanges:

$$\frac{a_c}{D_c} \left(1 - \frac{a_c}{D_c}\right) = \frac{2M_c}{\phi \lambda_c f_c' b_e D_c^2}$$

For bearing $\phi = 0.60$

$$\lambda_c = 3.0$$

$$b_e = \max [b_f, w_p] = 12.0''$$

$$\frac{a_c}{D_c} \left(1 - \frac{a_c}{D_c}\right) = \frac{2 \times 1404 \times 12}{0.6 \times 3.0 \times 5 \times 12 \times 39^2} = 0.205$$

$$\frac{a_c}{D_c} = 0.29 < 0.30 \quad - \text{OK}$$

3. Shear in steel panel:

$$\text{Shear cap. } V_{sp} = \phi (1/\sqrt{3}) F_{yp} t_{sp} D_c \left(1 - \frac{a_c}{D_c}\right)$$

For panel shear, $\phi = 0.90$

$$t_{sp} = t_w = 0.65''$$

$$V_{sp} = 0.9 \times (1/\sqrt{3}) \times 36 \times 0.65 \times 39 (1 - 0.29)$$

$$= 336.7 \text{ kips}$$

Actual shear in steel panel:

$$V_{hs} = \frac{2M_b}{d_b} - V_c \leq V_{sp}$$

$$d_b = D_b - t_f = 36.01 - 1.02 = 34.99''$$

$$V_{hs} = \frac{2 \times 1365 \times 12}{34.99} - 312 = 624.3 \text{ kips} > V_{sp}$$

$$\text{hence } V_{hs} = V_{sp} = 336.7 \text{ kips}$$

4. Shear in concrete panel:

$$\text{Shear cap. } V_{cp} = \phi \gamma \sqrt{f'_c} b_e D_c$$

For shear in concrete panel, $\phi = 0.85$

$$\frac{9\sqrt{f'_c} b_f}{F_{yp}} = \frac{9 \times \sqrt{5000} \times 12}{1000 \times 36} = 0.21''$$

$$t_{sp} = 0.65'' > 0.21''$$

hence $\gamma = 24$

$$V_{cp} = 0.85 \times 24 \times \sqrt{5000} \times 12 \times 39/1000$$

$$= 675 \text{ kips}$$

Actual shear in concrete panel:

$$V_{hc} = \frac{2M_b - V_{hs}d_b - V_c D_b}{d_p(1 - a_p/d_p)} \leq V_{cp}$$

$$d_p = D_b - 2t_f = 33.97 \text{ in.}$$

$$V_{hc} = \frac{2 \times 1365 \times 12 - 336.7 \times 34.99 - 312 \times 36.01}{33.97 (1 - 0.25)}$$

$$= 382.5 \text{ kips} < 675 \text{ kips} \quad - \text{OK}$$

5. Bearing on FBP:

$$\lambda_p = \frac{V_{hc}}{\phi f'_c w_p a_p}$$

For bearing $\phi = 0.60$

$$a_p = d_p (a_p / d_p) = 33.97 \times 0.25 = 8.49 \text{ in.}$$

$$\lambda_p = \frac{382.5}{0.6 \times 5 \times 12 \times 8.49}$$

$$= 1.251 < 3.0 \quad - \text{OK}$$

6. FBP thickness. Let us use FBP of A-36 material, $F_{yb} = 36$, $F_{ub} = 58$ ksi

(i) Shear fracture, Eq. 6.47a:

$$t_p = \frac{\sqrt{3} (V_{hc} - b_f t_w F_{yw})}{\phi b_f F_{ub}}$$

For shear fracture, $\phi = 0.75$

$$t_p = \frac{\sqrt{3} (382.5 - 12 \times .65 \times 36)}{.75 \times 12 \times 58} = 0.337''$$

(ii) Shear fracture, Eq. 6.47b

$$t_p = \frac{\sqrt{3} V_{hc}}{2 \phi b_f F_{ub}}$$

$$= \frac{\sqrt{3} \times 382.5}{2 \times .75 \times 12 \times 58} = 0.635"$$

(iii) Flexural bending, Eq. 6.47c

$$t_p = 0.2 \left(\frac{V_{hc} w_p}{\phi F_{yb} d_p} \right)^{0.5}$$

For plate bending, $\phi = 0.90$

$$t_p = 0.20 \left(\frac{382.5 \times 12}{.90 \times 36 \times 33.97} \right) = 0.834" \text{ controls}$$

Let us try 7/8 in. thick FBP

$$w_p/t_p = \frac{12}{7/8} = 13.71 < 22 \quad - \text{OK}$$

Use 12 x 33-7/8 x 7/8" FBP

7. Design support plates:

Not applicable

8. Check flange thickness:

$$t_f \geq 0.3 \left(\frac{b_f t_{sp} D_b F_{yp}}{\phi D_c F_{yf}} \right)^{0.5}$$

For plate bending $\phi = 0.90$

$$t_f \geq 0.3 \left(\frac{12 \times .65 \times 36 \times 36}{0.9 \times 39 \times 36} \right)^{0.5}$$

$$\geq 0.849 \text{ in.}$$

$$t_f = 1.02" > 0.849" \quad - \text{OK}$$

9. Calculate joint reinforcement:

$$(i) \quad A_{sh} = 0.3 \frac{S_h D_c f'_c}{f_{yh} A_c} \left(\frac{A_g}{A_c} - 1 \right)$$

Let us use GRD. 60 steel, $f_{yh} = 60 \text{ ksi}$

Concrete cover = 1-1/2" clear

$$\text{hence, } A_c = (39 - 2 \times 1.5)(39 - 2 \times 1.5) = 1296 \text{ in.}^2$$

$$A_g = 39 \times 39 = 1521 \text{ in.}^2$$

$$\frac{A_{sh}}{s_h} = 0.3 \times \frac{39 \times 5}{60} \left(\frac{1521}{1296} - 1 \right)$$

$$= 0.1692$$

$$(ii) \quad A_{sh} = 0.09 \frac{S_h D_c f'_c}{f_{yh}}$$

$$\frac{A_{sh}}{s_h} = 0.09 \times \frac{39 \times 5}{60} = 0.2925 \quad \text{controls}$$

$$\frac{A_{sh}}{s_h} = 0.2925 \text{ controls}$$

Provide #6 4-legged ties spaced vertically at 6" centers. Also provide two sets of ties at 3" spacing both above and below the beam.

10. Check size of vertical bars:

$$\frac{D_b}{d_{\text{bar}}} = \frac{36}{1.75} = 20.6 > 20 \quad - \text{OK}$$

Summary

Use 12 x 33-7/8 x 7/8" FBPs

Provide six sets of #6 4-legged ties spaced vertically at 6-in. centers. Also provide two sets of ties at 3-in. spacing both above and below the beam.

NOTE: The connection is designed for realistic forces in the lower stories of a 40-story building. It should be pointed out that by using wider or extended FBPs or higher strength concrete, the same connection could carry substantially higher forces. This shows the combination of structural steel beams and reinforced concrete columns can be used as a viable alternative.

LIST OF SELECTED NOTATIONS

a	distance along the beam as shown in Fig. 4.38
a_c	depth of stress block C_c . See Fig. 6.2
a_p	depth of stress block C_p . See Fig. 6.3(b)
A'	effective area of web in shear
A_c	confined area of column
A_g	gross area of column
A_{jh}	total area of horizontal shear reinforcement in the joint area
A_{jv}	total area of vertical shear reinforcement in the joint area
A_{sh}	total area of transverse reinforcement
A_{st}	required area of the stiffener
b	width of flange or moment connection plate. See Fig. A.5 and 2.1
b_b	overall width of beam
b_c	overall width of column
b_e	effective width of connection panel
b_f	flange width
b_s	width of stiffener plate
B_c	column width
$C_1 - C_9$	dimensionless constants
C_b	force in compression flange of beam
C_{bc}, C_{bs}	force C_b assigned to concrete and steel panels, respectively
C_c	Compressive stress block upon compression flanges. See Figs. 5.1 and 6.2.
C_{cc}, C_{cs}	force C_c assigned to concrete and steel panels, respectively

C'_c	compressive stress block upon tension flanges. See Fig. 5.3
C'_{cc}, C'_{cs}	force C'_c assigned to concrete and steel panels, respectively. See Fig. 5.4.
C_p	bearing stress block against face bearing plates. See Fig. 5.9
d_b	distance between centers of top and bottom flanges of beam. See Fig. 6.1
d_{bar}	diameter of the reinforcing bar
d_c	depth of column web
d_g	depth of girder. See Fig. A.8.
d_p	depth of face bearing plate as shown in Figs. 6.1 and 6.5.
d_{p1}	depth of face bearing plate between flanges when FBPs are extended above and below the beam. See Fig. 6.5.
D_b	overall depth of steel beam. See Fig. 6.1
D_c	overall depth of column. See Fig. 6.1
e_p	extension of the FBP. See Fig. 6.5
E	Young's modulus of elasticity
E_b	modulus of elasticity of beam material
E_c	modulus of elasticity of column material
E_s	modulus of elasticity of steel
E_{sh}	strain hardening modulus
f_b	bearing stress on concrete
f_c	concrete compressive strength in kg/cm^2
f_{ct}	concrete tensile strength
f'_c	compressive strength of concrete in psi
f_y	yield strength of reinforcing bars
f_{yh}	yield strength of transverse reinforcement

f_{yv}	yield strength of vertical shear reinforcement in the joint
F_b	force of the column vertical bars transmitted to the joint by bond. See Fig. 5.3
F_f	friction force under compression flanges. See Fig. 5.6
F_p	friction force against FBP
F_s	shear stress in steel panel
F_u	tensile strength of structural steel
F_{ub}	tensile strength of the FBP material
F_y	yield strength of structural steel
F_{yb}	yield strength of the FBP material
F_{yc}	yield strength of steel column
F_{yf}	yield strength of the beam flange
F_{yp}	yield strength of steel panel
F_{yst}	yield strength of the stiffener material
F_{yw}	yield strength of the beam web
G	shear modulus of elasticity
h	height of column, less joint size. See Fig. 4.38
h''	depth of column
H	height of column. See Fig. 4.38
ID	interstory drift. See Fig. 3.1(a)
I_b	moment of inertia of beam X-section
I_c	moment of inertia of column X-section
I_f	moment of inertia of flange about its own axis
k	distance between outer face of column flange and web toe of its fillet. See Fig. A.5
K_e	elastic panel stiffness
K_p	post-yielding stiffness of the panel
l	beam span, less joint size. See Fig. 4.38
l_{ab}	length between points a and b. See Fig. 5.9

l_{bc}	length between points b and c. See Fig. 5.9
L	beam span. See Fig. 4.38
m	width of central portion of flange as shown in Fig. A.6
M_b, M_c	moment in beam and column, respectively. See Fig. 6.1
M_p, M_{pf}	plastic moment capacity of flanges in bending about its own weak axis.
M_{sb}^u, M_{sc}^u	flexural capacity of the steel part of SRC beam and column, respectively
p	distance as shown in Fig. A.6
p_b	intensity of bearing stress. See Fig. 6.6
P	load at beam ends
P_{df}	force delivered by the flange
P_e	minimum axial compressive load on column
P_y	axial load capacity of column at yield
q	distance as shown in Fig. A.6
R_n	nominal strength of the panel in shear
S_h	spacing of hoops
t	column web thickness or panel thickness
t_b	thickness of flange or moment connection plate. See Fig. A.5
t_{cp}	thickness of concrete panel
t_p	thickness of face bearing plate
t_s	thickness of stiffener plate
t_{sp}	thickness of steel panel
T_b	force in tension flange of beam
T_{bc}, T_{bs}	force T_b assigned to concrete and steel panels, respective. See Fig. 5.5

T_c, T'_c	tension force in column vertical bars near tension and compression flanges, respectively. See Fig. 5.1
T_{cc}, T_{cs}	force T_c assigned to concrete and steel panels, respectively. See Fig. 5.5
T'_{cc}, T'_{cs}	force T'_c assigned to concrete and steel panels, respectively. See Fig. 5.5
V_b, V_c	shear force in beam and column, respectively
V_{bc}, V_{bs}	shear V_b assigned to concrete and steel panels, respectively. See Fig. 5.5
V_{cc}, V_{cs}	shear V_c assigned to concrete and steel panels, respectively. See Fig. 5.5
V_{ch}, V_{cv}	shear capacity of diagonal compression strut in the horizontal and vertical direction, respectively
V_h	total horizontal shear in the connection panel
V_{hc}, V_{hs}	horizontal shear in the concrete and steel panels, respectively
V_j	horizontal shear across the joint
V_{jh}, V_{jv}	design joint shear in the horizontal and vertical direction, respectively
V_{cp}, V_{sp}	shear capacity of the concrete and steel panel, respectively
V_u	net shearing force across the depth of the column web. See Fig. A.7
w_p	width of face bearing plate. See Fig 1.9(a)
x	distance X , less joint size. See Fig. 4.38
x_1	distance as shown in Fig. A.6
X	distance between two points on a beam where deflection is measured. See Fig. 4.38
Z_c	distance between centroids of tension reinforcement. See Fig. 5.8

γ normalized shear stress in concrete panel =

$$\frac{V_{hs}}{t_{cp} D_c \sqrt{f'_c}}$$

γ_y shear strain of the panel at yield
 Δ displacement between the two points on a beam. See Fig. 4.38
 ϵ_{sh} strain at the onset of strain hardening
 ϕ strength reduction factor
 λ_c coefficient of bearing stress on compression flange. See Fig. 6.2
 λ_p coefficient of bearing stress on FBP. See Fig. 6.3(b)
 ν ratio of shear strength of concrete panel to f_c
 ρ_s volumetric ratio of the spiral transverse reinforcement

REFERENCES

1. ACI-ASCE Committee 352, "Recommendations for Design of Beam-Column Joints in Monolithic Reinforced Concrete Structures", 1976.
2. ACI-ASCE Committee 352, "Recommendations for Design of Beam-Column Joints in Monolithic Reinforced Concrete Structures", Report ACI 352 R-85, 1985.
3. Adams, P.F., "Determination of the Static Yield Level of the Strain Hardening Modulus", Fritz Laboratory, Report No. 297-7, Lehigh University, March 64.
4. American Concrete Institute, "Building Code Requirements for Reinforced Concrete (ACI 318-83) and Commentary", American Concrete Institute, Detroit, 1983.
5. American Institute of Steel Construction, "Specification for the Design, Fabrication and Erection of Structural Steel for Buildings with Commentary", AISC, Chicago, Illinois, Nov. 1978.
6. American Institute of Steel Construction, "Specification for the Load and Resistance Factor Design, Fabrication and Erection of Structural Steel for Buildings", AISC, Chicago, Illinois, January 1986.
7. American Society for Testing Materials, "Standard Methods and Definitions for Mechanical testing of Steel Products", ASTM A370-77.
8. Ansourian, P., "Shear in Composite Beam-Column Connections", Proceedings, Institution of Civil Engineers, Part 2, Dec. 1981.
9. Ansourian, P., "Rigid-Frame Connections in Composite Structures", Transcripts, Institution of Engineers, Australia, Vol. CE22, Issue 2, May 80.
10. Aoyama, H., Umemura, H., and Minamino, H., "Tests and Analysis of SRC Beam-Column Subassemblages", Proceedings 6th WCEE, International Assoc. for Earthquake Eng., New Delhi, India, Jan. '77.

11. Belford, D., "Composite Steel-Concrete Building Frame", Civil Engineering, Am. Soc. of Civil Engineers, July '72.
12. Bjorhovde, R., and Fisher, J., "Wind Drift Criteria for Steel-Frame Buildings: An Introduction", Proceedings, The National Engineering Conference, Nashville, Tennessee, June 1986.
13. Blodgett, O.W., "Design of Welded Structures", 1966, The James F. Lincoln Arc Welding Foundation, Ohio.
14. Fielding, D., and Chen, W., "Steel Frame Analysis and Connection Shear Deformation", Journal of the Structural Div., Proceedings of the Am. Soc. of Civil Engineers, Jan. 1973.
15. Fielding, D., and Huang, J., "Shear in Steel Beam-to-Column Connections", Welding Journal, vol. 50, No. 7, Research Supplement, July 1971.
16. Fujimoto, M., Asai, K., et al., "Inelastic Behavior of Steel beam to Composite Column Connections", Trans. AIJ No. 301, April 1981 (Japanese).
17. Furlong, R., "Strength Implications of Connection Details to Composite Columns", Proceedings of the USA-Japan Seminar on Composite Structures and Mixed Structural Systems, Tokyo, Japan, 1980.
18. Griffis, L., "Design Considerations for Mixed Steel-Concrete Buildings", Proceedings, The National Engineering Conference, Nashville, Tennessee, June '86.
19. Hawkins, N., Mitchell, D. and Roeder, C., "Moment Resisting Connections for Mixed Construction", Engineering Journal, Am. Inst. of Steel Const., 1st Qtr., 1980.
20. Hawkins, N., and Roeder, C., "North American Analytical and Experimental Studies of Composite and Mixed Construction for Seismic Zones", Proceedings of the USA-Japan Seminar on Composite Structures and Mixed Structural Systems, Tokyo, Japan, 1980.
21. Hawkins, N.M., "The Bearing Strength of Concrete for Strip Loadings", Magazine of Concrete Research (London), V. 22, No. 71, June 1970.

22. Iyengar, H., "Systems Criteria for Mixed Steel-Concrete Systems", Proceedings of the USA-Japan Seminar on Composite Structures and Mixed Structural Systems, Tokyo, Japan, 1980.
23. Iyengar, H., "Mixing Steel and Concrete", Civil Engineering, Am. Soc. of Civil Engineers, Mar. '85.
24. Iyengar, H., "Recent Developments in Mixed Steel-Concrete Systems", Proceedings of the USA-Japan Seminar on Composite Structures and Mixed Structural Systems, Seattle, Washington, July, 1984.
25. Kato, B., and Tagami, J., "Beam-to-Column Connection of a Composite Structure", Proceedings of the USA-Japan Seminar on Composite Structures and Mixed Structural Systems, Seattle, Washington, July '84.
26. Krawinkler, H., "Shear in Beam-Column Joints in Seismic Design of Steel Frames", Engineering Journal, American Inst. of Steel Construction, 3rd Quarter, 1978.
27. Krawinkler, H., and Popov, E., "Seismic Behavior of Moment Connections and Joints", Journal of the Structural Div., Proceedings of the Am. Soc. of Civil Engineers, Feb., 1982.
28. Kriz, L.B., and Raths, C.H., "Connections in Precast Concrete Structures - Bearing Strength of Column Heads", Journal Prestressed Concrete Institute, V. 8, No. 6, Dec. 1963.
29. Lu, L., and Kato, B., "Research Needs in Composite and Mixed Structures", Proceedings of the USA - Japan Seminar on Composite Structures and Mixed Structural Systems, Seattle, Washington, July '84.
30. Manheim, D., and Popov, E., "Plastic Shear Hinges in Steel Frames", Journal of the Structural Div., Proceedings of the American Soc. of Civil Engineers, Oct. 1983.
31. Mattock, A. and Gaafar, G., "Strength of Embedded Steel Sections as Brackets", Journal of the Am. Conc. Institute, Mar.-April, 1982.
32. Meinheit, D.F., "The Shear Strength of reinforced Concrete Beam-Column Joints," Ph.D. dissertation, Department of Civil Engineering, University of Texas at Austin, Dec. 1983.

33. Miller, E., "Load and Resistance Factor Design of Moment Connections", Proceedings, The National Engineering Conference, Nashville, Tennessee, June '86.
34. Minami, K., "Stress Transferring Mechanism of Exterior Beam-Column Joints in Composite Structures", Proceedings of the USA-Japan Seminar on Composite Structures and Mixed Structural Systems, Seattle, Washington, July '84.
35. Moore, W., and Gosain, N., "Mixed Systems, Past Practices, Recent Experience and Future Direction", Proceedings of the USA-Japan Seminar on Composite Structures and Mixed Structural Systems, Seattle, Washington, July '84.
36. Naka, M., Unno, S., Morita, K. and Tachibana, M., "Experimental Study of the Strength of Steel Reinforced Concrete Beam-Column Joints", AIJ Convention, Chugoku, Japan, Oct. '77 (Japanese).
37. O'Leary, A., and Undrill, D., "A Steel Beam Concrete Column Frame System, Proceedings, Eighth World Conference on Earthquake Engr., San Francisco, CA, 1984.
38. Park, R., "New Zealand Design Recommendations for Beam-to-Column Connections", Paper presented at ACI Spring Convention, San Francisco, CA, Mar. 1986.
39. Paulay, T., "A Critique of the Special Provisions for Seismic Design of the Building Code Requirements for Reinforced Concrete (ACI 318-83)", Journal of the Am. Concrete Inst., Mar-April 1986.
40. Prestressed Concrete Institute, "PCI Design Handbook - Precast Prestressed Concrete", Prestressed Concrete Institute, Chicago, 1978.
41. Prestressed Concrete Institute, "PCI Manual for Structural Design of Architectural Precast Concrete", Prestressed Concrete Institute, Chicago, 1977.
42. Plastic Design in Steel, A Guide and Commentary Manual No. 41, 1971, American Society of Civil Engineers.
43. Popov, E., Amin, N., Louie J., and Stephen, R., "Cyclic Behavior of Large Beam-Column Assemblies", Engineering Journal, Am. Institute of Steel Constr., 1st quarter, 1986.

44. Raths, C., "Embedded Structural Steel Connections", PCI Journal, May-June 1974.
45. Roeder, C., and Popov, E., "Cyclic Shear Yielding of Wide-Flange Beams", Journal of the Engineering Mechanics Div., Proceedings of the American Society of Civil Engineers, Aug. 1978.
46. Sabnis, G.M., "Handbook of Composite Construction", Van Nostrand-reinhold, New York, 1979, Chapter 7.
47. Saenz, R., "The Influence of Floor Members on the Behavior of Reinforced Concrete Beam-Column Joints Subjected to Severe Cyclic Loading", Ph.D. dissertation, Department of Civil Engineering, Univ. of Texas at Austin, Dec. 1983.
48. Salmon, C.G. and Johnson, J.E., "Steel Structures, Design and Behavior", 2nd Edition, 1980, Harper and Row, Publishers, Inc., New York.
49. Shimizu, Y., Tada, A. and Yoshida, H., "The Reinforcing Effect on Steel-Reinforced Concrete Joints", AIJ Convention, Kento, Japan, Sept. '70 (Japanese).
50. Tanaka, A., and Nisigaki, T., "A Experimental Study of Steel Reinforced Concrete Column-Steel Beam Joints", AIJ Convention, Japan, Oct. '72, (Japanese).
51. Wakabayashi, M., "Experimental Studies on Composite Structures", Report of the Institute of Industrial Science, University of Tokyo, Japan, Vol. 6, No. 2 (Serial No. 45), Dec. '56.
52. Wakabayashi, M., "Seismic Design of Mixed Steel Concrete Structures in Japan", Proceedings of the International Colloquium on stability of Structures Under Static and Dynamic Loads, SSRC/ASCE, Washington, D.C., Mar. '77.
53. Wakabayashi, M., "Standards for the Design of Concrete Encased-Steel and Concrete Filled Tubular structures in Japan", Proceedings of the USA-Japan Seminar on Composite Structures and Mixed Structural Systems, Tokyo, Japan, 1980.
54. Wakabayashi, M., "Recent Japanese Developments in Mixed Structures", Proceedings of the Specialty Conference, Methods of Structural Analysis, University of Wisconsin-Madison, Aug. '76.

55. Wakabayashi, M., "Recent Research Activities on Composite Steel Reinforced Concrete Building Structures and Design Practices in Japan", Proceedings of the USA-Japan Seminar on Composite Structures and Mixed Structural Systems, Seattle, Washington, July '84.
56. Wakabayashi, M., and Minami, K., "Recent Experimental Studies on the Hysteretic Characteristics of Beam-to-Column Connections in Composite Structures", Proceedings of the USA-Japan Seminar on Composite Structures and Mixed Structural Systems, Tokyo, Japan, 1980.
57. Wakabayashi, M. and Minami, K., "Review of the Studies on the Shear Resistance of Composite Steel and Reinforced Concrete Beam-to-Column Connections in Japan", Proceedings of the U.S.-New Zealand-Japan Seminar, Monterrey, CA, Aug. '84.
58. Wakabayashi, M., Minami, K., and Nishimura, Y., "Design Method for Mixed Structures, Part 1, Stress Transfer Mechanism of Exterior Joints", Annual Report of the Disaster Prevent Center, No. 26, April '83.
59. Wakabayashi, M., Nakamura, T. and Morino, S., "An Experiment of Steel Reinforced Concrete Cruciform Frames", Bulletin of the Disaster Prevention Research Institute, Kyoto University, Japan, Vol. 23, Parts 3-4, No. 214, Dec. '73.
60. Williams, A., "The Bearing Capacity of Concrete Loaded Over a Limited Area", Technical Report No. 526, Cement and Concrete Association, London, Aug. 1979.
61. Winter, G., "Theme Report Mixed Steel-and-Concrete Buildings", Proceedings of the National Conference on Tall Buildings, Tokyo, Japan, Aug. 1973.
62. Yokoo, Y., Wakabayashi, M. and Suenaga, Y., "Experimental Studies on Steel-Reinforced Concrete, Study on the Shear Strength of the Panel at Beam-To-column Connections, Part 6", Trans. AIJ, No. 137, July 1967, (Japanese).
63. Yura, J.A., Unpublished Lecture Notes on "Advanced Steel Design", University of Texas at Austin, Austin, Texas, Fall '79.

VITA

Tauqir Muhammad Sheikh was born in Karachi, Pakistan, on May 11, 1954, the son of Mohammad Maqbool Ahmed and Rashida Maqbool. After completing his work at Muslim Model High School, Lahore, Pakistan, in 1968, he entered Government Intermediate College, Rawalpindi, Pakistan. He studied civil engineering at N.E.D. Government Engineering College, Karachi, Pakistan, from October 1970 until March 1973. He completed his Bachelor of Science degree at The University of Engineering and Technology, Lahore, Pakistan, in October 1975. Upon graduation, Tauqir worked for Gammon Pakistan, Ltd., Rawalpindi, as a Design Engineer. He was then employed at National Construction Company (PAK), Ltd., Islamabad, Pakistan, as a Junior Engineer. In May 1977, he was hired by Conforce Saudi Arabia, to work as a Site Engineer in Jeddah, Saudi Arabia. He received the degree of Master of Science from The University of Texas at Austin in May 1980. Subsequently, Tauqir worked with CBM Engineers, Inc., Houston Texas as Structural Engineer, before entering the Graduate School of The University of Texas at Austin in September, 1983. On April 16, 1987, he married Saba Waheed of Delhi, India.

Permanent address: House No. 7, Street 58, G-6/4
Islamabad, Pakistan

This dissertation was typed by Sharon Cunningham